Advances in Polymer Technology

Bio-Polymer Composites for High-Performance Applications

Lead Guest Editor: S. Indran
Guest Editors: Lee Chang Chuan and Parthiban A

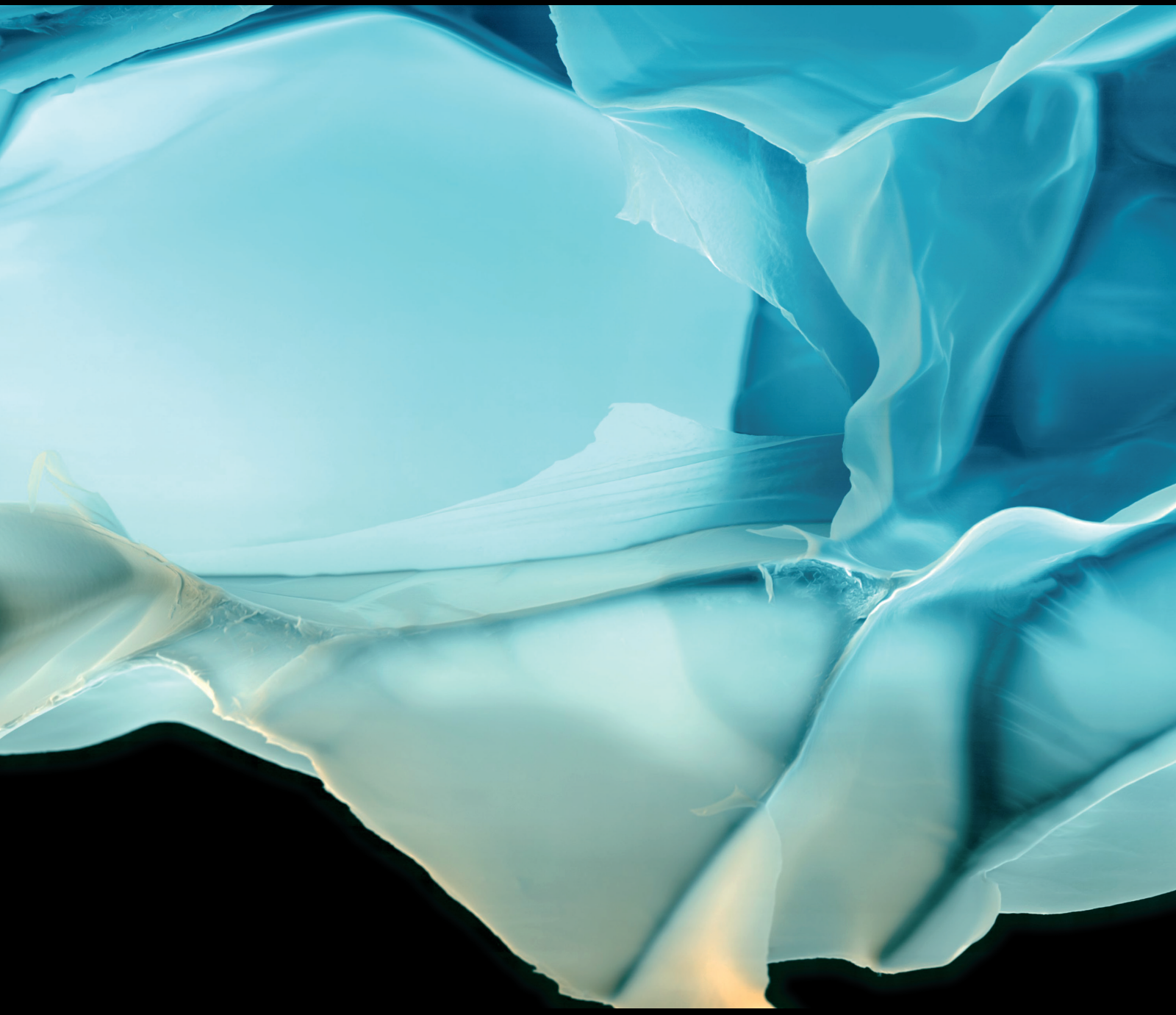

Bio-Polymer Composites for High-Performance Applications

Advances in Polymer Technology

Bio-Polymer Composites for High-Performance Applications

Lead Guest Editor: S. Indran
Guest Editors: Lee Chang Chuan and Parthiban A

Contents

A Decision-Making Carbon Reinforced Material Selection Model for Composite Polymers in Pipeline Applications

Mohammed Ahmed Mustafa, S. Raja, Layth Abdulrasool A. L. Asadi, Nashrah Hani Jamadon, N. Rajeswari, and Avvaru Praveen Kumar

Research Article (9 pages), Article ID 6344193, Volume 2023 (2023)

Hindawi
Advances in Polymer Technology
Volume 2023, Article ID 9452164, 9 pages
https://doi.org/10.1155/2023/9452164

Research Article

Physicochemical Characteristics of Chitosan–Alginate Scaffold Containing Atorvastatin

Hananeh Hamedfar,[1] Tayebeh Zivari-Ghader,[1] Abolfazl Akbarzadeh,[2] and Soodabeh Davaran[1,3]

[1]*Department of Medicinal Chemistry, Faculty of Pharmacy, Tabriz University of Medical Sciences, Tabriz, Iran*
[2]*Faculty of Pharmacy, Department of Medicinal Chemistry and Drug Applied Research Center, Tabriz University of Medical Sciences, Tabriz 51368, Iran*
[3]*Department of Toxicology, Faculty of Pharmacy, Yeditepe University, Ataşehir, Istanbul, Turkey*

Correspondence should be addressed to Soodabeh Davaran; davaran@tbzmed.ac.ir

Hananeh Hamedfar and Tayebeh Zivari-Ghader contributed equally to this work.

Received 19 November 2022; Revised 25 April 2023; Accepted 7 August 2023; Published 30 August 2023

Academic Editor: Chang Chuan Lee

In addition to being a lipid-lowering medication, atorvastatin (ATV) is an anti-inflammatory agent. When there is a bone defect or inflammation of adjacent tissues, it aids in bone repair. This study aimed to develop a chitosan–alginate (CS/ALG)–tripolyphosphate (TPP)–ATV hybrid hydrogel as a drug delivery system, using a tissue engineering scaffold for the first time. For this purpose, a CS/ALG hydrogel crosslinked with TPP was developed. The delivery profile of ATV and its physicochemical properties such as particle size and hydrogel swelling percentage were determined. The structure and morphology of the hydrogels were analyzed using Fourier transform infrared spectroscopy and scanning electron microscopy. As a result, an alginate–chitosan hydrogel with a TPP crosslinker was prepared. The results revealed that drug loading was nearly complete, and the first hour revealed a 25% explosive release. The drug was gradually released over 10 hr at approximately 35%. The amount of crosslinker used significantly influenced the encapsulation gain and release profiles. Owing to its high porosity and swelling, the CS/ALG hydrogel crosslinked with PPT is an ideal scaffold for loading drugs, macromolecules, and cells.

1. Introduction

Osteoporosis is a severe medical condition characterized by low bone mass and deterioration of bone structure, which increase bone fragility and fracture risk [1]. Patients with osteoporosis can lose up to 50% of their bone density at critical skeletal locations [2]. His illness is now treated with RANK ligand antibodies (denosumab), selective estrogen receptor modulators (SERMs), teriparatide, and bisphosphonates [3]. Most of these drugs prevent bone remodeling by reducing osteoclast activity and recruiting new osteoclasts. Although these medications help treat and manage this condition, their long-term use has significant drawbacks. For example, long-term bisphosphonate therapy has been linked to atrial fibrillation, jaw osteonecrosis, and severe bone turnover inhibition [4]. Long-term SERM (raloxifene) use has also been linked to venous thromboembolism and fatal strokes [5]. Therefore, effective therapy is required to improve bone mineral density and generate new bone without significant side effects associated with long-term medication [6, 7]. Statins have anti-inflammatory properties, because they lower the levels of interleukin-6 and interleukin-8. Mundy demonstrated for the first time an experimental study in which statins improved bone volume. The trabecular bone volume increased in rats whose ovaries were removed and administered 5–10 mg simvastatin daily for 35 days [8].

Simvastatin, another statin medication, has been shown to increase the amount of bone tissue, the rate at which bone tissue is produced, and the strength of spongy bone tissue [9]. Several processes involved in statin drugs and bone metabolism are of particular interest. These substances stimulate osteoblast activity, which is stimulated by bone morphogenetic protein-2. Statins also inhibit hydroxymethylglutaryl coenzyme-A reductase and

lower mevalonate production, thereby interfering with osteoclast function and increasing apoptosis, which prevents bone resorption. Statins have an anti-inflammatory effect, causing bone defects in the affected bone and surrounding tissues. Statin use may also aid bone healing [10].

The effect of atorvastatin (ATV) on the proliferation, migration, and invasiveness of primary smooth muscle cells isolated from human saphenous veins after loading into a hyaluronic acid hydrogel was studied. The results show that the hydrogel is a viable substrate for local drug administration because it allows for the steady release of ATV over hours, resulting in multiple changes in the vascular smooth muscle cells phenotype that are similar to those produced by the drug freely dissolved in the cell environment [11]. Another study used a crosslinked hyaluronic acid hydrogel/poly(lactic-co-glycolic acid) microparticle formulation loaded with ATV to develop a simple drug delivery system to prevent intimal hyperplasia (IH). A carotid artery ligation model was used to validate the in vivo proof of concept. The combination of rapid and continuous ATV release has a synergistic effect on IH development. There was no evidence of harm to the collected tissues [10]. In another study, Özdoğan et al. [12] discovered that combining ATV with chitosan improved anti-inflammatory activity and bone and tissue healing in periodontitis-induced rats. Therefore, using osteoimmunomodulatory biomaterials to create a local immunological environment that promotes bone regeneration and osseointegration may be an appropriate method for redressing this imbalance [13]. Natural source-based materials are promising for biomedical applications [14–19]. Nanobiomaterials are made using biological resources such as fungi, plants, and algae [20–23]. Chitin, as a fibrous substance in the cell walls of some fungi, is the source of chitosan. The most important characteristics of chitosan are its nonantigenicity, excellent biodegradability, biocompatibility, ease of processing under mild conditions, interaction with cell matrix components and cell surface receptors, reactive and changeable groups, and chelating capacity. However, its controlled degradation ensured long-term survival of the encapsulated cells. In addition, chitosan can create a dynamic environment for penetration of tissue defects, making it a suitable option for use in delivery systems or matrices for the regeneration of different tissues [24]. In this study, we aim to design a sensitive, fast, and routine method that can be implemented at a low cost in the shortest time, and on the other hand, can be used as a platform that can be developed.

2. Materials and Methods

2.1. Materials. Sodium alginate (Catalog no. 501785611), chitosan (Catalog no. NC0805453), disodium phosphate, pentasodium tripolyphosphate (TPP; Catalog no. 106999), and sodium dihydrogen phosphate were purchased from Sigma–Aldrich. Dimethylformamide (Catalog no. 103034) and acetic acid (Catalog no. 137000) were acquired from Merck Co., whereas ATV calcium was acquired from Sobhandarou.

2.2. CS/ALG Hydrogel Fabrication. Chitosan (0.2 g) was dissolved in 10 ml acetic acid (1%) under stirring conditions for 15 min, and the alginate solution was then prepared by dissolving sodium alginate (0.45 g) in deionized water (10 ml, conductivity at 25°C = 0.02 μS/cm) under stirring conditions with magnetic stirrer (1,000 rpm) at room temperature for 15 min. The above solutions were mixed at a specific ratio and stirred overnight with a magnetic stirrer (1,200 rpm) at room temperature to obtain chitosan–alginate (CS/ALG) as the final product.

2.3. CS/ALG/TPP Hydrogel Fabrication. Chitosan (0.2 g) dissolved in 10 ml acetic acid (1%), sodium alginate (0.45 g) dissolved in distilled water, and TPP (0.01 g) as a crosslinker were mixed. The solutions were stirred overnight with a magnetic stirrer (1,200 rpm) at room temperature [25] (Figure 1).

2.4. Preparation of Drug-Loaded Hydrogel. To load the drug, chitosan (0.1 g) was dissolved in 10 ml of acetic acid (1%), sodium alginate (0.0225 g) in 10 ml of deionized water, TPP (0.005 g) in 2 ml of deionized water, ATV in 10 ml of deionized water, and dimethyl fumarate (3 ml) in 10 ml of deionized water. The solutions were then mixed and stirred using a magnetic stirrer (1,200 rpm) overnight at room temperature. Finally, the CS/ALG/TPP hydrogel containing ATV was obtained.

2.5. Release Study in Phosphate-Buffered Saline. Three samples (average weight = 19.66 g) of CS/ALG/TPP loaded with ART were dispersed in 25 ml of phosphate-buffered saline (PBS) (pH = 7.4). The hydrogels were then placed in a shaker incubator (80 rpm) at 37°C. At specific times, PBS (3 ml) containing ART in the buffer solution was removed, measured using a UV–visible at 241.5 nm, and resupplemented with a fresh 3 ml of PBS. A set of standard solutions was used to calibrate the amount of ART present at each time point. The actual drug concentration was determined using Equation (1) [26]:

$$Cn = Cn.\text{meas} + \frac{\Delta v}{Vt}\sum_{s=1}^{n-1}(Cs.\text{meas}), \quad (1)$$

where n, n^{th} concentration measurement; Cn, corrected drug concentration; Cn.meas, the acquired drug concentration at the nth measurement; Δv, the withdrawn volume at each measurement; and Vt, the total volume of solution.

3. Physicochemical Properties of Hydrogels

3.1. Fourier Transform Infrared Spectroscopy. Fourier transform infrared spectroscopy (FTIR) (Equinox 55 LS 101, Bruker, Germany) was used to assess the chemical characteristics of the prepared CS/ALG/TPP. We used a wavelength range of 400–4,000 cm^{-1}, as in our previous work [27]. The Infrared (IR) spectra of all KBr-pressed samples were recorded in CO_2 nitrogen gas at room temperature [27].

3.2. Scanning Electron Microscopy of CS/ALG/TPP Hydrogel Loaded with ART. Scanning electron microscope (SEM) (LEO 1430 VP, Germany) was used to evaluate the surface morphology and structure of prepared material according to our previous works [28] at 15 kV acceleration voltage. Materials were sectioned into thin slices and vacuum-coated with Au–Pd thin layer by a Polaron SC7620 sputter coater as used previously [27].

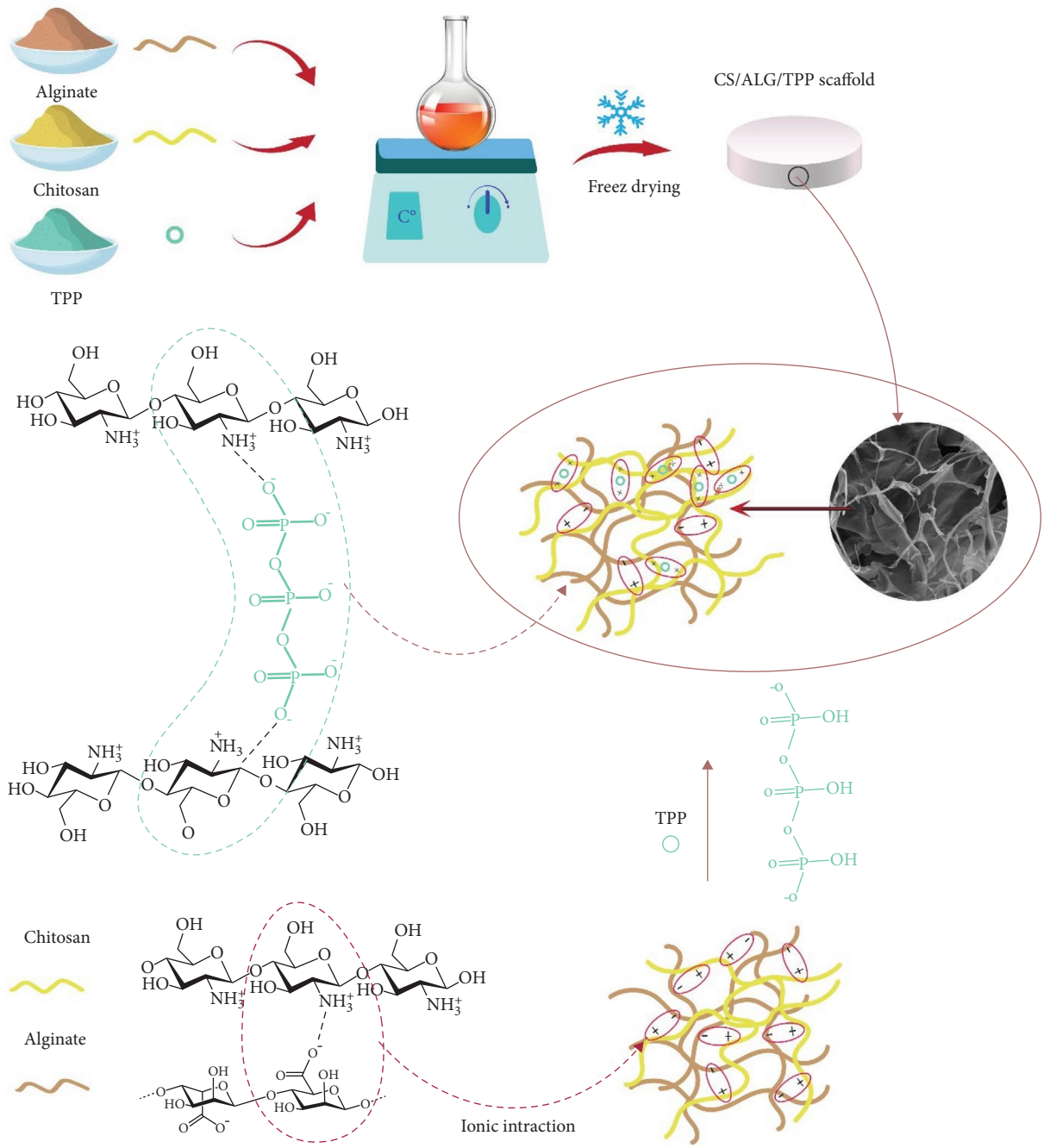

Figure 1: Schematic representation of the fabrication process of the CS/ALG/TPP scaffold.

3.3. Moisture Content and Swelling Ratio. To evaluate the swelling performance, freeze-dried hydrogel samples were immersed in PBS (pH 7.4) at 37°C and evaluated immediately after the liquid was removed from the hydrogel surface using a wet sponge. This process was repeated until total hydration was achieved. The swelling ratio (SR, g/g) was calculated using Equation (2) [25]:

$$\mathrm{SR}\,(\%) = \frac{W_s - W_d}{W_d} \times 100, \tag{2}$$

where W_d, hydrogel weight before floating in buffer (dry hydrogel) and W_s, weight of hydrogel after swelling in buffer (wet hydrogel).

4. Results and Discussion

4.1. Characterization of Fabricated CS/ALG/TPP Hydrogel. The hydrogels in this study were created by simply complexing chitosan, alginate, and TPP solutions (Figure 1). FTIR spectrometry was used to investigate the chemical structures of Gierszewska et al. [25]. One of the most important anionic

crosslinkers is TPP, which is widely used in the synthesis of scaffolds, membranes, nanoparticles, and various composites for medical purposes [29].

In addition, because phosphate groups are necessary for bone mineralization, TPP is widely used as a crosslinker in the development of biomimetic polymer systems for bone regeneration.

The degree of crosslinking can affect the homogeneity, porosity, hydrophilicity, and mechanical properties of scaffolds [30]. Consequently, a precise duration of the crosslinking stage is crucial for obtaining systems with exceptional performance. This negative phosphate crosslinker is frequently used to form positive ammonium chitosan crosslinks. Because instant gelation results in the formation of precipitates, simple mixing of chitosan and TPP solutions in tissue engineering applications is not an appropriate method for regulating the crosslinking reaction. Consequently, numerous methods for preparing CS-TPP systems with a controlled degree of crosslinking have been developed, such as those based on the ionic strength of the CS solvent in the presence of NaCl or the slow diffusion of TPP in the CS solution. This was used to create uniform membranes. In this study, CS/ALG scaffolds were crosslinked by immersion in TPP solution. To investigate the effects of various experimental conditions on scaffold performance, scaffolds were prepared with various concentrations of CS (1% and 2% w/w) and alginate, as well as two concentrations of TPP (1% and 2% w/w), and various reaction times (2, 4, and 8 hr). FTIR spectral range: the formation of chitosan crosslinks was confirmed by the crosslink scaffold composed of CS/ELG/TPP.

Figure 2(a)–2(c) depicts the FTIR spectra of chitosan, alginate, pentasodium TPP, and their mixtures [31].

Except for TPP, all spectra exhibited a strong and broad antisymmetric band at approximately 3,430 cm^{-1}, which was caused by the overlap of O–H and N–H stretching vibrations of the functional groups involved in hydrogen bonding. Chitosan possesses characteristic bands at 1,650 cm^{-1} (associated with the stretching vibrations of carbonyl amide 1), 1,598 cm^{-1} (associated with the bending vibrations of the first type of nonacetylated aminoglycoside), and 1,560 cm^{-1} (related to the bending vibrations of the N–H group of amide type 2).

Chitosan's saccharide structure is characterized by absorption bands at 2,253 cm^{-1} (asymmetric stretching vibrations of C–O–C bonds), 1,083 cm^{-1}, and 1,031 cm^{-1} (skeletal vibrations including C–O bonds). When chitosan was crosslinked with TPP, a new absorption band was observed at 1,635 cm^{-1}, owing to the antisymmetric vibration of N–H in the NH_2 groups. After the ion crosslinking of chitosan with TPP, additional changes in the IR spectrum were observed. The absorption at 1,215 cm^{-1} was due to the stretching vibrations of the C = O bond of the crossphosphate linker groups [25].

4.2. Swelling Study of CS/ALG/TPP Hydrogel. The SR was measured to evaluate the swelling performance of the prepared CS/ALG/TPP hydrogel containing ART and quantify its water uptake ability. The SR values of the prepared hydrogels are shown in Figure 3. Swelling is caused by liquid absorption by the polymer, and can be calculated by measuring the hydrogel mass. The mass SR data revealed that the Chit/Alg/TPP hydrogels exhibited 700%–800% swelling in the first few hours and 1,000% swelling after 30 hr, before decreasing to approximately 800% [32]. The swelling behavior and structural stability of hydrogels are critical for their practical use in tissue engineering. Most natural polymers, including chitosan, rapidly swell in biological fluids. Previous research indicates that early swelling is favorable and that the resulting increase in pore size promotes cell adhesion and development in a three-dimensional structure [33]. On the other hand, persistent swelling may result in loss of mechanical integrity and maceration of the surrounding tissue [32].

4.3. SEM Study of CS/ALG/TPP Hydrogel. SEM was used to investigate the morphological and surface properties of CS/ALG/TPP-containing ART hydrogels. Figure 4 shows the SEM images of the hydrogels. Images captured by SEM of the CS/ALG/TPP freeze-dried hydrogel containing ART revealed the morphology of the hydrogel. Examination of the hydrogel architecture revealed that the scaffold had a highly porous structure with interconnected pores generated by phase separation during lyophilization. The hydrogel structure is completely permeable. The holes are approximately 30 μm in size, which facilitates bone cell adhesion and development and is advantageous for cell attachment and migration [34].

4.4. Porosity Determination of CS/ALG/TPP Hydrogel. SEM was used to investigate the morphological and surface properties of CS/ALG/TPP-containing ART hydrogels. Figure 4 shows the SEM images of the hydrogels. Images captured by SEM of the CS/ALG/TPP freeze-dried hydrogel containing ART revealed the morphology of the hydrogel. Examination of the hydrogel architecture revealed that the scaffold had a highly porous structure with interconnected pores generated by phase separation during lyophilization. The hydrogel structure is completely permeable. The holes are approximately 30 μm in size, which facilitates bone cell adhesion and development and is advantageous for cell attachment and migration [35]:

$$P = \frac{(V_1 - V_3)}{(V_2 - V_3)} \times 100\%, \tag{3}$$

where $V_1 = 9$, $V_2 = 9.05$, $V_3 = 8.4$, and $P = 92\%$.

After crosslinking, the hydrogel was 92% porous (Figure 3), and after 24 hr in water, it swelled by a shock of 98.6%.

Numerous studies have reported the amount of water absorption and swelling of alginate and chitosan hydrogels crosslinked with TPP. After approximately 24 hr, the maximum swelling percentage of the crosslinked CS/ALG hydrogel was 98.6%, which is greater than the values reported in the literature [36, 37]. The results showed that using a TPP crosslinker is beneficial, and because the structure of the hydrogel is highly porous (92%), the expansion percentage can be significantly increased.

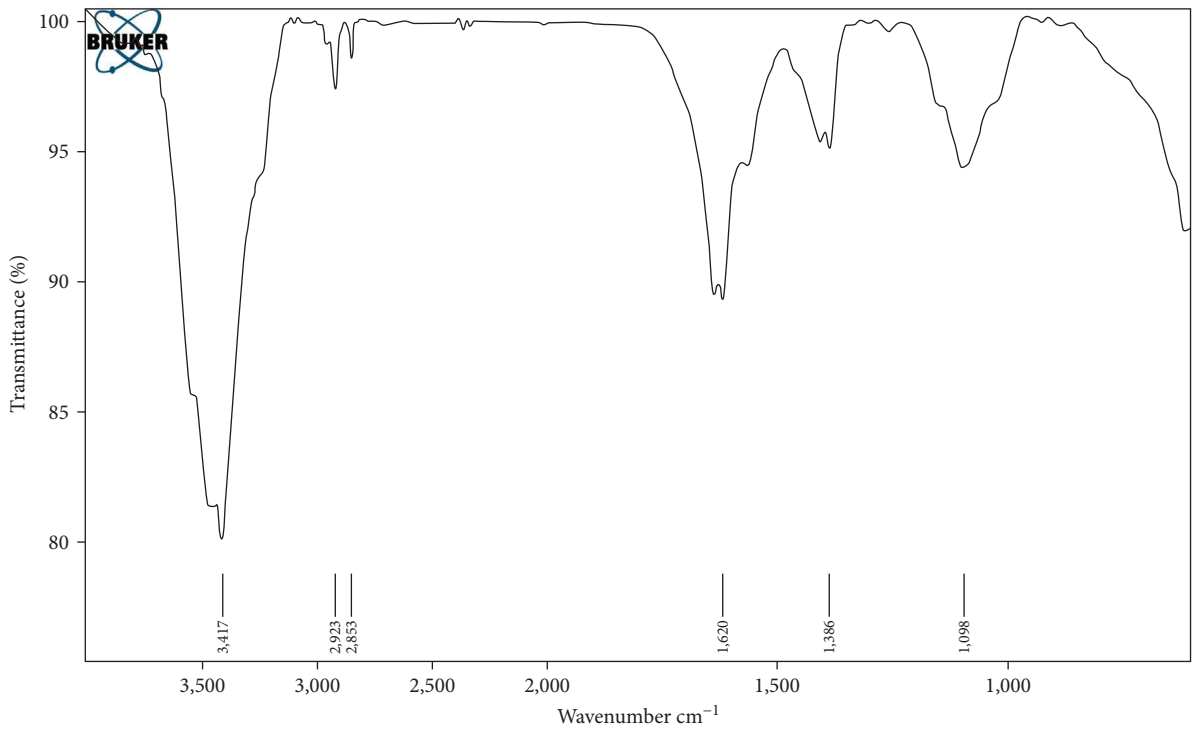

(a)

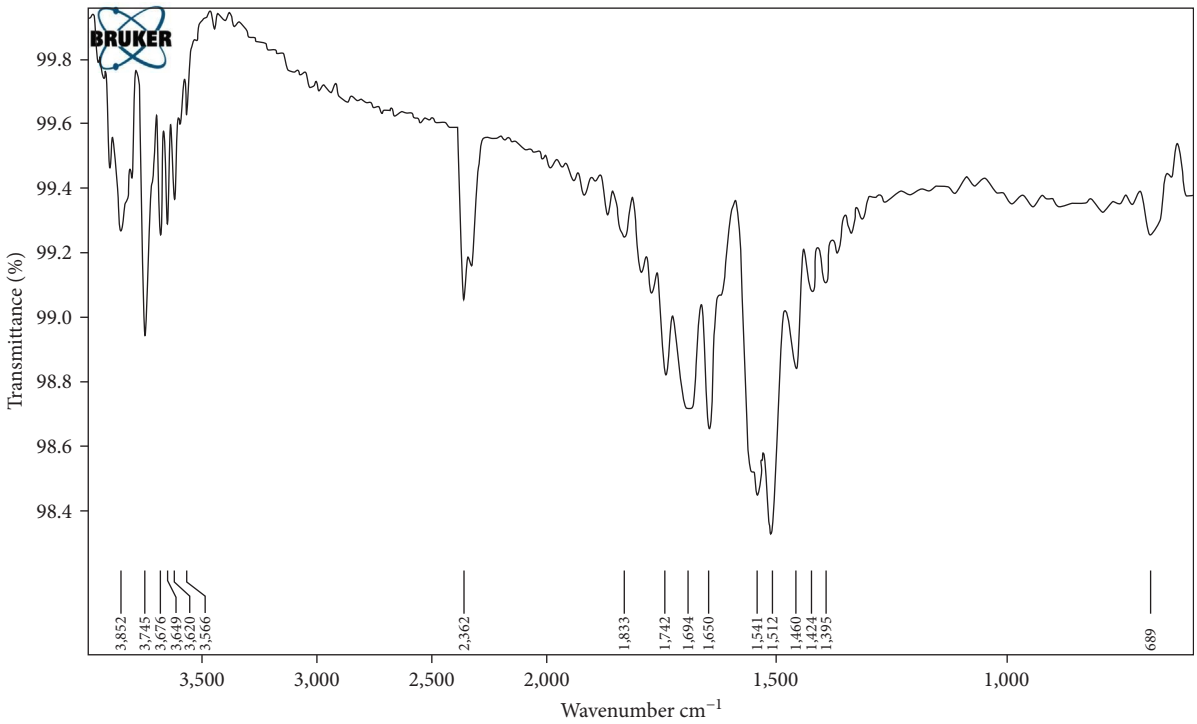

(b)

Figure 2: Continued.

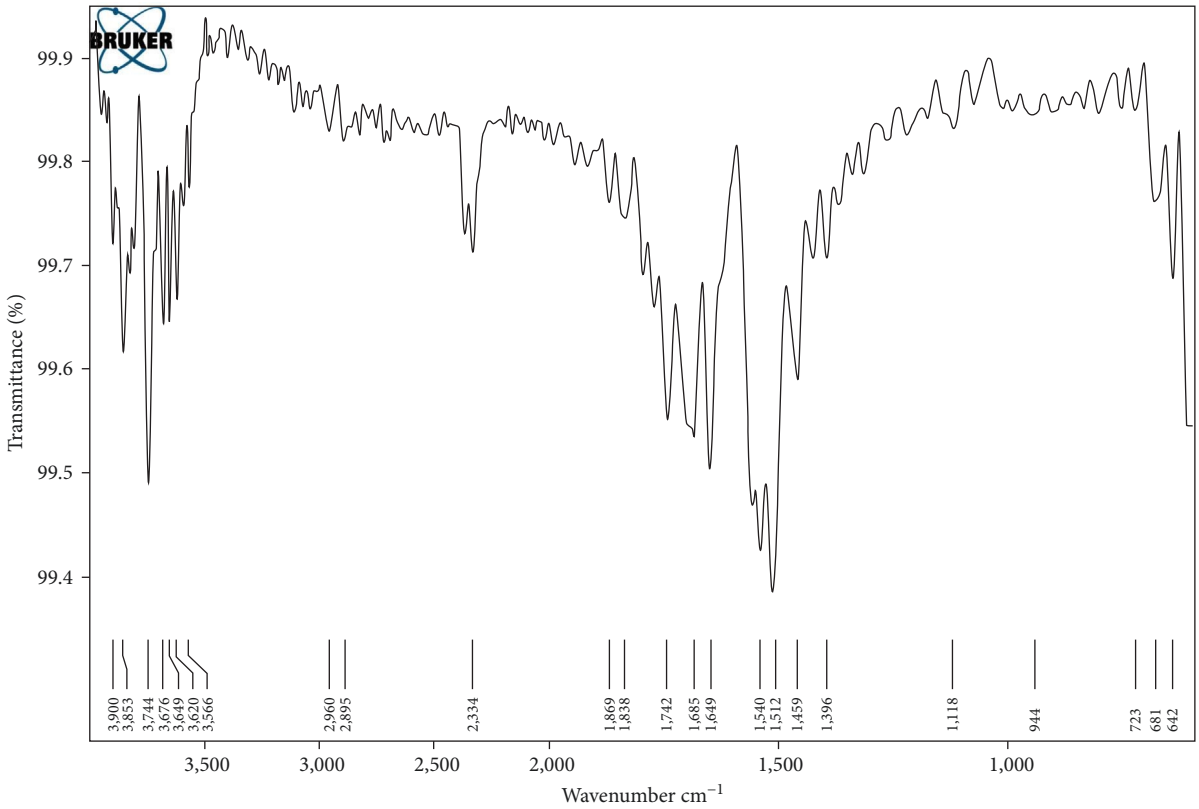

(c)

Figure 2: (a) FTIR spectrum of CS/ALG hydrogel, (b) FTIR spectra of CS/ALG/TPP hydrogel, and (c) FTIR spectra of CS/ALG/TPP scaffold containing ART.

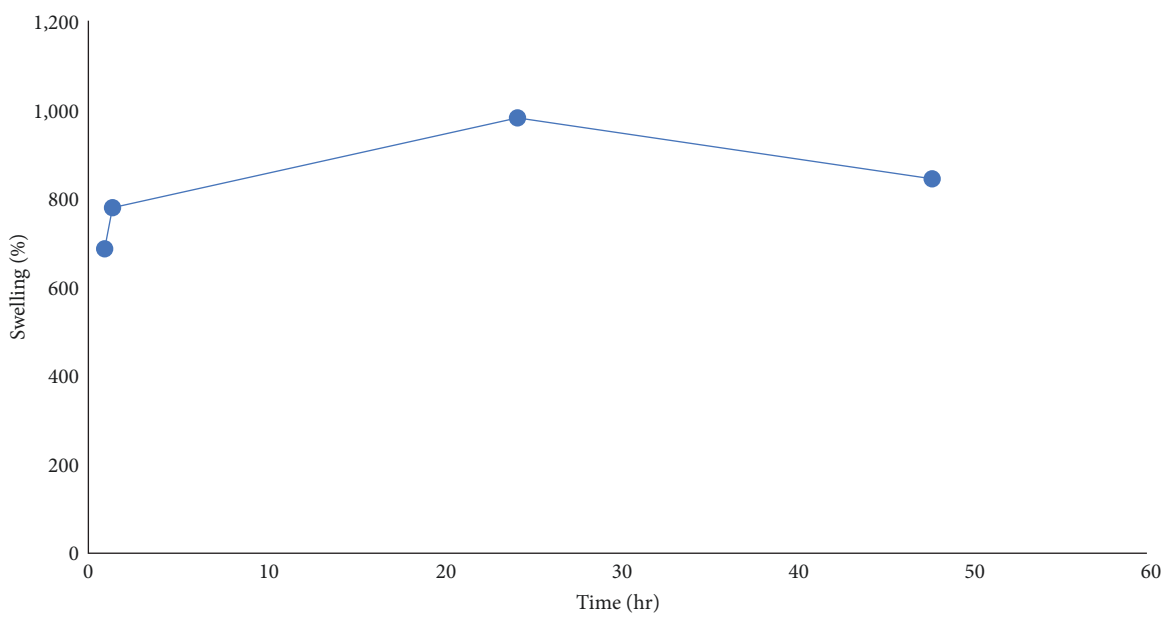

Figure 3: Swelling percentage graph of CS-AlG-TPP freeze-dried hydrogel containing atorvastatin in phosphate buffer after hours.

4.5. Cumulative Release Study. This study investigated the release of ART from CS/ALG/TPP hydrogels in PBS (pH 7.4) at 37°C for 10 and 24 hr (Figure 5). Standard deviations of the samples were calculated. The drug release profile was examined at 37°C and a pH of 7.4. The results revealed that the drug was released explosively in the first hour at approximately 25% (Figures 5(a) and 5(b)) and then gradually for 10 hr, at a rate of approximately 35%. After 24 hr,

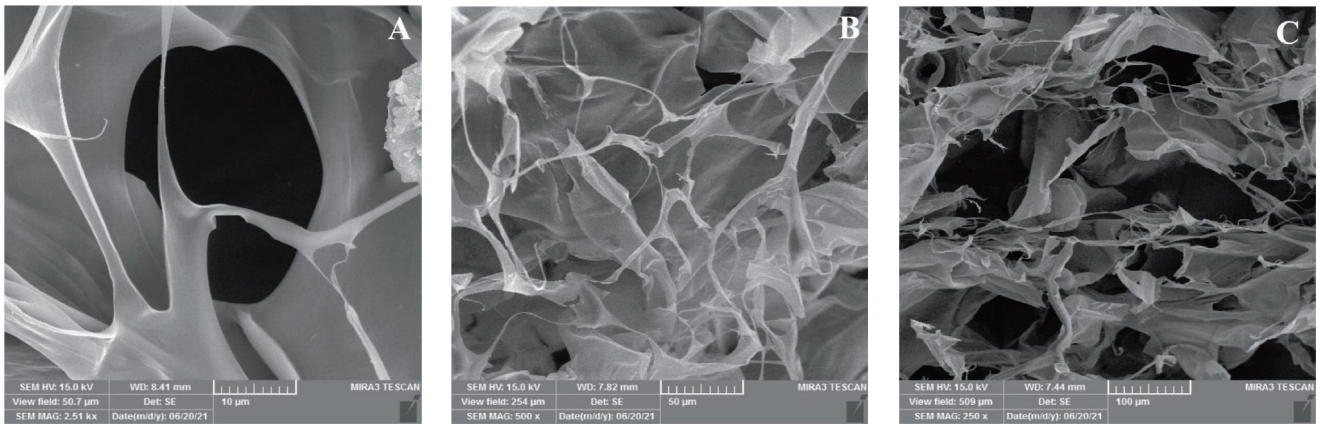

Figure 4: Scanning electron microscope images of CS-AlG-TPP freeze-dried hydrogel containing ATV with magnifications of (a) 10 μm, (b) 50 μm, and (c) 100 μm.

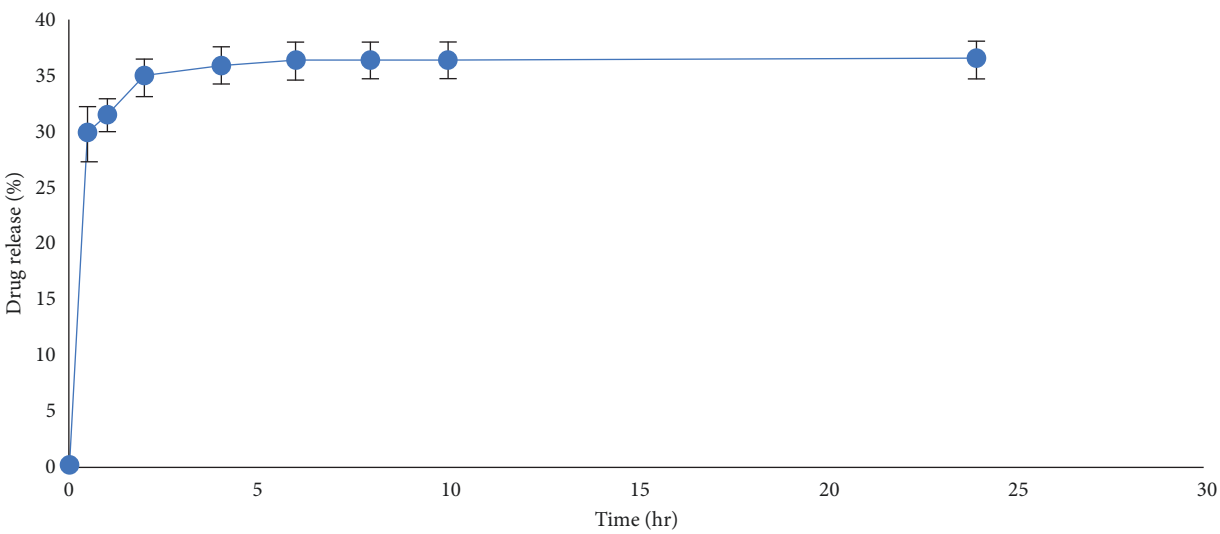

(a)

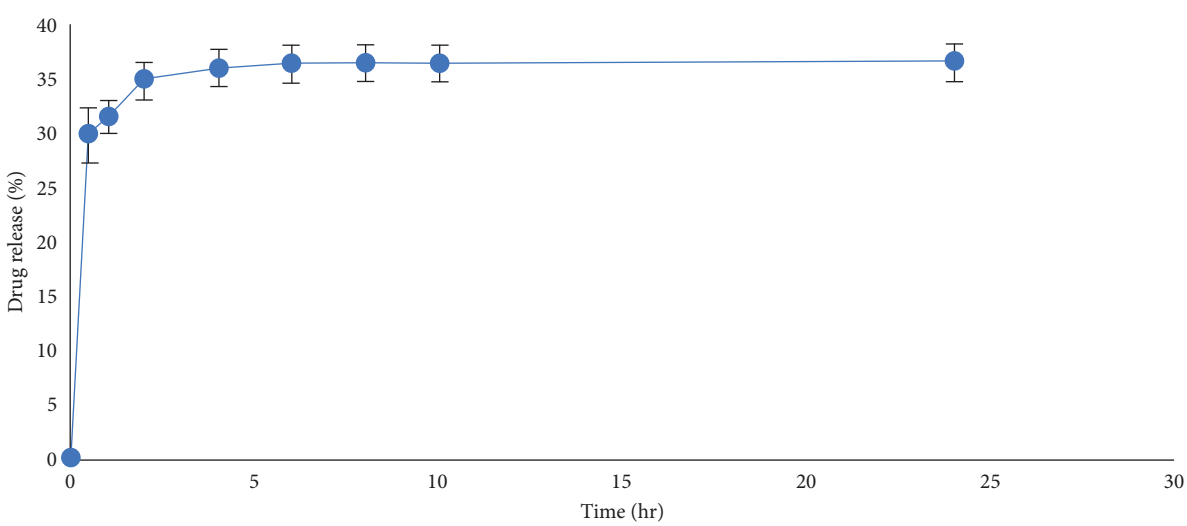

(b)

Figure 5: Graph of release percentage of atorvastatin in certain time intervals. (a) After 10 hr and (b) after 24 hr.

there was no significant increase in the percentage of drug released (Figure 5(b)). The gradual release of ATV from the alginate–chitosan microspheres was studied. Because TPP crosslinking does not occur in this system, the swelling percentage and amount of drug loading are lower, and drug release from these microspheres is slow and complete after 25 hr [38]. This suggests that the drug was retained in the three-dimensional network formed by TPP, and that the drug molecules entrapped within the porosity of the hydrogel were slowly released. During the first hour, 20% of the drug attached to the hydrogel is released via surface absorption. The percentage of crosslinkers significantly influenced the encapsulation gain and release profiles. Increasing the proportion of crosslinkers is expected to increase the proportion of drug loading while decreasing and limiting the proportion of drug release; thus, optimizing the proportion of crosslinkers is critical.

5. Conclusion

CS/ALG hydrogels were prepared and loaded with ATV at various ratios and percentages of TPP crosslinker. The results showed that the drug was loaded with an approximately 100% gain during crosslinking. The drug release profile from the hydrogel was investigated, and the results showed that the percentage of drug release was relatively low owing to drug retention in the three-dimensional TPP network. The results of this study demonstrated that the crosslinked CS/ALG hydrogel could be a suitable scaffold for loading all types of drugs, macromolecules, and cells because of its swelling percentage and high porosity. The drug loading and percentage of release are expected to be controlled by adjusting the ratio of the two polymers and crosslinker. Future studies should consider scaffold cell compatibility tests, such as hemolysis and cytotoxicity. Furthermore, stability studies, biodegradability determination, and modification of the drug release profile via a change in the crosslinker ratio will help to improve this study. Finally, the scaffolds mentioned above can be studied further in cell and animal studies for bone tissue engineering and stem cell differentiation in the presence of ATV.

Data Availability

The data used to support the findings of this study have been included in this article.

Conflicts of Interest

The authors declare that they have no conflicts of interest.

Authors' Contributions

Hananeh Hamedfar and Tayebeh Zivari Ghader contributed equally to this work.

Acknowledgments

The authors are grateful for the financial support of the Tabriz University of Medical Sciences, Tabriz, Iran. Grant no. 4221 was provided by the Department of Medicinal Chemistry, Faculty of Pharmacy, Tabriz University of Medical Sciences, Tabriz, Iran.

References

[1] S. L. Bonnick, "Osteoporosis in men and women," *Clinical Cornerstone*, vol. 8, no. 1, pp. 28–39, 2006.

[2] M. Shahrezaee, A. Oryan, F. Bastami, S. Hosseinpour, M. H. Shahrezaee, and A. Kamali, "Comparative impact of systemic delivery of atorvastatin, simvastatin, and lovastatin on bone mineral density of the ovariectomized rats," *Endocrine*, vol. 60, no. 1, pp. 138–150, 2018.

[3] G. Mazziotti, J. Bilezikian, E. Canalis, D. Cocchi, and A. Giustina, "New understanding and treatments for osteoporosis," *Endocrine*, vol. 41, no. 1, pp. 58–69, 2012.

[4] K. A. Kennel and M. T. Drake, "Adverse effects of bisphosphonates: implications for osteoporosis management," *Mayo Clinic Proceedings*, vol. 84, no. 7, pp. 632–638, 2009.

[5] W. Ledger and P. C. Ho, *Gynecological Drug Therapy*, p. 315, CRC Press, Boca Raton, 1st edition, 2016.

[6] A. Oryan, A. Kamali, and A. Moshiri, "Potential mechanisms and applications of statins on osteogenesis: current modalities, conflicts and future directions," *Journal of Controlled Release*, vol. 215, pp. 12–24, 2015.

[7] A. Moshiri, M. Shahrezaee, B. Shekarchi, A. Oryan, and K. Azma, "Three-dimensional porous gelapin–simvastatin scaffolds promoted bone defect healing in rabbits," *Calcified Tissue International*, vol. 96, no. 6, pp. 552–564, 2015.

[8] G. Mundy, R. Garrett, S. Harris et al., "Stimulation of bone formation in vitro and in rodents by statins," *Science*, vol. 286, no. 5446, pp. 1946–1949, 1999.

[9] M. Takenaka, K. Hirade, K. Tanabe et al., "Simvastatin stimulates VEGF release via p44/p42 MAP kinase in vascular smooth muscle cells," *Biochemical and Biophysical Research Communications*, vol. 301, no. 1, pp. 198–203, 2003.

[10] I. Mylonaki, F. Strano, S. Deglise et al., "Perivascular sustained release of atorvastatin from a hydrogel-microparticle delivery system decreases intimal hyperplasia," *Journal of Controlled Release*, vol. 232, pp. 93–102, 2016.

[11] C. Dubuis, L. May, F. Alonso et al., "Atorvastatin-loaded hydrogel affects the smooth muscle cells of human veins," *Journal of Pharmacology and Experimental Therapeutics*, vol. 347, no. 3, pp. 574–581, 2013.

[12] A. I. Özdoğan, Y. D. İlarslan, K. Kösemehmetoğlu et al., "In vivo evaluation of chitosan based local delivery systems for atorvastatin in treatment of periodontitis," *International Journal of Pharmaceutics*, vol. 550, no. 1-2, pp. 470–476, 2018.

[13] X. Yin, C. Yang, Z. Wang et al., "Alginate/chitosan modified immunomodulatory titanium implants for promoting osteogenesis in vitro and in vivo," *Materials Science and Engineering: C*, vol. 124, Article ID 112087, 2021.

[14] P. Vahedi, R. Moghaddamshahabi, T. J. Webster et al., "The use of infrapatellar fat pad-derived mesenchymal stem cells in articular cartilage regeneration: a review," *International Journal of Molecular Sciences*, vol. 22, no. 17, Article ID 9215, 2021.

[15] A. Nasibova, "Generation of nanoparticles in biological systems and their application prospects," *Advances in Biology & Earth Sciences*, vol. 8, no. 2, pp. 140–146, 2023.

[16] V. Ramazanli, "Effect of pH and temperature on the synthesis of silver nano particles extracted from olive leaf," *Advances in Biology & Earth Sciences*, vol. 6, no. 2, 2021.

[17] I. Ahmadov and V. Ramazanli, "Synthesis of nanoparticles in biological systems and their physical chemical characteristics-green synthesis," *Advances in Biology & Earth Sciences*, vol. 4, no. 3, 2019.

[18] A. Jafarova and V. Ramazanli, "Antibacterial characteristics of Ag nanoparticle extracted from olive leaf," *Advances in Biology & Earth Sciences*, vol. 5, no. 3, 2020.

[19] E. Ahmadian, A. Eftekhari, D. Janas, and P. Vahedi, "Nanofiber scaffolds based on extracellular matrix for articular cartilage engineering: a perspective," *Nanotheranostics*, vol. 7, no. 1, pp. 61–69, 2023.

[20] A. Baran, M. Fırat Baran, C. Keskin et al., "Investigation of antimicrobial and cytotoxic properties and specification of silver nanoparticles (AgNPs) derived from *Cicer arietinum* L. green leaf extract," *Frontiers in Bioengineering and Biotechnology*, vol. 10, Article ID 855136, 2022.

[21] A. Baran, M. F. Baran, C. Keskin et al., "Ecofriendly/rapid synthesis of silver nanoparticles using extract of waste parts of artichoke (*Cynara scolymus* L.) and evaluation of their cytotoxic and antibacterial activities," *Journal of Nanomaterials*, vol. 2021, Article ID 2270472, 10 pages, 2021.

[22] M. F. Baran, C. Keskin, A. Baran et al., "Green synthesis of silver nanoparticles from *Allium cepa* L. peel extract, their antioxidant, antipathogenic, and anticholinesterase activity," *Molecules*, vol. 28, no. 5, Article ID 2310, 2023.

[23] A. Baran, C. Keskin, M. F. Baran et al., "Ecofriendly synthesis of silver nanoparticles using ananas comosus fruit peels: anticancer and antimicrobial activities," *Bioinorganic Chemistry and Applications*, vol. 2021, Article ID 2058149, 8 pages, 2021.

[24] T. Zivari-Ghader, S. Dolati, A. Mehdizadeh, S. Davaran, M. R. Rashidi, and M. Yousefi, "Recent scaffold-based tissue engineering approaches in premature ovarian failure treatment," *Journal of Tissue Engineering and Regenerative Medicine*, vol. 16, no. 7, pp. 605–620, 2022.

[25] M. Gierszewska, J. Ostrowska-Czubenko, and E. Chrzanowska, "Characteristics of ascorbic acid release from TPP-crosslinked chitosan/alginate polyelectrolyte complex membranes," *Progress on Chemistry and Application of Chitin and its Derivatives*, vol. 23, pp. 76–87, 2018.

[26] F. Esmaeili and M. Babazadeh, "Targeted and controlled release of indomethacin from polyacrylic carrier systems," *Der Pharmacia Lettre*, vol. 7, no. 2, pp. 40–48.

[27] F. Rad, S. Davaran, M. Babazadeh, A. Akbarzadeh, and H. Pazoki-Toroudi, "Biodegradable electrospun polyester-urethane nanofiber scaffold: codelivery investigation of doxorubicin-ezetimibe and its synergistic effect on prostate cancer cell line," *Journal of Nanomaterials*, vol. 2022, Article ID 8818139, 10 pages, 2022.

[28] S. Same, J. Kadkhoda, G. Navidi et al., "The fabrication of halloysite nanotube-based multicomponent hydrogel scaffolds for bone healing," *Journal of Applied Biomaterials & Functional Materials*, vol. 20, Article ID 22808000221111875, 2022.

[29] I. Silvestro, I. Francolini, V. Di Lisio et al., "Preparation and characterization of TPP-chitosan crosslinked scaffolds for tissue engineering," *Materials*, vol. 13, no. 16, Article ID 3577, 2020.

[30] S. Shahi, F. Dehghani, E. D. Abdolahinia et al., "Effect of gelatinous spongy scaffold containing nano-hydroxyapatite on the induction of odontogenic activity of dental pulp stem cells," *Journal of King Saud University—Science*, vol. 34, no. 8, Article ID 102340, 2022.

[31] M. Gierszewska-Drużyńska and J. Ostrowska-Czubenko, "The effect of ionic crosslinking on thermal properties of hydrogel chitosan membranes," *Progress on Chemistry and Application of Chitin and its Derivatives*, vol. 15, pp. 25–32, 2010.

[32] A. Ehterami, M. Salehi, S. Farzamfar et al., "Chitosan/alginate hydrogels containing alpha-tocopherol for wound healing in rat model," *Journal of Drug Delivery Science and Technology*, vol. 51, pp. 204–213, 2019.

[33] N. Shanmugasundaram, P. Ravichandran, P. N. Reddy, N. Ramamurty, S. Pal, and K. P. Rao, "Collagen–chitosan polymeric scaffolds for the in vitro culture of human epidermoid carcinoma cells," *Biomaterials*, vol. 22, no. 14, pp. 1943–1951, 2001.

[34] S. Yang, K. F. Leong, Z. Du, and C. K. Chua, "The design of scaffolds for use in tissue engineering. Part I. Traditional factors," *Tissue Engineering*, vol. 7, no. 6, pp. 679–689, 2001.

[35] Z. Wang, T. Gao, L. Cui, Y. Wang, P. Zhang, and X. Chen, "Improved cellular infiltration into 3D interconnected microchannel scaffolds formed by using melt-spun sacrificial microfibers," *RSC Advances*, vol. 6, no. 3, pp. 2131–2134, 2016.

[36] H. Hamedi, S. Moradi, A. E. Tonelli, and S. M. Hudson, "Preparation and characterization of chitosan–alginate polyelectrolyte complexes loaded with antibacterial thyme oil nanoemulsions," *Applied Sciences*, vol. 9, no. 18, Article ID 3933, 2019.

[37] M. Tavakol, E. Vasheghani-Farahani, and S. Hashemi-Najafabadi, "The effect of polymer and $CaCl_2$ concentrations on the sulfasalazine release from alginate-*N*,*O*-carboxymethyl chitosan beads," *Progress in Biomaterials*, vol. 2, no. 1, pp. 1–8, 2013.

[38] A. M. Gorabi, N. Kiaie, M. Pirro, V. Bianconi, T. Jamialahmadi, and A. Sahebkar, "Effects of statins on the biological features of mesenchymal stem cells and therapeutic implications," *Heart Failure Reviews*, vol. 26, no. 5, pp. 1259–1272, 2021.

Hindawi
Advances in Polymer Technology
Volume 2023, Article ID 4379941, 10 pages
https://doi.org/10.1155/2023/4379941

Research Article

Fabrication and Characterization of Partial Bio-nano-silica Inclusion in Fibre-Reinforced Concrete for High-performance Applications

D. Vivek,[1] **C. Aravind**,[1] **S. Gokulkumar**,[2] **M. Aravindh**,[2] **and Yalew Asres**[3]

[1]*Department of Civil Engineering, KPR Institute of Engineering and Technology, Arasur, Coimbatore, Tamil Nadu 641407, India*
[2]*Department of Mechanical Engineering, KPR Institute of Engineering and Technology, Arasur, Coimbatore, Tamil Nadu 641407, India*
[3]*Department of Mechanical Engineering, Faculty of Manufacturing, Institute of Technology, Hawassa University, Hawassa, Ethiopia*

Correspondence should be addressed to D. Vivek; viveksiga91@gmail.com and Yalew Asres; yalewa@hu.edu.et

Received 15 December 2022; Revised 29 April 2023; Accepted 29 June 2023; Published 10 August 2023

Academic Editor: Chang Chuan Lee

Ultra-high-performance fibre-reinforced concrete (UHPFRC) is a specialized type of concrete (to create a very dense matrix) that is used for both new construction and renovation projects in order to improve the lifespan of structures. Researchers analyse and evaluate only the microstructure, porosity, and fresh and hardened concrete properties of UHPFRC but limited their exploration on the reduction of the mechanical properties of UHPFRC due to the presence of metallic particles and micro-fractures that occur during the generation of hydrogen. Hence, the present study aims to eliminate the existing problem by hybridization approach (mixing of bio-nano-silica (nS) and polypropylene) with different percentages to further improve the strength properties of UHPFRC. The result showed that the compressive strength is increased by 15.5% compared to traditional concrete due to the filling ratio of nS in the pores of the concrete; in addition, the fibre's surface and roughness also contributed to the strength enhancement.

1. Introduction

Concrete is regarded as a broadly used resource on the globe, with an anticipated yearly manufacture of 28.2 billion tones during 2017, resulting in a standard of roughly 2.8 m^3 for every person on the planet. Concrete is considered to be primary element in construction industry. The need for infrastructure industry accounts for almost 70% of all carbon. CO_2 outflows account for 5%–7% of total CO_2 discharges on our planet. By 2060, the need for concrete is expected to increase by about 200%, reaching 7,000 million tons per year. As a result, the primary management problems for the next several years will be developing and producing concrete that uses fewer clinkers and emits less carbon dioxide than ordinary concrete while providing the same performance unchanging quality and somewhat more strength [1–3]. It was portrayed as the importance of toughness in construction materials for eco-effectiveness, stating that an augment in considerable resilience for 60 years to 600 years might reduce the climate's influence by up to 10%. It was calculated that by increasing the significant compressive strength, the consumption of supported steel might be reduced by as much as half. All things considered, the main concern for its future production is long-lasting concrete [4]. This research intended at use of bio-nanoparticles to enhance the resilience and mechanical characteristics of cementitious composites. In late 1980s, the use of bio-nanoscience in cement materials was recognized and became dynamic for over a quarter-century. Bio-nano-materials offer incredible features and capacities, and they can be afforded as cementitious composites with top performance, good mechanical, and durability properties, as well as multifunctionality and insight [5]. Cementitious composites made of bio-nanoscale metallic and non-metallic compounds were initially employed on the way by altering or improving the characteristics of cementitious resources. Other inventions of

superior performance of building materials may be reorganized created, developed by seeing the structure at its bio-nano-level. The design at the nuclear level, the composite, may be seen as technology advances, and their distinct qualities of each successive phase are able to be measured at the bio-nano-level. Perception on bio-nanoparticles can thus be used to improve the presentation of composites [6–8]. The analysts were persuaded to use bio-nanoparticle and bio-nano-filaments to increase the strength, durability and handling property of concrete composites. Novel features of bio-nanoparticles with diameters ranging from 1 to 100 nm have piqued the curiosity of many people in recent years [9–11]. One of the key advantages of bio-nanoparticles is their huge quantity at the surface [12–14]. Some bio-nanoparticles are being used as a bio-nano-added ingredient in concrete-based products to improve their quality and increase their utility; nS have become common among such bio-nano-sized particles [15]. The parameter nS, also known as silicon dioxide bio-nanoparticles, could be used as additives to improve the mechanical and toughness qualities of concrete. The influence of nS on the bio-nanostructure in concrete also confirmed the enhancement of significant strength [16–19]. The results discovered that nS is an outstanding solution for reducing the use of concrete in the production of high-strength concrete. Incorporating nS as a cement substitute makes significant sense and reduces the CO_2 impact of the significant goods [20, 21]. Because of their superior performance in filling effect and molecular size appropriation, nS has gained special attention in comparison to other mineral admixtures, reduced permeability in concrete, and widened their pozzolanic reaction by calcium hydroxide to generate calcium-silicate hydrate (C-S-H). In terms of availability, nS is produced on a large scale, making it relatively accessible for industrial and commercial purposes. However, the production process of nS can be challenging and requires specialized equipment, which can result in higher costs compared to the production of traditional silica materials. The cost of nS depends on several factors, including the production method, purity, and quantity being purchased. Generally, larger quantities of nS are more cost-effective than smaller quantities. Such nS behaviour results in enhanced mechanical characteristics in the significant blend [22–24]. When compared to silica exhaust, nS improved the concrete setting process, reduced drainage, and increased the isolation and cohesion of new mixes [25, 26]. Because of its high pozzolanic activity, bio-nano-silica (nS) can consume and change calcium hydroxide into C-S-H gel at an early stage, improving the mechanical properties of the substance [27–30]. The biggest limitation hindering the widespread production of UHPFRC is its high cost [31]. Therefore, there is an increasing need to replace expensive key ingredients such as cement and silica fume to overcome this limitation [32]. Such substitution may be achieved using by-product materials with disposal processes that raise environmental concerns [33]. Some by-product materials have also been incorporated into his UHPFRC to improve its performance and reduce overall costs [34]. Concrete curing is the result of chemical reactions that occur throughout cement hydration and is referred as a set of concrete. Environmental factors, such as reactions, may influence the concrete's properties throughout setting. High temperatures, low humidity, wind, and other factors are considered throughout concrete setting. Strong wind, high temperature, and a dry environment may all have an impact on the speed of two phenomena which impact concrete curing: moisture evaporation owing to cement hydration. To address this issue, one potential strategy is to explore filaments, which may effectively limit growth to avoid the utilization of non-sustainable normal rock as well as to keep Stay away from excessive ground filling. The main objective of this study is to find the effect of utilizing combination of bio-nS and steel fibre in ultra-high-performance fibre-reinforced concrete (UHPFRC). UHPFRC has become an important component in the construction industry due to its excellent properties. Therefore, many researchers recently tested UHPFRC properties under the influence of additional cementitious materials obtained using industrial waste [35]. Previous studies have demonstrated the high potential for using industrial waste as a partial cement substitute in UHPFRC production, such as rice husk ash being effectively used to partially replace silica fume or cement in concrete mixes.

Figure 1: Bio-nano-silica.

2. Research Significance

This study is the first to use a combination of bio-nS and polypropylene fibres as a partial substitute for cement. This study investigates the impact of using a combination of bio-nS and polypropylene fibres in various ratios as a partial substitute for cement on freshness and mechanical micro-structural properties.

3. Materials and Methods

Industrially accessible bio-nS is chosen as the pozzolanic material as shown in Figure 1, and its XRD analysis is done to study the primary characteristics as illustrated in Figure 2. Further, we used two sorts of filaments which is straight steel fibre varying from 1% to 2% and small polypropylene fibre. Table 1 displays additional information on used resources. Ordinary Portland cement of grade of 53 grade, confirming to IS: 12269–1987, was used, and polycarboxylate ether is used as a water-reducing agent. Preliminary test on cement was

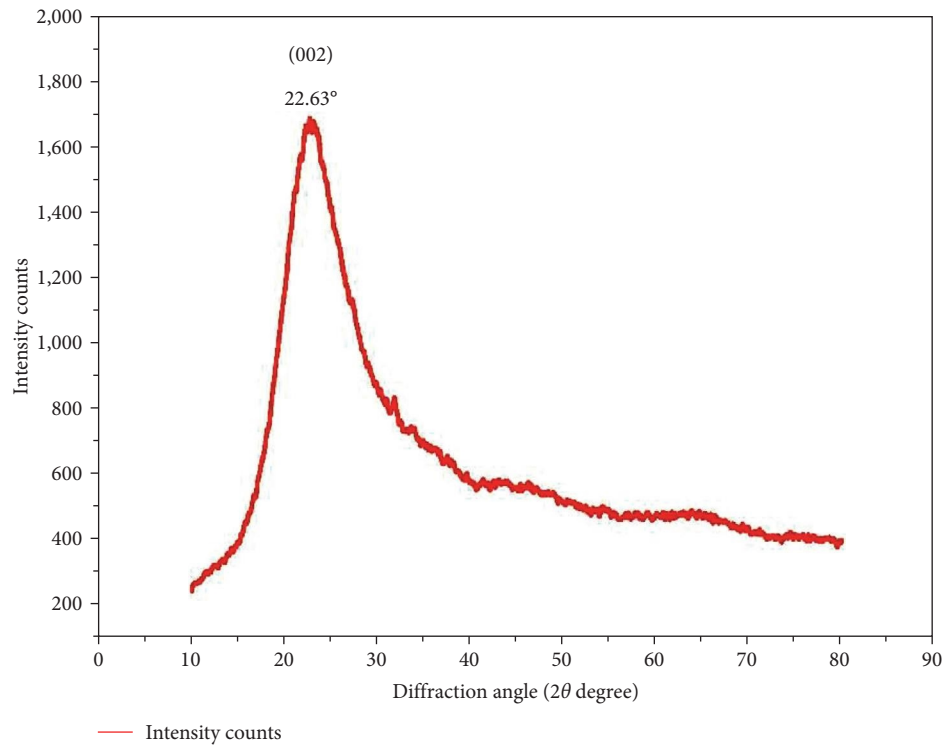

Figure 2: XRD analysis of bio-nano-silica.

Table 1: Material properties.

Materials	Specific density (g/cm^3)
Cement	3.16
Fine aggregate	2.54
Coarse aggregate	2.43
Superplasticizer	1.01
Bio-nano-silica	2.10
Polypropylene fibre	8.90

Table 3: Fresh concrete properties.

Percentage of polypropylene fibre	Slump flow (mm)
0	158
1	179
1.5	183
2	186
2.5	190

Table 2: Mix proportions.

Properties	Percentage of polypropylene fibre				
	0	1.0	1.5	2.0	2.5
Cement (kg/m^3)	612	605	602	600	596
NS (percentage)	0	1	1	2	2
Water (kg/m^3)	200	200	200	200	200
Fine aggregate (kg/m^3)	680	680	680	680	680
Coarse aggregate (kg/m^3)	1,020	1,020	1,020	1,020	1,020
Superplasticizer (%)	0.2	0.2	0.2	0.2	0.2

Table 4: Bionano-silica properties.

Particulars	Range
Specific surface area (m^2/gm)	204
pH value	4.2
Loss on drying (%)	0.66
Loss of ignition (%)	0.72
Silica content	99.9
Carbon content	0.07

conducted as per IS 4031-1988. Tables 1 and 2 provide information on the mix proportions of the concrete's material properties, while Tables 3 and 4 display the properties of fresh concrete and bio-nS, respectively.

4. Experimental Methodology

4.1. Compressive Strength. Materials used for this research are well graded and dry condition is maintained. Concrete cubes of size (150 × 150 × 150 in mm) are casted to test compressive strength and curing is carried out for 28 days by immersing specimen in water. As stated below, an intrinsic grain size distribution technique of regular variety of factors presents a potential for mix design in which extremely tiny particles may be added with comparatively little effort. The first attempts to explain an intended formulation of concrete blends that frequently comprise regularly scaled elements can be traced back more than a century. Gong et al. [34]

proved through his experimentation that the stacking of concrete particles may change the characteristics of the resulting concrete. It was accomplished that a spatial uninterrupted gradation of particles in the created concrete mixes can facilitate to develop the characteristics of concrete. An ideal particle shape of the applied particle components in the mix might potentially yield a minimum porosity, as demonstrated in Equation (1).

$$P(D) = \frac{(D)}{(D_{\max})} \tag{1}$$

Here D would be the element dimension (μm), P (D) is proportion of entire solids that are lesser than dimension D, and $D_{\max}$ is major element size (μm). However, the minimal particles are not included in Equation (1), notwithstanding the fact that the stocking model has a finite smaller size limit with which it may be enhanced. The modified model is shown below in Equation (2).

$$P(D) = \frac{D^q - D^q_{\min}}{D^q_{\max} - D^q_{\min}}, \tag{2}$$

where $D_{\min}$ – Particle size in μm

Using Equation (2), various types of concrete may be constructed by varying the dispersion modulus q, which defines the percentage of fine and coarse grains in the combination. Greater value of dispersion modulus ($q > 0.5$) often results in coarse mixes, but lesser values ($q = 0.25$) result in fine-particle-rich concrete blends. It was proved that a q range of 0–0.28 will potentially affect optimum packing. The suggestions provided that even in self-compacting concrete, a q in range of 0.22–0.25 are used (SCC). As a result, it is used to design UHPFRC in this case, given that a significant number of fine particles are present. In this study, the frequency of q is set at 0.23 since it is used to construct the UHPFRC. In this investigation, the adapted model Equation (2) serves while a goal task for optimizing the composition of granular material mixtures. By means of an optimization process based on least squares method, the scope of each individual constituent in the mix is modified until an optimal match between the assembled mix and the goal curve is achieved, as shown in Equation (3). While the divergence among goal curve and its constructed blend is minimized, as shown by addition of square of residuals (RSS) for set element size, the concrete composition is considered optimum.

$$\mathrm{RSS} = \sum_{i=1}^{n} \left(P_{\mathrm{mix}}\left(D_i^{i+1}\right) - P_{\mathrm{tar}}\left(D_i^{i+1}\right)\right) \tag{3}$$

$P_{\mathrm{mix}}\left(D_i^{i+1}\right)$–Composed mix, $P_{\mathrm{tar}}\left(D_i^{i+1}\right)$–Target grading calculated from Equation (2).

This study will design thirty batches of UHPFRC in total. Furthermore, nS is incorporated in amounts ranging from 1% to 2% of the overall binder quantity. According to the literature, the proportion of steel fibre is approximately 3% by concrete volume, whereas the content of polymer fibre is not as much as 2.5% by concrete volume. As a result, steel and polypropylene fibres account for 0%–2.5% of the volume of concrete correspondingly. As a result of examining the characteristics of various UHPFRCs, it will be feasible to assess the various impacts of nS and hybrid fibres here on characteristics of UHPFRC. Mixing duration intended UHPFRC is about ten minutes and lower binder proportion. Furthermore, incorporation is usually done in a laboratory setting using dried and toughened aggregates and powder components. While combining and testing, the room temperature remains constant at roughly twenty-one degrees Celsius.

4.2. Porosity of UHPFRC. The intended UHPFRC's porosity is calculated using the vacuum saturation system that is known as highest effective saturation method. Saturation is performed on at least three samples (100 × 100 × 20) mm for every combination, as described as per ASTM C1202. The following Equation (4) is used to compute the water-permeable porosity.

$$\varphi_{v,\,\mathrm{water}} = \frac{m_s - m_d}{m_s - m_w} \times 100 \tag{4}$$

$\varphi_{v,\,\mathrm{water}}$–Permeable water porosity, m_s–saturated sample mass in surface dry condition, m_w–mass of saturated water sample, m_d–mass of oven-dried sample.

5. Result and Discussion

Preliminary investigations revealed that the addition of nS and fibres will reduce its workability of concrete. The flowability of intended concrete decreases from 35.6 cm to roughly 29.0 cm. This incident is capable of recognizing the nS permeable surface, which is capable of absorbing a lot of water. Moreover, the impact of nS and hybrid fibres incorporation into the slump flow capacity of new UHPFRC blends. The data exhibit the link between the nS and composite fibre content as well as flowability of fresh UHPFRC. It is vital to note that the flowability of all UHPFRC combinations diminishes linearly with the incorporation of polypropylene fibres. The determining coefficients, R^2 in every regression outline, are close to one, indicating a good relationship between the numbers of polypropylene fibres, and also, the workability is developed by UHPFRC. Furthermore, the inclusion of nS lowers the UHPFRC's workability. For example, the slump flow value in the sample material (excluding nS and fibres) is around 29 cm, but it lowers to roughly 25.6 and 22.5 cm if nS (2%) or steel fibre (2% by volume) is added, respectively. When nS (2%) and Steel fibre (2% by volume) was concurrently introduced to the UHPFRC, the slump flow is reduced to around 23.5 cm. Furthermore, when nS, Steel fibre and polypropylene fibre (0.5%) are combined in UHPFRC and Slump flow is the smallest, measuring approximately 12.8 cm. Impact of nS on concrete flowability is supposed to be accredited to an increase in cement paste viscosity. The considerable water-holding capacity of cement paste with nS is due to immediate

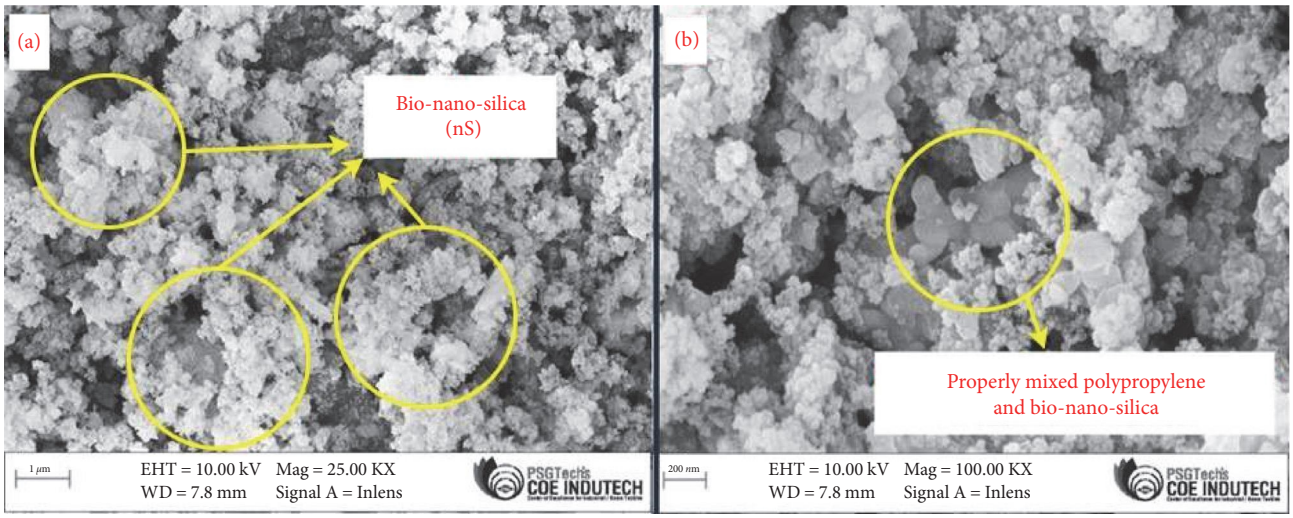

Figure 3: Scanning electron microscope of NS at (a) 1 μm (b) 200 nm.

reactions in the nS slurry as well as the liquid of cement paste. The existence of nS reduces the quantity of lubricating water accessible inside the inter-particle gaps, causing an increase in yield stress. Because of the numerous impacts of bio-nS and hybrid fibres on the workability of UHPFRC, the flowability of a sample comprising nS (5%), steel fibres 3% by volume, and polypropylene fibre (0.4% or 0.5% by volume) can be reduced to zero. Furthermore, the addition of bio-nS, steel, and synthetic fibre can limit the flow property of the UHPFRC even further. As a result, it is critical to carefully tune the liquid and admixtures quantities in order to achieve a flowable UHPFRC. Scanning Electron Microscope analysis was carried out for nS, and the results are shown in Figures 3(a) and 3(b). From the results, it is evident that the average range of particles is 30 nm. Because of the extreme fineness of the bio-nS particles, the microstructure could be upgraded in terms of packing efficiency. The extremely tiny particle size enabled the filling of very small pores which cement particles could not reach.

5.1. Porosity of the UHPFRC. The porousness of UHPFRC is higher, at roughly 17% of volume. Primary investigations revealed that perhaps the porosity of the planned UHPFRC is around 10%, implying that the addition of fibres should account for roughly 7% of the porosity. Furthermore, the inclusion of steel fibres can greatly enhance the permeability of the UHPFRC, whereas Polypropylene fibres only minimally enhance the porousness of the UHPFRC. These effects should be ascribed to the steel fibre that might alter the granular skeleton's structure, whereas extensible fibres bridge the void between both the large particles. However, it is significant to mention that perhaps the permeability of the UHPFRC drops marginally with the addition of nS. For example, in samples without fibres, the addition of roughly 4% of nS can lower the porosity of the UHPFRC from 17.8% to 18.5%.

The nucleation as well as the pozzolanic impact of nS in cement hydration should be attributed to this. As it is well recognized, due to the nucleation effect, the creation of CSH phase is no longer limited to the cement grain surface only, resulting in a greater hydration degree of cement and more holes that may be filled by the recently created CSH phase. In general, the incorporation of fibres and other admixtures results in a rather high porosity of the proposed UHPFRC. Furthermore, the combination of steel fibres may develop the permeability of the concrete. The inclusion of nS might decrease the permeability of the concrete and the results are shown in Figure 4.

5.2. Compressive Strength of UHPFRC. The inclusion of the steel fibre greatly boosts the mechanical properties of UHPFRC. For example, a mechanical property with no steel fibres varies at 80 MPa. The compressive strength of concrete with steel fibre increased up to 120 MPa. As the amount of bio-nS in the concrete grows, so does its compressive strength. Furthermore, it can be seen that the influence of fibres on the compressive strength is negligible. Nonetheless, mechanical properties of the developed UHPFRC are much less than those of other UHPFRC. This can be attributable to the subsequent factors such as utilization of nS that can influence the microstructure improvement of concrete, potentially increasing the porosity and reducing the concrete's mechanical properties. It is obvious that when the nS is added to concrete, mechanical properties drop dramatically, but the flexural strength remains reasonably equivalent. However, including nS, steel fibres, and polypropylene fibres at the same time can greatly increase the mechanical characteristics of the concrete. Figure 5 shows variation of compressive strength for different percentages of polypropylene fibre and nS. There is an increase in compressive strength of 15.5% observed for concrete with 2% of nS and polypropylene fibre when compared to conventional concrete. For mix containing 1% of nS and 2% of fibre, there is an enhancement in compressive strength of 12.2% when compared to nominal concrete. The above phenomenon is mainly due to pore filling effect of nS and other properties such as the surface of the fibre, surface roughness and bond between mortar and aggregates. Addition of fibres and nS

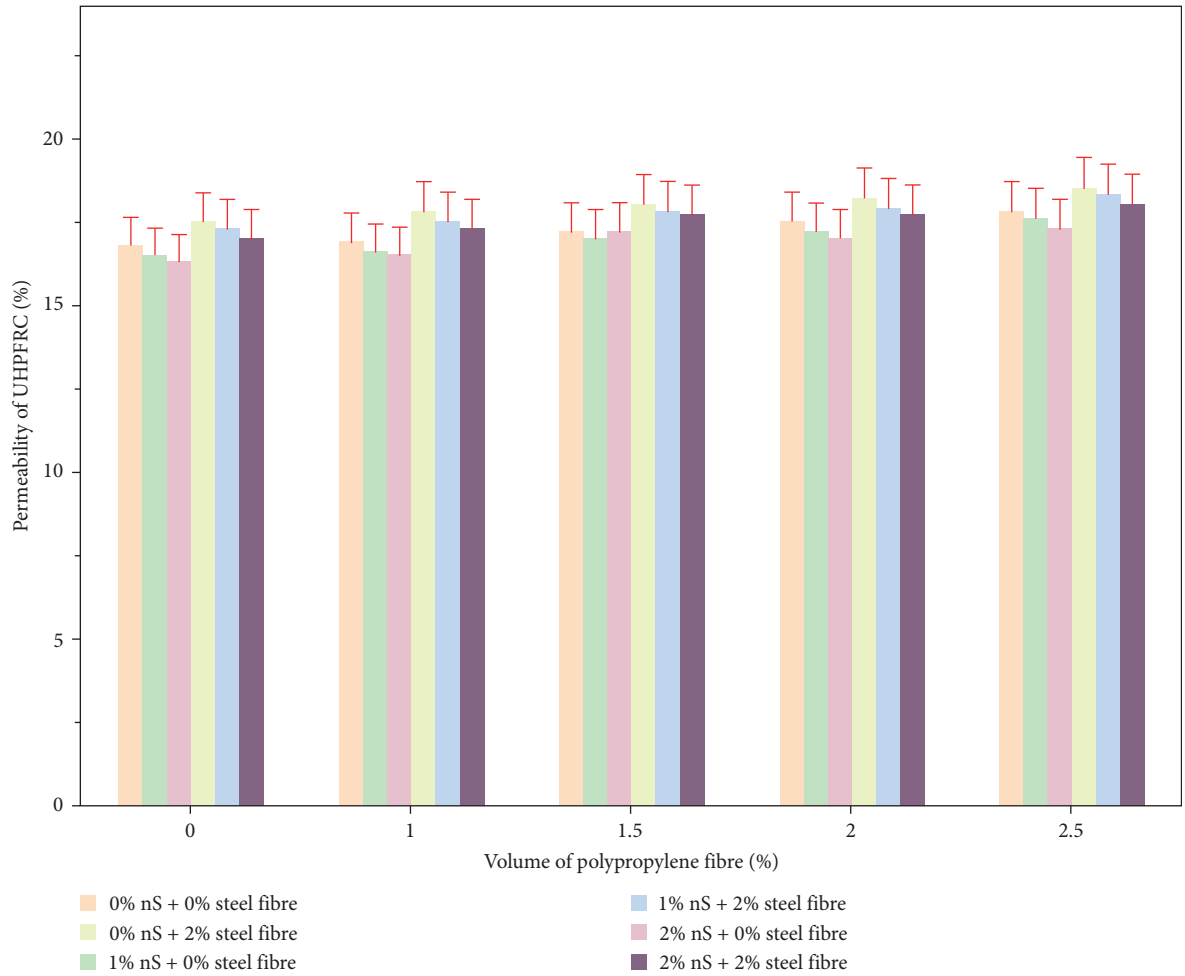

Figure 4: Effect on porosity of UHPFRC.

prevents the formation of micro-cracks and alters the crack propagation pattern. As a result, UHPFRC may be manufactured and used in applications requiring high flexural strength.

5.3. Hydration Process of the UHPFRC. Furthermore, the inclusion of nS may considerably speed cement hydration, and as the amount of nS increases, so does the cement hydration rate. Finally, in this investigation, the extra nS might compensate for the unfavourable effect on cement hydration. The aggregation and cementitious action of nS must be related to this process. The nanoparticles in concrete are equally disseminated after mixing. When the hydration process starts, the hydration products disperse and enclose nanoparticles as kernels, promoting cement hydration and making the cement structure highly homogenous and compact. As a result, more reactive kernels will be produced in this investigation as the amount of nS increases, and as a result, the cement's hydration rate is quickened.

5.4. Chloride Penetration Resistance. Chloride penetration was studied as a result of migration and diffusion (two of the major components of ion transport inside concrete). Migration is caused by an electrical potential gradient, while diffusion is caused by a gradient of concentration. The chloride migration in all of the samples was much lesser than in the control concrete, with differences at about 2 orders of magnitude. At 28 days, the mean Dnssm (m^2/s) value of the coefficient in concretes 2% nS and steel fibre and control specimen was 1.010×10^{-13} m^2/s and 1.2×10^{-13} m^2/s, respectively. Multiple factors contribute to (UHPFRC) high resistance to chloride penetration. On the one side, there is a very closely packed microstructure with low porosity as nS acts as filling agent, a quite fine porous structure, and capillary network segmentation, all of which reduce water permeability (when chlorides are dissolved in water).

5.5. Effect of Curing Temperature. High curing temperatures can help create a stronger concrete structure by promoting the formation of a dense and compact skeleton. The high temperatures also reduce capillary stress by creating a coarser porous structure. On the other hand, reducing the water-to-cement ratio (w/c) can increase autogenous strains, as the lower water content can lead to insufficient hydration and an incompletely developed microstructure. The relationship between curing temperature, w/c ratio, and concrete strength is complex and requires careful consideration to produce high-quality concrete with the desired properties.

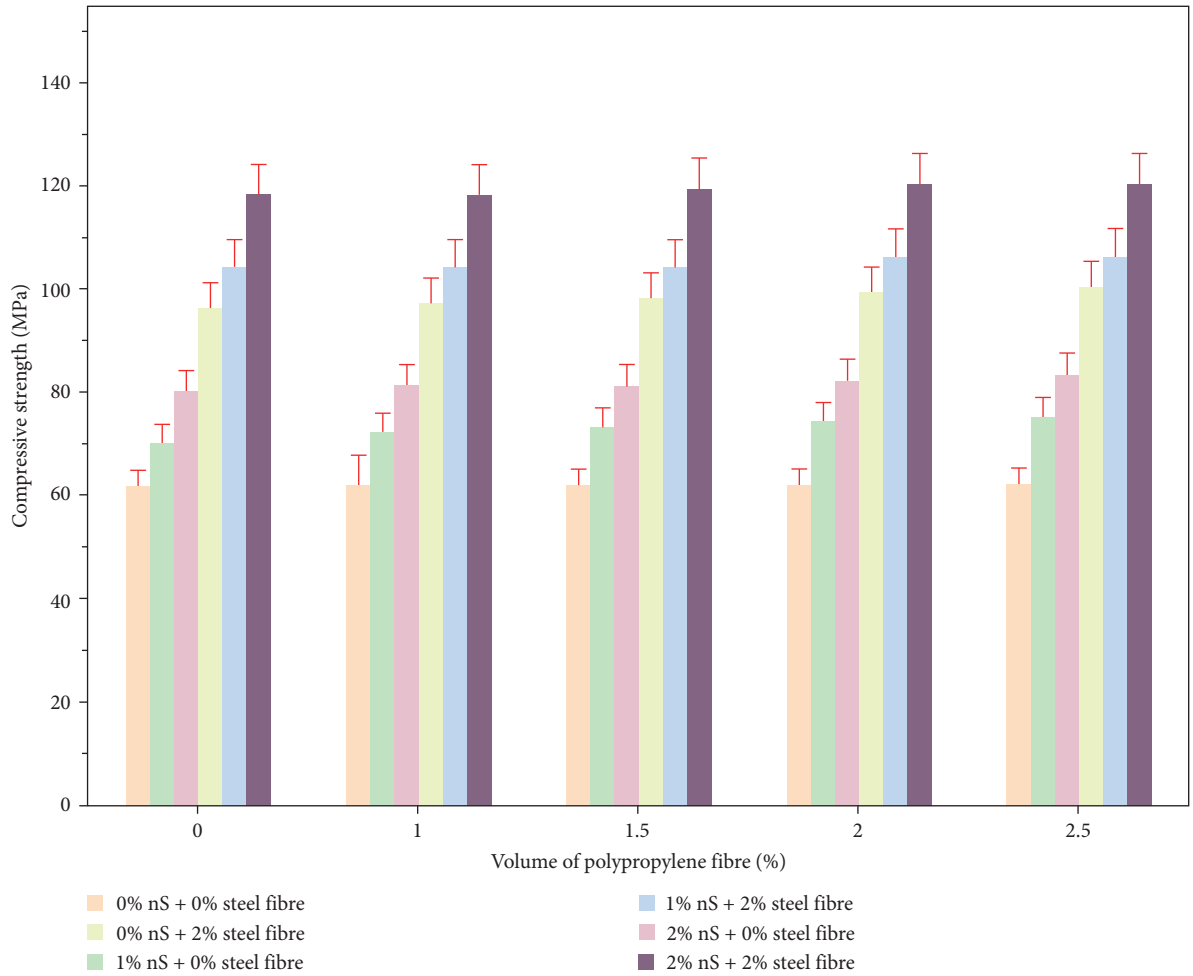

Figure 5: Compressive strength of UHPFRC.

5.6. Comparison with Previous Work. The comparison literature highlights various research studies that have investigated the effects of incorporating steel fibre and non-steel fibres in concrete. The results obtained from Zhang et al. [35] showed that adding 2% of steel fibre can increase the impact resistance of concrete by up to 150%. However, a high composition of steel fibre can reduce the impact durability of concrete. They also found a linear relationship between the ductility ratio and impact strength, which can be used to estimate the impact strength of concrete with varying steel fibre levels.

Larsen et al. [36] showed that the addition of non-steel and polypropylene fibres enhances the mechanical properties of concrete over time. Meanwhile, Zhou et al. [37] found that steel fibre bond strengths in UHPC are increased by approximately 50% when coated with nS. The nS coating also improves the inter-facial adherence between the fibre and the concrete matrix, as evidenced by the outer layer of the ns-coated steel fibre having more scratches and hydrates than the plain steel fibre after pull-out. The coating also doubles the energy capacity for absorption, thus increasing the tensile strength of UHPFRC.

Similarly, Chen et al. [38] utilized a hybrid approach to improve the mechanical properties of UHPFRC by incorporating silica fume, polypropylene fibres, and graphene oxide. The results showed that the compressive and flexural strengths of UHPFRC were significantly enhanced due to the synergistic effect of the hybrid approach. The addition of graphene oxide and polypropylene fibres helped in improving the mechanical properties of UHPFRC, similar to the approach used in the study mentioned above. Likewise, Ozbakkaloglu et al. [39] evaluated the mechanical properties of UHPFRC under impact loading conditions. The results showed that the addition of steel fibres in UHPFRC improved the impact resistance and energy absorption capacity of the material. This study highlights the importance of incorporating fibres in UHPFRC to enhance its mechanical properties, similar to the approach taken in this present study.

Wang et al. [40] studied the mechanical properties and durability of hybrid fibre-reinforced ultra-high-performance concrete with nS and polyvinyl alcohol fibres. The study aimed to improve the mechanical properties and durability of UHPFRC by adding both nS and polyvinyl alcohol fibres. The results showed that the hybridization approach led to

significant improvements in both compressive and flexural strength compared to UHPFRC without fibres or with only one type of fibre. The addition of nS also improved the durability of the concrete, reducing the deterioration caused by water and chloride ion penetration. In similar manner, Jain et al. [41] experimented the effect of steel fibre on the mechanical properties of ultra-high-performance concrete with nS. The study investigated the effect of adding steel fibres and nS to UHPFRC on its mechanical properties. The results showed that the addition of both steel fibres and nS significantly improved the compressive and flexural strength, as well as the toughness, of UHPFRC. The study also found that the optimum dosage of steel fibres and nS was 2% and 3%, respectively, for achieving the best mechanical properties.

Hence, the comparison literature highlights the benefits of incorporating fibres in concrete to enhance its mechanical properties, such as impact resistance and tensile strength. It also suggests that the optimal composition of fibres depends on the specific application and desired outcome. Therefore, it is crucial to carefully consider the type and composition of fibres used in concrete mix design.

6. Conclusions

The impact of nS and hybrid fibres on the characteristics of (UHPFRC) using fibres is discussed in this research. The concrete mixes were designed with the goal of achieving a highly compacted cementitious matrix. The following conclusions are reached from the data discussed in this paper:

(i) The inclusion of nS, steel fibres can limit its flow properties of UHPFRC. As a result, it is critical to carefully tune both fluid and superplasticizer quantities in order to achieve a flowable UHPFRC.

(ii) The water-permeable porosity of the planned UHPFRC is rather high around 18%. Furthermore, fibres might both enhance the permeability of concrete. Nonetheless, a suitable number of nS about 4% might marginally lower the permeability of the concrete.

(iii) The addition of nS and hybrid fibres to concrete can greatly increase its mechanical qualities. Moreover, very little number of additional nS might counteract for slowing impact on cement hydration, which is related to the nucleation impact of nS.

(iv) The incorporation of nS in concrete considerably reduces crack propagation and enhances the mechanical properties of concrete.

(v) Despite their significant cost, UHPFRC mixtures are presently used in building projects such as high-rise building structures, bridge girder construction, defence, aerospace, and marine industries due to their high durability as well as reduced maintenance needed during project's service life.

Data Availability

The data used to support the findings of this study are included in the article.

Conflicts of Interest

The authors declare that they have no conflicts of interest.

Authors' Contributions

Conceptualization: Vivek D, Yalew Asres; Methodology: Vivek D, Aravind C; Formal analysis and investigation: Vivek D, Yalew Asres; Writing—original draft preparation: Vivek D, Gokulkumar S; Writing—review and revise: Yalew Asres, Gokulkumar S, Aravindh M; Supervision: Yalew Asres; Ideology: Vivek D, Gokulkumar S, Aravindh M.

References

[1] H. Assaedi, T. Alomayri, F. Shaikh, and I.-M. Low, "Influence of nano silica particles on durability of flax fabric reinforced geopolymer composites," *Materials*, vol. 12, no. 9, Article ID 1459, 2019.

[2] Y. Du, S. Wang, W. Hao et al., "Investigations of the mechanical properties and durability of reactive powder concrete containing waste fly ash," *Buildings*, vol. 12, no. 5, Article ID 560, 2022.

[3] H. Ş. Arel and F. U. A. Shaikh, "Effects of fly ash fineness, nano silica, and curing types on mechanical and durability properties of fly ash mortars," *Structural Concrete*, vol. 19, no. 2, pp. 597–607, 2018.

[4] A. M. Zeyad, I. Y. Hakeem, M. Amin, B. A. Tayeh, and I. S. Agwa, "Effect of aggregate and fibre types on ultra-high-performance concrete designed for radiation shielding," *Journal of Building Engineering*, vol. 58, Article ID 104960, 2022.

[5] M. Amin, B. A. Tayeh, M. A. Kandil, I. S. Agwa, and M. F. Abdelmagied, "Effect of rice straw ash and palm leaf ash on the properties of ultrahigh-performance concrete," *Case Studies in Construction Materials*, vol. 17, Article ID e01266, 2022.

[6] M. Hanafi, E. Aydin, and A. Ekinci, "Engineering properties of basalt fiber-reinforced bottom ash cement paste composites," *Materials*, vol. 13, no. 8, Article ID 1952, 2020.

[7] I.-H. Yang and J. Park, "A study on the thermal properties of high-strength concrete containing CBA fine aggregates," *Materials*, vol. 13, no. 7, Article ID 1493, 2020.

[8] T.-Y. Liu, P. Zhang, J. Wang, and Y.-F. Ling, "Compressive strength prediction of PVA fiber-reinforced cementitious composites containing nano-sio_2 using BP neural network," *Materials*, vol. 13, no. 3, Article ID 521, 2020.

[9] Q. Alam, Y. Hendrix, L. Thijs, A. Lazaro, K. Schollbach, and H. J. H. Brouwers, "Novel low temperature synthesis of sodium silicate and ordered mesoporous silica from incineration bottom ash," *Journal of Cleaner Production*, vol. 211, pp. 874–883, 2019.

[10] B. Vafaei, K. Farzanian, and A. Ghahremaninezhad, "Effect of hydrogels containing nanosilica on the properties of cement pastes," *Journal of Composites Science*, vol. 5, no. 4, Article ID 105, 2021.

[11] G. B. de Abreu, S. M. M. Costa, A. G. Gumieri et al., "Mechanical properties and microstructure of high performance concrete containing stabilized nano-silica," *Revista Matéria*, vol. 22, no. 2, 2017.

[12] D. Vivek, K. S. Elango, R. Saravanakumar et al., "Effect of nano-silica in high performance concrete," *Materials Today: Proceedings*, vol. 37, Part 2, pp. 1226–1229, 2021.

[13] M. Ghosal and A. K. Chakraborty, "A compatibility study of ordinary Portland cement and flyash based cement with nano-silica," *AIP Conference Proceedings*, vol. 2158, no. 1, Article ID 020001, 2019.

[14] J. Sridhar and D. Vivek, "Influence of non-biodegradable wastes on mechanical properties of concrete—a neural network approach," *IOP Conference Series: Materials Science and Engineering*, vol. 1025, Article ID 012007, 2021.

[15] P. Zhang, Q.-F. Li, J. Wang, Y. Shi, and Y.-F. Ling, "Effect of PVA fiber on durability of cementitious composite containing nano-sio_2," *Nanotechnology Reviews*, vol. 8, no. 1, pp. 116–127, 2019.

[16] H. E.-D. Ahmed, B. A. E.-G. Sabrah, S. A. E.-A. Mohamed, and N. M. Mostafa, "Chemical and engineering properties of blended cement containing micro- and nano-silica," *American Journal of Chemical Engineering*, vol. 5, no. 5, pp. 111–121, 2017.

[17] T. Rai, B. B. Mukharjee, and S. V. Barai, "Beam-column joints made of self-compacting concrete containing recycled coarse aggregates and nano-silica," *International Journal of Sustainable Materials and Structural Systems*, vol. 4, no. 1, pp. 91–104, 2020.

[18] F. U. A. Shaikh, T. Nishiwaki, and S. Kwon, "Effect of fly ash on tensile properties of ultra-high performance fiber reinforced cementitious composites (UHP-FRCC)," *Journal of Sustainable Cement-Based Materials*, vol. 7, no. 6, pp. 357–371, 2018.

[19] T. Ali, A. S. Buller, F. ul Rehman Abro et al., "Investigation on mechanical and durability properties of concrete mixed with silica fume as cementitious material and coal bottom ash as fine aggregate replacement material," *Buildings*, vol. 12, no. 1, Article ID 44, 2022.

[20] I.-H. Yang, J. Park, K.-C. Kim, and S.-W. Yoo, "A comparative study on the thermal conductivity of concrete with coal bottom ash under different drying conditions," *Advances in Civil Engineering*, vol. 2021, Article ID 7449298, 12 pages, 2021.

[21] S. A. Mangi, M. H. W. Ibrahim, N. Jamaluddin, M. F. Arshad, S. H. Khahro, and R. P. Jaya, "Influence of coal ash on the concrete properties and its performance under sulphate and chloride conditions," *Environmental Science and Pollution Research*, vol. 28, pp. 60787–60797, 2021.

[22] P. Zhang, H. Zhang, G. Cui, X. Yue, J. Guo, and D. Hui, "Effect of steel fiber on impact resistance and durability of concrete containing nano-sio_2," *Nanotechnology Reviews*, vol. 10, no. 1, pp. 504–517, 2021.

[23] A. Hosan and F. U. A. Shaikh, "Compressive strength development and durability properties of high volume slag and slag-fly ash blended concretes containing nano-$CaCO_3$," *Journal of Materials Research and Technology*, vol. 10, pp. 1310–1322, 2021.

[24] K. S. Elango, P. R. Remya, D. Vivek, R. Gopi, V. Rajeshkumar, and R. Saravanakumar, "Strength and durability studies on ficus exasperata leaf ash concrete," *Materials Today: Proceedings*, vol. 37, Part 2, pp. 999–1002, 2021.

[25] G. Miruthun, D. Vivek, P. R. Remya, K. S. Elango, R. Saravanakumar, and S. Venkatraman, "Experimental investigation on strengthening of reinforced concrete beams using GFRP laminates," *Materials Today: Proceedings*, vol. 37, Part 2, pp. 2744–2748, 2021.

[26] R. Embong, A. Kusbiantoro, K. Muthusamy, and N. Ismail, "Recycling of coal bottom ash (CBA) as cement and aggregate replacement material: a review," *IOP Conference Series: Earth and Environmental Science*, vol. 682, Article ID 012035, 2021.

[27] D. N. Jabbar, M. K. Abed, and Z. D. Habeeb, "Early and long-term assessment of high-performance concrete contained nano-silica exposed to sulfate attack," *IOP Conference Series: Materials Science and Engineering*, vol. 1090, Article ID 012074, 2021.

[28] P. Sikora, T. Rucinska, D. Stephan, S.-Y. Chung, and M. A. Elrahman, "Evaluating the effects of nanosilica on the material properties of lightweight and ultra-lightweight concrete using image-based approaches," *Construction and Building Materials*, vol. 264, Article ID 120241, 2020.

[29] K. S. Elango, D. Vivek, G. Krishna Prakash, M. J. Paranidharan, S. Pradeep, and M. Prabhukesavaraj, "Strength and permeability studies on PPC binder pervious concrete using palm jaggery as an admixture," *Materials Today: Proceedings*, vol. 37, Part 2, pp. 2329–2333, 2021.

[30] M. H. Abd-Elrahman, I. S. Agwa, Y. Elsakhawy, and M. S. Rizk, "Effect of utilising ferrosilicon and recycled steel fibres on ultra-high-strength concrete containing recycled granite," *Case Studies in Construction Materials*, vol. 18, Article ID e01903, 2023.

[31] B. A. Tayeh, A. S. Aadi, N. N. Hilal, B. H. Abu Bakar, M. M. Al-Tayeb, and W. N. Mansour, "Properties of ultra-high-performance fiber-reinforced concrete (UHPFRC)—a review paper," *AIP Conference Proceedings*, vol. 2157, no. 1, Article ID 020040, 2019.

[32] A. Tafraoui, G. Escadeillas, and T. Vidal, "Durability of the ultra high performances concrete containing metakaolin," *Construction and Building Materials*, vol. 112, pp. 980–987, 2016.

[33] B. A. Tayeh, D. M. Al Saffar, A. S. Aadi, and I. Almeshal, "Sulphate resistance of cement mortar contains glass powder," *Journal of King Saud University - Engineering Sciences*, vol. 32, no. 8, pp. 495–500, 2020.

[34] C. Gong, J. Zhang, S. Wang, and L. Lu, "Effect of aggregate gradation with fuller distribution on properties of sulphoaluminate cement concrete," *Journal of Wuhan University of Technology-Mater. Sci. Ed.*, vol. 30, pp. 1029–1035, 2015.

[35] P. Zhang, L. Kang, J. Wang, J. Guo, S. Hu, and Y. Ling, "Mechanical properties and explosive spalling behavior of steel-fiber-reinforced concrete exposed to high temperature—a review," *Applied Sciences*, vol. 10, no. 7, Article ID 2324, 2020.

[36] I. L. Larsen and R. T. Thorstensen, "The influence of steel fibres on compressive and tensile strength of ultra high performance concrete: a review," *Construction and Building Materials*, vol. 256, Article ID 119459, 2020.

[37] M. Zhou, Z. Wu, X. Ouyang, X. Hu, and C. Shi, "Mixture design methods for ultra-high-performance concrete—a review," *Cement and Concrete Composites*, vol. 124, Article ID 104242, 2021.

[38] L. Chen, H. Cao, J. Zhang, W. Sun, and S. Hu, "Improving the mechanical properties of ultra-high-performance concrete by hybridizing silica fume, polypropylene fiber and graphene

oxide," *Construction and Building Materials*, vol. 251, Article ID 118962, 2020.

[39] T. Ozbakkaloglu, J. W. Lim, and G. Ma, "Performance of ultra-high performance fiber reinforced concrete under impact loading," *Cement and Concrete Composites*, vol. 73, pp. 84–93, 2016.

[40] H. Wang, Z. Li, and J. Li, "Mechanical properties and durability of hybrid fiber-reinforced ultra-high performance concrete with nano-silica and polyvinyl alcohol fibers," *Construction and Building Materials*, vol. 221, pp. 668–679, 2019.

[41] A. Jain, A. Vyas, and S. Jain, "Effect of steel fiber on the mechanical properties of ultra-high-performance concrete with nano-silica," *Construction and Building Materials*, vol. 205, pp. 512–522, 2019.

Hindawi
Advances in Polymer Technology
Volume 2023, Article ID 6685060, 8 pages
https://doi.org/10.1155/2023/6685060

Research Article

Mechanical Interlocking Approaches to the Prediction of Mechanical and Tribological Behavior of Natural Fiber-Reinforced Polymer Hybrid Nanocomposites or Automotive Applications

R. Venkatesh,[1] P. C. Santhosh Kumar,[2] A. Senthilkumar,[3] J. Phani Krishna,[4] P. Chandramohan,[5] V. N. Aneesh,[6] Avinash Malladi,[7] C. B. Priya,[8] and Elangomathavan Ramaraj[9]

[1]*Department of Industrial Engineering, Saveetha School of Engineering, SIMATS, Chennai 602105, Tamil Nadu, India*
[2]*Department of Mechanical Engineering, K.Ramakrishnan College of Engineering, Trichy 621112, Tamil Nadu, India*
[3]*Department of Mechanical Engineering, Aarupadai Veedu Institute of Technology, Vinayaka Mission's Research Foundation (DU), Chennai 603104, Tamil Nadu, India*
[4]*Design Engineering, Powder Handling Solutions, RIECO Industries Ltd., Pune 411005, India*
[5]*Department of Mechatronics Engineering, Rajalakshmi Engineering College, Chennai 602105, Tamil Nadu, India*
[6]*Department of Mechanical Engineering, UKF College of Engineering and Technology, Parippally 691302, Kerala, India*
[7]*Department of Mechatronics Engineering, ICFAI Tech., ICFAI Foundation for Higher Education, Hyderabad 501203, Telangana, India*
[8]*Department of Mechanical Engineering, OASYS Institute of Technology, Trichy 621006, Tamil Nadu, India*
[9]*Department of Biology, College of Natural and Computational Sciences, Debre Tabor University, Amhara Region, Ethiopia*

Correspondence should be addressed to Elangomathavan Ramaraj; elanmath@dtu.edu.et

Received 21 December 2022; Revised 19 May 2023; Accepted 13 July 2023; Published 2 August 2023

Academic Editor: Milan Mari

Polymer matrix composites synthesized with biodegradable natural fiber obtain a predominant structure with specific properties at a low-processing cost. The unique characteristics of polymer matrix composites were magnetized in automotive parts like top roof, panel, and seat frame applications. American Society for Testing and Materials (ASTM) G99 analyzed the wear characteristics of synthesized composites through a pin-on-disc wear tester with an EN32 steel disc. The epoxy hybrid composites have been synthesized via a conventional casting process assisted with a mechanical interlock technique to obtain a predominant structure with specific properties at a low-processing cost. The advanced composite contained different jute weights (50, 25, 50, and 75 g) and coconut coir (50, 70, 45, and 20 g) hybridized with graphite particles. ASTM D2240, D638, and D790 standards evaluated the fabricated composite hardness, tensile, and flexural strength. The Sample 4 hybrid composite found maximum hardness, tensile, and flexural strength of 27.41 ± 0.99 Hv, 51.69 ± 1.01 MPa, and 55.94 ± 0.78 MPa, respectively. Sample 4 offered good wear resistance of their volumetric wear rate of 0.043 cm^3 on 40 N average load at 0.25 m/s sliding speed. It is increased by 12% compared to Sample 1 at 40 N applied load on 2.5 m/s sliding speed.

1. Introduction

Natural and synthetic fibers are familiar in fabricating polymer matrix composite, attaining good mechanical, tribological, and thermal characteristics compared with conventional plastics [1–3]. The hastened development of different fabrication industries is brought on by the requirement to increase the material properties via natural composites [4]. Natural fibers are more beneficial than synthetic fibers due to less weight, nonexpensive, good mechanical strength, increased surface quality, flexibility, biodegradability, and availability from renewable sources [5]. Recent research integrates different kinds of natural fibers utilized as reinforcement in the polymer matrix, resulting in superior physical and mechanical

characteristics of composites [6]. As well as it has durability, economical, and lightweight [7]. The features of polymer matrix composite depend on the choice of polymer, reinforcement fiber, and processing route [8]. The effective processing of hybrid polymer matrix composite hybridization with the different fiber combinations enhances the mixed characteristics utilized in various industrial applications [9–11].

In recent years, nonabrasive natural fiber/filler bonded polymer matrix composites are progressively augmented in the automotive, construction, structural, sports, and other applications due to their low density, nontoxic, better-damping properties, enhanced flexural, flame retardancy, water absorption behavior, and tensile strength, and economic operation [12, 13]. Researchers [14] examined the mechanical characteristics of polymer matrix composite with coconut coir combinations via American Society for Testing and Materials (ASTM) standard. It was found that the tensile strength of the composite increased with the increase in coconut coir and was suggested for nonstructural and structural applications. The nanoparticle-bonded natural fiber composite combination offers a high-melting temperature [15]. The nano-SiO_2 discovered natural fiber composite having excellent dynamic behavior and obtained an extraordinary quality [16]. The feasibility of replacing glass fiber with jute fiber natural composite in tribological applications has been studied. The investigational results showed that the jute fiber-reinforced epoxy composite has superior tribological properties to glass fiber composites [17]. In the past decades, granite powder and jute fiber synthesized epoxy composite, which offered maximum yield strength and good dynamic behavior for wind turbine applications [18].

Similarly, the jute fiber reinforced composite was great potential to replace the glass fiber composite in automotive front bonnet applications [19]. The jute and hemp fiber bonded polymer composite was prepared by hand layup technique and studied the mechanical properties of composites. They reported that the triple layer offered maximum strength and stiffness [20]. However, the jute fiber has been bonded with various natural fibers like tetracarpidiumconophorum [21], chicken feather, and lignocellulose Ceiba Pentandra [22], egg shell powder/nanoclay [23], coconut shell microparticle reinforced with *Cissus quadrangularis* [24], and coconut leaf sheath/glass stem fiber [25] found increased mechanical and tribological characteristics. The sansevieria ehrenbergii fiber incorporated polymer composite enriched with coconut shell ash powder via hand layup technique and reported that 10% fiber facilitated maximum yield strength, good thermogravimetric behavior, and reduced thermal conductivity [26]. Recently, polypropylene composite was fabricated by combining jute and tetracarpidiumconophorum for automotive applications. The wear loss of composite was reduced by 3.8 times that of conventional polypropylene materials [21]. The conventional method prepared the bambusaflexuosa to stem fiber-reinforced polymer composite for lightweight applications. They found improved thermal stability compared to untreated fiber [27]. Phenolic composites were synthesized using sugar palm fiber via hot press technique, and studied their mechanical performance. The results showed that the composite contained 30 vol % offered 32.23 and 61.66 MPa compressive strength, and 4.12 kJ/m^2 impact strength compared to the unreinforced composite [28].

Biodegradable reinforcements like sisal fiber, pineapple fiber, and its fly ash synthesized hybrid composite mechanical and wear properties were studied, and 30–50 wt% fiber combinations showed good mechanical and wear resistance [29]. Hemp/sisal fiber reinforced epoxy composites were enhanced by adding silica nanoparticles and studied the physical, mechanical, and tribological properties. The 3 wt% of silica exhibited high flexural, tensile, and impact strength compared to unreinforced hemp/sisal fiber composite [30]. The polyester-based hybrid composite was developed with basalt and banana fiber via a hand layup technique-assisted compression molding route. 2.5 wt% of basalt and banana fiber facilitates good mechanical and thermal performances [31]. Agrowaste-based cellulosic microfiller reinforced polymer matrix composite was developed by conventional technique and studied its surface morphology [32]. Similarly, fiber epoxy composite is synthesized by using micro-red mud filler [33], sisal/glass [34], and basalt/alumina [35].

However, the hybridization of polymer matrix composite with natural fiber (jute fiber) found poor adhesive properties due to its hydrophilic nature. To overcome the above various chemical treatments were adopted during the fabrication. This present investigation exposes the combinations of graphite nanopowders assisted jute fiber reinforced polymer matrix composite developed through mechanical interlocking approaches. The developed composite samples are shaped as per ASTM test standard requirements. Three trials are considered for the composite's performance evaluation, and average test results' average values are considered the final value. Finally, the characteristics of developed mixed results were compared and beat combinations of composite with enhanced characteristics samples to be recommended for top automobile roof, panel, and seat frame applications.

2. Materials and Methods

2.1. Material Selection. The jute fiber of 100 mm in length and nanographite powder (50 μm) is reinforced due to its high stiffness, lightweight, mechanical strength, thermal stability, and hardness [17–19]. Figure 1(a)–1(c) illustrates the jute, coconut coir, and graphite nanoparticles.

The basic properties of matrix and reinforcement materials are mentioned in Table 1. Before fabrication. The jute fibers are chemically treated with a 2% NaOH solution at room temperature for 24 hr, facilitating good adhesive behavior and offering superior mechanical interlocking between the matrix and fiber. It increases the mechanical and tribological properties [28]. The graphite nanopowder and treated jute fibers are mixed with epoxy resin settled with a hardener (triethylenetetramine) of 10 : 1 ratio. It has suitable viscosity and better dimensional stability [29].

2.2. Fabrication of Polymer Hybrid Nanocomposites. The compositions for fabricating polymer hybrid nanocomposites are detailed in Table 2. Figure 2 represents the

(a) (b) (c)

Figure 1: Reinforcements (a) jute fiber, (b) coconut coir, and (c) graphite nanoparticles.

Table 1: Properties of reinforcements/matrix.

Reinforcements/ matrix	Density (g/cc)	Tensile strength (MPa)	Young's modulus (GPa)	Thermal conductivity ($Wm^{-1} K^{-1}$)	Size
Jute fiber	1.4	393–779	26.5	427.3	100 mm length and 50 μm Dia
Coconut coir	1.2	175	2–8	–	0.1–0.4 μm
Graphite	2.25	–	–	24	50 nm
Epoxy	1.1	–	–	–	–
Triethylenetetramine	0.72	–	–	–	–

Table 2: Weight of percentages of matrix and fillers.

Sample no.	Weight of the matrix and filler materials in g			
	Epoxy resin	Jute fiber	Coconut coir	Graphite
1	500	50	50	0
2	355	25	70	50
3	355	50	45	50
4	355	75	20	50

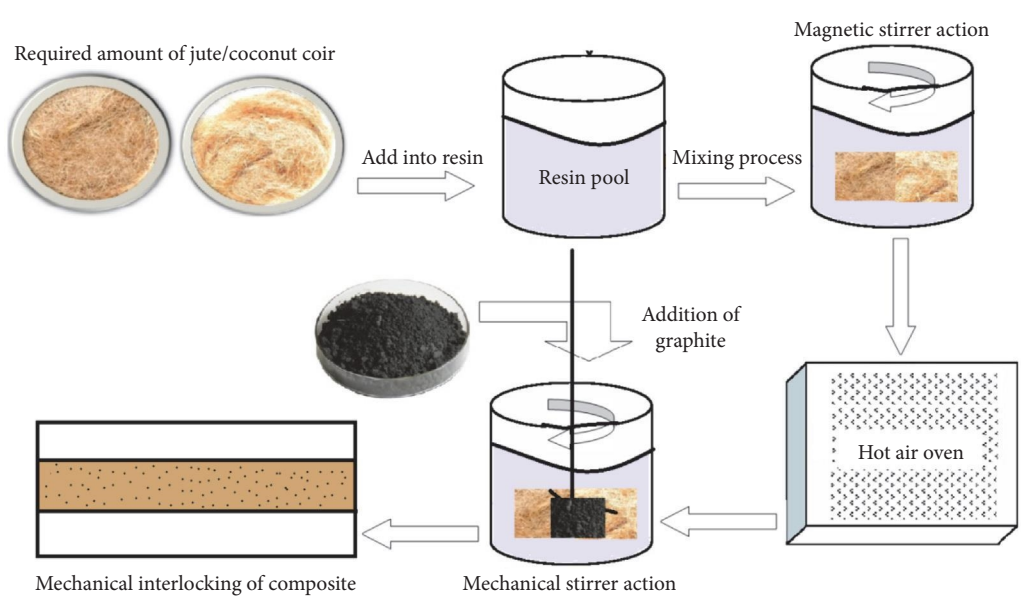

Figure 2: Conceptual diagram for mechanical interlocking fabrication of polymer hybrid nanocomposite.

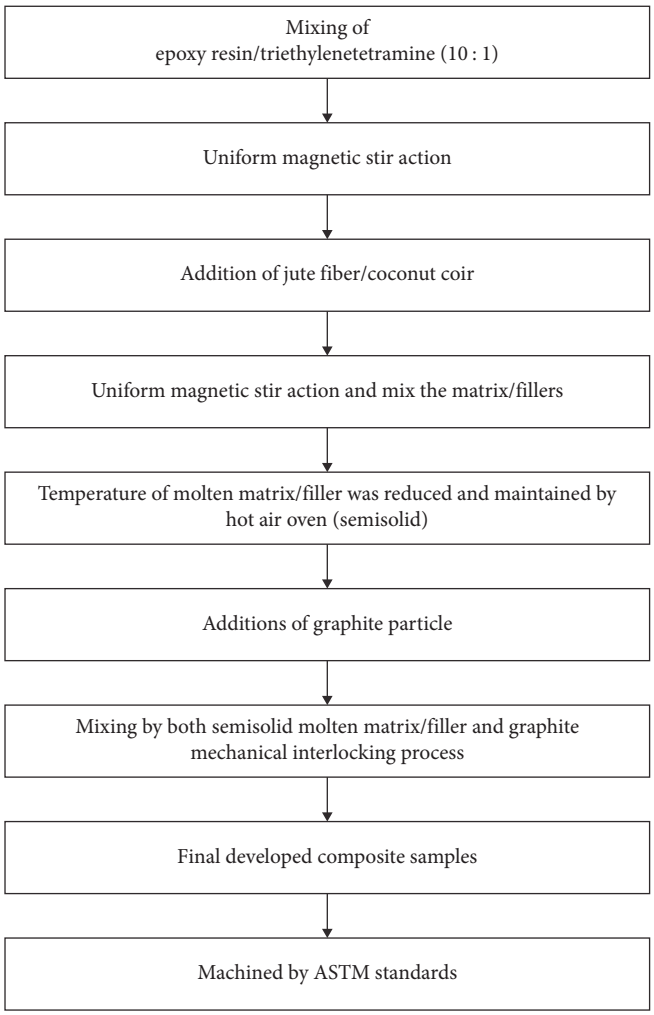

Figure 3: Flow process diagram for the fabrication of hybrid composites.

step-by-step process for polymer hybrid nanocomposite fabrication. Before the fabrication, the jute fiber and coconut coir are cleaned using distilled water and then dried in the oven for 10 hr at 65°C temperature. Particularly, chopped jute fibers are chemically soaked with 2% NaOH solution for 24 hr at 24°C temperatures. The preprocessing treatment of natural fiber gained good adhesive properties [28].

Figure 3 illustrates the flow process diagram for the fabrication of hybrid composites. Initially, the treated chopped jute fiber and coconut coir are weighed by a digital weighing machine with an accuracy of ±0.001 g per the constitutions (Table 2). Both natural fibers are manually added into the epoxy pool and mixed uniformly with the help of a magnetic stirrer (1,000 rpm) for 20 min. The high-stir speed helps to remove the acetone gas and increase the adhesion properties [17]. After adding both fibers, the preheated graphite nanoparticles were added into the mixed natural fiber pool and mechanical action was carried out for fine mixing for 20 min. The mixed composite slurry is

Figure 4: Developed composite samples.

preheated at 65°C for 20 min to eliminate the residual stress. Finally, the hardener is added in epoxy composite slurry and mixed via mechanical action for 20 min. The prepared composite mixture is in a steel mold, and 50 kN of the load is applied over the mold for 24 hr. The developed composites are shown in Figure 4.

2.3. Characterization Details. The developed polymer hybrid nanocomposites are subjected to various mechanical characteristics evaluation followed by ASTM standards (the revision year 2021). In the same way, fabricated composite samples were evaluated by ASTM [33, 34]. ASTM D638 evaluates the tensile strength of the composite, ASTM D2240 is adapted to measuring the hardness of the composite, and its flexural strength is examined via ASTM D790. During the evaluation, three trials are chosen from each sample, and the average of three trials is treated as the mean value of the corresponding test. All the tests are evaluated at room conditions.

The dry sliding volumetric wear behavior of advanced polymer matrix composites is evaluated by a DUCOM pin-on-disc wear testing machine arranged with EN32 steel counter disc. It is analyzed by ASTM G99 standard followed by two approaches like the constant sliding speed of 2.5 m/s with a varied load of 10, 20, 30, and 40 N and another condition is 40 N applied load with a varied sliding speed of 1, 2, 3, and 4 m/s, respectively. The 6 mm diameter and 30 mm length wear test samples are vertically loaded with a perpendicular arm. Before (w1) and after (w2), the wear test of entire samples is weighted by a digital electronic weighing machine with an accuracy of ±0.001 g. The weight loss ratio calculates the volumetric wear to composite density [29] as follows:

$$\text{Volumetric wear} = \frac{\text{weight loss}(\text{w2} - \text{w1})}{\text{density}(\rho)}. \quad (1)$$

Scanning electron microscopy (SEM) analyzed the wear debris area of the tested wear sample. SEM and Image software observed a similar tendency, the presence of filler materials in the polymer matrix composite [32].

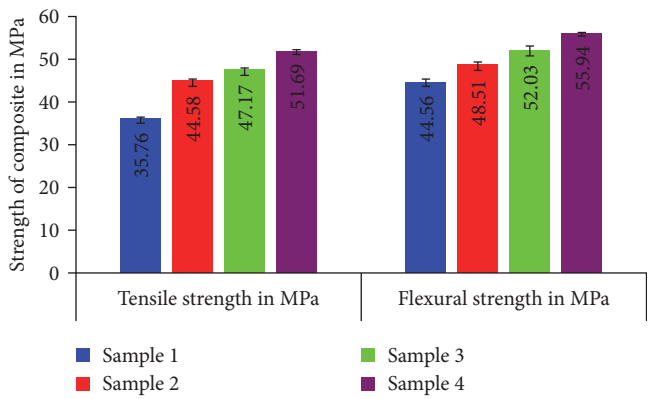

FIGURE 5: Tensile and flexural strength of composites.

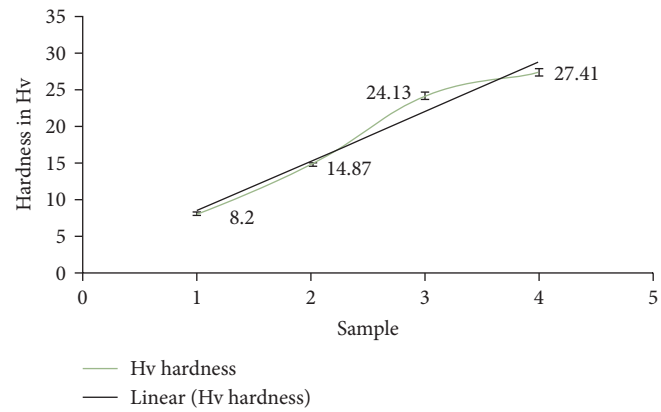

FIGURE 6: Hardness of composite.

3. Results and Discussion

3.1. Mechanical Characteristics Studies

3.1.1. Tensile and Flexural Strength of Composite. ASTM standard evaluated test results on tensile and flexural strength of the polymer matrix composite with and without graphite particles is shown in Figure 5. It shows the variations in mechanical characteristics due to their effect on reinforcement, processing, and adhesion behavior of ingredients.

The tensile strength of the composite is progressively increased with an increase in jute fiber and reduced coconut coir at constant weight percentages (5 wt%) of graphite particles. The tensile strength of Sample 1 without graphite particle predicted 35.76 ± 0.81 MPa.

However, incorporating 5 wt% graphite nanoparticle into the polymer matrix established higher tensile strength of more than 10% compared to each sample. The maximum tensile strength of 51.69 ± 1.01 MPa is predicted for Sample 4, having 75 wt% of jute fiber/20 wt% coconut coir/5 wt% graphite nanoparticles, which is increased by 44.5% compared to Sample 1. While the tensile strength of Sample 4 was compared to the recent investigation reported [31] by the basalt/banana fiber-based hybrid polymeric composite bonded with 5 wt% of the oil cake biomass waste derived cellulose microfillers found a 6% improvement. The increase in tensile strength is due to its good adhesive properties between the matrix and reinforcement achieved by the highly forced mechanical interlocking process. However, the high-tensile load applied on the composite can weaken the interfacial bonding between the matrix and reinforcements, resulting in decreased tensile strength [8]. In comparison, introducing inorganic silica particles increased the tensile strength with effective adhesive performance on polymer matrix composite [29].

It was observed from Figure 5; the flexural strength of polymer matrix composite reinforced with jute fiber/coconut coir (50 : 50) shows a 44.56 ± 1.21 MPa. At the same time, the introduction of 5 wt% graphite nanoparticles in a polymer matrix showed increased flexural strength. The composite contained 25 wt% jute fiber/70 wt% coconut coir/5 wt% graphite nanoparticles, which enhanced the flexural strength of 9% compared to Sample 1. Further increase in jute fiber content found superior flexural strength. Increased content of jute fiber predicts the highest flexural strength of 55.94 ± 0.78 MPa as 75 wt% with a reduced weight percentage of coconut coir under-maintained constant weight percentage of (5 wt%) graphite nanoparticles. About (Sample 4) 25.55% improvement in flexural strength compared to Sample 1. The higher weight percentage of jute fiber mixed with coconut coir via epoxy leads to increased flexural strength, and the presence of graphite nanoparticles to adhesive characteristics is the prime reason for the increased flexural strength of the composite. The same trend was reported by one of the researchers during the analysis of cissus quadrangularis stem fiber/epoxy composite with micro-red mud filler [33] and alumina nanofillers bonded with basalt/epoxy hybrid composites.

3.1.2. Hardness of Composite. The effect of graphite nanoparticles on the hardness of polymer matrix hybrid nanocomposite is shown in Figure 6.

The immobilization of polymer resin adhesive with jute/coconut coir and graphite nanoparticles is shown by the improvement in the hardness of the hybrid nanocomposite. It is revealed that Sample 1 composite without graphite was found to be 8.2 ± 1.20 Hv. The hardness of Sample 2 was identified as 14.87 ± 1.01 Hv and 24.13 ± 1.03 Hv noted by Sample 3. However, the hardness of the composite increased with reduced coconut coir maintained with a constant weight percentage of graphite nanoparticles. The maximum hardness of 27.41 ± 0.99 Hv was noted on Sample 4 due to its enhanced particle distribution and graphite nanoparticles, enhancing adhesive characteristics via mechanical interlocking technique.

Moreover, the optimum dispersion of graphite nanoparticles at higher loading resists indentation. About 2.34 times increase in hardness value compared to Sample 1. It was due to the best combinations of jute fiber/coconut coir/graphite in polymer resin is proved. Similar trends for improvement in the hardness of polymer matrix

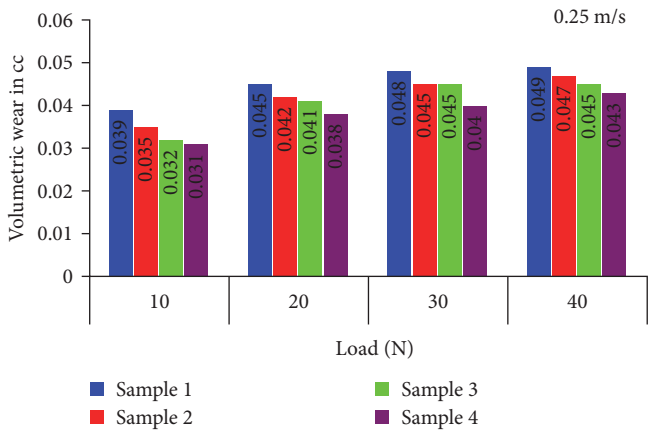

FIGURE 7: Volumetric wear characteristics of polymer matrix composites on varied average load.

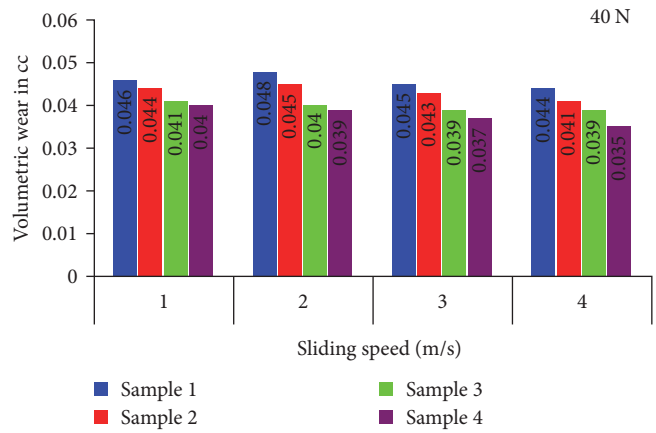

FIGURE 8: Volumetric wear characteristics of polymer matrix composites on varied sliding speed.

composites were observed with the additions of silica nanoparticles [30].

3.2. Wear Characteristics Studies

3.2.1. Effect of Load on Wear Characteristics of Polymer Hybrid Nanocomposites. The volumetric wear characteristics of polymer matrix hybrid nanocomposite with a varied weight percentage of jute fiber/coconut coir/graphite nanoparticles are examined by different loading conditions of 10, 20, 30, and 40 N with 0.25 m/s sliding speed operated by the constant sliding distance of 1,000 m is shown in Figure 7. It is noted from Figure 7, that the volumetric wear behavior of polymer matrix composite is increased progressively with increase in average load from 10 to 40 N an interval of 10 N at 0.25 m/s sliding speed. The volumetric wear behavior of the composite is reduced with the incorporation of graphite nanoparticles. The volumetric wear properties of Sample 1 increased from 0.039 to 0.049 cc. Adding jute fiber with the decreased weight percentages of coconut coir-reinforced graphite nanoparticles predicted reduced volumetric wear. The decreasing tendency of volumetric wear properties is due to the complex graphite nanoparticles in the polymer matrix.

The presence of a complex ceramic particle in polymer matrix composite is the main reason for decreased volumetric wear. The complex graphite nanoparticles facilitate good resistance against abrasive wear. Sample 4 found minimum volumetric wear of 0.031, 0.038, 0.04, and 0.043 cc on the applied average load of 10, 20, 30, and 40 N at 0.25 m/s sliding speed. It exhibited a minimum volumetric wear percentage of 12% compared to Sample 1 at 40 N applied load on 2.5 m/s sliding speed. One researcher reported a similar trend in evaluating silica-reinforced polymer matrix composite [14]. Moreover, the composite containing 75 wt% jute fiber produces high-thermal stability and strength during high-frictional force [17–20]. However, the jute fiber can withstand the increased frictional force, and the coconut coir to resist wear against the applied load.

3.2.2. Effect of Sliding Speed on Wear Characteristics of Polymer Hybrid Nanocomposites. The volumetric wear characteristics of polymer matrix composites on the varied sliding speed of 1, 2, 3, and 4 m/s on a constant applied load of 40 N is shown in Figure 7. While applied 40 N load of different sliding speeds showed decreased volumetric wear of Sample 4 is 0.04 to 0.039 cc. Sample 1 predicted the highest volumetric wear remains lower than Sample 1. It is observed from Figure 8 that the volumetric wear of polymer matrix composite containing 5 wt% graphite nanoparticles showed decreased value.

However, more than 3 m/s sliding speed found enhanced volumetric wear compared to 1 and 2 m/s. It was due to the increased content of jute fiber (75 wt%) offering a high-resistance force against the 3 m/s sliding force. While an increase in the content of jute fiber with decreased content of coconut coir assisted with 5 wt% graphite nanoparticle in polymer matrix predicted by 20% of volumetric wear is limited on Sample 4. The presence of ceramic nanofillers enhanced the wear resistance [31].

3.3. SEM Micrograph of Sample 4 (40 N Average Load at 0.25 m/s). Figure 9 depicts the SEM of epoxy hybrid composite Sample 4. Figure 9(a) represents Sample 4 and is measured by 40 N average load with 23.78 N frictional force at 0.25 m/s sliding speed. It was noted that the filler and graphite particles were present in the epoxy platform. It was observed from Figure 9(b) that the high load of 40 N with increased frictional force results in wear debris and adhesive layer formation at 38°C temperature. However, the jute fiber could withstand the high-frictional force and be formed as adhesive accumulated layers diffused by the adjutant layer decreased the volumetric wear rate. The incorporated graphite particles were seen as a white dotted field of the SEM micrograph, as illustrated by Figure 9. The graphite particles were led to maximum resistance against high-frictional force and temperature.

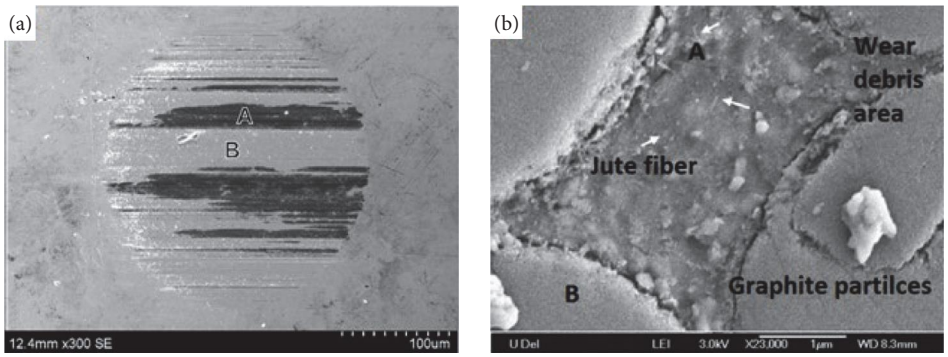

Figure 9: (a) Test Sample 4 (b) SEM micrograph of Sample 4 on 40 N load at 0.25 m/s. Where A—worn surface bonded with epoxy and B—epoxy layer covered with reinforcements.

4. Conclusions

The graphite hybridized epoxy composites were successfully made using the varied weight of natural jute/coconut fiber via a conventional casting process assisted with the mechanical interlocking route. The following conclusions are mentioned below:

(i) Among the various samples, Sample 4 performed enhanced mechanical hardness, the tensile, and flexural strength of 27.41 ± 0.99 Hv, 51.69 ± 1.01 MPa, and 55.94 ± 0.78 MPa.

(ii) While compared to without graphite epoxy composite Sample 1, the hardness, tensile, and flexural strength were improved by 2.3 times, 44.5% and 25.55%, respectively.

(iii) The volumetric wear properties of epoxy hybrid composites with graphite particles showed good wear resistance. Sample 4 facilitated a low-volumetric wear rate of 0.043 cm^3 under 40 N average load with 23.78 N frictional force at 0.25 m/s sliding speed. The wear resistance of Sample 4 was improved by 12% compared to Sample 1 under maximum load and low-sliding speed of 40 N and 2.5 m/s.

(iv) The SEM micrograph of Sample 4 revealed that the adhesive wear and its debris area is shown in Figure 9.

Data Availability

All the data required are available within the manuscript.

Conflicts of Interest

The authors declare that they have no conflicts of interest.

References

[1] M. J. John and S. Thomas, "Biofibres and biocomposites," *Carbohydrate Polymers*, vol. 71, no. 3, pp. 343–364, 2008.

[2] P. Sahu and M. K. Gupta, "Sisal (Agave sisalana) fibre and its polymer-based composites: a review on current developments," *Journal of Reinforced Plastics and Composites*, vol. 36, no. 24, pp. 1759–1780, 2017.

[3] J. Praveenkumara, P. Madhu, T. G. Yashas Gowda, M. R. Sanjay, and S. Siengchin, "A comprehensive review on the effect of synthetic filler materials on fiber-reinforced hybrid polymer composites," *The Journal of The Textile Institute*, vol. 113, no. 7, pp. 1231–1239, 2022.

[4] D. B. Dittenber and H. V. S. GangaRao, "Critical review of recent publications on use of natural composites in infrastructure," *Composites Part A: Applied Science and Manufacturing*, vol. 43, no. 8, pp. 1419–1429, 2012.

[5] N. Chand and M. Fahim, "Natural fibers and their composites," in *Tribology of Natural Fiber Polymer Composites*, Woodhead Publishing Series in Composites Science and Engineering, pp. 1–58, Woodhead Publishing, 2008.

[6] N. Saba, P. M. Tahir, and M. Jawaid, "A review on potentiality of nano filler/natural fiber filled polymer hybrid composites," *Polymers*, vol. 6, no. 8, pp. 2247–2273, 2014.

[7] M. Ramesh, L. N. Rajeshkumar, N. Srinivasan, D. V. Kumar, and D. Balaji, "Influence of filler material on properties of fiber-reinforced polymer composites: a review," *e-Polymers*, vol. 22, no. 1, pp. 898–916, 2022.

[8] C. Dong, "Review of natural fibre-reinforced hybrid composites," *Journal of Reinforced Plastics and Composites*, vol. 37, no. 5, pp. 331–348, 2018.

[9] Y. Li, Y.-W. Mai, and L. Ye, "Sisal fibre and its composites: a review of recent developments," *Composites Science and Technology*, vol. 60, no. 11, pp. 2037–2055, 2000.

[10] T. Gurunathan, S. Mohanty, and S. K. Nayak, "A review of the recent developments in biocomposites based on natural fibres and their application perspectives," *Composites Part A: Applied Science and Manufacturing*, vol. 77, pp. 1–25, 2015.

[11] G. M. Pinto, J. M. O. Cremonezzi, H. Ribeiro, R. J. E. Andeade, N. R. Demarqurtte, and G. J. M. Fechine, "From two-dimensional materials to polymer nanocomposites with emerging multifunctional applications: a critical review," *Polymer Composites*, vol. 44, no. 3, pp. 1438–1470, 2023.

[12] N. Saba, M. T. Paridah, and M. Jawaid, "Mechanical properties of kenaf fibre reinforced polymer composite: a review," *Construction and Building Materials*, vol. 76, pp. 87–96, 2015.

[13] J. Sun, J. Shen, S. Chen et al., "Nanofiller reinforced biodegradable PLA/PHA composites: current status and future trends," *Polymers*, vol. 10, no. 5, Article ID 505, 2018.

[14] P. N. E. Naveen and T. Dharma Raju, "Evaluation of mechanical properties of coconut coir fiber reinforced polymer matrix composites," *Journal of Nano Research*, vol. 24, pp. 34–45, 2013.

[15] M. Adamu, M. R. Rahman, and S. Hamdan, "Bamboo nanocomposite: impact of poly (ethylene-alt-maleic anhydride)

and nanoclay on physicochemical, mechanical, and thermal properties," *BioResources*, vol. 15, no. 1, pp. 331–346, 2019.

[16] R. K. Sinha, K. Sridhar, R. Purohit, and R. K. Malviya, "Effect of nano SiO_2 on properties of natural fiber reinforced epoxy hybrid composite: a review," *Materials Today: Proceedings*, vol. 26, Part 2, pp. 3183–3186, 2020.

[17] G. Raghavendra, S. Ojha, S. K. Acharya, and S. K. Pal, "Jute fiber reinforced epoxy composites and comparison with the glass and neat epoxy composites," *Journal of Composite Materials*, vol. 48, no. 20, pp. 2537–2547, 2014.

[18] M. J. Pawar, A. Patnaik, and R. Nagar, "Investigation on mechanical and thermo-mechanical properties of granite powder filled treated jute fiber reinforced epoxy composite," *Polymer Composites*, vol. 38, no. 4, pp. 736–748, 2017.

[19] A. K. Rana, A. Mandal, B. C. Motra, R. Jacobson, R. Rowell, and A. N. Banejee, "Short jute fiber-reinforced polypropylene composites: effect of compatibilizer," *Applied Polymer*, vol. 69, no. 2, pp. 329–338, 1998.

[20] S. P. Singh, A. Dutt, and C. K. Hirwani, "Mechanical, modal and harmonic behavior analysis of jute and hemp fiber reinforced polymer composite," *Journal of Natural Fibers*, vol. 20, no. 1, Article ID 2140328, 2023.

[21] O. A. Balogun, O. O. Daramola, A. A. Adediran, A. A. Akinwande, and O. S. Bello, "Investigation of *Jute/Tetracarpidium conophorum* reinforced polypropylene composites for automobile application: mechanical, wear and flow properties," *Alexandria Engineering Journal*, vol. 65, pp. 327–341, 2023.

[22] S. M. Rangappa, J. Parameswaranpillai, S. Siengchin, M. Jawaid, and T. Ozbakkaloglu, "Bioepoxy based hybrid composites from nano-fillers of chicken feather and lignocellulose Ceiba Pentandra," *Scientific Reports*, vol. 12, Article ID 397, 2022.

[23] K. Ganesan, C. Kailasanathan, M. R. Sanjay, P. Senthamaraikannan, and S. S. Saravanakumar, "A new assessment on mechanical properties of jute fiber mat with egg shell powder/nanoclay-reinforced polyester matrix composites," *Journal of Natural Fibers*, vol. 17, no. 4, pp. 482–490, 2020.

[24] I. Jenish, S. G. V. Chinnasamy, S. Basavarajappa et al., "Tribo-mechanical characterization of carbonized coconut shell micro particle reinforced with Cissus quadrangularis stem fiber/epoxy novel composite for structural application," *Journal of Natural Fibers*, vol. 19, no. 8, pp. 2963–2979, 2022.

[25] K. N. Bharath, D. Roopa, S. Indran, S. Basavarajappa, M. R. Sanjay, and S. Siengchin, "Influence of the stacking sequence and coconut husk micro fillers on the drilling parameters of coconut leaf sheath/glass/jute fiber hybrid phenol formaldehyde composites," *Materials Today: Proceedings*, vol. 52, Part 5, pp. 2427–2431, 2022.

[26] J. Iyyadurai, F. S. Arockiasamy, T. Manickam, S. Rajaram, I. Suyambulingam, and S. Siengchin, "Experimental investigation on mechanical, thermal, viscoelastic, water absorption, and biodegradability behavior of sansevieria ehrenbergii fiber reinforced novel polymeric composite with the addition of coconut shell ash powder," *Journal of Inorganic and Organometallic Polymers and Materials*, vol. 33, pp. 796–809, 2023.

[27] R. Srisuk, L. Techawinyutham, A. Vinod, S. M. Rangappa, and A. Siengchin, "Agro-waste from *Bambusa flexuosa* stem fibers: a sustainable and green material for lightweight polymer composites," *Journal of Building Engineering*, vol. 73, Article ID 106674, 2023.

[28] B. Rashid, Z. Leman, M. Jawaid, M. J. Ghazali, and M. R. Ishak, "The mechanical performance of sugar palm fibres (ijuk) reinforced phenolic composites," *International Journal of Precision Engineering and Manufacturing*, vol. 17, pp. 1001–1008, 2016.

[29] K. R. Sumesh, V. Kavimani, G. Rajeshkumar, P. Ravikumar, and S. Indran, "An investigation into the mechanical and wear characteristics of hybrid composites: influence of different types and content of biodegradable reinforcements," *Journal of Natural Fiber*, vol. 19, no. 8, pp. 15440–15478, 2022.

[30] T. Singh, B. Gangil, L. Ranakoti, and A. Joshi, "Effect of silica nanoparticles on physical, mechanical, and wear properties of natural fiber reinforced polymer composites," *Polymer Composites*, vol. 42, no. 5, pp. 2396–2407, 2021.

[31] R. Jagadeesan, I. Suyambulingam, D. Divakaran, and S. Siengchin, "Novel sesame oil cake biomass waste derived cellulose micro-fillers reinforced with basalt/banana fibre-based hybrid polymeric composite for lightweight applications," *Biomass Conversion and Biorefinery*, vol. 13, pp. 4443–4458, 2023.

[32] N. P. Sunesh, S. Indran, D. Divya, and S. Suchart, "Isolation and characterization of novel agrowaste-based cellulosic micro fillers from Borassus flabellifer flower for polymer composite reinforcement," *Polymer Composites*, vol. 43, no. 9, pp. 6476–6488, 2022.

[33] V. C. Sathish Gandhi, I. Jenish, S. Indran, and D. Yugendra Rajan, "Mechanical and thermal analysis of *Cissus Quadrangularis* stem fiber/epoxy composite with micro-red mud filler composite for structural application," *Transactions of the Indian Institute of Metals*, vol. 75, pp. 737–747, 2022.

[34] G. R. Arpitha, M. R. Sanjay, P. Senthamaraikannan, C. Barile, and B. Yogesha, "Hybridization effect of sisal/glass/epoxy/filler based woven fabric reinforced composites," *Experimental Techniques*, vol. 41, pp. 577–584, 2017.

[35] S. S. Vinay, M. R. Sanjay, S. Siengchin, and C. V. Venkatesh, "Effect of Al_2O_3 nanofillers in basalt/epoxy composites: mechanical and tribological properties," *Polymer Composites*, vol. 42, no. 4, pp. 1727–1740, 2021.

Hindawi
Advances in Polymer Technology
Volume 2023, Article ID 8832582, 11 pages
https://doi.org/10.1155/2023/8832582

Research Article

Analysis of the Multiwalled Carbon Nanotubes Reinforced Polymethyl Methacrylate Bone Cement's Characteristics and *In Vitro* Bioactivity to Prolong Its Functionality in Orthopedic Application

T. V. Vineeth Kumar,[1] **N. Shanmugapriya**,[1] **S. Arun**,[2] **and G. Ramasubramanian**[3]

[1]*Department of Mechanical Engineering, Siddaganga Institute of Technology (Autonomous Institution Affiliated to Visvesvaraya Technological University, Belagavi), Tumakuru, 572 103 Karnataka, India*
[2]*Advanced Composites Division, CSIR-National Aerospace Laboratories, Bengaluru, 560 017 Karnataka, India*
[3]*Department of Chemistry, Seenu Atoll School, Addu City, Maldives*

Correspondence should be addressed to G. Ramasubramanian; raman@satollschool.edu.mv

Received 24 December 2022; Revised 23 March 2023; Accepted 27 April 2023; Published 30 May 2023

Academic Editor: Indran Suyambulingam

Polymethyl methacrylate (PMMA) bone cement is being used to fill voids that are created due to vertebral compression fractures. It is also a grouting medium in orthopedic joint replacement surgeries as they possess fast primary fixation to the bone. Considering the cement properties and *in vitro* bioactivity of bone cement is essential for cemented hip and knee joint replacement surgeries. In this study, commercial Simplex P bone cement (SPBC) is modified with carboxyl- (-COOH-) functionalized multiwalled carbon nanotubes (MWCNTs) to overcome high polymerization temperature, volumetric shrinkage, surface wettability, and *in vitro* bioactivity. A geometric dilution method is used to incorporate MWCNTs with the PMMA powder, which is in unequal proportions. The PMMA/MWCNT nanocomposite with different concentrations of reinforcements, such as 0.1, 0.3, 0.5, and 0.7 weight percentages, is prepared for the investigation. It was observed that the MWCNTs had a beneficial impact on PMMA bone cement (PMMA-BC) by enhancing its setting time (2.94%↑) and surface wettability (23.58%↑). Also, diminished polymerization temperature (29%↓) and volumetric shrinkage (40.9%↓) are observed for an optimum concentration of 0.7 wt. %. The bioactivity of the cement surface is validated by the *in vitro* bioactivity observed in simulated body fluid (SBF) through the development of primary and secondary apatite. It is concluded that the synthesized PMMA/MWCNT nanocomposites are found to have enhanced cement properties compared to PMMA-BC.

1. Introduction

PMMA bone cement has been used to secure prosthetic joints in humans for over fifty years [1]. The PMMA is a self-polymerizing polymer that allows for a fast primary fixation to the bone and helps in speedy patient recovery after surgery. Also, it is simple to handle during the preparation and positioning of cement mantles [2]. This self-setting PMMA bone cement fills the gap and distributes the load between the bone and implant in hip and knee joint replacement surgeries [3]. The compression fracture voids were filled by the percutaneous injection of PMMA-BC into the vertebral body [4]. The PMMA was observed to lose its properties after its prolonged usage, which leads to revision surgery. The prominent reasons for the failure of cemented joint replacements are aseptic loosening, volumetric shrinkage, and breakdown of the cement mantle [5, 6]. PMMA-BC undergoes a high exothermic polymerization reaction that generates temperatures beyond 100°C. These high polymerization temperatures can result in significant thermal necrosis and aseptic loosening [7]. According to reports, bone tissue experiences thermal necrosis after being exposed to

temperatures beyond 50°C for more than one minute. It has been revealed that the reasons for volumetric shrinkage are thermal contraction (upon cooling) and variation in density during polymerization [8]. Gilbert et al. [9] reported 5.1% to 6.5% volumetric shrinkage as a result of density change brought on by exothermic polymerization. Thus, the technical issues with the current use of bone cement are listed as high polymerization temperature causing thermal necrosis, excessive volumetric shrinkage leading to mechanical loosening, and short working times causing uneven filling [10].

The aforesaid shortcomings of PMMA bone cement attracted researchers to work on bone cement properties by incorporating different fillers like graphene oxide, silver nanoparticles, silica nanoparticles, carbon nanotubes, and other fillers [11–13]. It can be noted from the literature that nanomaterials have been used prominently as fillers because they differ from bulk materials of the same composition in terms of strong reactivity and the substantial surface area-to-mass ratio [14]. The properties of nanomaterials are intrinsic only if they are distributed uniformly in the matrix. The MWCNTs were reinforced with PMMA-BC to enhance the cement properties. The agglomeration of MWCNTs within the bone cement matrix is governed mainly by the method used to distribute them into the bone cement matrix [15]. The distribution of MWCNTs in the bone cement matrix was achieved by the following three methods [16]:

(1) *Ultrasonic Disintegrator.* MWCNTs were incorporated into liquid monomer by dispersion

(2) *High-Temperature Mechanical Shear Mixing.* MWCNTs were dispersed with MMA powder

(3) *Magnetic Stirring.* MWCNTs were incorporated into liquid monomers using a magnetic stirrer

The thermal properties obtained by Ormsby et al. [16] for 0.1 wt.% unfunctionalized and -COOH-functionalized MWCNT-reinforced bone cement using the above three methods are summarized in Table 1. The amount of heat released during the exothermic polymerization of PMMA-BC was greatly influenced by the addition of functionalized MWCNTs.

The literature review indicates that MWCNTs were dispersed in the liquid component of the bone cement using sonication and magnetic-stirring methods. MWCNTs were added to the MMA powder component in the dry blending technique. However, these methods required additionally a sophisticated instrument and postprocessing methods for the incorporation of MWCNTs. Although the results were encouraging, it is a difficult task to significantly improve the overall performance of the nanocomposites without compromising mechanical and physical properties. The scientific community is still grappling with the issues of PMMA-BC processing methods for uniform disaggregation and poor chemical interface with the matrix [17].

In this study, MWCNTs are incorporated into the powder part of PMMA-BC using a geometric dilution method, which is often used in the pharmaceutical industry to mix two powders of unequal proportions [18]. This method is used as an alternative to sonication and magnetic stirring methods to incorporate MWCNTs to reduce possible agglomeration. The effect of 0.1, 0.3, 0.5, and 0.7 wt. % MWCNT-COOH on commercial SPBC in terms of cement properties and *in vitro* bioactivity is reported in this work. Fourier transform infrared (FTIR) was used to investigate the chemical interaction (identification of compounds) with the PMMA-BC matrix. The physical interface of MWCNTs with PMMA is detected using Transmission electron microscopy (TEM).

2. Materials and Methods

2.1. Materials. The surgical Simplex P radiopaque bone cement is purchased from Stryker Howmedica Osteonics, Republic of Ireland. It is a two-part acrylic-based mixture with liquid and powder components. The powder component contains polymethyl methacrylate polymer units, barium sulfate as a radiopaque agent, and benzoyl peroxide as the polymerization initiator. The composite composition uses carboxyl functionalized MWCNTs as nanofillers, purchased from Platonic Nanotech Pvt. Ltd. (Kachwa Chowk, Mahagama, Jharkhand) that are 2–10 m in length and 10–15 nm in outer diameter.

2.2. Formulation of Composite Bone Cement. According to manufacturer recommendations, the powder and liquid medium are combined in a 2 : 1 ratio, initiating the polymerization of free radicals to form a rigid polymer. In Table 2, the weight ratios of the composite bone cement are displayed. Briefly, MWCNTs were dispersed using a geometrical dilution method with measured size, combining fine powders of unequal proportions of MWCNTs with MMA powder to ensure uniform distribution. This MMA powder and MWCNT blend are added to the MMA liquid monomer solution to initiate self-polymerization. Nanocomposite bone cement samples are prepared for 0.1, 0.3, 0.5, and 0.7 wt. % MWCNT concentration.

Mixing of liquid and powder components involves sticky, working, and hardening phases. The mixture is poured into the mould of 6 mm diameter and 12 mm height when it is seen to approach the dough stage. The curing is done at room temperature for 24 hours. The cylindrical specimens are cut into sections after curing and polished with SiC paper with grits ranging from 220 to 2400.

3. Thermal Characterization

3.1. Polymerization Temperature Measurements. The exothermic polymerization temperatures are measured for the nanocomposite bone cement samples using a digital infrared thermometer. The thermometer is calibrated at an ice point (0°C) and boiling point of water (100°C) for its precision. The temperatures are measured at 30 seconds intervals at the center and different locations of the cylindrical mould ($\phi 6 \times 12$ mm), during the different stages of curing. The sample temperatures are recorded at different locations on the specimen to obtain a better estimation and the average of three maximum values are recorded.

Table 1: Thermal properties of PMMA-BC (Colacryl B866) with different methods of incorporation [16].

Methods of incorporation	Type of MWCNT	Maximum temperature % decrease	Setting time % increase
Ultrasonic disintegration	Unfunctionalized	9.57	51.87
	-COOH functionalized	8.05	55.90
Dry blending	Unfunctionalized	16.86	96.54
	-COOH functionalized	25.41	146.68
Magnetic stirring	Unfunctionalized	29.08	81.55
	-COOH functionalized	52.75	207.06

Table 2: Composite identification and composition.

Sl. No.	Sample identification	Material composition
1	BC	PMMA (control)
2	BC1	PMMA+0.1% MWCNT
3	BC2	PMMA+0.3% MWCNT
4	BC3	PMMA+0.5% MWCNT
5	BC4	PMMA+0.7% MWCNT

3.2. Setting Time. The prepared samples are tested for their setting time using a Vicat instrument. The initial and final setting times are measured by following the ASTM C191-08 standard [19]. The dial gauge measures the needle's vertical travel at a constant 100 g load. The needle is used to pierce a 10×50 mm bone cement mould. The tip's distance is measured at every 5 seconds until the cement gets cured.

3.3. Thermal Gravimetric Analysis. The thermal gravimetric analysis (TGA) of bone cement is investigated using differential scanning calorimetry (DSC)-TGA SDT2960 from ambient temperature to 700°C at 10°C/minute in nitrogen gas atmosphere. Before the DSC/TGA studies, the samples are hardened in a pH 7.4 phosphate-buffered saline solution. The samples are crushed, dried for 24 hours in the open air, and then tested.

4. Contact Angle

Contact angle measurements are used to quantify the surface wettability of the PMMA-BC samples. The static sessile drop method is employed to determine the contact angle using a fabricated contact angle measuring instrument. The contact angles are measured on five randomly chosen regions of each sample using distilled water droplets. As previously noted, samples of $\phi 10 \pm 2$ mm in size are made. Phosphate-buffered saline, which has a pH of 7.4, is used to harden the samples. SiC papers of 800 and 1200 grits are used to polish the bone cement samples to achieve a flat smooth surface. Before testing, the samples are dried for 24 hours after being sonicated for 30 min in an ultrasonic cleaner bath.

4.1. Volumetric Shrinkage. The volumetric shrinkage of the prepared nanocomposite bone cement is investigated after curing to observe the effect of MWCNTs on PMMA-BC volume change. The samples with different MWCNTs wt. % having a diameter of 6 mm and thickness of 12 mm are prepared and allowed to harden, as mentioned earlier. The samples are dried for 24 hours, and the final volume is estimated as per ASTM D 792–20 by measuring densities using Archimedes' principle with a Mettler electronic balance—ME204. Standard specimen is used to calibrate the instrument. The density accuracy of ±0.0001 g/cc is obtained using this method. The volumetric shrinkage is calculated using Equation (1),

$$\begin{aligned} \%\text{Volumetric Shrinkage} &= -\left(\frac{v_f - v_i}{v_i}\right)100 \\ &= -\left(\frac{\rho_m - \rho_p}{\rho_p}\right)100, \end{aligned} \tag{1}$$

where v_i is the initial volume (mL), v_f is the final volume (mL), ρ_m is the density of the monomer, (g/cc), and ρ_p is the density of the polymer (g/cc).

4.2. Fourier Transform Infrared Spectroscopy (FTIR). As previously stated, $\phi 10 \times 2$ mm samples are prepared for FTIR characterization. The samples are air dried for 24 hours before being powdered with an agate mortar and pestle. A Bruker Alpha II FTIR spectrophotometer is used to examine the functional groups of the pulverized composite. In transmission mode, spectra of the composite are observed in the spectral range of 4000–400 cm^{-1} to determine the chemical interactions between the MWCNTs and PMMA.

4.3. Electron Microscopy. The nanocomposite bone cement specimens are observed for morphology by using scanning electron microscopy (SEM) (JEOL 6500, JSM) at a working voltage of 5.0 kV and 4-Torr vacuum pressure. The prepared samples for SEM are dried for 24 hours and then polished using SiC paper (220–2400 grits), and they are sputter coated. Energy dispersive spectroscopy is used to investigate the elemental composition of the composite bone cement.

The powdered samples of nanocomposite bone cement are studied for morphology at the MWCNT–PMMA interphase using transmission electron microscopy (TEM)–HRTEM (JEOL/JEM 2100, Japan) having a point resolution of 0.23 nm operated at 120 kV.

4.4. In Vitro Bioactivity. The formation of apatite in the SBF has been used as an indication that an orthopedic material is bioactive. Samples ($n = 3$) of uniform size (8×2 mm) are examined for bioactivity by submerging them in SBF. Tris/HCl is added to set the pH of the solution as 7.4. The SBF-immersed samples are incubated at 37°C for a period of 7,

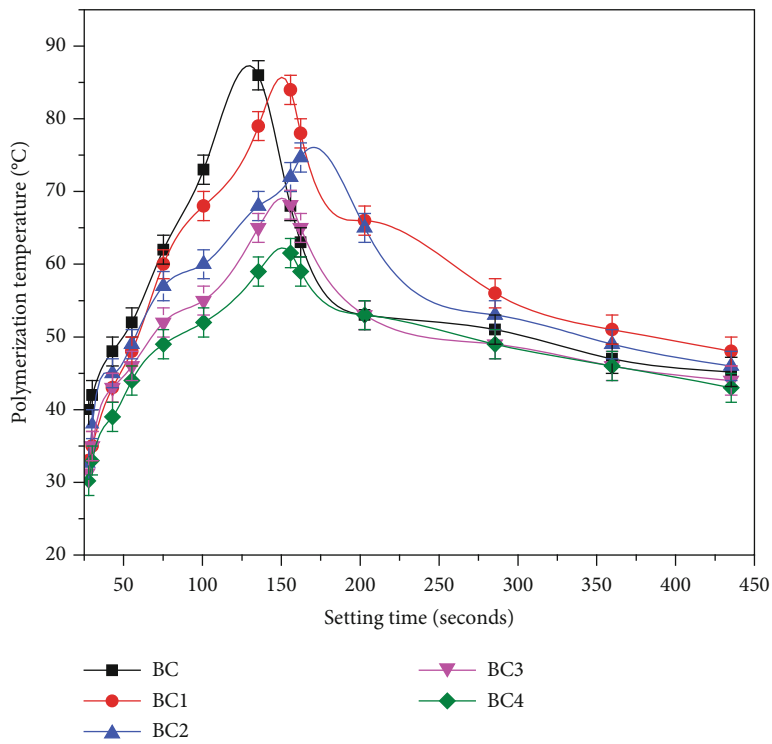

Figure 1: Setting time v/s polymerization temperatures.

14, and 21 days. After the designated incubation period, samples are rinsed with deionized water to eliminate adsorbed minerals and dried; then, SEM and EDS are analyzed for apatite deposition.

4.5. Statistical Analysis. The data for polymerization temperature, setting time, and contact angle are statistically analyzed using a two-sample t-test. To illustrate the results, the mean standard deviation is employed. The level of statistical significance is set at $p < 0.05$.

5. Results and Discussion

5.1. Thermal Characterization. The setting time concerning the polymerization temperature for different bone cement compositions is shown in Figure 1. The maximum polymerization temperature (T_{max}) is reduced for all compositions of the prepared composites. The maximum (84°C) and minimum (61°C) values of T_{max} are recorded for 0.1 and 0.7 wt. % of MWCNT loading, respectively. The temperature evolution of the PMMA-BC reached 86°C, whereas the inclusion of 0.7 wt.% MWCNTs reduced the peak polymerization temperature to 61°C in 160 seconds.

The variation of peak polymerization temperature (T_{max}) for different bone cement compositions with varying MWCNT loading is shown in Figure 2. The addition of 0.1, 0.3, 0.5, and 0.7 wt. % MWCNT to PMMA-BC resulted in a decrease of T_{max}. This decrease in T_{max} is influenced by the thermal conductivity of MWCNT, which is reported as 3000 W/mK [20]. Also, the MWCNTs within the PMMA matrix are observed to exhibit chemical interaction because of the -COOH functional group and physical interaction due to the large surface area during the polymerization reaction [15]. These interactions helped to dissipate the heat energy produced during polymerization.

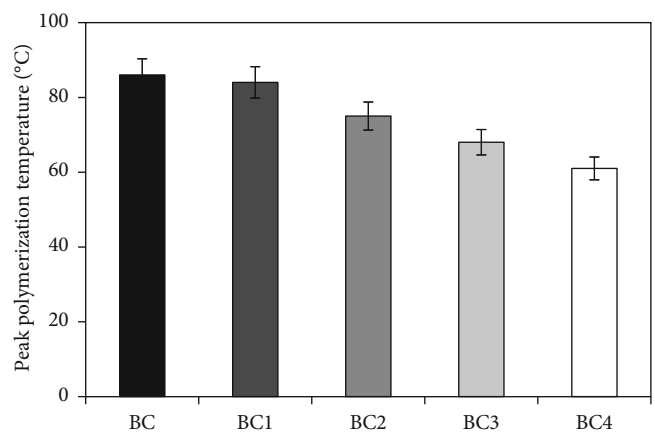

Figure 2: Variation in the peak polymerization temperature of composite bone cement.

TEM analysis is carried out to explore PMMA-MWCNT physical interaction and morphology of the nanocomposite particles. The TEM pictures, Figure 3(a) and 3(b), of the 0.7 wt. % MWCNT-loaded composite bone cement powder show that the agglomerated particles are observed as in the shape of beads and are about 75 nm in size. The TEM pictures also show the well-dispersed MWCNTs surrounded by PMMA particles, which ensures the physical interphase between PMMA-MWCNT.

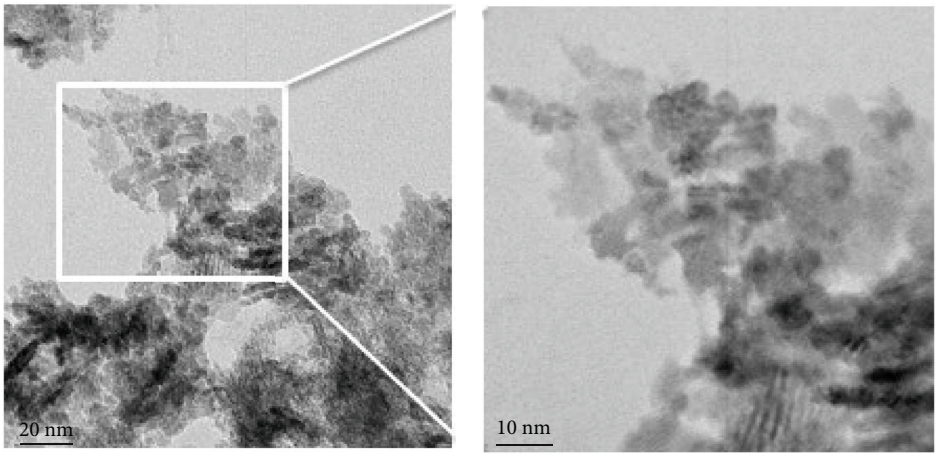

(a) (b)

Figure 3: TEM images of PMMA with 0.7 wt. % MWCNT bone cement. (a) 20 nm scale and (b) 10 nm scale.

The heat dissipated during polymerization must be reduced to avoid thermal damage to the surrounding cells during *in situ* application. Berman et al. [21] reported that decreasing the operative temperature of PMMA-BC below 70°C might avoid severe bone necrosis at the bone and cement interface. Here, the percentage of damage to the bone cells is calculated as a damage function $D(T)$, which is defined as the time required to cause bone cell necrosis [22]. For instance, bone cell necrotizes and damage reaches 100% when it receives 60°C for 410 seconds. The amount of damage per second is calculated using Equation (2).

$$D(T) = \frac{1}{410} \times 100. \quad (2)$$

The thermal damage for the control, 0.1, 0.3, 0.5, and 0.7 wt. % MWCNT-loaded composite is noted as 0.73%, 0.64%, 0.61%, 0.63%, and 0.65%, respectively. It is observed that among the composites, thermal damage is minimal for 0.3 wt.% and maximum for 0.7 wt. % MWCNT loading. The heat dissipation duration is observed to influence thermal damage minimization. From this, it is evident that the curing kinetics of the PMMA-BC is affected by the inclusion of MWCNTs. The curing kinetics involves the setting time and duration of the polymerization reaction [23]. The increase in setting time provides additional time for processing/working during bone cement mixing. PMMA cement with varying amounts of MWCNTs and their respective setting times are summarized in Table 3. The initial and final setting times for PMMA-BC are found to be 605 ± 12 and 612 ± 15 seconds, respectively. The percentage increase in setting time for the prepared samples compared with PMMA-BC is found to be 0.65%, 1.15%, 2.30%, and 2.95% for BC1, BC2, BC3, and BC4, respectively.

The uniformly dispersed -COOH-functionalized MWCNTs are primarily responsible for the slow polymerization reaction (setting time) by physically impeding cross-linking of the polymer chains. The chemical functionalization of MWCNTs is found to improve the chemical interphase,

Table 3: Percentage variation in setting time and contact angle.

Bone cement samples	Setting time %↑		Contact angle %↓
	Initial	Final	
BC1	0.82↑	0.49↑	1.25↓
BC2	1.32↑	0.98↑	2.95↓
BC3	2.47↑	2.12↑	5.85↓
BC4	2.97↑	2.94↑	7.45↓

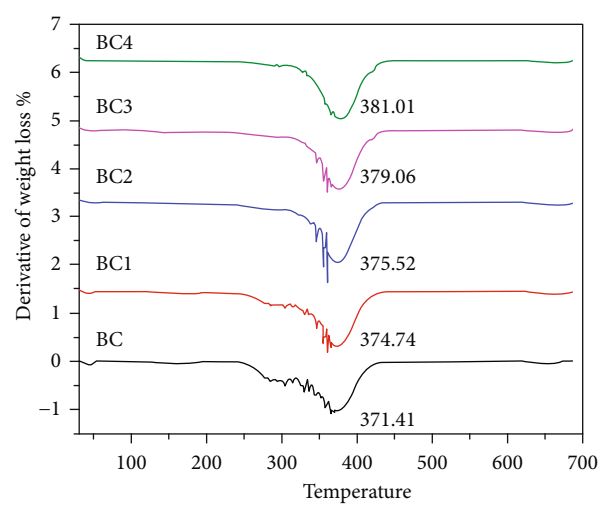

Figure 4: Derivative of TGA curves of composite bone cement.

and it is found to be the most predominant factor for a reduction in the peak polymerization temperature [24].

The derivative thermogravimetric analysis (DTG) of PMMA/MWCNTs composites is illustrated in Figure 4. The DTG plot revealed that the addition of MWCNTs delayed the thermal degradation of PMMA and increased its thermal stability. The degradation temperature of PMMA was determined as 371.41°C, which is increased by 0.89%,

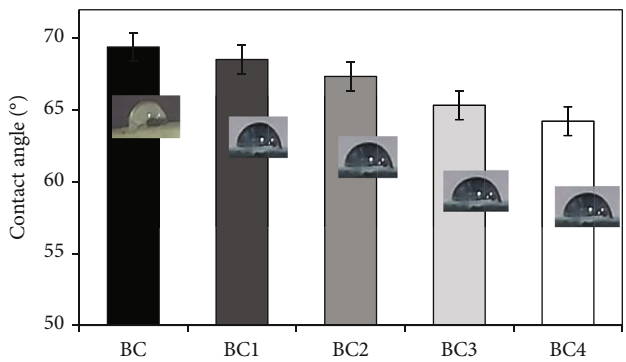

Figure 5: Contact angle of water droplets on composite bone cement.

1.1%, 2.1%, and 2.58% for 0.1, 0.3, 0.5, and 0.7 wt. % MWCNTs, respectively. This increase in thermal stability prevents the breakdown of PMMA beads of thickness 4–10 mm due to heat stresses when they are placed in the gap between the implant and bone [25].

6. Contact Angle

The contact angles for the distilled water droplets measured on the cement surface are presented in Figure 5. Water droplet photos revealed that the PMMA and PMMA/MWCNT composite bone cement surfaces are hydrophilic. However, nanocomposite bone cement samples have demonstrated a substantially lesser contact angle compared to PMMA-BC ($p < 0.04$). The contact angle for PMMA-BC is found as 69.40°. The percentage decrease in the contact angle for the composite bone cement samples is 1.25%, 2.95%, 5.85%, and 7.45% for BC1, BC2, BC3, and BC4, respectively. The contact angle is used to determine the surface energy (S_E) of the composite bone cement using Equation (3).

$$S_E = S_{\mathrm{EWA}} \cos\theta \frac{J}{\mathrm{m}^2}, \tag{3}$$

where S_{EWA} represents the surface energy between pure water and air at ambient temperature and pressure (72.8 mJ/m^2 at 20°C) [19] and "θ" represents the static contact angle. The percentage increase in surface energy for composite bone cement samples is found to be 4.03%, 9.45%, 18.59%, and 23.58% for BC1, BC2, BC3, and BC4, respectively.

Thus, it can be observed from the results of contact angle and surface energy that the reinforcement of -COOH-functionalized MWCNTs increased the wettability by decreasing hydrophobicity. Further, this facilitated the liquid monomer to wet the nanofillers effectively and improves the surface adhesion of the composite bone cement. The increase in surface wettability can also be verified by comparing it to the *in vitro* bioactivity studies. This improved surface wettability is found to increase mineral absorption and cell adhesion in simulated body fluid solution [19].

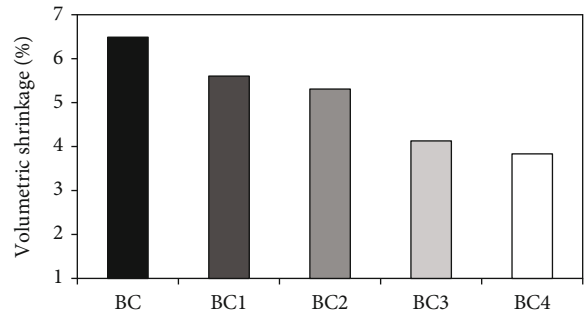

Figure 6: Volumetric shrinkage of composite bone cement.

Table 4: Volumetric shrinkage of the bone cement composition.

Material	% increase in density	% increase in the final volume	% reduction in volumetric shrinkage
BC1	4.06	0.94	13.63
BC2	4.40	1.26	18.18
BC3	6.10	2.52	36.36
BC4	7.03	2.83	40.90

7. Volumetric Shrinkage

The volume contraction of the prepared bone cement samples after curing is shown in Figure 6 as a volumetric shrinkage percentage. The initial volume (v_i) is calculated from the mould dimensions ($v_i = 0.339$ mL), and Archimedes' principle is used to measure the final volume (v_f) by measuring density. The volumetric shrinkage for PMMA-BC is found to be 6.49% after curing, whereas for nanocomposite bone cement it is observed to be 5.60%, 5.31%, 4.13%, and 3.83% for BC1, BC2, BC3, and BC4, respectively.

Table 4 summarizes the density variations, dimensional changes, and reduction in shrinkage for the cured nanocomposite samples. The volume shrinkage of PMMA/MWCNT composite bone cement is observed to be 13.63%, 18.18%, 36.36%, and 40.90% for BC1, BC2, BC3, and BC4, respectively, compared with PMMA-BC. The maximum reduction in volumetric shrinkage occurred in BC4, which indicates that the volumetric shrinkage is directly proportional to the MWCNT concentration.

Volumetric shrinkage is an extrinsic property inversely proportional to the density of the polymer (Equation (1)). The density of MMA was specified by the manufacturer as 0.938-0.940 g/cc before curing. However, the density of PMMA-BC is noted as 1.18 g/cc after curing. The density of the composite bone cement is increased with the reinforcement of MWCNTs [26]. This increased density is the consequence of the reduction in the number of cross-connections between MWCNTs and the PMMA matrix [27]. The rise in density is observed to increase the molecular weight, and it leads to a reduction in volumetric shrinkage [28]. It is observed that the polymerization shrinkage is extensive in the viscous phase of the cement curing. The volumetric shrinkage may be attributed to polymerization

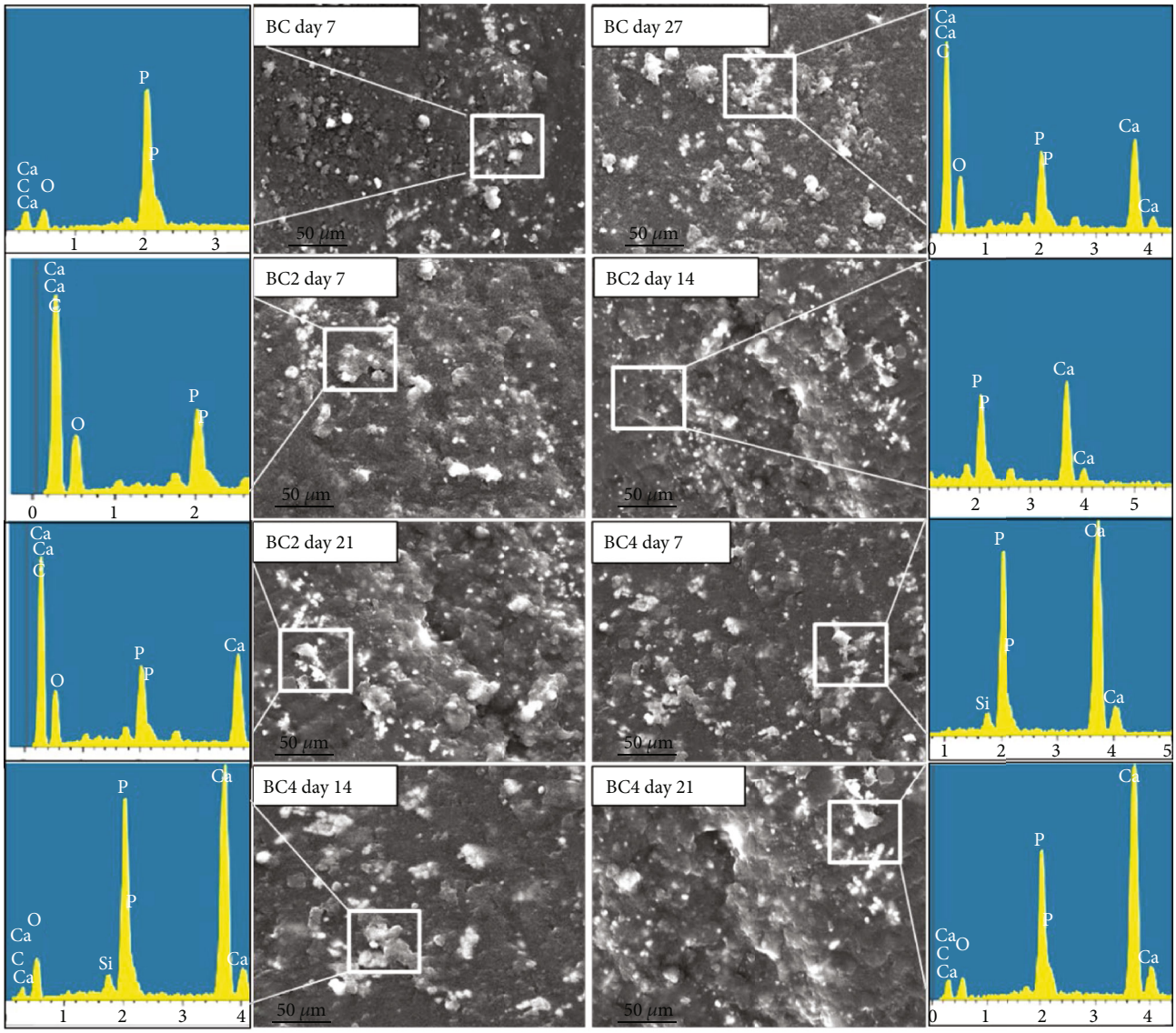

Figure 7: SEM pictures with boxed EDS spectra show bone cement biomineralization in SBF.

shrinkage, thermal contraction after the exothermic reaction, and cement density [29]. Another important parameter responsible for volume shrinkage is the mixing method, and it is a fact that the bone cement shrinks in a confined environment forming pores at the cement implant interface anywhere during polymerization. In this study, the hand mixing method is used, during which some shrinkage occurred at the pore sites, which is notable in the volume reduction. Therefore, better mechanical properties can be expected at the cement-implant interface with lower volumetric shrinkage.

7.1. In Vitro Bioactivity. The nanocomposite bone cement sample disks containing 0.3 and 0.7 wt. % MWCNTs are subjected to *in vitro* bioactivity studies. Because of its intended application in bone tissue, bone cement requires bioactivity to ensure a reliable bonding of PMMA-BC right after the surgery. SEM images of the composite bone cement sample after soaking in SBF for 7, 14, and 21 days (Figure 7) revealed that the nucleation of primary apatite has a nodular structure. The samples are subjected to EDS analysis on the selected area and the deposition of Ca and P elements are observed. The increased intensities of Ca and P peaks are observed on the sample surface, confirming the deposition of mineral phases through SEM-EDS spectra [21]. The increased deposition with grown individual nuclei and a reticular layer composed of secondary apatite (numerous flakes) due to coalescence are observed after 21 days. Despite certain deposits being visible on the surface of the sample, the EDS examination after 7 days of immersion revealed the absence of Ca or P elements.

FTIR is used to identify functional groups and characterize the chemical structures based on the interaction of infrared radiation with matter. The peaks observed in the transmission spectra are depicted in Figure 8. The peaks observed in the range of 1395–1440 cm^{-1} correspond to the

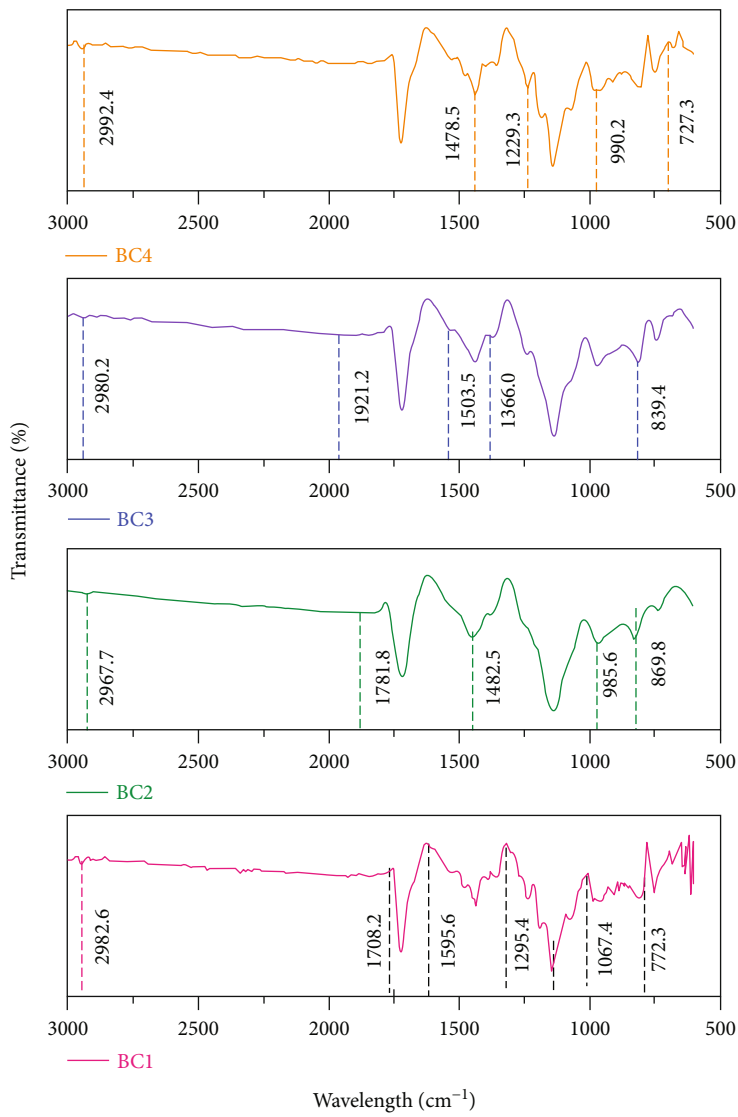

Figure 8: FTIR spectra of the PMMA composite bone cement.

O–H bond. The peaks observed from 815 to 930 cm^{-1} can be assessed to the valence C=O bond. The CC stretching vibration bands of MWCNT are found at the peaks of 1503 and 1482 cm^{-1}. The sharp peaks could be attributed to the existence of the -COOH functional groups. These results are observed to indicate the physical bonding between the MWCNT-COOH and PMMA matrix, which has influenced the nanocomposite for more wettability. Thus, the enhanced bioactivity is observed after 21 days of immersion, and it is mainly due to the incorporation of -COOH-functionalized MWCNTs.

8. Discussion

In this study, it is shown that adding a small amount of carboxyl functionalized MWCNT enhanced the bioactivity and cement characteristics of proprietary Simplex P bone cement. The decrease in polymerization temperature, reduction in volumetric shrinkage, and increased surface wettability are observed after MWCNT-COOH incorporation. The homogeneous distribution of MWCNT within the PMMA-BC matrix is considered an important parameter for the enhancements in cement properties [30]. It is possible that the -COOH groups attached to the MWCNTs, which are negatively charged, contributed to the uniform dispersion [31]. The existence of uniformly dispersed MWCNT-COOH inside the PMMA-BC matrix leads to a decrease in agglomerations. Agglomerations can further contribute as a site for the stress concentration, leading to crack initiation and early fracture of the cement mantle [16, 32]. Subsequently, the uniform dispersion would also expedite a higher amount of chemical interaction between the MWCNT-COOH and the PMMA-BC matrix, resulting in effective stress transfer. Therefore, the evenly distributed MWCNTs in the novel nanocomposite bone cement could be able to prolong the functionality of the existing PMMA-BC.

This study found the reduction in Simplex P bone cement's exothermic polymerization reaction, which would

reduce thermal shrinkage-induced residual stresses [33]. Incorporating a 0.1-0.7 wt. % of MWCNT-COOH helped to dissipate heat from the nanocomposite bone cement's exothermic polymerization reaction. Interestingly, the MWCNT-COOH used in this study has a thermal conductivity of more than 3000 W/mK (Platonic data sheet), indicating that it acted as a heat sink in the nanocomposite to dissipate the heat produced during polymerization. The addition of 0.3 wt. % MWCNT reduced the thermal damage $D(T)$ per second by 16% (maximum) compared with PMMA bone cement. Ormsby et al. [30] also reported that the incorporation of MWCNTs into acrylic bone cement has reduced the peak polymerization temperature by 34% and the thermal necrosis index values are significantly reduced at ≥44°C and ≥55°C (28% and 27%) compared to PMMA bone cement. In this study, it can be noted that the thermal damage is minimum at 0.3 wt. %, and it is also lesser than the thermal necrosis index values which were observed from the published work. The slower rate of polymerization and lower $T_{\max}$ decreased the exposure time of bone tissue to high temperatures. This helps to reduce the damage function $D(T)$ and provides adequate workability in preparing and placing the cement mantle. The DSC analysis carried out in this study revealed an increase in thermal stability, which would also support this observation.

The workability of any bone cement depends on its initial and final setting time. Shaping and filling of bone cement are required enough initial setting time. Disturbing the prepared cement until it hardens will cause fractures and weaken it. It needs the shortest final setting time to avoid wound closure delays. The initial setting time shows the end of the workability of cement after wetness, whereas the final setting time signifies the cement hardening. Ormsby et al. [16] observed a 3–24% increase in setting time when 0.1 wt. % of MWCNTs incorporated into PMMA-BC. However, these variations were observed for different methods of incorporation and functionalized/nonfunctionalized groups. In this study, the setting times for the prepared composite bone cement samples are well within the admissible setting time for orthopedic applications [34].

Bone cement shrinkage is another aspect hypothesized to contribute to implant loosening. In this study, the volumetric shrinkage for PMMA-BC is found to be 6.49% after curing, whereas for BC1, BC2, BC3, and BC4, it is observed to be 5.60%, 5.31%, 4.13%, and 3.83%, respectively. Gilbert et al. [9] also reported that volumetric shrinkage for Simplex P bone cement as a result of density variation, due to the exothermic polymerization, was between 5.1% and 6.5%, depending on the mixing method employed and the type of cement. Jasty et al. [35] discovered cracks emanating from the inner surface of the cement mantle and indicated that they were caused by hoop stresses due to acrylic cement shrinkage during polymerization. Hence, the reduction in volumetric shrinkage observed in this study is better compared to the previous results and helps in avoiding cracks by reducing the hoop stresses.

The wettability of the cement helps in the adsorption of more proteins and minerals leading to enhance binding sites for cell attachment on the cement surface. In this study, the wettability is calculated using the contact angle of bone cement with distilled water droplets. The addition of MWCNTs decreased the contact angle and increased the wettability. The surface energy of PMMA-BC is increased to 31.64 mJ/m^2 by the addition of 0.7 wt. % MWCNT-COOH, whereas for the PMMA bone cement, it is observed to be 25.60 mJ/m^2. Jayasree and Sampath Kumar [19] also studied the effect of wettability in improving the bioactivity of commercially available orthopedic bone cement, where the surface energy of Simplex P bone cement is measured to be 25.67 mJ/m^2 with the addition of 25 wt. % calcium-deficient hydroxyapatite.

The current research has a few limitations that are acknowledged. Firstly, just one type of cement (Simplex P) was employed because other varieties with various chemical compositions and viscosities could produce different results. Since total hip and knee replacements is using Simplex P as one of the most popular bone cement formulations, this particular cement was chosen [36]. Secondly, the mechanical properties of the MWCNT-loaded cement were not evaluated, although they play a significant role in *in vivo* cement failure. Mechanical characterization is found to be out of the scope of the current investigation. Thirdly, only *in vitro* bioactivity tests were carried out, but antimicrobial studies would have revealed distinct effects. However, *in vitro* testing greatly simplifies the *in vivo* situation, and care must be given when interpreting biocompatibility data.

9. Conclusion

The results of earlier research have been expanded in this study to improve the cement properties and thermal characteristics of commercially available Simplex P bone cement by incorporating MWCNT-COOH using the geometric dilution method. The influence of 0.1, 0.3, 0.5, and 0.7 wt. % MWCNTs on cement properties and *in vitro* bioactivity studies of the polymerizing and cured cement are examined. The uniform distribution of MWCNT-COOH was assumed to reduce the exothermic polymerization reaction. Here, the maximum reduction in the peak polymerization temperature of 29% is found in the BC4 samples. This reduction in $T_{\max}$ is influencing the setting time of the samples, and for BC4, the setting time is prolonged by 2.94%. The increase in surface wettability (23.58%↑) and setting time (2.94%↑) and decrease in maximum polymerization temperature (29.06%↓) and volumetric shrinkage (40.9%↓) are observed for MWCNT-loaded composite bone cement relative to the control cement (without MWCNTs). The *in vitro* bioactivity test results indicate that the mineral deposition is observed to be proportional with MWCNTs wt.% which is increased wettability of the cement. These findings imply that *in vitro* and *in vivo* biocompatibility studies of -COOH-functionalized MWCNT-loaded with PMMA-BC may be tested for their feasibility to understand the clinical usage complications.

Data Availability

The data used to support the results of this study are included in the article.

Conflicts of Interest

The authors declare that they have no known competing financial interests or personal connections that could have influenced the findings of this study.

Acknowledgments

The authors are thankful to the Siddaganga Institute of Technology, Tumakuru, for providing a research facility, the Visvesvaraya Technological University, Belagavi, Karnataka, India, for supporting this research work, and the Biotechnology Department, Siddaganga Institute of Technology, Tumakuru, and the BioEdge Solutions, Peenya, Bengaluru 560058, for supporting in conducting biocompatibility studies. The authors appreciate the support from the Seenu Atoll School, Maldives, for the preparation of the manuscript. The authors thank the generous support from the Department of Applied Sciences (Nanotechnology), Visvesvaraya Technological University, Center for Post Graduate Studies, Bengaluru Region, Muddenahalli, Chikkballapura 562101, Karnataka, India, for supporting the characterizations. The authors thank the Vision Group on Science and Technology, Department of Electronics, Information Technology, Biotechnology and Science & Technology, Government of Karnataka, the Advanced Composites Division, CSIR-National Aerospace Laboratories, Bengaluru 560017, Karnataka, India, and the Center of Applied Research and Nanotechnology, Siddaganga Institute of Technology, Tumakuru, for conducting this research work.

References

[1] L. Hasandoost, O. Rodriguez, A. Alhalawani et al., "The role of poly(methyl methacrylate) in management of bone loss and infection in revision total knee arthroplasty: A Review," *Journal of Functional Biomaterials*, vol. 11, no. 2, p. 25, 2020.

[2] M. E. Zapata, C. D. Tovar, and J. H. Hernandez, "The role of chitosan and graphene oxide in bioactive and antibacterial properties of acrylic bone cements," *Biomolecules*, vol. 10, no. 12, p. 1616, 2020.

[3] D. O. Ko, S. Lee, K. T. Kim, J. Il Lee, J. W. Kim, and S. M. Yi, "Cement mantle thickness at the bone cement interface in total knee arthroplasty: comparison of PS150 RP and LPS-flex knee implants," *Knee Surgery & Related Research*, vol. 29, no. 2, pp. 115–121, 2017.

[4] A. Rajan, V. Thirunarayanan, D. R. Ramprasath, J. D. V. Kumar, and K. Muthulingam, "Vertebroplasty in osteoporotic vertebral fractures: technical considerations and complications," *Journal of Orthopedics and Joint Surgery*, vol. 2, no. 1, pp. 17–21, 2020.

[5] N. Dunne, J. Clements, and J.-S. Wang, "Acrylic cements for bone fixation in joint replacement," in *Joint Replacement Technology*, pp. 212–256, Elsevier, 2014.

[6] P. A. Revell, "Biological causes of prosthetic joint failure," in *Joint Replacement Technology*, pp. 299–371, Elsevier, 2021.

[7] R. Vaishya, M. Chauhan, and A. Vaish, "Bone cement," *Journal of Clinical Orthopaedics and Trauma*, vol. 4, no. 4, pp. 157–163, 2013.

[8] N. Dunne and W. Ross, "MWCNT used in orthopaedic bone cements," in *Carbon Nanotubes - Growth and Applications*, IntechOpen, 2011.

[9] J. L. Gilbert, J. M. Hasenwinkel, R. L. Wixson, and E. P. Lautenschlager, "A theoretical and experimental analysis of polymerization shrinkage of bone cement: a potential major source of porosity," *Journal of Biomedical Materials Research*, vol. 52, no. 1, pp. 210–218, 2000.

[10] A. De Mori, E. Di Gregorio, A. P. Kao et al., "Antibacterial PMMA composite cements with tunable thermal and mechanical properties," *ACS Omega*, vol. 4, no. 22, pp. 19664–19675, 2019.

[11] J. Slane, J. Vivanco, W. Rose, H.-L. Ploeg, and M. Squire, "Mechanical, material, and antimicrobial properties of acrylic bone cement impregnated with silver nanoparticles," *Materials Science and Engineering: C*, vol. 48, pp. 188–196, 2015.

[12] K. Letchmanan, S. C. Shen, W. K. Ng et al., "Mechanical properties and antibiotic release characteristics of poly(methyl methacrylate)-based bone cement formulated with mesoporous silica nanoparticles," *Journal of the Mechanical Behavior of Biomedical Materials*, vol. 72, pp. 163–170, 2017.

[13] F. Pahlevanzadeh, H. R. Bakhsheshi-Rad, A. F. Ismail, M. Aziz, and X. B. Chen, "Development of PMMA-Mon-CNT bone cement with superior mechanical properties and favorable biological properties for use in bone-defect treatment," *Materials Letters*, vol. 240, pp. 9–12, 2019.

[14] N. Baig, I. Kammakakam, and W. Falath, "Nanomaterials: a review of synthesis methods, properties, recent progress, and challenges," *Materials Advances*, vol. 2, no. 6, pp. 1821–1871, 2021.

[15] S. Soleymani Eil Bakhtiari, H. R. Bakhsheshi-Rad, S. Karbasi et al., "Polymethyl methacrylate-based bone cements containing carbon nanotubes and graphene oxide: an overview of physical, mechanical, and biological properties," *Polymers*, vol. 12, no. 7, p. 1469, 2020.

[16] R. Ormsby, T. McNally, C. Mitchell, and N. Dunne, "Incorporation of multiwalled carbon nanotubes to acrylic based bone cements: effects on mechanical and thermal properties," *Journal of the Mechanical Behavior of Biomedical Materials*, vol. 3, no. 2, 2010.

[17] K. D. Patel, R. K. Singh, and H.-W. Kim, "Carbon-based nanomaterials as an emerging platform for theranostics," *Materials Horizons*, vol. 6, no. 3, pp. 434–469, 2019.

[18] S. Tantavisut, J. Leanpolchareanchai, and A. Wongrakpanich, "Influence of chitosan and chitosan oligosaccharide on dual antibiotic-loaded bone cement: in vitro evaluations," *PLoS One*, vol. 17, no. 11, article e0276604, 2022.

[19] R. Jayasree and T. Sampath Kumar, "Acrylic cement formulations modified with calcium deficient apatite nanoparticles for orthopaedic applications," *Journal of Composite Materials*, vol. 49, no. 23, pp. 2921–2933, 2015.

[20] G. Lewis, "Properties of nanofiller-loaded poly (methyl methacrylate) bone cement composites for orthopedic applications: a review," *Journal of Biomedical Materials Research Part B: Applied Biomaterials*, vol. 105, no. 5, pp. 1260–1284, 2017.

[21] A. T. Berman, J. S. Reid, D. R. Yanicko, G. C. Sih, and M. R. Zimmerman, "Thermally induced bone necrosis in rabbits," *Clinical Orthopaedics and Related Research*, vol. 186, pp. 284–292, 1984.

[22] H. Fukushima, Y. Hashimoto, S. Yoshiya et al., "Conduction analysis of cement interface temperature in total knee

arthroplasty," *Kobe Journal of Medical Sciences*, vol. 48, no. 1–2, pp. 63–72, 2002.

[23] R. Ormsby, T. McNally, C. Mitchell, and N. Dunne, "Influence of multiwall carbon nanotube functionality and loading on mechanical properties of PMMA/MWCNT bone cements," *Journal of Materials Science. Materials in Medicine*, vol. 21, no. 8, pp. 2287–2292, 2010.

[24] R. Ormsby, T. McNally, C. Mitchell et al., "Effect of MWCNT addition on the thermal and rheological properties of polymethyl methacrylate bone cement," *Carbon*, vol. 49, no. 9, pp. 2893–2904, 2011.

[25] S. K. Smart, A. I. Cassady, G. Q. Lu, and D. J. Martin, "The biocompatibility of carbon nanotubes," *Carbon*, vol. 44, no. 6, pp. 1034–1047, 2006.

[26] B. Pei, W. Wang, N. Dunne, and X. Li, "Applications of carbon nanotubes in bone tissue regeneration and engineering: superiority, concerns, current advancements, and prospects," *Nanomaterials*, vol. 9, no. 10, p. 1501, 2019.

[27] H. Kim, B. Goh, S. Lee, K. Lee, and J. Choi, "Computational study on interfacial interactions between polymethyl methacrylate-based bone cement and hydroxyapatite in nanoscale," *Applied Sciences*, vol. 11, no. 7, p. 2937, 2021.

[28] N. Dunne, A. Tzagiollari, M. Sahebalzamani, and T. J. Dunne, "Acrylic cements for bone fixation in joint replacement," in *Joint Replacement Technology*, pp. 213–262, Elsevier, 2021.

[29] A. Alnazzawi and D. C. Watts, "Simultaneous determination of polymerization shrinkage, exotherm and thermal expansion coefficient for dental resin-composites," *Dental Materials*, vol. 28, no. 12, pp. 1240–1249, 2012.

[30] R. W. Ormsby, M. Modreanu, C. A. Mitchell, and N. J. Dunne, "Carboxyl functionalised MWCNT/polymethyl methacrylate bone cement for orthopaedic applications," *Journal of Biomaterials Applications*, vol. 29, no. 2, pp. 209–221, 2014.

[31] M. Chao, Y. Li, G. Wu, Z. Zhou, and L. Yan, "Functionalized multiwalled carbon nanotube-reinforced polyimide composite films with enhanced mechanical and thermal properties," *International Journal of Polymer Science*, vol. 2019, Article ID 9302803, 12 pages, 2019.

[32] B. Marrs, R. Andrews, T. Rantell, and D. Pienkowski, "Augmentation of acrylic bone cement with multiwall carbon nanotubes," *Journal of Biomedial Materials Research Part A*, vol. 77A, no. 2, pp. 269–276, 2006.

[33] N. J. Dunne and J. F. Orr, "Curing characteristics of acrylic bone cement," *Journal of Materials Science. Materials in Medicine*, vol. 13, no. 1, pp. 17–22, 2002.

[34] E. Şahin, "Calcium phosphate bone cements," in *Cement Based Materials*, INTECH, 2018.

[35] M. Jasty, W. Maloney, C. Bragdon, D. O'Connor, T. Haire, and W. Harris, "The initiation of failure in cemented femoral components of hip arthroplasties," *Journal of Bone and Joint Surgery (British Volume)*, vol. 73-B, no. 4, pp. 551–558, 1991.

[36] S. Kim, A. R. Bishop, M. W. Squire, W. E. Rose, and H.-L. Ploeg, "Mechanical, elution, and antibacterial properties of simplex bone cement loaded with vancomycin," *Journal of the Mechanical Behavior of Biomedical Materials*, vol. 103, article 103588, 2020.

Hindawi
Advances in Polymer Technology
Volume 2023, Article ID 9964610, 10 pages
https://doi.org/10.1155/2023/9964610

Research Article

Effect of Curing Temperature and Time on Mechanical Properties of Vinyl Polymer Material for Sealing Applications in Industry Using Machine Learning Techniques

Sudheer D. Kulkarni,[1,2] **B. Manjunatha**,[3] **U. Chandrasekhar**,[4] **G. K. Siddesh**,[5] **Haiter Lenin**,[6] **and Sujin Jose Arul**[7]

[1]*New Horizon College of Engineering, Visvesvaraya Technological University, Bangalore, India*
[2]*Department of Industrial Engineering and Management, Ramaiah Institute of Technology, Bangalore 560054, India*
[3]*Professor, Department of Mechanical Engg, New Horizon College of Engineering, Bengaluru, Karnataka, India*
[4]*AddWize-Wipro 3D, Bangalore 560058, India*
[5]*ECE Department and Deputy Dean Research, ALVA'S Institute of Engineering and Technology, Moodbidri, DK, Karnataka, India*
[6]*Department of Mechanical Engineering, WOLLO University, Kombolcha Institute of Technology, Kombolcha, Ethiopia Post Box No: 208*
[7]*Department of Automobile Engineering, New Horizon College of Engineering, Bangalore, India*

Correspondence should be addressed to Haiter Lenin; haiter@kiot.edu.et

Received 24 January 2023; Revised 11 March 2023; Accepted 29 April 2023; Published 16 May 2023

Academic Editor: Indran Suyambulingam

A seal is a mechanism or a piece of material that securely shuts a hole so that air, liquid, or other substances cannot enter or exit the system. Seals are an essential component of practically all machinery and engines and have several applications in industry. The development of novel materials for sealing applications is essentially required on these days. In this research, an attempt is made to find the polymer material for the said application. Poly vinyl rubber material has been taken, and the specimens are prepared for testing the tensile properties and hardness. The specimens were prepared by using die with various temperatures and curing time. Sixteen specimens were prepared by changing the curing temperature, curing time, postcuring temperature, and postcuring time. The curing temperature 150°C and 170°C, postcuring temperature 100°C and 50°C, curing time 14 mins and 18 mins, postcuring time 120 mins and 60 mins, and the pressure of 150 kg/cm^2 for all the specimens were maintained. The tensile strength and hardness analysis were done as per the ASTM standard, and it was found that the specimen prepared on 150°C curing temperature, 18 min curing time, 50°C postcuring temperature, and 120 min postcuring time provides the higher tensile strength. DOE analysis is also done to determine the best values of the factors impacting the mechanical characteristics of the seal material. Simple regression analysis is used to find the influence of curing temperature and curing time on the tensile strength and hardness for every 1°C temperature rise and 1 sec curing time.

1. Introduction

A versatile and cost-effective material, "polyvinyl chloride (PVC, or vinyl) is used in plumbing and siding, blood bags, tubing, wire and cable insulation, windshield system components, and more, in the building and construction, health care, electronics, automobile industries, and others." Vinyl can range in hardness from plastic wrap to industrial pipes to thin and flexible wall covering. Additionally, it can be completely translucent or colored to any desired shade. The majority of vinyl produced is employed in long-term building and construction applications—roughly 75%. PVC/vinyl is advantageous for environmental protection because of its low greenhouse gas emissions and ability to conserve resources and energy, according to life-cycle studies. Since vinyl is strong and resistant to moisture and

abrasion, it is ideal for cladding, windows, roofs, fences, decks, wall coverings, and flooring. Contrary to some building materials, vinyl is not prone to corrosion, does not need to be painted frequently, and can be cleansed using straightforward cleaning solutions. VTI employs RF welding, also known as dielectric welding. This is a procedure that uses radio frequency waves to molecularly fuse two films or textiles together, forming a hermetic connection [1]. This is a procedure with several names, and you may have heard one of them: dielectric sealing, RF sealing, RF welding, and heat sealing [2]. They all refer to the same high-tech approach of connecting thermoplastic sheets that use radio frequency (RF) radiation. RF waves excite the molecules of the materials, causing them to fuse together from the inside out [3, 4]. Depending on your use, it does not leak air, moisture, water, or fuel. High frequency radio waves are used to heat the material in RF sealing, which is similar to heat sealing [5]. Radio waves (typically between 15 kHz and 70 kHz) cause polymer molecules to vibrate, which generates a significant amount of heat quickly. In this way, RF seals are faster, more consistent, and stronger than conventional heat seals. Because exposed seals are transparent and flawless, this procedure is also suitable for them [6]. It is more expensive and requires more energy to perform RF sealing than a traditional heat seal; nevertheless, the field of RF sealing is rapidly evolving and becoming more efficient [7]. The use of RF sealing to polyvinyl chloride or vinyl fabric is known as PVC sealing. Because of its flexibility and polarity, PVC is an excellent choice for RF heat sealing. It is also ideal for generating hermetic seals and waterproofing applications. PVC sealing is a high-frequency welding procedure that allows PVC (polyvinyl chloride) to be applied to a soft fabric or film [8, 9]. PVC is used in waterproofing textiles because it is lightweight, resilient, and abrasion resistant. Because of its high dipolar moment and other chemical features, PVC is regarded as a suitable material for radio frequency welding [10, 11]. PVC welding is a comparable procedure in which PVC is used as the material of choice when welding textiles, plastics, or other materials together. Another name for RF sealing is HF welding, which is used interchangeably [12, 13]. Both words refer to the method of joining two thermoplastic polymers using high-frequency radio waves. This procedure is also known as RF heating, HF heating, and dielectric sealing.

PVC sheets and boards, in particular, can benefit from the strong seams produced by RF welding [14, 15]. The products of the PVC sealing technique can be flexible and elastic while yet having shear strength and durability [16]. PVC is a versatile and cost-effective material in and of itself. Its primary advantages are as follows:

Electrical insulation: because PVC has a high dielectric strength, it is an excellent insulation material for electrical purposes. Abrasion, weathering, oily residues, greases, chemical degradation, corrosion, and pressure all resist PVC [17, 18]. Since durability is a primary requirement for many outdoor products, it makes sense that it is the material of choice. Because of their high chlorine content, PVC goods are self-extinguishing [19]. This offers a great fire resistance and mechanical qualities.

High performance at a low cost: the durability and other features listed above enable for completed goods that require little maintenance and replacement in a variety of environmental circumstances [20]. Because PVC is abrasion-resistant, lightweight, and durable, it is the material of choice for completed items that will be subjected to weathering or hard use.

Poly vinyl seal material is being evaluated experimentally for its mechanical characteristics in relation to process factors. The particular aims, technique to be used to achieve the objectives, and possible outcomes are detailed in the following sections. Dong et al. [21] examined the effect of poly vinyl alcohol/aluminum microcapsule expansion agents on cement-based drilling sealing materials, and the effect of delayed expansion on mechanical strength, porosity, and pore connectivity of the sealing material is quantitatively examined using uniaxial compression and NMR experiments. Ethylene-propylene diene monomer rubber was proposed as a viable option for recycling end-of-life poly vinyl chloride foams by Mahmood et al. [22]. The effects of high-pressure processing on the properties of multilayer flexible packaging are made of polyamide and ethylene vinyl alcohol. The findings of this study have implications for the food packaging industry, particularly in terms of developing packaging materials that can withstand high-pressure processing while maintaining their mechanical and thermal properties [23]. A variety of volumes of ethylene-propylene diene monomer (EPDM) rubber and carbon black (CB) were combined with EoL PVC cross-linked foams at 60°C for 15 minutes. Compression moulding of EPDM-CB-PVC composites was achieved by vulcanizing the rubber mixtures for 20 minutes at 160°C.In tensile tests, EPDM-CB's modulus gradually increased with increasing PVC content, while its elongation-at-break decreased. In the EPDM-CB matrix, PVC particles were dispersed uniformly by SEM. A multidisciplinary approach to biomedical applications using poly vinyl pylori done electro spun nanofibers and bioprinted scaffolds was established by Kurakula et al. and Kibirkštis et al. [24, 25]. The tensile strength of polymer specimens with varying infill density is better than the specimens with single infill density [26–30]. Through the study, it is concluded that the vinyl polymer will be the best alternative for sealing material.

2. Materials and Methods

2.1. Materials. Poly vinyl rubber has been taken as a material for making seal and underwent the mechanical property analysis. The test specimens were prepared in M/s Seal Industries Pvt. Ltd., Bangalore, Karnataka State, India, for conducting the experiment trials. The procured material has the density of 1.05 gm/cm^3.

2.2. Specimen Preparation. The specimens were prepared using die for testing that was shown in Figure 1. The die was preheated to a temperature of 150°C, and the poly vinyl rubber compound was placed on the cavity of die. The die closed, and the pressure of 150 kg/cm^2 was applied on the die, and it was allowed for 14 minutes of curing. In the same

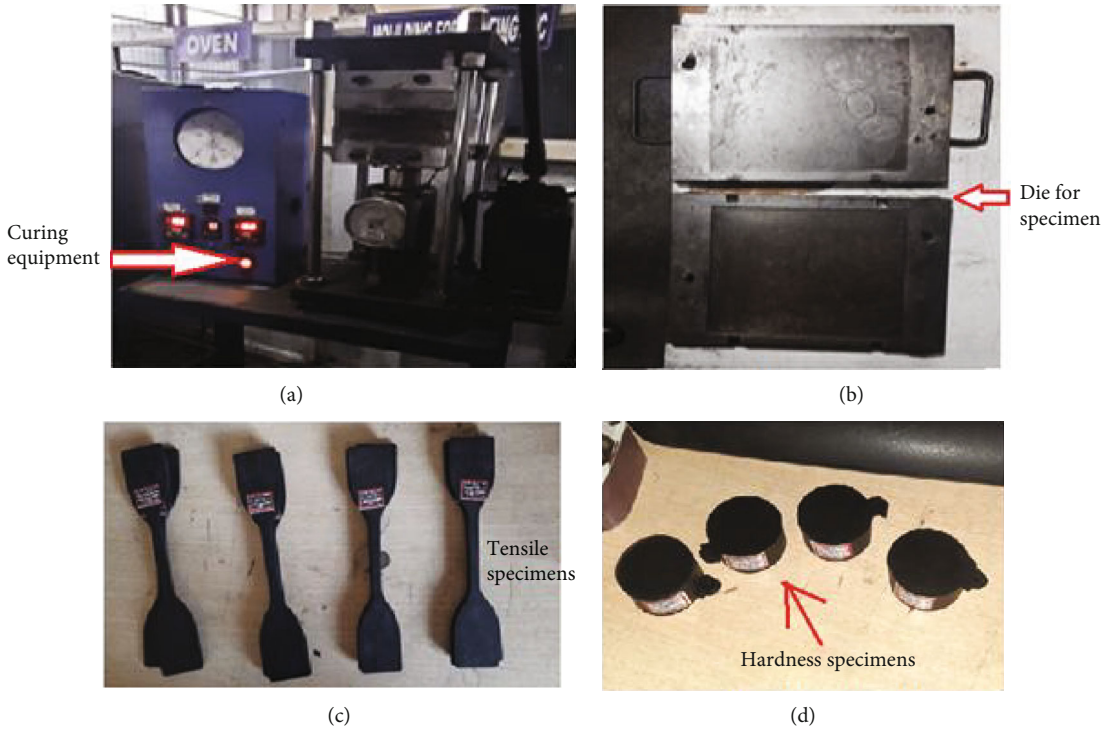

Figure 1: (a) Curing equipment. (b) Die set. (c) Tensile specimens. (d) Hardness specimens.

Table 1: Process control parameters and specimens.

Specimen number	Curing temp. in °C	Curing time in mins	Postcuring temp. in °C	Postcuring time in mins
1	150	14	100	60
2	150	14	100	120
3	150	14	50	60
4	150	14	50	120
5	150	18	100	60
6	150	18	100	120
7	150	18	50	60
8	150	18	50	120
9	170	14	100	60
10	170	14	100	120
11	170	14	50	60
12	170	14	50	120
13	170	18	100	120
14	170	18	100	60
15	170	18	50	60
16	170	18	50	120

way, another specimens were prepared by changing the die preheating temperature as well as curing time. After curing time, the pressure was released, and the die opened. The desired rubber sheet was taken out from the die and allowed to aging for 24 hours at a room temperature. After aging, the tensile and hardness specimens were cut from the sheet as per the ASTM dimensions.

2.3. Tensile Test. Tensile tests were performed using a universal testing machine to measure tensile strength, load at break, and % elongation at various combinations. ASTM D903 was used as the testing standard. With a grip gap of 25 mm, the specimen is mounted between the grips. The system's readings are reset to zero. A load is applied gradually until the specimen fails.

3. Results and Discussions

The tensile strength of various specimens tested and taken 3 trials as per the ASTM standard, and the optimization was done on the results.

3.1. Design of Experiment Analysis. For this investigation, the response variables were tensile strength, modulus at 100%, and percentage elongation. The experiment used 24 designs with three repetitions to determine the best values of the factors impacting the mechanical characteristics of the seal material. The run order for these tests was generated using Minitab software. Table 1 shows the factors examined and their range values. Table 2 represents the performance analysis. The experiment was conducted using the DOE approach, with two levels and four components, for a total of 24 complete factorial designs. Pilot runs were carried out to check that the equipment worked properly. The procedure was meticulously watched to ensure that everything went as planned. According to the experimental design, the settings were chosen. In order to account for the operational peculiarities, standard order was created. To avoid the influence of noise, the experiment was conducted in a random sequence. The experiments were all random. Standard and

Table 2: Average tensile strength and hardness values of specimens.

Specimen number	Extension (mm)	Displacement (mm)	Peak load (N)	Yield load (N)	Tensile strength N/mm^2	Hardness (HB)
1	42.60	102.50	86.595	86.595	7.2167	69
2	41.90	113.90	85.222	85.222	7.1001	71
3	49.80	121.50	85.22	85.22	7.1001	67
4	43.70	102.50	75.61	75.61	6.3008	68
5	43.00	107.50	89.635	89.635	7.4687	70
6	42.90	102.50	94.049	94.049	7.8375	69
7	48.10	122.50	94.54	94.54	7.8777	69
8	53.10	129.10	99.34	99.34	8.2778	70
9	48.20	122.70	94.931	94.931	7.911	71
10	42.90	102.50	91.891	91.891	7.657	71
11	51.10	126.10	95.422	95.422	7.9512	69
12	47.80	122.70	94.931	94.931	7.91102	68
13	47.70	124.00	98.462	98.462	8.2042	69
14	54.50	134.10	95.814	95.814	7.9836	68
15	52.70	128.20	87.95	87.95	7.3292	68
16	50.00	124.00	94.049	94.049	7.8375	69

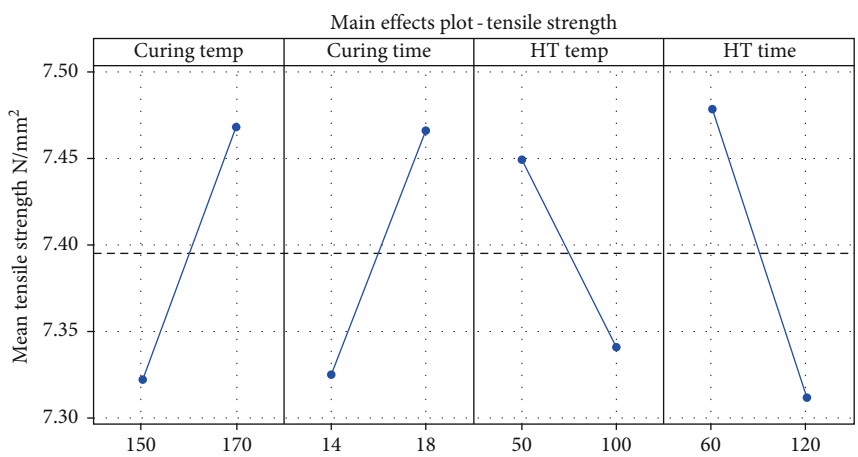

Figure 2: Effects of tensile strength.

run orders must be specified. Minitab software was used to create plots of main effects and interaction effects. Figure 2 illustrates the effects of tensile strength, and Figure 3 is its interaction plot.

Figure 4 displays the specimens' weight vs. infill density, break load, and peak load. The break value and peak load of specimen C were found to be the lowest, measuring "686.5 N and 725.7 N," respectively. Among the single infill density specimens A, B, and C, specimen A had the highest value, which was determined to be "1088.6 N and 1127.8 N," respectively. The experimental data clearly show that load-bearing capacity rises with a positive incremental change in infill density. The highest break and peak load among the specimens of combined infill density are determined to be "1000.3 N and 1122.9 N" in specimen ABA from the results. The least break and peak load values for the specimen CBC are "779.7 N and 872.85 N," respectively. The experimental data set aids in understanding how the specimen fails and how the crack spreads from the outside layer to the inside layer. In the following section, this event is explained in more detail. One of the significant elements affecting the tensile property is the variation in the density of the filling layers in their layering order.

3.2. Correlation Analysis on Factors Affecting Tensile Strength. Correlation analysis has been done using the Pearson correlation coefficient (Equation (1)) to understand the correlation between the independent variables and dependent variable. Curing times and curing temperatures are the independent variables which are affecting the tensile strength. Tensile strength is the dependent variable which varying based on the variable curing temperature and curing time.

$$r = \frac{n\Sigma xy - (\Sigma x)(\Sigma y)}{\sqrt{[n\Sigma x.x - (\Sigma x.\Sigma x)][n\Sigma y.y - (\Sigma y\Sigma y]}}. \quad (1)$$

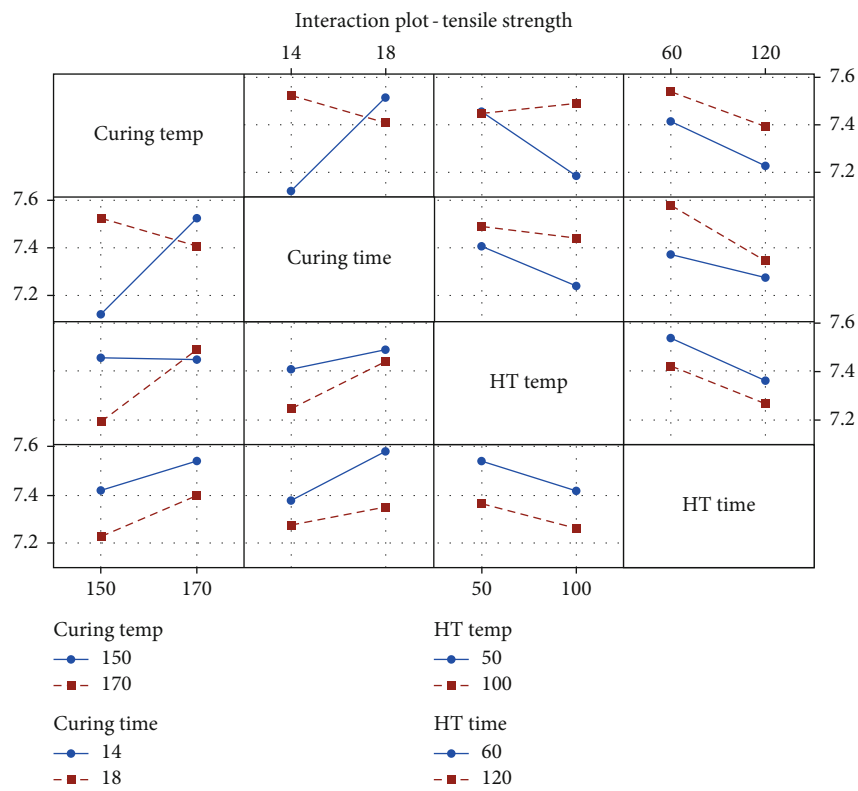

Figure 3: Interaction plot for tensile strength.

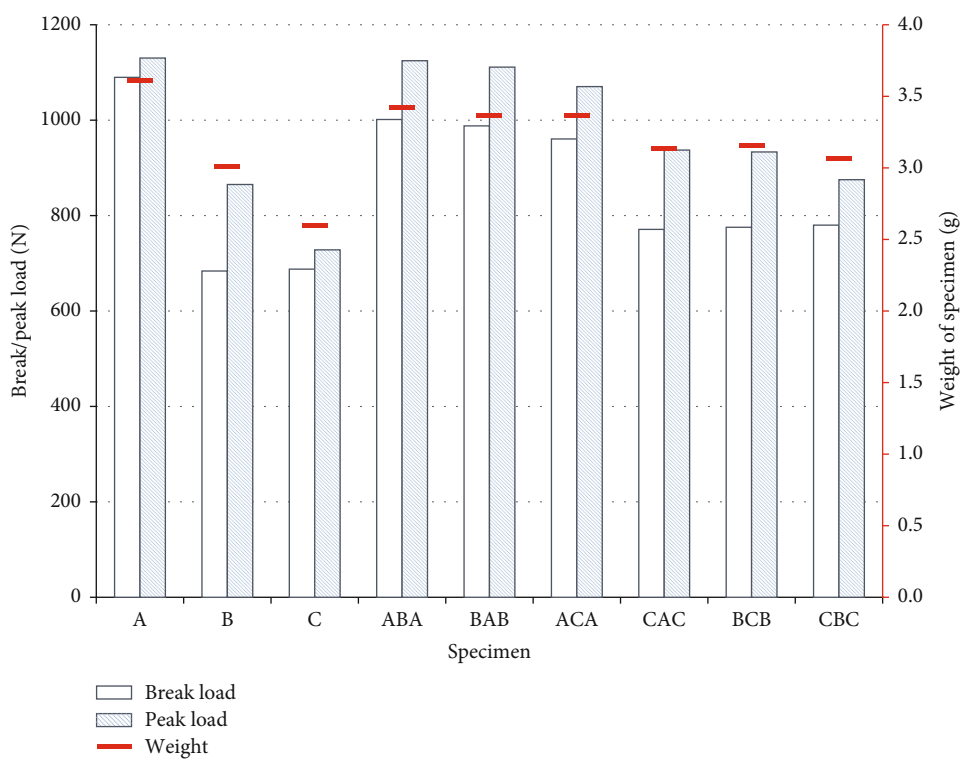

Figure 4: Peak load and break load during a tensile test are compared.

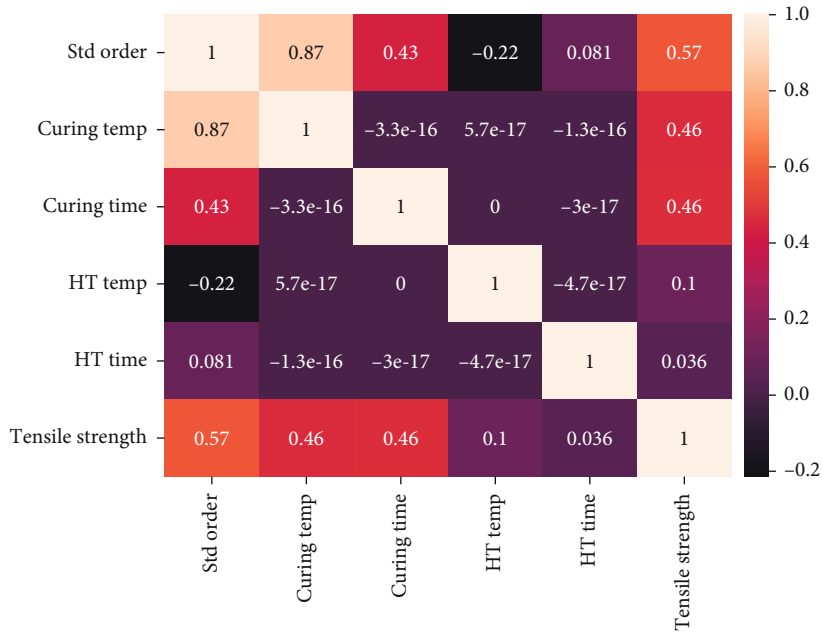

Figure 5: Correlation map.

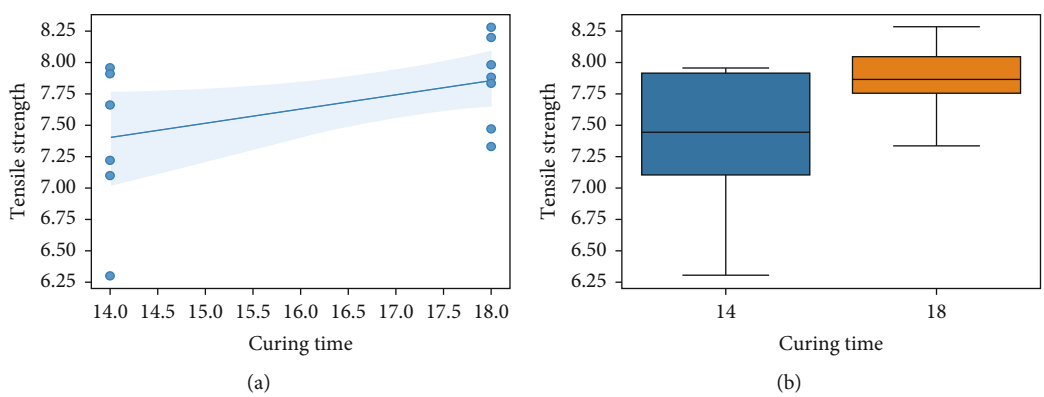

Figure 6: Tensile strength vs. curing time: (a) scatter plot and (b) box plot.

Results: Ordinary least squares

Model:	OLS	Adj. R-squared:	0.182
Dependent variable:	Tensile strength	AIC:	19.3050
Date:	2023-02-22 11:56	BIC:	20.2748
No. observations:	12	Log-likelihood:	−7.6525
Df model:	1	F-statistic:	3.448
Df residuals:	10	Prob (F-statistic):	0.0930
R-squared:	0.256	Scale:	0.25154

	Coef.	Std. err.	t	P > | t |	[0.025	0.975]
Const	5.3794	1.2079	4.4536	0.0012	2.6881	8.0707
Curing time	0.1363	0.0734	1.8568	0.0930	−0.0273	0.2999

Omnibus:	0.843	Durbin-Watson:	1.854
Prob (Omnibus):	0.656	Jarque-Bera (JB):	0.476
Skew:	−0.454	Prob (JB):	0.788
Kurtosis:	2.641	Condition no.:	138

Figure 7: Linear model summary for tensile strength vs. curing time.

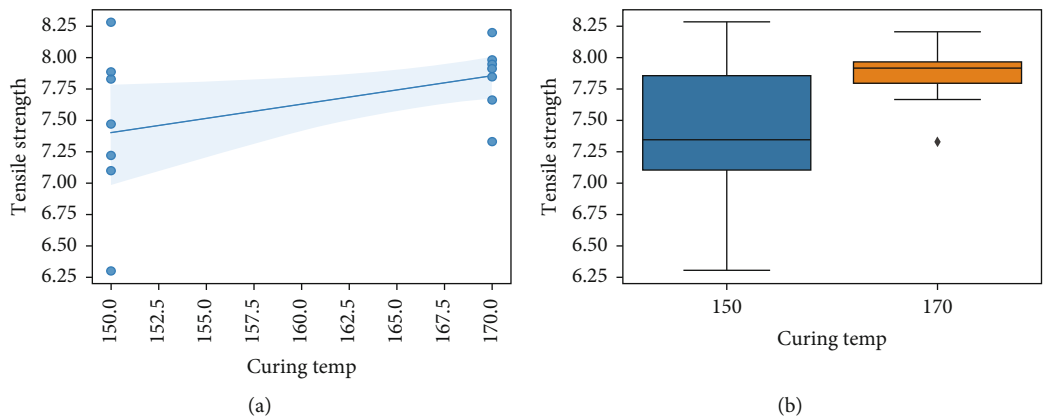

(a) (b)

Figure 8: Tensile strength vs. curing temperature: (a) scatter plot and (b) box plot.

Results: Ordinary least squares

Model:	OLS	Adj. R-squared:	0.051
Dependent variable:	Tensile strength	AIC:	21.0911
Date:	2023-02-22 12:06	BIC:	22.0609
No. observations:	12	Log-likelihood:	−8.5455
Df model:	1	F-statistic:	1.588
Df residuals:	10	Prob (F-statistic):	0.236
R-squared:	0.137	Scale:	0.29191

	Coef.	Std. err.	t	P > | t |	[0.025	0.975]
Const	4.4498	2.5094	1.7733	0.1066	−1.1415	10.0410
Curing temp	0.0199	0.0158	1.2602	0.2362	−0.0153	0.0552

Omnibus:	2.430	Durbin-Watson:	2.869
Prob (Omnibus):	0.297	Jarque-Bera (JB):	0.783
Skew:	−0.608	Prob (JB):	0.676
Kurtosis:	3.294	Condition no.:	2552

Figure 9: Linear model summary for tensile strength vs. curing temperature.

The correlation between the independent variables and dependent variable is shown in Figure 5. This statistical measure indicates how far the variables changes according to each other. As shown in Figure 5, there is a positive correlation between the independent variables such as curing time and temperatures and the expected tensile strength.

3.3. Effect of Curing Time on Tensile Strength. The tensile strength is influenced by curing time which is shown in Figure 6. Figure 6(a) reveals the correlation between the curing time and tensile strength. The variation of tensile strength is calculated by Equation (2). Figure 6(b) represents the numerical data used to understand the variability of the data and the presence of out layers which describes the statistics of various quartiles, the maximum and minimum values of tensile strength and interquartile range.

$$y = \alpha + \beta x. \tag{2}$$

The linear model summary is used to diagnose the regression model which is shown in Figure 7.

The independent parameter is chosen to be curing time (x), and the linear model is given as

$$\text{Tensile strength} = 5.379 + 0.136 \times \text{curing time}. \tag{3}$$

From the analysis, it is clear that, for every 1 sec increase of curing time, the tensile strength will increase by 0.136 N/mm^2.

3.4. Effect of Curing Temperature on Tensile Strength. Curing temperature and postcuring temperature are also making the influence on tensile strength of the specimen. The scatter plot (Figure 8(a)) reveals the correlation between the curing temperature and tensile strength. The tensile strength variation with respect to curing temperature is calculated by Equation (2). The variability of the data and the presence of out layers which describes the statistics of various quartiles described by the numerical data are shown in Figure 8(b) also which reveals the maximum and minimum values of tensile strength and interquartile range.

Figure 9 describes the linear model summary which is used to diagnose the regression model.

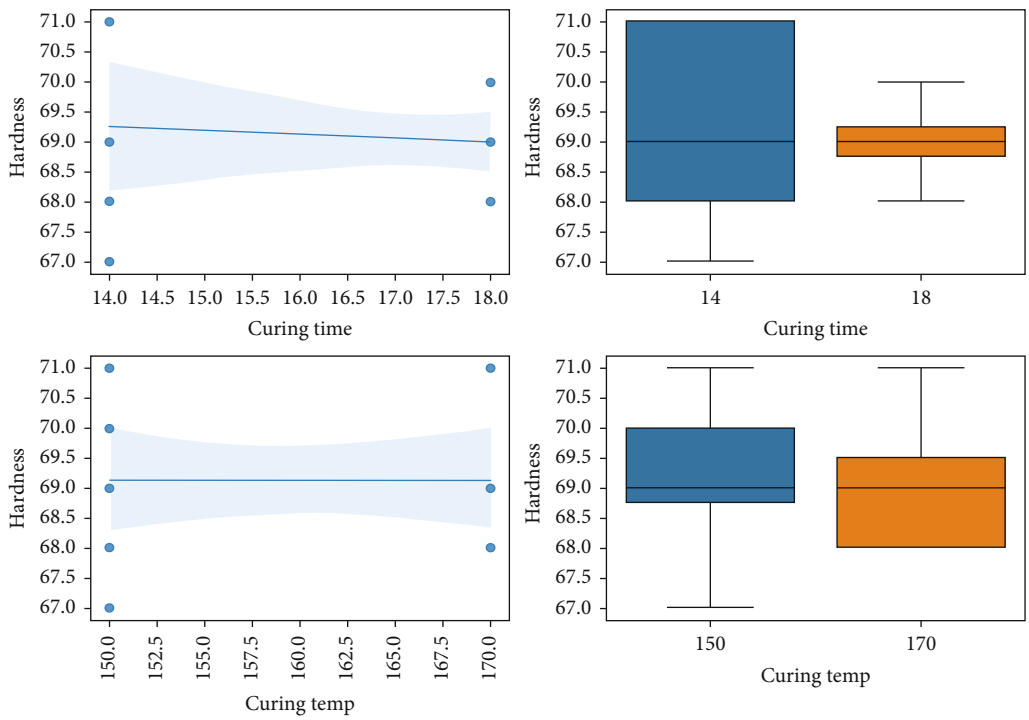

Figure 10: Hardness vs. curing time and hardness vs. curing temperature.

Results: Ordinary least squares

Model:	OLS		Adj. R-squared:		−0.095
Dependent variable:	Hardness		AIC:		38.8824
Date:	2023-02-22	16:26	BIC:		39.8523
No. observations:	12		Log-likelihood:		−17.441
Df model:	1		F-statistic:		0.04630
Df residuals:	10		Prob (F-statistic):		0.834
R-squared:	0.005		Scale:		1.2857

	Coef.	Std. err.	t	P > | t |	[0.025	0.975]
Const	67.7857	5.2664	12.8714	0.0000	56.0515	79.5199
Curing temp	0.0071	0.0332	0.2152	0.8340	−0.0668	0.0811

Omnibus:	0.087	Durbin-Watson:	2.176
Prob (Omnibus):	0.957	Jarque-Bera (JB):	0.191
Skew:	0.147	Prob (JB):	0.909
Kurtosis:	2.457	Condition no.:	2552

Results: Ordinary least squares

Model:	OLS		Adj. R-squared:		−0.027
Dependent variable:	Hardness		AIC:		38.1115
Date:	2023-02-22	16:34	BIC:		39.0813
No. observations:	12		Log-likelihood:		−17.056
Df model:	1		F-statistic:		0.7129
Df residuals:	10		Prob (F-statistic):		0.418
R-squared:	0.067		Scale:		1.2057

	Coef.	Std. err.	t	P > | t |	[0.025	0.975]
Const	66.7000	2.6445	25.2226	0.0000	60.8078	72.5922
Curing time	0.1357	0.1607	0.8443	0.4182	−0.2224	0.4939

Omnibus:	3.583	Durbin-Watson:	1.714
Prob (Omnibus):	0.167	Jarque-Bera (JB):	1.280
Skew:	0.754	Prob (JB):	0.527
Kurtosis:	3.533	Condition no.:	138

Figure 11: Linear model summary for hardness vs. curing time and hardness vs. curing temperature.

The independent parameter is chosen to be curing temperature (x), and the linear model is given in

$$\text{Tensile strength} = 4.4498 + 0.0199 \times \text{curing temperature}. \tag{4}$$

From the analysis, it is clear that, for every 1°C increase of curing temperature, the tensile strength will increase by 0.0199 N/mm^2.

3.5. Effect of Curing Time and Temperature on Hardness. Figure 10 shows the effect of curing time and curing temperatures on hardness which clearly shows the correlation between the independent variables and dependent variables. The box plot shows the variability of data and the statistics of various quartiles. The maximum and minimum hardness values of the specimens are also described by the scatter and box plots. From Figure 10 and the linear model summary in Figure 11, it is clearly identified that the correlation between the hardness and independent variables such as curing temperature is very less compared with the variable curing time. This result indicates that there is very little influence on hardness of the fabricated vinyl polyester rubber due to curing temperature. The curing time makes an influence on hardness. But very small amount of hardness variation is recorded compared with tensile strength. The variation quantity is calculated by Equations (5) and (6).

The independent parameter is chosen to be curing time and curing temperature, and the linear model is given in

$$\text{Hardness} = 67.7857 + 0.0071 \times \text{curing temperature}, \quad (5)$$

$$\text{Hardness} = 66.7000 + 0.1357 \times \text{curing time}. \quad (6)$$

From the analysis, it is clear that, for every 1°C increase of curing temperature, the hardness value will increase by 0.0071HB N/mm^2, and 0.1357HB increases for every 1 sec curing time.

4. Conclusion

The development of poly vinyl rubber material for sealing applications has been successful, and the mechanical properties of the material have been investigated using various factors such as curing temperature, curing time, postcuring temperature, and postcuring time. The tensile strength and hardness of the material were analyzed using ASTM standard, and it was found that the specimen prepared at 150°C curing temperature, 18 min curing time, 50°C postcuring temperature, and 120 min postcuring time provides the highest tensile strength and better hardness value. A design of experiment (DOE) analysis was performed to determine the best values of the factors impacting the mechanical characteristics of the seal material. Simple regression analysis was used to find the influence of curing temperature and curing time on the tensile strength and hardness. The analysis showed that for every 1 second increase of curing time, the tensile strength will increase by 0.136 N/mm2, and the hardness value will increase by 0.1357HB. Similarly, for every 1°C increase of curing temperature, the tensile strength will increase by 0.0199 N/mm2, and the hardness value will increase by 0.0071HB. The study provides valuable information on the development and optimization of poly vinyl rubber material for sealing applications, and the results can be used to improve the mechanical properties of the material for better performance in sealing applications.

Data Availability

There is no data availability statement in this study.

Conflicts of Interest

The authors declare that they have no conflicts of interest.

References

[1] W.-J. Lan, H.-X. Wang, X. Zhang, and S.-S. Chen, "Sealing properties and structure optimization of packer rubber under high pressure and high temperature," *Petroleum Science*, vol. 16, no. 3, pp. 632–644, 2019.

[2] Y. Bai, Y. Yang, Z. Xiao, M. Zhang, and D. Wang, "Process optimization and mechanical property evolution of AlSiMg0.75 by selective laser melting," *Materials & Design*, vol. 140, pp. 257–266, 2018.

[3] A. Dey and N. Yodo, "A systematic survey of FDM process parameter optimization and their influence on part characteristics," *Journal of Manufacturing and Materials Processing*, vol. 3, no. 3, p. 64, 2019.

[4] E. Dhanumalayan and G. M. Joshi, "Performance properties and applications of polytetrafluoroethylene (PTFE)—a review," *Advanced Composites and Hybrid Materials*, vol. 1, no. 2, pp. 247–268, 2018.

[5] D. Kai, N. Guanhua, X. Yuhang et al., "Effect of optimized pore structure on sealing performance of drilling sealing materials in coal mine," *Construction and Building Materials*, vol. 274, article 121765, 2021.

[6] G. K. Gupta, P. K. Gupta, and M. K. Mondal, "Experimental process parameters optimization and in-depth product characterizations for teak sawdust pyrolysis," *Waste Management*, vol. 87, pp. 499–511, 2019.

[7] W. Huang, G. Feng, H.-L. He, J.-Z. Chen, J.-Q. Wang, and Z. Zhao, "Development of an ultra-high-pressure rotary combined dynamic seal and experimental study on its sealing performance in deep energy mining conditions," *Petroleum Science*, vol. 19, no. 3, pp. 1305–1321, 2022.

[8] G. Hu, P. Zhang, G. Wang, M. Zhang, and M. Li, "The influence of rubber material on sealing performance of packing element in compression packer," *Journal of Natural Gas Science and Engineering*, vol. 38, pp. 120–138, 2017.

[9] P. Lu and R. J. K. Wood, "Tribological performance of surface texturing in mechanical applications—a review," *Surface Topography: Metrology and Properties*, vol. 8, no. 4, article 043001, 2020.

[10] Y. Ding, R. Liu, J. Yao, Q. Zhang, and L. Wang, "Stellite alloy mixture hardfacing via laser cladding for control valve seat sealing surfaces," *Surface and Coatings Technology*, vol. 329, pp. 97–108, 2017.

[11] K. Mohan, A. Seal, O. Krejcar, and A. Yazidi, "Facial expression recognition using local gravitational force descriptor-based deep convolution neural networks," *IEEE Transactions on Instrumentation and Measurement*, vol. 70, pp. 1–12, 2021.

[12] D. A. D. Genuino, M. D. G. de Luna, and S. C. Capareda, "Improving the surface properties of municipal solid waste-derived pyrolysis biochar by chemical and thermal activation: optimization of process parameters and environmental application," *Waste Management*, vol. 72, pp. 255–264, 2018.

[13] A. Karlekar, A. Seal, O. Krejcar, and C. Gonzalo-Martin, "Fuzzy k-means using non-linear *S-distance*," *Access*, vol. 7, pp. 55121–55131, 2019.

[14] A. C. Bouali, E. A. Straumal, M. Serdechnova et al., "Layered double hydroxide based active corrosion protective sealing of plasma electrolytic oxidation/sol-gel composite coating on AA2024," *Applied Surface Science*, vol. 494, pp. 829–840, 2019.

[15] Y. Bai, Y. Yang, D. Wang, and M. Zhang, "Influence mechanism of parameters process and mechanical properties evolution mechanism of maraging steel 300 by selective laser melting," *Materials Science and Engineering: A*, vol. 703, pp. 116–123, 2017.

[16] A. M. Guerra, N. Mokni, P. Delage et al., "In-depth characterisation of a mixture composed of powder/pellets MX80 bentonite," *Applied Clay Science*, vol. 135, pp. 538–546, 2017.

[17] H. A. Abdel-Aal, "Functional surfaces for tribological applications: inspiration and design," *Surface Topography: Metrology and Properties*, vol. 4, no. 4, article 043001, 2016.

[18] C. L. Brown, D. E. Mulcahy, and R. A. Mittermaier, "Protein conformational dynamics measured by NMR relaxation," *Methods in Molecular Biology*, vol. 1688, pp. 227–258, 2018.

[19] E. K. Oikonomou, G. Zachos, and P. Tsiakaras, "Hydrogen production via steam reforming of bio-ethanol: A review," *Renewable and Sustainable Energy Reviews*, vol. 100, pp. 286–305, 2019.

[20] M. A. Hossain, K. H. Kim, J. H. Ahn, and J. J. Lee, "Recent advances in photocatalytic CO2 reduction using metal-organic frameworks," *Journal of CO2 Utilization*, vol. 39, article 101161, 2021.

[21] K. Dong, G. Ni, B. Nie et al., "Effect of polyvinyl alcohol/aluminum microcapsule expansion agent on porosity and strength of cement-based drilling sealing material," *Energy*, vol. 224, article 119966, 2021.

[22] H. Mahmood, F. Nart, and A. Pegoretti, "Effective recycling of end-of-life polyvinyl chloride foams in ethylene–propylene diene monomers rubber," *Journal of Vinyl and Additive Technology*, vol. 28, no. 3, pp. 494–501, 2022.

[23] M. H. Alaaeddin, S. M. Sapuan, M. Y. M. Zuhri, E. S. Zainudin, and F. M. AL-Oqla, "Polyvinyl fluoride (PVF); its properties, applications, and manufacturing prospects," *IOP Conference Series: Materials Science and Engineering*, vol. 538, no. 1, article 012010, 2019.

[24] S. Khouri, M. Behun, L. Knapcikova, M. S. AnnamariaBehunova, and A. Rosova, "Characterization of customized encapsulant polyvinyl butyral used in the solar industry and its impact on the environment," *Energies*, vol. 13, no. 20, p. 5391, 2020.

[25] M. Kurakula and G. K. Rao, "Moving polyvinyl pyrrolidone electrospun nanofibers and bioprinted scaffolds toward multidisciplinary biomedical applications," *European Polymer Journal*, vol. 136, article 109919, 2020.

[26] M. Q. Tanveer, A. Haleem, and M. Suhaib, "Effect of variable infill density on mechanical behaviour of 3-D printed PLA specimen: an experimental investigation," *SN Applied Sciences*, vol. 1, no. 12, p. 1701, 2019.

[27] P. Jagadeesh, S. Mavinkere Rangappa, S. Siengchin et al., "Sustainable recycling technologies for thermoplastic polymers and their composites: a review of the state of the art," *Polymer Composites*, vol. 43, no. 9, pp. 5831–5862, 2022.

[28] P. Jagadeesh, M. Puttegowda, S. M. Rangappa et al., "A comprehensive review on 3D printing advancements in polymer composites: technologies, materials, and applications," *The International Journal of Advanced Manufacturing Technology*, vol. 121, no. 1-2, pp. 127–169, 2022.

[29] L. M. Júnior, L. M. de Oliveira, P. F. J. Bócoli, M. Cristianini, M. Padula, and C. A. R. Anjos, "Morphological, thermal and mechanical properties of polyamide and ethylene vinyl alcohol multilayer flexible packaging after high-pressure processing," *Journal of Food Engineering*, vol. 276, article 109913, 2020.

[30] E. Kibirkštis, V. Mayik, R. Zatserkovna et al., "Study of physical and mechanical properties of partially biodegradable LDPE polymeric films and their application for printing and packaging," *Polymer Testing*, vol. 112, article 107646, 2022.

Hindawi
Advances in Polymer Technology
Volume 2023, Article ID 3684253, 7 pages
https://doi.org/10.1155/2023/3684253

Research Article

Influences of Nanosilica Particles on Density, Mechanical, and Tribological Properties of Sisal/Hemp Hybrid Nanocomposite

K. Dhanasekar,[1] A. Mohana Krishnan,[2] Gopal Kaliyaperumal,[3] Melvin Victor De Poures,[4] P. Chandramohan,[5] N. Parthipan,[6] C. B. Priya,[7] R. Venkatesh,[8] and Kassu Negash[9]

[1]*Department of Civil Engineering, Adi Shankara Institute of Engineering and Technology, Ernakulam, 683574 Kerala, India*
[2]*Department of Mechanical Engineering, K.Ramakrishnan College of Engineering, Trichy, 621112 Tamilnadu, India*
[3]*Department of Mechanical Engineering, New Horizon College of Engineering, Bengaluru, Karnataka 560103, India*
[4]*Department of Thermal Engineering, Saveetha School of Engineering, SIMATS, Chennai, 602105 Tamilnadu, India*
[5]*Department of Mechatronics, Rajalakshmi Engineering College, Chennai, 602105 Tamilnadu, India*
[6]*Department of Mechanical Engineering, M.Kumarasamy College of Engineering, Karur, 639113 Tamilnadu, India*
[7]*Department of Mechanical Engineering, OASYS Institute of Technology, Trichy, 621006 Tamilnadu, India*
[8]*Department of Industrial Engineering, Saveetha School of Engineering, SIMATS, Chennai, 602105 Tamilnadu, India*
[9]*Department of Mechanical Engineering, Faculty of Manufacturing, Institute of Technology, Hawassa University, Ethiopia*

Correspondence should be addressed to Kassu Negash; kassun@hu.edu.et

Received 5 January 2023; Revised 17 March 2023; Accepted 28 April 2023; Published 15 May 2023

Academic Editor: Kinga Pielichowska

Focusing on natural fibers are the prominent substitution for synthetic fiber and reinforced into polymer matrices found unique properties such as lightweight, cost-effectiveness, and good mechanical and wear properties. Incompatibility and low adhesive behavior are the primary drawbacks found during the fabrication of natural fiber-bonded polymer matrix composites. The constant weight percentage (10 wt%) of sisal and hemp fiber is treated with a 5% NaOH solution for improving adhesive behavior and bonded with epoxy. The prepared sisal/hemp/epoxy combination is blended with 0 wt%, 3 wt%, 6 wt%, and 9 wt% silica nanoparticles, which results in reduced voids (1.32%) and increased flexural strength (56.98 MPa). Based on the compositions of fiber and reinforcement, the density of the composite varied. Samples 3-6 wt% of silica nanoparticle-blend sisal/hemp/epoxy composite offered maximum tensile and impact strength of 52.16 MPa and 2.1 J. An optical microscope analyzed the tensile fracture surface, and the failure nature was reported. The dry sliding wear performance of composite samples is tested by pin-on-disc setup with a 10 N-40 N load of 10 N interval at 0.75 m/sec. Sample 3 found good wear resistance compared to others.

1. Introduction

Due to beneficial features, the polymer matrix composites were considered significant in structural, sports equipment, automotive interior structure, electrical, housewares, and aerospace [1, 2]. The historical evaluation and measurement of composite properties have varied by choice of processing method, process parameters, choice of reinforcement fiber, and other relevant concerns [3, 4]. The interest in natural fibers from natural plants was more advantageous than synthetic fiber because of ease of availability, accessibility, lightweight, nonexpansive, biodegradability, superior flexural, strength, and renewable [5, 6]. Natural fiber-bonded polymer matrix composites were hybridized with nanofiller additions and found to have significant physical, mechanical, and wear performance compared to conventional materials [7, 8]. Moreover, the life cycle of plantfiber reinforced polymer matrix composites was addressed with various environmental aspects, and its life cycle assessment was proved with the incorporation of plant fiber [9] and to decide the cost and life span of polymer matrix composite [10].

Recently, the growth of hybrid polymer matrix composites containing more than one fiber helps enhance composites' mechanical and wear properties. The composites were prepared by combining polymer or epoxy matrix bonded with reinforcements such as natural, synthetic, natural/synthetic, and fiber/ceramic particles. Moreover, various researchers reported that the adhesive bonding strength between matrix and reinforcement could decide the properties of polymer matrix composite. Fiber with nanofiller (ceramic particles) enhanced the interfacial adhesive action, increasing mechanical strength, and void reduction [11–16]. Cost-effective natural coir, hemp, jute, sisal, bamboo, and natural flax fibers in the polymer matrix composite found an extended life span and biodegradability. The natural fibers were gained from natural biodegradable waste and utilized as filler material for polymer matrix composite fabrication [17–19]. The lightweight automobile components were fabricated from epoxy composite bonded with natural sisal fiber and found to have enhanced mechanical properties as compared to unreinforced polymer composite [20]. The mechanical tensile strength of the hybrid epoxy composite was enhanced via jute/sisal/silica. The presence of silica microparticles in epoxy hybrid composite tensile strength increased by 77% compared to jute/sisal fiber composite [21].

The polyethylene composite was synthesized using montmorillonite/silica nanoparticles blended with wood flour through conventional technique. The presence of silica nanoparticles enhances the composite's rigidity, tensile, and impact strength [22]. The mechanical characteristic of hybrid polyethylene (HDPE) composite was prepared with 5 wt% of natural wood powder and different weight percentages of silica were studied by ASTM. The polyethylene composite containing 3 wt% silica was found to have higher impact strength, and 5 wt% of silica had superior tensile and flexural strength [23].

Similarly, a kenaf/sisal fiber-reinforced epoxy composite was hybridized with a small number of silica nanoparticles and observed to have high mechanical strength [24]. The effect of multiwalled CNT (carbon nanotubes) on the mechanical characteristics of banana/jute/flex fiber-bonded hybrid epoxy composite, which is the increased content of multiwalled CNT in epoxy composite tensile strength, was improved [25]. The ASTM G99 standard studied fly ash-reinforced polymer matrix composites' wear properties for brake applications [26]. The short natural fiber-reinforced thermoplastic composite's thermal and mechanical characteristics were studied by ASTM and found the enhanced flexural strength in 30 wt% of the natural fiber-reinforced composite [27]. Recently, polymer matrix composites were synthesized from chicken feather fiber [28, 29], nonwoven waste cellulose fabric [30], human hair [31], and silicon carbide [32] and found improvement in mechanical performance.

However, the literature studied above shows limited literature on sisal/hemp fiber-bonded epoxy composite. The novelty of the present research is to enhance the adhesive behavior of epoxy composite by adding NaOH-treated natural fiber, and its composite hybridization using different weight percentages of silica nanoparticles helps reduce the voids. The effect of NaOH-treated natural fiber and silica nanoparticles on composite density and mechanical and wear properties is studied. The adhesion effects are proven by mechanical and wear performance. The presence of silica nanoparticles in epoxy composites is expected to enhance tribomechanical characteristics compared to conventional and unreinforced composites. From the above, no report is available on the combinations of sisal/hemp/different weight percentages of silica nanoparticles incorporated in an epoxy composite made by conventional fabrication methods.

Table 1: Compositions of epoxy hybrid nanocomposites.

Matrix/reinforcements/sample		1	2	3	4
Epoxy	Weight percentages in Wt%	80	77	74	71
Sisal fiber			10		
Hemp fiber			10		
Silica nanoparticles		0	3	6	9

2. Experimental Details

2.1. Details of Material Selection. Araldite epoxy resin (AW106) and hardener (HV935) are chosen as matrix materials. Natural sisal and hemp fibers (10-12 mm fiber length) are selected as filler materials and have good mechanical strength, better thermal properties, more durability, UV light resistance, and good dying capabilities [24]. A silica nanoparticle of 50 nm is chosen as a secondary filler material, enhancing the composite's mechanical and wear properties.

2.2. Processing of Natural Fibers. Initially, the natural sisal and hemp fibers were cleaned with distilled water in test room conditions and dried at ambient temperature (27°C) for 48 hrs. After the processing, each fiber was kept in a separate bowl containing 5% NaOH, soaked for 24 hrs to remove the waste dust particles, and cured as clean fiber. The NaOH chemical treatment helps to increase the adhesive and interlocking properties between the matrix and reinforcements [25]. The NaOH-treated fibers were dried in test room condition for 24 hrs. After the NaOH treatment, the fibers were immersed in distilled water for 30mins and then dried via oven heat for 10 hours duration at 65°C temperature. Finally, the fibers were sheared to 10-12 mm length via a fine cutter and used as filler phase. The constitution of epoxy hybrid composite fabrication weight percentage is tabulated in Table 1.

2.3. Fabrication of Composites. Figure 1 presents the actual flow process fabrication layout for epoxy hybrid nanocomposite containing constant weight percentages (10 wt%) of sisal/hemp fiber and hybridization with different weight percentages of silica nanoparticles, as the details were mentioned in Table 1.

The 10 : 1 ratio of epoxy resin and hardener was blended using a mechanical stirrer. The chemically treated chopped sisal and hemp fibers were weighed by a digital weighing machine and mixed into an epoxy resin blend pool. An applied speed of 500 rpm for 30 mins uniformly stirred the epoxy resin pool and natural fibers. Meanwhile, the silica nanoparticles were preheated by a muffle furnace to remove

Figure 1: Actual flow process fabrication layout for epoxy hybrid nanocomposite.

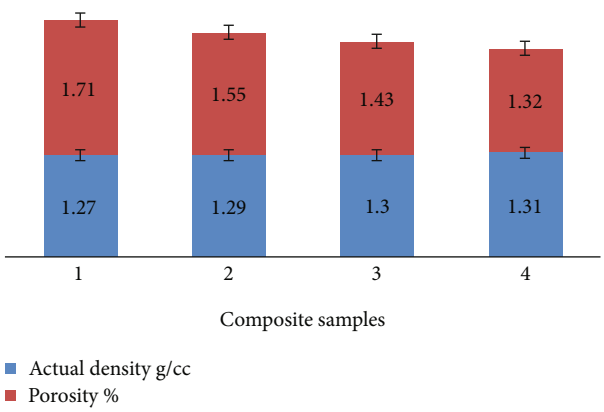

Figure 2: Density and porosity of developed epoxy hybrid nanocomposites.

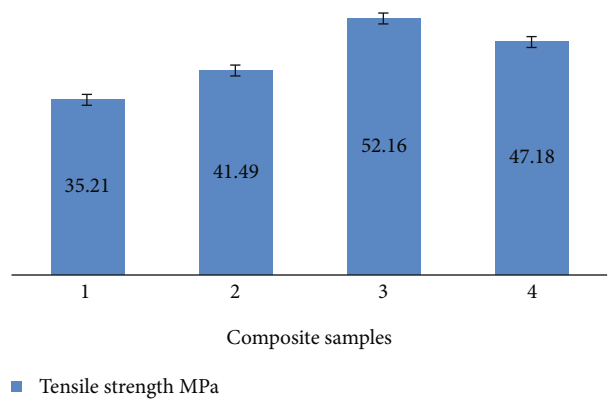

Figure 3: Tensile strength of developed epoxy hybrid nanocomposites.

the moisture content. After the blending process, the externally preheated silica nanoparticles were forced to epoxy and blend with continuous stir action, and 70°C raised their temperature via an electrical heater, increasing the composite's adhesive properties. The epoxy resin pool containing natural fibers and silica nanoparticles was blended at 500 rpm stir speed for 20 mins at a temperature range of 55°C to 70°C. Finally, blended compositions were transferred to a steel mold with an applied load of 0.5 tons.

2.4. Test Details. The rule of mixture measures the density of the composite, and its voids are estimated by the Archimedes principle at test room conditions. The Instron 3367 model, a tensile/compression testing machine, was utilized to evaluate composites' tensile and flexural strength at a 5 mm/min cross-slide speed. The tensile and flexural strengths of the composite were followed by the standard of ASTM D638 and ASTM D790 standards [15, 23]. The IT30-impact machine performed the impact toughness as per ASTM D6110. The wear performance of the developed composite is evaluated with hardened gray cast-iron material under 10 N, 20 N, 30 N, and 40 N average loads at 0.75 m/sec sliding velocity, followed by the ASTM G99 standard [3, 11, and 26].

3. Results and Discussions

3.1. Density and Porosity Percentages of Epoxy Hybrid Nanocomposites. The density and porosity percentages of epoxy hybrid nanocomposite synthesized using sisal/hemp fiber bonded with different weight percentages of silica nanoparticles results are addressed in Figure 2. The principle of Archimedes measured the actual experimental density of an epoxy hybrid nanocomposite. The actual experimental density of epoxy hybrid nanocomposite without silica nanoparticles was 1.27 ± 0.28 g/cc, and the impact of silica nanoparticles on the epoxy hybrid nanocomposite density was progressively increased by 1.29 ± 0.21 g/cc, 1.30 ± 0.11, and 1.31 ± 0.12 g/cc of 3 wt%, 6 wt%, and 9 wt% of silica

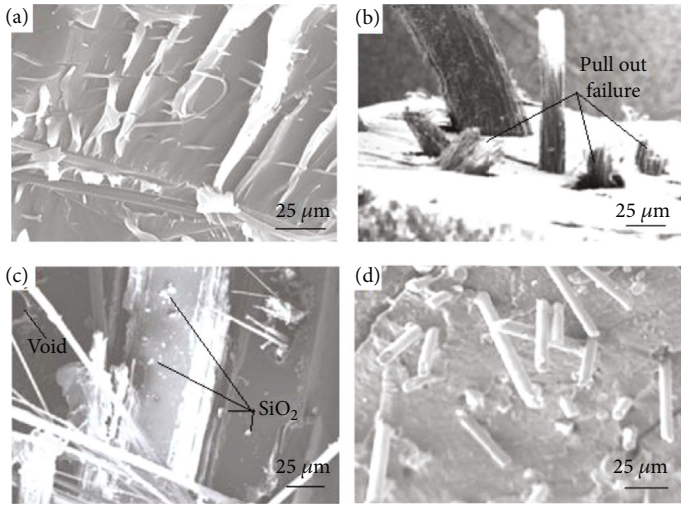

Figure 4: Tensile fracture surface morphology. (a) Sample 1. (b) Sample 2. (c) Sample 3. (d) Sample 4.

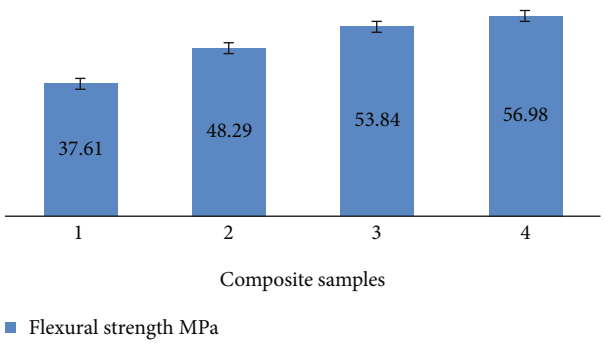

Figure 5: Flexural strength of developed epoxy hybrid nanocomposites.

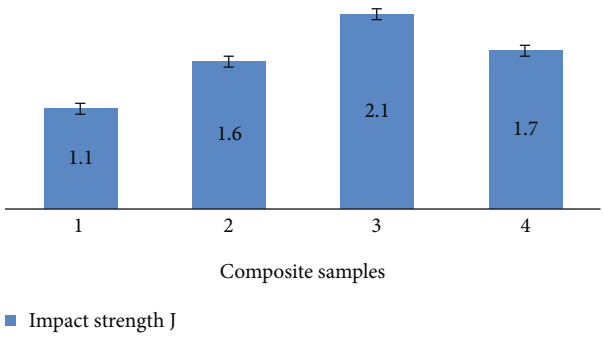

Figure 6: Impact strength of developed epoxy hybrid nanocomposites.

nanoparticles, respectively. The improvement in epoxy composite density was mainly featured by the choice of silica nanoparticle content and low-density epoxy resin. However, the porosity percentages of epoxy hybrid composites decreased with increased silica nanoparticles due to its effective dispersion of silica nanoparticles in the epoxy resin.

The uniform presence of silica nanoparticles was the main reason for the composite's increased density and reduced porosity. It helps to improve the mechanical and tribological properties [26].

3.2. Effect of Silica Nanoparticles on Tensile Strength of Epoxy Hybrid Nanocomposites. ASTM D638 standards evaluated the tensile strength of developed epoxy composites through the Instron 3367 tensile testing machine with an applied crosshead speed of 5 mm/min. Figure 3 illustrates the tensile strength of an epoxy composite reinforced with 10 wt% of sisal and 10 wt% of hemp fiber via conventional technique. The epoxy/sisal/hemp combinations were enriched with silica nanoparticles via a uniform stir speed of 500 rpm. The tensile strength of an unreinforced epoxy/sisal/hemp fiber composite was 35.21 ± 1.34 MPa, and 3 wt% of silica nanoparticles incorporated into an epoxy hybrid nanocomposite was observed at 41.49 ± 2.11 MPa. There was evidence of silica nanoparticles present.

The constitutions of 6 wt% of silica nanoparticles in the hybrid nanocomposites identified the maximum tensile strength as 52.16 ± 1.91 MPa. The increase in the tensile of the composite was due to the good interfacial bonding between epoxy and sisal/hemp fiber was increased by the presence of silica nanoparticles. The minor porous was occupied and silica nanoparticles increased its composite bonding strength. The tensile strength of the composite varied due to the processing, selection of matrix, and reinforcement [15, 20]. Further additions of silica nanoparticles into epoxy composite found decreases in tensile strength of 47.18 ± 1.87 MPa. However, the 6 wt% of silica nanoparticles-reinforced epoxy composite was found to have higher tensile strength and increased by 48.13% compared to sample 1 (unreinforced epoxy/sisal/hemp composite).

3.3. Tensile Fracture Surface Analysis. Figure 4 represents the tensile fracture micrograph of a natural fiber-reinforced epoxy composite with and without silica (SiO_2) nanoparticles. Figure 4(a) shows the tensile fracture surface micrograph of an epoxy/natural fiber composite without silica content. It showed elongated failure during the tensile test, and the layers are deflecting with their natural fiber. The tensile failure of sample 2 is illustrated in Figure 4(b). The micrograph indicates the pullout failure during the high tensile force. However, the silica nanoparticles were effectively

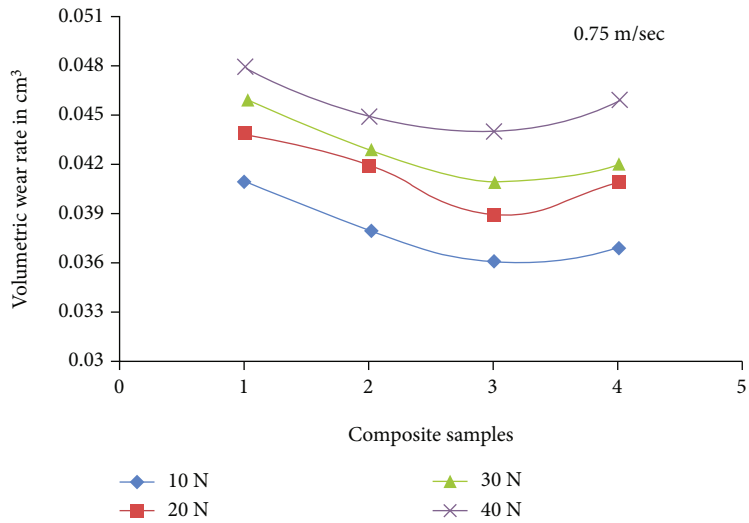

Figure 7: Volumetric wear rate of developed epoxy hybrid nanocomposites.

bonded with the epoxy layer, and the fracture surface of sample 3 is shown in Figure 4(c). A few voids were found during the evaluation of the tensile fracture surface and were due to the air gap. Figure 4(d) indicates the tensile fracture surface morphology of sample 4 composite contained 9 wt% of silica particles. It clearly shows adequate bonding with uniformly distributed SiO_2 particles in epoxy and also formed the microcrack during high tension.

3.4. Effect of Silica Nanoparticles on Flexural Strength of Epoxy Hybrid Nanocomposites. The flexural strength of epoxy hybrid composites reinforced with different weight percentages of silica nanoparticles was evaluated by ASTM D790 standards, and its values are summarized in Figure 5. The flexural strength of epoxy composite without silica nanoparticles showed 37.61 ± 1.09 MPa, and it was improved by 28.3% with the addition of 3 wt% of silica nanoparticles. The flexural strength of sample 3 hybrid nanocomposite was 53.84 ± 2.13 MPa, which increased by 43.15% compared to sample 1 epoxy composite. The higher flexural strength of 56.98 ± 1.12 MPa was noted by 6 wt% of silica nanoparticle-reinforced epoxy composite. It was increased by 51.5% compared to sample 1 epoxy composite without silica nanoparticles. However, the epoxy composite's improved fiber orientations and silica nanoparticle content must attain maximum flexural strength. One of the researchers reported a similar tendency while evaluating a silica-reinforced sisal/glass fiber hybrid composite [20].

3.5. Effect of Silica Nanoparticles on the Impact Strength of Epoxy Hybrid Nanocomposites. The Charpy impact energy on developed epoxy composites with and without silica nanoparticles was experimentally measured in ASTM D6110 standards, and its measured values are illustrated in Figure 6. The inclusion of silica nanoparticles in the epoxy composites impact strength was progressively improved with constant weight percentages of sisal and hemp fiber. It was noted from Figure 6 bar chart that the epoxy composite contained 10 wt% of each sisal and hemp fiber and offered an impact strength of 1.1 ± 0.5 J, and the epoxy/sisal/hemp fiber composite was hybridized with different weight percentages of silica nanoparticles. The impact strength of the composite was increased from 1.6 ± 0.45 J to 2.1 ± 0.75 J with the incorporation of 3 wt% and 6 wt% of silica nanoparticles, respectively. The increase in impact strength of the composite was due to the presence of sisal and hemp fibers which were able to resist the high impact load because both sisal and hemp fibers have good mechanical properties. Moreover, the adequate void-free interfacial bonding quality has increased by incorporating silica nanoparticles. With more than 6 wt% of silica nanoparticles, the impact strength of the composite was reduced by 23.5% compared to sample 3. The decreased impact strength was due to the higher content of silica which led to its brittle nature [20]. The variation in impact strength was due to fiber orientations and the processing method [23, 24].

3.6. Effect of Silica Nanoparticles on the Wear Rate of Epoxy Hybrid Nanocomposites. The wear rate characteristics of a developed hybrid nanocomposite containing different weight percentages of silica nanoparticles were investigated by ASTM G99 standards through a pin-on-disc wear tester consisting of a hardened steel counter-disc with an applied load of 10-40 N of a 10 N interval under 0.75 m/sec sliding velocity. Figure 7 shows the wear rate of developed epoxy hybrid nanocomposited with and without silica nanoparticles.

It was observed in Figure 6 that the volumetric wear rate of epoxy hybrid nanocomposites increased with improved average load from 10 N to 40 N, respectively. The volumetric wear rate of sample 1 epoxy composite without silica nanoparticles was increased progressively from 0.041 cc to 0.048 cc. While the incorporations of silica nanoparticles in the epoxy composite volumetric wear rate also increased gradually but were lower than the sample 1 composite, similarly, samples 2 and 3 observed a reduction in wear rate with the addition of silica nanoparticles by 3 wt% and 6 wt%, respectively. Due to the presence of nanosilica particles that resisted the indentation against the high sliding

speed, natural fibers performed better in elongation. The natural fibers had good tensile and Young's modulus characteristics that resist or withstand the maximum frictional force [18, 25]. The content of silica nanoparticles of more than 6 wt% showed an increased volumetric wear rate. It was due to increased silica content that led to the breaking and deboning of the fiber layer. However, the content of nanosilica particles enhanced the composite's wear properties, and sample 3 was identified as having a low volumetric wear rate compared to all. It was reduced by 9% with the applied 40 N load and 0.75 m/sec sliding velocity.

4. Conclusions

The epoxy composite containing sisal and hemp fiber was successfully hybridized using different weight percentages of silica nanoparticles, and its physical, mechanical, and wear properties were enhanced. The test results and main conclusions are made below.

(i) The epoxy/sisal/hemp composite was enriched with the addition of nanosilica particles at 0, 3, 6, and 9 wt% via conventional processing to minimize the cost

(ii) The composite density gradually increased, and sample 4 found a higher density of 1.31 ± 0.12 g/cc with a reduced porosity of 1.32%

(iii) The epoxy composite containing 6 wt% of nanosilica particles identified higher tensile and impact strength. It was enriched by 48.13% and had 1.9 times tensile and impact strength compared to sample 1 unreinforced silica nanoparticles epoxy composites

(iv) The composite contained 6 wt% of silica nanoparticles owing to good flexural strength and increased by 51.5% compared to sample 1 epoxy composite without silica nanoparticles

(v) The influences of silica nanoparticles in the epoxy composite have reduced the volumetric wear rate, and sample 3 was observed as good wear behavior on high load and sliding speed compared to others

(vi) In the future, silica will be derived from natural wastes like rice husk ash, bamboo leaves, and others and utilized as a secondary phase filler material for polymer matrix composites

(vii) The natural fiber is extracted from various natural waste leaves and chemically treated to increase the properties of fiber instead of synthetic fiber

Data Availability

All the data required are available within the manuscript.

Conflicts of Interest

The authors declare that there are no conflicts of interest regarding the publication of this paper.

References

[1] H. S. Kim, J. U. Jang, H. Lee et al., "Thermal management in polymer composites: a review of physical and structural parameters," *Advanced Engineering Materials*, vol. 20, no. 10, article 1800204, 2018.

[2] M. J. Mochane, T. E. Motaung, and S. V. Motloung, "Morphology, flammability, and properties of graphite reinforced polymer composites. Systematic review," *Polymer Composites*, vol. 39, no. S3, pp. E1487–E1499, 2018.

[3] S. Pradhan, S. K. Acharya, and V. Prakash, "Mechanical, morphological, and tribological behavior of Eulaliopsis binata fiber epoxy composites," *Journal of Applied Polymer Science*, vol. 138, no. 12, p. 50077, 2021.

[4] J. Chen, L. Yan, W. Song, and D. Xu, "Thermal and electrical properties of carbon nanotube-based epoxy composite materials," *Material Research Express*, vol. 5, no. 6, article 65051, 2018.

[5] M. Ramesh, K. Palanikumar, and K. H. Reddy, "Plant fibre based bio-composites: sustainable and renewable green materials," *Renewable and Sustainable Energy Reviews*, vol. 79, pp. 558–584, 2017.

[6] Natural fibers and their composites, "Natural fibers and their composites," *Tribology of Natural Fiber Polymer Composites*, vol. 5, pp. 1–58, 2008.

[7] P. Jagadeesh, M. Puttegowda, Y. G. T. Girijappa, S. M. Rangappa, and S. Siengchin, "Effect of natural filler materials on fiber reinforced hybrid polymer composites: an overview," *Journal of Natural Fibers*, vol. 19, no. 11, pp. 4132–4147, 2022.

[8] N. Saba, P. Tahir, and M. Jawaid, "A review on potentiality of nano filler/natural fiber filled polymer hybrid composites," *Polymers*, vol. 6, no. 8, pp. 2247–2273, 2014.

[9] M. Ramesh, C. Deepa, L. R. Kumar, M. R. Sanjay, and S. Siengchin, "Life-cycle and environmental impact assessments on processing of plant fibres and its bio-composites: a critical review," *Journal of Industrial Textiles*, vol. 51, Supplement 4, pp. 5518S–5542S, 2022.

[10] S. Jayavani, H. Deka, T. O. Varghese, and S. K. Nayak, "Recent development and future trends in coir fiber-reinforced green polymer composites: review and evaluation," *Polymer Composites*, vol. 37, no. 11, pp. 3296–3309, 2016.

[11] M. Gupta, "Thermal and dynamic mechanical analysis of hybrid jute/sisal fibre reinforced epoxy composite," *Proceedings of the Institution of Mechanical Engineers, Part L: Journal of Materials: Design and Applications*, vol. 232, no. 9, pp. 743–748, 2018.

[12] R. Z. A. A. Ramadhan, A. R. Abu Talib, A. S. Mohd Rafie, and R. Zahari, "High velocity impact response of Kevlar-29/epoxy and 6061-T6 aluminum laminated panels," *Materials & Design*, vol. 43, pp. 307–321, 2013.

[13] P. Sahu and M. K. Gupta, "Sisal (Agave sisalana) fibre and its polymer-based composites: a review on current developments," *Journal of Reinforced Plastics and Composites*, vol. 36, no. 24, pp. 1759–1780, 2017.

[14] M. Ramesh, L. N. Rajeshkumar, N. Srinivasan, D. V. Kumar, and D. Balaji, "Influence of filler material on properties of

fiber-reinforced polymer composites: a review," *e-Polymers*, vol. 22, no. 1, pp. 898–916, 2022.

[15] C. Dong, "Review of natural fibre-reinforced hybrid composites," *Journal of Reinforced Plastics and Composites*, vol. 37, no. 5, pp. 331–348, 2018.

[16] S. Doagou-Rad, A. Islam, and T. D. Merca, "An application-oriented roadmap to select polymeric nanocomposites for advanced applications: a review," *Polymer Composites*, vol. 41, no. 4, pp. 1153–1189, 2020.

[17] R. A. Braga and P. A. Magalhaes, "Analysis of the mechanical and thermal properties of jute and glass fiber as reinforcement epoxy hybrid composites," *Material Science and Engineering Part C*, vol. 56, pp. 269–273, 2015.

[18] K. Bledzki, S. Reihmane, and J. Gassan, "Properties and modification methods for vegetable fibers for natural fiber composites," *Journal of Applied Polymer Science*, vol. 59, no. 8, pp. 1329–1336, 1996.

[19] M. Shamsuyeva, O. Hansen, and H. J. Endres, "Review on hybrid carbon/flax composites and their properties," *International Journal of Polymer Science*, vol. 2019, Article ID 9624670, 17 pages, 2019.

[20] B. T. Ferreira, L. J. da Silva, T. H. Panzera, J. C. Santos, R. T. S. Freire, and F. Scarpa, "Sisal-glass hybrid composites reinforced with silica microparticles," *Polymer Testing*, vol. 74, pp. 57–62, 2019.

[21] A. M. Kazi, D. V. A. Ramasastry, and S. Waddar, "Characterization of interwoven roselle/sisal fiber reinforced epoxy composites," *Polymer Composites*, vol. 43, no. 3, pp. 1421–1428, 2022.

[22] J. Jiang, C. Mei, M. Pan, and J. Cao, "Improved mechanical properties and hydrophobicity on wood flour reinforced composites: incorporation of silica/montmorillonite nanoparticles in polymers," *Polymer Composites*, vol. 41, no. 3, pp. 1090–1099, 2020.

[23] T. Buddi, B. N. Rao, S. K. Singh, R. Purohit, and R. S. Rana, "Development and analysis of high density poly ethylene (HDPE) nano SiO2and wood powder reinforced polymer matrix hybrid nano composites," *Journal of Experimental Nanoscience*, vol. 13, Supplement 1, pp. S24–S30, 2018.

[24] L. M. G. Vieira, J. C. . Santos, T. H. Panzera et al., "Hybrid composites based on sisal fibers and silica nanoparticles," *Polymer Composites*, vol. 39, no. 1, pp. 146–156, 2018.

[25] K. Mohan and T. Rajmohan, "Fabrication and characterization of MWCNT filled hybrid natural fiber composites," *Journal of Natural Fibers*, vol. 14, no. 6, pp. 864–874, 2017.

[26] V. Ahlawat, S. Kajal, and P. Anuradha, "Tribo-performance assessment of milled fly ash brake friction composites," *Polymer Composites*, vol. 41, no. 2, pp. 707–718, 2020.

[27] Y. Kısmet and A. Dogan, "Characterization of the mechanical and thermal properties of rape short natural-fiber reinforced thermoplastic composites," *Iranian Polymer Journal*, vol. 31, no. 2, pp. 143–151, 2022.

[28] A. Verma, P. Negi, and V. K. Singh, "Physical and thermal characterization of chicken feather fiber and crumb rubber reformed epoxy resin hybrid composite," *Advances in Civil Engineering Materials*, vol. 7, no. 1, pp. 20180027–20180557, 2018.

[29] A. Verma, P. Negi, and V. K. Singh, "Experimental analysis on carbon residuum transformed epoxy resin: chicken feather fiber hybrid composite," *Polymer Composites*, vol. 40, no. 7, pp. 2690–2699, 2019.

[30] S. Rastogi, A. Verma, and V. K. Singh, "Experimental response of nonwoven waste cellulose fabric–reinforced epoxy composites for high toughness and coating applications," *Materials Performance and Characterization*, vol. 9, no. 1, article 20190251, 2020.

[31] A. Verma and V. K. Singh, "Mechanical, microstructural and thermal characterization of epoxy-based human hair–reinforced composites," *Journal of Testing and Evaluation*, vol. 47, no. 2, pp. 1193–1215, 2019.

[32] N. Bisht, A. Verma, S. Chauhan, and V. K. Singh, "Effect of functionalized silicon carbide nano-particles as additive in cross- linked PVA based composites for vibration damping application," *Journal of Vinyl and Additive Technology*, vol. 27, no. 4, pp. 920–932, 2021.

Hindawi
Advances in Polymer Technology
Volume 2023, Article ID 8838766, 15 pages
https://doi.org/10.1155/2023/8838766

Review Article

Nontraditional Natural Filler-Based Biocomposites for Sustainable Structures

K. Mohan Kumar,[1,2,3,4] **Venkatesh Naik**,[2] **Vijayanand Kaup**,[2] **Sunil Waddar**,[1] **N. Santhosh**,[1] **and H. V. Harish**[5]

[1]*Department of Mechanical Engineering, MVJ College of Engineering, Bangalore 560067, India*
[2]*Department of Mechanical Engineering, CMR Institute of Technology, Bangalore 560037, India*
[3]*Department of Mechanical Engineering, Visvesvaraya Technological University, Jnana Sangama, Belagavi, Karnataka, India*
[4]*Research Center-Department of Mechanical Engineering, CMR Institute of Technology, Bangalore 560037, Affiliated to Visvesvaraya Technological University, Belagavi, Karnataka, India*
[5]*Department of Mechanical Engineering, Debre Markos University, Debre Markos, Gozamn, Misrak Gojam, Amhara Zipcode 269, Ethiopia*

Correspondence should be addressed to K. Mohan Kumar; mohankumark2019@gmail.com and H. V. Harish; harish_hv@dmu.edu.et

Received 14 December 2022; Revised 9 January 2023; Accepted 20 March 2023; Published 2 May 2023

Academic Editor: Indran Suyambulingam

In recent years, there has been a growing awareness and demand for global sustainability, as well as a mandate for the use of renewable and environmentally sustainable materials and processes. Due to which, massive efforts are being made to develop and nurture the next generation of composite materials that are energy efficient, environmentally friendly, and biodegradable. Light weight, lower coefficient of thermal expansion, and comparable tensile strength exhibited by natural fibers render them the choice for use in several industrial products and applications over the last decade. Natural fibers as the reinforcing entity are pitted against their synthetic variants primarily because of the superior aspects like biodegradability and excellent strength-to-weight ratio. This article presents the review on various nonconventional natural fibers such as tamarind seed and shell, Luffa cylindrica, groundnut shell, coconut coir, papaya bast, okra, and Ashoka tree seed. The flow of the chapter includes the introduction, extraction methodologies, and fabrication, and investigations of mechanical properties, applications, and sustainability are dealt in detail for nontraditional natural fibers. The okra fibers possess greater tensile strength of up to 262.8 MPa in comparison with other fibers, while the Ashoka tree seed fibers are known to possess a maximum flexural strength of up to 125 MPa. Further, these fibers are used as reinforcements in potential applications in interiors and automobile and aircraft panels and wood-based particle board composites owing to the increase in tensile and flexural strengths of composites.

1. Introduction

Development and use of natural fiber-based composite materials are steadily increasing due to the superior properties offered by these fibers and their abundant availability [1]. In the recent past, various types of plant and fruit fibers are explored and studied. The natural fibers, which are extracted from various plants, mineral sources, and animals, seem to have better specific properties and weight saving potential. The properties of plant fibers are dependent on the age of plant, extraction technique adopted, and interaction with the environment [2, 3]. Nevertheless, natural fiber composites find applications in automobiles, naval, household items, and chemical industries [4].

The plant fibers such as banana [5, 6], jute [7, 8], kenaf [9, 10], abaca [11, 12], pineapple [13], sisal [14, 15], agave [16], flax [17], hemp [18], cotton [19], and roselle [20] are the traditionally used natural fibers for making the composites. Various thermoplastic [21, 22] and thermosetting [23, 24] resins are used as matrix material. Most of the studies

are related to the mechanical characterization of these novel composites. The quality of these composites depends on the mode of adhesion and the strength of the constituent elements. Few researchers have demonstrated that the surface treatment of the naturally available fibers enhances the adhesion between the constituents, leading to improved properties owing to a better load transfer mechanism. Animal fibers such as wool obtained from sheep, goat hair, horsehair, and yak are explored by researchers [25]. The fiber extraction methods and fabrication of composites are dealt in these articles [26].

Due to the desired properties exhibited by these composites, researchers have taken steps to explore the possibilities of extracting and using these new materials for several engineering applications [27] and in particular low load-bearing structures [28]. Hence, in the present study, the processing methodology, characterization methods, and their consequences are elaborated for newer natural fibers and animal fiber composites. In this paper, a comprehensive review of the newly explored natural fibers such as tamarind, Ashoka tree, fish scale, and groundnut shell which are extracted and studied for their mechanical and thermal properties is dealt in detail. The review articles presented the mechanical properties and applications of natural fibers such as jute, banana, kenaf, and sisal for the multiutilities [29] and structural applications [30]. However, the findings on the nontraditional natural fiber-reinforced biopolymer composites are incipient to utilize them for structural applications. In this regard, the present chapter provides a detailed review of the use of nontraditional natural fibers for advanced applications, particularly related to load-bearing low weight structural applications. Figure 1 gives a schematic of some of the nontraditional natural fiber sources that can be utilized for the synthesis of biocomposites for structural applications.

These natural fiber sources provide an additional advantage of high strength-to-low weight ratios. The densities of some of the conventional natural fibers in comparison with the nonconventional fibers are herewith given in Figure 2.

From the graphs of variation of densities for different natural fibers, it is herewith evident that the nonconventional natural fiber sources like gold cane, vakka, jackfruit stem fiber, and waste boom grass have relatively lower densities. However, they provide higher strength, thus providing composites with high strength with relatively lesser weights.

Jagadeesan et al. [31] have accomplished research on sesame oil cake biomass waste-derived cellulose microfillers reinforced with basalt/banana fiber-based hybrid polymeric composite for lightweight applications and have ascertained the need for nontraditional filler materials for natural fiber-reinforced biocomposites. Further, Rantheesh et al. [32] have worked on the characterization of novel microcellulose from *Azadirachta indica* A. Juss agroindustrial residual waste oil cake for futuristic applications. The higher cellulose content (73.53%), better crystallinity (66.23%), lower density (1.59 g/cm^3), considerable thermal stability (335.71°C), kinetic activation energy (83.06 kJ/mol), particle size (17.93 μm), and good surface roughness (47.004 nm) make neem cake cellulose

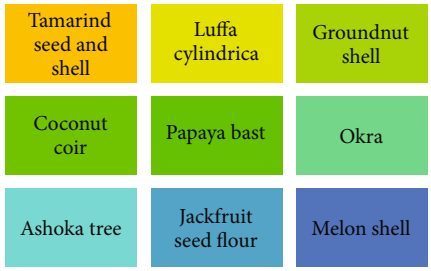

Figure 1: Schematic of some of the potential nontraditional natural filler and fiber sources reviewed in the article.

(NCC) suitable to be incorporated as a biofiller material in polymer matrices to manufacture ecofriendly composites.

Sunesh [33] has worked on the novel agrowaste-based cellulosic microfillers from *Borassus flabellifer* flower for polymer composite reinforcement. The results have showed that an agricultural residue can be converted into a valuable microsized cellulosic filler material for polymeric composite applications that can withstand processing temperature up to 200°C.

Ramesh et al. [34] have reviewed the influence of filler material on properties of fiber-reinforced polymer composites and have concluded that the use of filler material alongside the natural fibers enhances the performance attributes of the composite materials.

R Vijay et al. [35] have carried out the thermomechanical characterization studies on bio-fillers, namely *Azadirachta indica* seed powder, spent Camellia sinensis powder, and their combinations filled with jute fabrics in the epoxy matrix. The synthesized composites are evaluated both analytically and experimentally and compared with the neat epoxy. The test results revealed that the *Azadirachta indica* seed powder-filled composites exhibit better mechanical properties with lesser voids, while spent Camellia sinensis powder and its composites exhibit better thermal stability.

Ravikumar et al. [36] have explored the consequence of ecofriendly sodium bicarbonate treatment on the drilling behavior of jute fiber-reinforced polyester composites. The use of response surface methods for optimizing the composition, curing time, and process parameters has improved the machinability of natural filler-based jute fiber-reinforced composites.

Sumesh et al. [37] have focused on the impact of biowaste filler in mechanical applications. The biowastes from banana, pineapple, and coconut plants were used for preparing banana fly ash (BFA), pineapple fly ash (PFA), and coir fly ash (CFA) fillers. The results revealed that the flexural and impact properties enhanced up to 22.11% and 21.77%, with filler incorporation. The SEM results exhibited good bonding nature due to the application of filler powders. The EDX results proved the presence of silica and other inorganic content in the polymer composites adding to the improvement in properties of the composites.

Sumesh et al. [38] have studied the effect of banana, pineapple, and coir fly ash filled with hybrid fiber epoxy-based composites for mechanical and morphological study

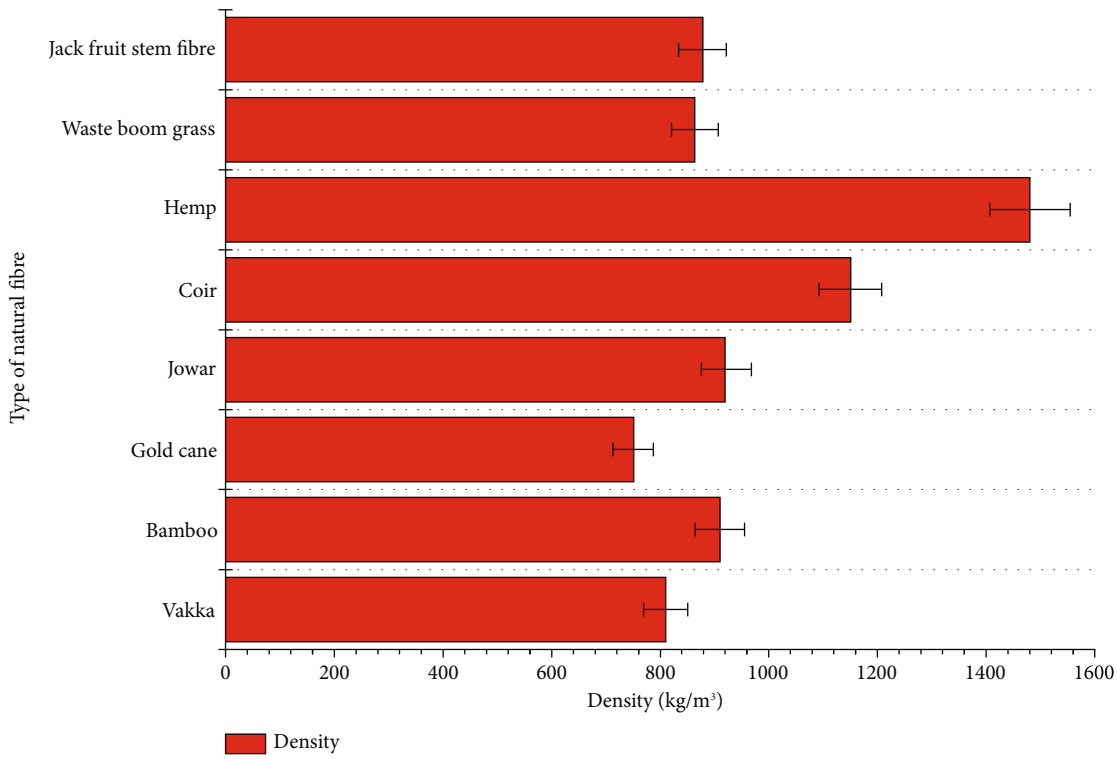

Figure 2: Type of natural fiber and their densities.

and have reported that the inclusion of the filler powders enhances the tensile strength from 23.78 to 33.79 MPa owing to the improved adhesion between the fibers and the matrix due to the addition of the filler.

Sumesh and Kanthavel [39] have carried out optimization studies by the Taguchi method and gray relational analysis to evaluate the influence of Al_2O_3 nanopowder, NaOH treatment, and compression pressure on free vibration and damping behavior of natural hybrid-based epoxy composites. The gray relational analysis concluded that 20 wt.% sisal and 15 wt.% coir with 2 wt.% nanoalumina and treatment with 5% NaOH at a compression pressure of 10 MPa provided optimized working condition for synthesis of the composite plates for better vibration behavior.

Sumesh et al. [40] have further studied the influence of different parameters in tribological characteristics of pineapple/sisal/TiO_2 filler incorporation by Taguchi optimization techniques, and the optimization results showed lower specific wear rate (SWR) by the incorporation of high TiO_2 filler (5 wt.%) addition in the pineapple/sisal fiber-reinforced epoxy composites.

The nontraditional filler-based natural fiber composites have been tried with ANN, GRA, and Taguchi approaches for optimization. In this regard, the works of Sumesh et al. [41] aim to optimize the mechanical performance of ramie/kenaf fibers under various parameters using GRA/TOPSIS methods.

This article encompasses a complete review of the literatures related to the use of nontraditional filler materials to improve the characteristics of the composites, which is a novel concept in comparison with the existing review particles based more on synthetic fibers and synthetic filler materials, as the need for ecocompatible and sustainable composite materials for structural applications is evolving day by day.

2. Different Nontraditional Filler Materials

The sourcing of different nontraditional natural fillers is an important aspect of the study. In this regard, a detailed review of the different nontraditional natural fibers is essential. Thus, the extraction methods of the naturally available materials like *Tamarindus indica* (tamarind) seed, *Arachis hypogaea* (groundnut) shell, coconut shell powder, Luffa cylindrica, coir powder, Abutilon (Indian mallow plant), and *Saraca asoca* (Ashoka tree fruit) are reviewed and discussed in detail in this section.

2.1. Mono Nontraditional Natural Filler-Based Biocomposites

2.1.1. Tamarindus indica. The *Tamarindus indica* is also known as the tamarind plant. The plant is widely grown in India, and its seed is used to make a hybrid composite. Initially, the tamarind seed (Figure 3) is extracted manually from the fruit and washed and treated with alkali solution to remove the stickiness. Later, the brownish layer of seed is removed and ground to a fine powder using commercially available flour grinders. Tamarind shells are washed to remove any impurities and dried to render them free of moisture. They are then ball milled into powder form. Epoxy resin of grade HSC-7101 is used as a matrix and HSC-9222 as the hardener. The composite was prepared using the hand

Figure 3: Tamarind seed with brown shell.

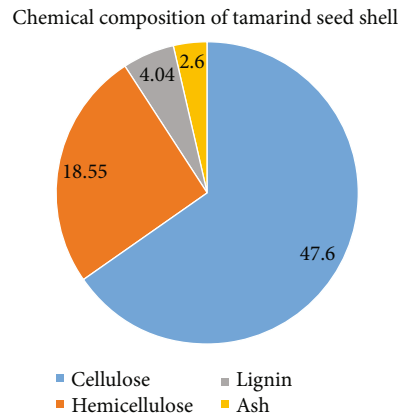

Figure 4: Chemical composition of the tamarind seed shell [43].

layup method. To obtain enhanced mechanical behavior such as impact resistance, shock resistance, vibration resistance, and water resistance, thixotropic high viscosity epoxy resin can be used with a variety of hardeners to create natural fiber-reinforced composites. Prior to the layup, tamarind powder and epoxy are mixed according to weight ratios such as 30 : 70 and 50 : 50. The samples were cured for 1 day. Cured samples were subjected to mechanical tests like the tensile test (ASTM D3039-20) and flexural test (ASTM D7264-20), followed up by water absorption test (ASTM D785). Baig and Mushtaq [42] concluded that laminates containing less tamarind shell have a lower rate of water absorption and thus a higher flexural modulus and bending strength, whereas laminates containing more tamarind shell have a higher tensile strength and hardness number.

Several findings have been reported on the variation of the mechanical characteristics of the composites with the varying wt.%. The research on the tamarind seed shell by Naik et al. [43] has revealed that the enhanced characteristics, the tensile strength, and Young's modulus of composites are 27.69 MPa and 362.39 MPa for 10% and 20% composition of tamarind seed shell in polymer matrix, respectively. The impact strength increased steadily up to 30% composition of tamarind seed shell. The hardness number varies from 72.33 to 53.33 HRN for the composite materials. This improvement is attributed to the microcoring and stronger bonding of the matrix and the reinforcements, particularly due to the inoculation brought about by the tamarind seed. The chemical composition of the tamarind shell comprises of greater weight percent of cellulose, which makes it a potential candidate for its use in composites, particularly for enhanced flexural and tensile strengths. Figure 4 gives the chemical composition of the tamarind seed shell.

2.1.2. Groundnut Shell. The biological name for groundnut is *Arachis hypogaea*. The powdered forms of groundnut shell (Figure 5(a)) are used as reinforcements. To extract the powder, the dirt present over the groundnut shells is removed by cleaning them with plain water. This is followed by alkali solution (of 4% concentration) treatment for around 2 hours. The groundnut shells are then washed again with plain water and sun-dried. The sun-dried shells are then ground into a fine powder (Figure 5(b)) and then sieved with different grades (0.5, 1, 2, and 3 mm) of sieve [44].

The particle board with varying ratios of groundnut shell powder and epoxy matrix (60 : 40, 65 : 35, and 70 : 30) is prepared by manual stirring and open molding and tested. The prepared composites are tested for its tensile behavior (ASTM D638), impact (ASTM D256), flexural behavior (ASTM D790), and water absorption (IS: 2380 (PART XVI)). The results showed that the composites exhibited moderate mechanical properties and low water absorption. Groundnut shell particle composites can be used as a substitute for wood in the production of particle board for use in indoor environments. This material has the potential to be used in structural, packaging, and other general applications [45].

2.1.3. Coconut Shell Powder. Coconut shell is an agricultural residue, usually disposed of through open burning. Toxic gases have been emitted from the open burning phase and can therefore be detrimental to human health and the environment. Thus, to reduce the risk of pollution, researchers have developed a new technology by using agrowastes to produce biocomposites. Coconut shell powder (CSP) is a solid nonfood waste, which can be potentially exploited to reduce the usage of synthetic fiber. Coconut shell is also a low-cost and low weight material that can be used to reduce the production cost of and fuel consumption for transportation [46]. This review has focused on the research carried out on the CSP loaded into different types of matrices, highlighting the fundamental, mechanical, physical, and thermal properties of CSP composites. This article also provides critical review of the development for CSP composite and the summary of the results presented in the literature, focusing in the properties of CSP with polymeric matrices and the application design for economical products.

2.1.4. Luffa cylindrica. The Luffa cylindrica, commonly known as sponge gourd, is mostly grown in European countries. The sponge gourd contains an inner fiber core and an outside mat core, with a multidirectional array of fibers forming a natural mat. They are extracted just by separating

(a) (b)

Figure 5: (a) Groundnut shell. (b) Groundnut shell powder after pretreatment [44].

Figure 6: Luffa cylindrica fiber [47].

and peeling the skin manually. Figure 6 gives the photographic image of the Luffa cylindrica fiber.

Saw et al. [47] and Noone et al. [48] investigated the effect of alkali treatment on Luffa cylindrica-reinforced composites and compared with glass-reinforced composites. Alkaline treatment is found to disrupt hydrogen bonds and helps to remove certain quantity of wax, lignin, and oils present on the exterior surface of cell walls of the fibers. It also depolymerizes cellulose and uncovers the small length. The spongy mat is treated with alkaline solution (5% NaOH), ClO_2 (oxidation), and furfuryl alcohol (FA) to remove impurities and to increase surface topology. Hand layup method and compression molding are employed to prepare the composites of treated and untreated Luffa fiber mats with epoxy resin in a mold of size $100 \times 100 \times 3\,mm^3$. The matrix-to-fiber weight ratio is kept constant at 70 : 30 in each composite. The tensile properties obtained for untreated Luffa fibers, alkali-treated Luffa fibers, and grafted Luffa fibers are represented in a tabular format for comparison. FA-grafted Luffa fiber composites show enhanced tensile properties as compared to alkaline-treated and untreated Luffa fiber composites, due to improved adhesion among the fibers and the matrix material. The properties obtained from the works of Saw et al. [47] and Noone et al. [48] are summarized in Table 1. The extracted Luffa fibers are further treated with 10 to 15 ml of sodium hydroxide (NaOH) solution and thoroughly dried for the preparation of composites. The composite material specimen is developed by the traditional hand layup process. The Luffa fiber composite ratio of 80 : 20 is prepared using LY556 (epoxy resin) and HY951 as the hardener and cured. The mechanical properties of the hybrid Luffa and glass fiber composites obtained from the works of Sreeramulu and Ramesh [49] are also summarized in Table 1. Luffa treated with alkaline solution showed better results as compared to glass-reinforced and untreated Luffa fiber, which indicates the possibility to replace glass fiber composites in structures of automobiles and other general applications.

The inclusion of the Luffa fiber reinforcements improves the mechanical characteristics of the composites owing to the stronger bonding between the matrix and reinforcements facilitated by the cellulose content in the fiber that enhances the adhesive strengthening.

Premalatha et al. [50] have studied the structural and thermal properties of chemically modified Luffa cylindrica fibers and have reported that the appropriate stearic acid treatment of the fibers improves the thermal stability and bonding capabilities.

2.1.5. Ashoka Tree Seed. Ashoka tree is commonly known as *Polyalthia longifolia*. The seeds collected after harvest are washed, and upper coats are removed and retreated with plain water and dried under sunlight for 12 days. The dried seeds are ball-milled to a particle size of 25 μm to 50 μm. The combination of powder and untreated vinyl ester is used to fabricate composites using compression molding. The composite is baked in an oven followed by accelerators N-dimethylaniline and styrene; the catalyst and promoters like methyl ethyl ketone peroxide (MEKP) and cobalt naphthenate are used. The prepared samples are cured for one day under a pressure of 100 kPa. The mechanical properties and thermal properties are determined by various ASTM standards like ASTM D638 for tensile test, ASTM D790-10 for flexural, and ASTM D256 for impact strength. Thermal properties like thermogravimetric and differential thermal analyses were conducted, and water absorption test was done for the sample specimen where the sample was submerged in water for 1 day. The test results revealed that

Table 1: Mechanical properties of hybrid Luffa and glass fiber composite [47–49].

Sample	Tensile strength (MPa)	Flexural strength (MPa)	Tensile modulus (MPa)	Flexural modulus (MPa)
Untreated Luffa fiber [47]	178.20	—	4263.84	—
Alkali-treated Luffa fiber	192.70	—	5184.62	—
FA-grafted Luffa fiber	226.40	—	5865.70	—
Luffa fiber under alkali treatment/epoxy [48]	34.1	57.2	—	—
Untreated Luffa fiber/epoxy	31.4	54.4	—	—
Glass-reinforced epoxy composite	23.3	50.2	—	—
Luffa fiber (5 gm)+glass fiber (15 gm) [49]	17.97	106.67	1331.24	4858.08
Luffa fiber (10 gm)+glass fiber (10 gm)	4.51	7.86	327.39	490.94
Luffa fiber (15 gm)+glass fiber (5 gm)	9.13	14.10	446.16	760.08

(a) (b)

Figure 7: (a) Okra plant. (b) Extracted okra fiber [52].

Table 2: Mechanical properties of okra fiber composites [52].

Tensile strength (MPA)	Tensile modulus (MPa)	Flexural modulus (MPa)	Impact strength (J/mm^2)	Density (g/cc)
263.5	7319.996	48.85	1.66	1.11

tensile strength increased up to 30 wt.% which leads to the use of these composites in the interior part of an automobile and aircrafts. Going beyond this limit, a weak interfacial adhesion ensued between the filler and matrix leading to a reduction in the strength. The addition of up to 35 wt.% filler to the samples had a significant impact on the flexural and impact strengths. The composite flexural and impact strengths were raised by factors of 1.60 and 2.63, respectively, over neat vinyl ester resin [51].

2.1.6. Okra (Ladies' Finger) Plant. Okra (gumbo or ladies' finger) plant (Figure 7(a)) is treated with water for 6 days to remove dirt from the roots of the stem. The fibers are then extracted from the stem of the plant (Figure 7(b)) and are dried under ambient conditions for 7 days. The fabrication process used is manual hand layup. The fibers are placed in layers so that they bind up with the epoxy resin. Catalyst and accelerator are added to reduce the curing time. A small load is applied over the mold and cured for 24 hrs. Postcuring is carried out for 2 hours, at 70°C. Mechanical tests like tension (ASTM D638-89), 3-point bending (ASTM D790 M-86), impact test (ASTM D256-10), and density test are performed. Table 2 depicts the mechanical properties of 60% volume fraction of fibers which exhibit optimal properties as compared to any other volume fractions from among the tested specimens. The study also showed that an increase in the volumetric fraction resulted in a significant improvement in tensile strength and tensile modulus. Figure 4 shows the images of the okra plant and the extracted okra fiber considered in the works of Potluri et al., while Table 2 gives the mechanical properties of the okra fiber in composites [52].

2.1.7. Artocarpus heterophyllus (Jackfruit). Artocarpus heterophyllus is commonly known as jackfruit. The rough skin of jackfruit is used as reinforcement for composite material in particulate form. Jackfruit skin is peeled manually, crushed, dried, and finally ground to 0.5 mm size. Ground skin particles are sieved to obtain 250 μm to 500 μm particulates. To remove excess lignin, the holocellulose bleaching is carried out on particles. This is further washed with plain water followed by heating to a temperature of around 70°C. For removing debris and odour, additives like sodium chlorite and acetic acid are added every 1 hr over a time period of

5 hrs. Initially, the uniform mixing of particles and polylactic acid (PLA) is carried out in Brabender Plasti-Corder, where the particles are infused at intermediate stages at a temperature of 170°C and mixed for 10 mins. The sample is then dried for 1 day at a constant temperature of 60°C. The composite granules obtained are fed in compression molding and sheets are obtained. The specimens from the prepared sheets are cut as per the ASTM standards and tested. Characterization such as infrared spectroscopy, scanning electron microscopy, and tensile testing was done under ASTM D638, and differential scanning calorimetry, thermogravimetric analysis, degradation test, and antimicrobial activity are performed. The results showed that the jackfruit skin can be used as the reinforcement up to 30% by weight and save the usage of plastics. The tensile characteristics of the composites improved when the fiber content was increased [53].

(1) Jackfruit Seed Flour. Marzuki et al. [54] studied the tensile properties of jackfruit flour reinforced in low-density polyethylene matrix. To start with, seeds are ground to particle sizes of 63 μm to 100 μm and are dried in an oven at 60°C. The content is mixed thoroughly, and the sample is extruded through a twin screw extruder at a temperature of 150°C and motor speed of 50 rpm. Extruded samples were then molded according to ASTM D638 for tensile test. The results showed that the use of higher percentage of filler content is not recommended due to the decline of tensile properties of the blends.

2.1.8. Melon Shell (Abutilon). Melon shell, also called cantaloupes, is dried under the sun for 7 days and ground. The resulting content is called uncarbonized melon shell. The dried shell is jammed in a graphite crucible and heated to 1200°C in a muffle furnace for the formation of carbonized melon shell. Hand layup technique is used to fabricate the samples using epoxy matrix LY556 and hardener of HY951. Different weight ratios (5, 10, 15, 20, and 30 wt.%) of carbonized and uncarbonized melon shells are attempted. The samples thus obtained are tested for mechanical properties like ASTM D638 for tensile behavior and ASTM D256-10 for impact behavior. The results showed weight saving potential with increase in carbonized melon content in epoxy matrix. As the amount of melon shell particles in the epoxy matrix increases, the compressive strength, elastic modulus, dielectric constant, and capacitance of the composites increased. The epoxy/carbonized melon shell composites had higher tensile strength, modulus, and impact energy than epoxy/uncarbonized melon shell particle composites. Melon shell particles added to the epoxy matrix boosted tensile strength and impact energy to a maximum of 20%. Melon shell particles can be employed to improve the mechanical and electrical properties of epoxy matrix composites for indoor and outdoor structural applications, according to the findings [55].

2.1.9. Fish Scale. Sekaran et al. utilized fish scales of bony fishes (*Osteichthyes*) as the reinforcing component in their composite material. Fish scales like ctenoid scales or ganoid scales are used to develop the composites using epoxy (LY556) as the matrix component and HY951 as the hardener. The prepared samples are tested for tensile behavior (ASTM D638), flexural behavior (ASTM D790), impact strength (ASTM D256), and hardness (ASTM E18-19). The sample with the volume fraction of 40% fish scale powder showed best results for tensile load; the sample with volume fraction of 30% fish scale powder showed best results for flexural load; and the sample with volume fraction of 25% fish scale powder showed best results for impact loads. The hardness of the composite material increased with an increase in the volume fraction of fish scale powder. The fish scale-reinforced polymeric composites are potential materials for pipes to carry pulverized coal in power plants, conveyor belt rollers, and low-cost housing materials [56].

Babu et al. reinforced fish scales in particulate form with epoxy grade of LY556 and hardener of HY951 and developed a new composite material using manual hand layup process and compression molding. Weight fractions of the filler were varied in percentages of 10, 15, 20, 25, 30, 35, and 40 in the epoxy matrix. Mechanical characteristics of the above samples were studied. It was found that increasing the filler material in the composite sample brought about an improvement in its mechanical properties to some degree. An optimum tensile strength is achieved at 30 percent weight fraction of fish scale filler. For 30% and 25% weight fractions of filler material, optimum flexural and impact strength are obtained, respectively. However, adding more fish scale fillers decreased the mechanical properties, which may be due to inadequate dispersion of filler in the epoxy matrix. The findings are very promising, and fish scale natural filler can be used with epoxy resin to make composite materials useful in applications such as [57].

Abhishek et al. have worked on the development of new hybrid Phoenix pusilla/carbon/fish bone filler-reinforced polymer composites and have reported that the addition of bionanofillers in hybrid polymer composites permits the enhancement of the tensile strength, flexural strength, and hardness by 22.5, 200, 100, and 15.2%, respectively [58].

2.1.10. Papaya Bast Mass. Coura et al. [59] have extensively worked on the papaya bast fibers that were extracted from the stem of the plant and soaked in water for 15 days. The fibers are then extracted, washed with plain water, and sun-dried for 7 days. The fabrication process used was manual hand layup and followed by compression molding. Epoxy resin of grade RenLam-M and Aradur HY96 as the hardener was used as the matrix. The fibers were cut to 5 mm to 20 mm lengths before the hand layup. Composite material specimens were prepared with 40% to 60% weight fraction of fiber content. The sample was pressured cured for 1 day at a temperature of 50°C. Mechanical testing of the samples is carried out as per ASTM standards: tensile test (ASTM D638-14), flexural test (ASTM D790-15), and density of fiber (ASTM D3800-99). They have concluded that mechanical properties of laminates prepared through longitudinal alignment of the bast fibers and without any internal voids showed superior tensile strength.

2.2. Hybrid Nontraditional Natural Filler-Based Biocomposites

2.2.1. Tamarind Seed and Shell-Based Filler-Based Hybrid Biocomposites. The hybrid composites of tamarind powder, Borassus tree trunk, and palmyra palm fiber (treated and untreated) and epoxy (LY556) matrix resin with hardener (HY906) are prepared with compression molding. The prepared composites are tested for its tensile behavior (ASTM D3039M), flexural behavior (ASTM D790-20), impact (ASTM D256-20), and active absorption (ASTM D590-20). The results showed that the particulate form of tamarind seed in the composite increases the strength significantly [60]. These types of composites have potential industrial applications such as room partitioning and false roofing.

Felix Sahayaraj et al. [61] have studied the effect of hybridization on properties of tamarind seed nanopowder incorporated Luffa cylindrica fruit waste fiber-reinforced polymer composites. They have reported that the tensile and flexural properties of the composites improved owing to the stronger bonding due to the hybridization reactions between the tamarind seed shell and the fiber in the matrix. Thus, the tamarind seed shell is a potential candidate for its use in real-time applications for improving the properties of the natural fiber-reinforced polymer composites.

2.2.2. Coconut Coir and Groundnut Shell. The hybrid of coconut coir and groundnut shell composites was formed and compared for its tensile and flexural strengths. The coconut coir and groundnut shell were pretreated with NaOH and washed with water and dried under the sun for 1 day. The fibers were crushed to different grain sizes of 1 mm, 1.5 mm, and 2 mm. Fabrication of the composite is done by hand layup and compression molding. Epoxy grade of LY556 was used, followed by a hardener HY951. Sample of composites was prepared by weight ratios of epoxy to fiber with different grain sizes. The samples are then cured for 15 hours. Water absorption test was carried out by keeping the samples under water for 1 day. The results revealed higher flexural strength and a lower rate of water absorption when the particulate fiber size is 1 mm. In respect of mechanical properties, coir fiber composite showed superior behavior as compared to groundnut shell-powdered composites [62]. Such properties will make these composites as the better substitutes for wood-based material in many applications. This composite is also having the potential for its use in structural, packaging, and other general applications.

2.2.3. Coconut Shell Powder and Areca Palm Fibers. Hybrid composites with continuous areca palm fibers and coconut shell in particulate form as the reinforcements and epoxy matrix are fabricated by hand layup technique. Initially, the areca fibers are extracted from the stem of the plant and pretreated in plain water for 15 days. The dry coconut shells are broken into smaller pieces and then ground to fine particles. The particles are then sieved using 150 μm sieve. Physical tests like density test, void content, and water absorption tests are performed as per ASTM D 792-21, ASTM D 2734-70, and ASTM D 570-98, respectively. The thermal conductivity of the prepared samples is also investigated using ASTM E1530. The results revealed that areca-coconut shell powder/epoxy composites are considerably influenced by the fiber loading. Thermal conductivity decreased with an increase in the fiber loading. Also, with an increase in fiber loading, the theoretical and experimental densities of hybrid composites see a fall, whereas void content and water absorption capacities of hybrid composites were found to increase [63].

2.2.4. Coconut Shell and Tamarind Shell Powder. Somashekhar et al. [64] used coconut shell in powdered form and strained in standard sieve BS 1377-1990. The particle size was around 300 μm. Polyethylene pellets were crushed in a shredder, and the tamarind shell was powdered in a grinder. Hand layup was used to create samples of three distinct composites. Epoxy resin was used as a matrix, and five separate combinations of constituents were generated by varying the matrix proportion from 5% to 25%. The samples were hot pressed at 140°C for 15 to 20 mins at a pressure of 2 MPa. The samples were cured at room temperature for 30 mins. Mechanical properties, water absorption test, and hardness tests were performed. It was discovered that combining tamarind shell powder with coconut shell powder enhanced the tensile property by around 50%. The optimum results and mechanical properties are obtained when the content is 50% coconut shell powder, 5% tamarind shell powder, and 45% epoxy resin.

3. Comparison of the Strength Characteristics of Different Nontraditional Natural Fibers and Their Composites

The nontraditional natural fiber-reinforced composites have significant advantages over the conventional composites due to the higher cellulose and hemicellulose contents that enhance the adhesive characteristics of the composites owing to stronger bonding and greater strength [65]. These materials are critically useful for their applications in sustainable solutions, viz., automotive dashboards, window panels, doors, and other components ranging from aerospace to marine domains [66]. Table 3 gives the comparisons of the mechanical properties of some of the nontraditional fiber-/filler-reinforced composites.

The critical review of some of the properties of these nontraditional natural fiber-reinforced composites has given a comprehensive picture of their performance capability, and it is herewith noted that the tensile, flexural, and impact properties are important for using these composites in structural applications. A comparative evaluation of the mechanism behind these enhanced properties is accomplished by morphological studies and is reported in this section. The increase in the mechanical properties is attributed to the stronger bonding between the fiber and matrix due to the homogeneous distribution of the filler in the matrix. From the works of Hariprasad et al. [69], the *Sansevieria trifasciata* fiber-reinforced polyester composites containing 15% SiO_2 exhibit higher mechanical strength due to the homogeneous distribution of the filler in polyester because

Table 3: Comparisons of the mechanical properties of some of the nontraditional fiber-/filler-reinforced composites.

Authors, year	Natural reinforcements used	Matrix used	Major properties studied
Felix Sahayaraj et al., 2021 [67]	Tamarind (*Tamarindus indica* L.) seed nanopowder incorporated jute-hemp fibers	Epoxy resin	The authors have studied the tensile, flexural, and interlaminar shear strength and impact properties. The tensile strength and modulus of the composites are 39.52 MPa and 2.648 GPa, and the flexural strength and modulus values are 89.62 MPa and 9.24 GPa, respectively. The impact strength and ILSS values were found to be 2.35 J and 3.62 MPa.
Iyyadurai Jenish et al., 2022 [68]	*Cissus quadrangularis* stem fiber with red mud nanofillers	Epoxy resin	The authors have studied the hardness and wear characteristics of the composites. The hardness of the samples increased by 10.7% for 5 wt.% red mud addition and 14.2% for 10 wt.% of red mud addition.
Hariprasad et al., 2022 [69]	Sansevieria trifasciata fiber with SiO_2 and B4C filler	Polyester resin	The authors have studied the tensile, flexural, and impact properties. The polyester resin-based composite with 20 wt.% STF fiber and 15 wt.% SiO_2 exhibits a maximum flexural strength of 103.58 MPa and impact strength of 27.4 kJ/m^2 in comparison with the neat and other compositions of the composites.
Felix Sahayaraj et al., 2022 [61]	*Tamarindus indica* seed powder (TISP) incorporated *Luffa cylindrica* fruit (LCF)	Epoxy resin	The authors have studied the density, tensile, compression, flexural, impact, hardness, and water absorption behavior and thermogravimetric analysis. The results revealed that the inclusion of 7.5 wt.% TISP resulted in better physicomechanical and thermal properties.
Premkumar et al., 2022 [70]	Sansevieria trifasciata fibers	Polyester resin	The authors have studied the tensile, flexural, and impact strength of NaOH-treated and NaOH-untreated fiber-reinforced composites. It is reported that the tensile strength of the composites increases up to 48.47 MPa, the flexural strength up to 69.17 MPa, and the impact strength up to 16.34 kJ/m^2, with the inclusion of treated fibers.
Prem Kumar et al., 2022 [71]	Jute/snake grass/kenaf fiber *Annona reticulata* seed filler addition	Epoxy resin	The authors have studied the tensile, ILSS, and wear properties of the composites. The tensile, flexural, inter-lamina, and impact strengths of the composite with an equal amount of snake grass and kenaf fibers filled with *Annona reticulata* seed filler were 50.12 MPa, 132.53 MPa, 1.952 MPa, and 2.23 J, respectively.

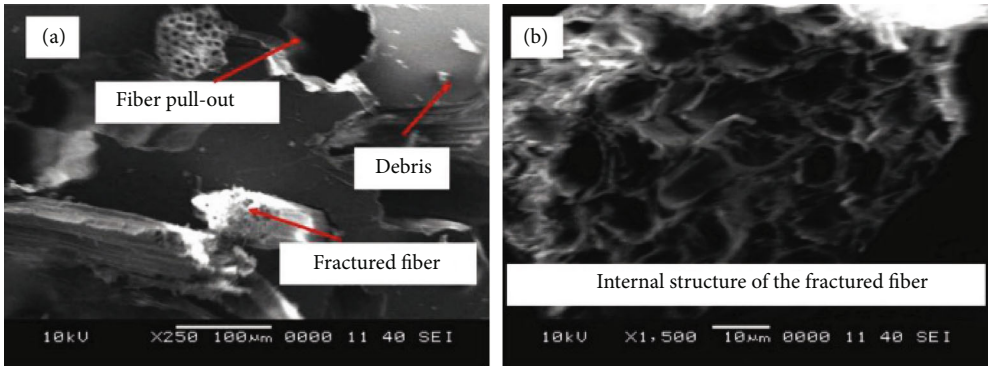

Figure 8: SEM images of *Sansevieria trifasciata* fiber-reinforced polyester composites with (a) 15 wt.% SiO_2 and (b) 20 wt.% SiO_2 nanofiller [72].

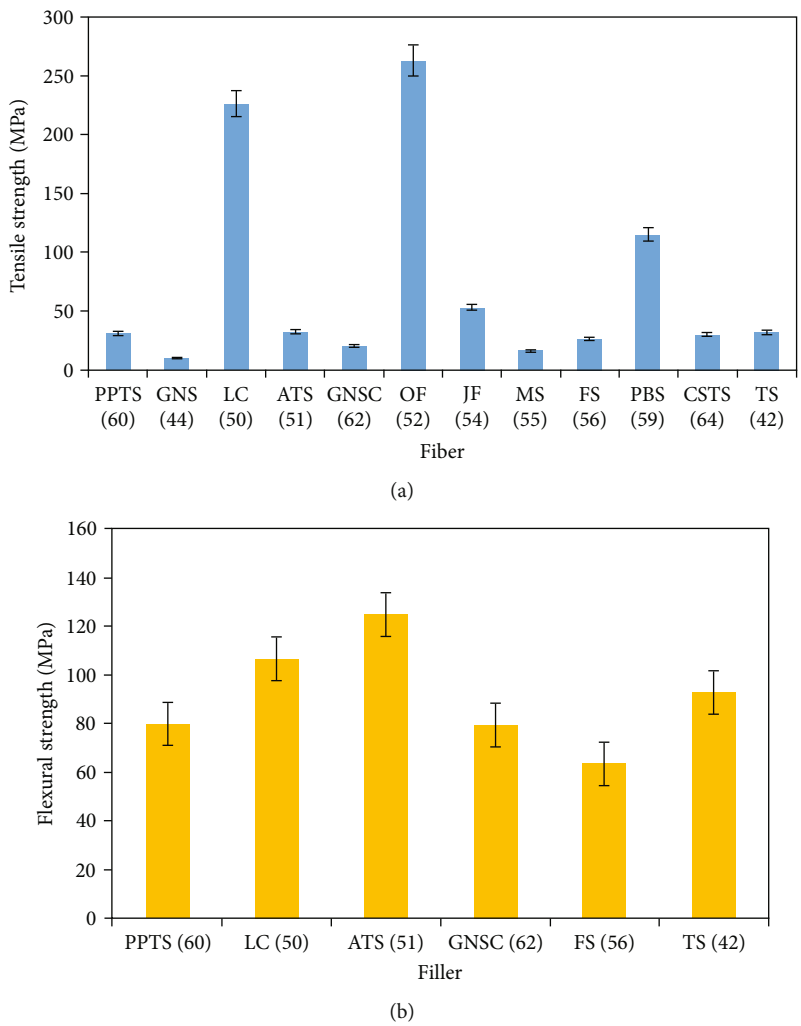

Figure 9: Comparison of (a) tensile strength and (b) flexural strength of various nontraditional fillers from various literature.

the uniform distribution of filler improves the fiber bonding significantly. However, when the SiO_2 concentration rises beyond 15 wt.%, the agglomerates form, resulting in a reduced bonding strength.

Further, the properties of different natural fibers are accomplished and provided in the graphical format in Figures 8(a) and 8(b), respectively. Figure 9(a) depicts the tensile properties of various nonconventional natural fiber composites. It is observed that okra fiber composites exhibited better tensile properties followed by Luffa cylindrica. The least tensile properties are represented by groundnut shell composites due to improper bonding between the

Table 4: List of abbreviations used in the graphs in Figures 8(a) and 8(b).

PPTS (60)	Palmyra palm and tamarind seed powder
GNS (44)	Groundnut shell
LC (50)	Luffa cylindrica
ATS (51)	Ashoka tree seed
GNSC (62)	Groundnut shells and coir fiber
OF (52)	Okra fibers
JF (54)	Jackfruit skin powder
MS (55)	Melon shell
FS (56)	Fish scale
PBS (59)	Papaya bast fiber
CSTS (64)	Coconut shell powder and tamarind shell powder
TS (42)	Tamarind shell

constituents. The maximum flexural strength was shown by Ashoka tree seed composites compared to other composites which are represented in Figure 9(b). The abbreviation used in the graphs is given in Table 4.

Jagadeesh et al. [73] have reviewed the effect of natural filler materials on fiber-reinforced hybrid polymer composites and have reported that the natural fiber-reinforced polymer composites are the new innovative class of sustainable materials having good mechanical properties for practical applications. Further, to increase the performance of composites, researchers pointed out that using filler materials essentially increases the mechanical properties and in turn minimizes the organic contents in the composite laminates. Hemath et al. [72] work on the effect of TiC nanoparticles on accelerated weathering of coir fiber filler, and basalt fabric-reinforced bio/synthetic epoxy hybrid composites have further reiterated the significance of stronger bonding between the filler content and the fiber that facilitates greater strength characteristics.

4. Sustainability of the Nontraditional Natural Fibers

Nontraditional fibers are considered one of the arising accoutrements of the present time, and the "sustainability" term is frequently associated with these nontraditional fiber-reinforced composites [74]. It is due to the biocompatibility and ecosustainability of the nontraditional natural fiber-reinforced composites that the utilization of these composites for real-time applications is increasing [75]. Biodegradability and recyclability can have a significant effect on both future and present-day requirements of ecocompatible developments [76].

Ecofriendly accoutrements are gaining attention throughout the world owing to continually raising environmental concerns and several research on the sustainability indices of renewability, recyclability, commercial viability, biodegradability, and ecocompatibility [77]. In this paper, the review of the sustainability aspects of the traditional natural fiber-reinforced composites is also accomplished and the key factors are identified [78]. The major attributes which make the nontraditional fibers sustainable and very much vital for their use in green composites are depicted in the schematic block diagram given in Figure 10 [79, 80].

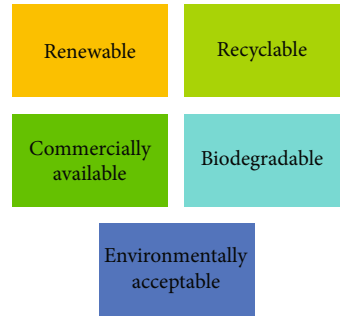

Figure 10: Factors influencing the sustainability of the nontraditional natural fillers for green composites.

The need for sustainable biocomposites for real-time applications has facilitated substantial research to be accomplished in the domain of nontraditional natural filler-based polymer-based biocomposites [81], and this review has considered all the aspects of ecocompatibility and sustainability.

5. Conclusion and Future Scope of Work

The review paper has made an attempt to present the summary of various works carried out by researchers on the use of nontraditional natural fibers in green composite materials while keeping different engineering applications in the perspective.

(i) An increase in the usage of these nontraditional natural fibers will reduce carbon footprints and greenhouse gas emissions

(ii) Among all the nontraditional filler-based composites studied in the present work, the okra fiber-filled composites exhibited better tensile properties, and Ashoka tree seed composites show better flexural properties, while fish scale-reinforced polymer composites showed higher impact strength

(iii) The hybrid combination of okra fibers with Ashoka tree seed powder and fish scale-reinforced composites can be used for the load-bearing applications

(iv) The manufactured composites are economical and can be processed at locations where they are available abundantly

(v) The nontraditional natural filler-based composites are environment friendly and can be recycled

(vi) These composites may eventually replace man-made synthetic fiber composites for different engineering applications such as interiors of automobiles and aircrafts, as the tensile, flexural, hardness, wear, impact, and thermomechanical stability of these natural filler-based composites are relatively higher

than the composites fabricated from the conventional synthetic sources

The review provides a comprehensive text on the non-traditional fillers for the researchers to look for the alternative filler materials which are suitable for the applications in low load-bearing structures. The researchers shall further explore the possible avenues, for the usage of mango shell powder, tamarind shell powder, tamarind seed powder, tamarind fiber, and walnut shell powder in polymeric composites for various applications.

Data Availability

The data supporting the review is already included in the manuscript, and any other additional data are readily available from the corresponding authors and will be furnished upon request.

Conflicts of Interest

The authors declare that they have no known competing financial interests or personal relationships that could have appeared to influence the work reported in this paper.

References

[1] A. Karimah, M. R. Ridho, S. S. Munawar et al., "A review on natural fibers for development of eco-friendly bio-composite: characteristics, and utilizations," *Journal of Materials Research and Technology*, vol. 13, pp. 2442–2458, 2021.

[2] M. Ramesh, C. Deepa, L. R. Kumar, M. R. Sanjay, and S. Siengchin, "Life-cycle and environmental impact assessments on processing of plant fibres and its bio-composites: a critical review," *Journal of Industrial Textiles*, vol. 51, 4_suppl, pp. 5518S–5542S, 2022.

[3] U. S. Gupta, M. Dhamarikar, A. Dharkar, S. Tiwari, and R. Namdeo, "Study on the effects of fibre volume percentage on banana-reinforced epoxy composite by finite element method," *Advanced Composites and Hybrid Materials*, vol. 3, no. 4, pp. 530–540, 2020.

[4] Y. Chen, O. Chiparus, L. Sun, I. Negulescu, D. V. Parikh, and T. A. Calamari, "Natural fibers for automotive nonwoven composites," *Journal of Industrial Textiles*, vol. 35, no. 1, pp. 47–62, 2005.

[5] M. Jannah, M. Mariatti, A. Abu Bakar, and H. P. S. Abdul Khalil, "Effect of chemical surface modifications on the properties of woven banana-reinforced unsaturated polyester composites," *Journal of Reinforced Plastics and Composites*, vol. 28, no. 12, pp. 1519–1532, 2009.

[6] L. A. Pothan, C. N. George, M. Jacob, and S. Thomas, "Effect of chemical modification on the mechanical and electrical properties of banana fiber polyester composites," *Journal of Composite Materials*, vol. 41, no. 19, pp. 2371–2386, 2007.

[7] W. M. Wang, Z. S. Cai, and J. Y. Yu, "Study on the chemical modification process of jute fiber," *Journal of Engineered Fibres and Fabrics*, vol. 3, no. 2, p. 155892500800300203, 2008.

[8] E. A. Elbadry, M. S. Aly-Hassan, and H. Hamada, "Mechanical properties of natural jute fabric/jute mat fiber reinforced polymer matrix hybrid composites," *Advances in Mechanical Engineering*, vol. 4, Article ID 354547, 2012.

[9] A. Guo, Z. Sun, and J. Satyavolu, "Experimental and finite element analysis on flexural behavior of mortar beams with chemically modified kenaf fibers," *Construction and Building Materials*, vol. 292, article 123449, 2021.

[10] Y. Y. Sim and K. L. Nyam, "Application of *Hibiscus cannabinus* L. (kenaf) leaves extract as skin whitening and anti-aging agents in natural cosmetic prototype," *Industrial Crops and Products*, vol. 167, article 113491, 2021.

[11] E. A. Simbaña, P. E. Ordóñez, Y. F. Ordóñez, V. H. Guerrero, M. C. Mera, and E. A. Carvajal, "Abaca: cultivation, obtaining fibre and potential uses," in *Handbook of Natural Fibres*, pp. 197–218, Elsevier, 2020.

[12] A. Sinha, H. Narang, and S. Bhattacharya, "Tensile strength of abaca epoxy laminated composites," *Materials Today: Proceedings*, vol. 5, no. 14, pp. 27861–27864, 2018.

[13] T. Singh, C. I. Pruncu, B. Gangil, V. Singh, and G. Fekete, "Comparative performance assessment of pineapple and Kevlar fibers based friction composites," *Journal of Materials Research and Technology*, vol. 9, no. 2, pp. 1491–1499, 2020.

[14] S. Waddar, J. Pitchaimani, M. Doddamani, and E. Barbero, "Buckling and vibration behaviour of syntactic foam core sandwich beam with natural fiber composite facings under axial compressive loads," *Composites Part B: Engineering*, vol. 175, article 107133, 2019.

[15] A. Gilorkar, R. Murugan, and J. Pitchaimani, "Thermal buckling of sisal and glass hybrid woven composites: experimental investigation," *Composites Part C: Open Access*, vol. 2, article 100012, 2020.

[16] O. Huerta-Cardoso, I. Durazo-Cardenas, V. Marchante-Rodriguez, P. Longhurst, F. Coulon, and A. Encinas-Oropesa, "Up-cycling of agave tequilana bagasse-fibres: A study on the effect of fibre- surface treatments on interfacial bonding and mechanical properties," *Results in Materials*, vol. 8, article 100158, 2020.

[17] M. Puttegowda, S. M. Rangappa, M. Jawaid, P. Shivanna, Y. Basavegowda, and N. Saba, "15 - Potential of natural/synthetic hybrid composites for aerospace applications," in *Sustainable Composites for Aerospace Applications*, M. Jawaid and M. Thariq, Eds., pp. 315–351, Woodhead Publishing, 2018.

[18] B. Mazhoud, F. Collet, S. Prétot, and C. Lanos, "Effect of hemp content and clay stabilization on hygric and thermal properties of hemp-clay composites," *Construction and Building Materials*, vol. 300, article 123878, 2021.

[19] Z. Kamble, B. K. Behera, R. Mishra, and P. K. Behera, "Influence of cellulosic and non-cellulosic particle fillers on mechanical, dynamic mechanical, and thermogravimetric properties of waste cotton fibre reinforced green composites," *Composites Part B: Engineering*, vol. 207, article 108595, 2021.

[20] A. M. Kazi, D. Devika, S. Waddar, and D. V. A. Ramasastry, "Characterization of roselle fiber composites for low load bearing structures," *Polymer Composites*, vol. 42, no. 5, pp. 2589–2597, 2021.

[21] S. Malagi, R. Anawal, S. V. Gorabal, and M. Doddamani, "Tensile characteristics of HDPE/walnut shell composites," *IOP Conference Series: Materials Science and Engineering*, vol. 561, no. 1, article 012089, 2019.

[22] S. Kanakannavar and J. Pitchaimani, "Fracture toughness of flax braided yarn woven PLA composites," *International Journal of Polymer Analysis and Characterization*, vol. 26, no. 4, pp. 364–379, 2021.

[23] V. Naik, M. Kumar, and V. Kaup, "Study on the mechanical properties of alkali treated screw pine root fiber reinforced in epoxy matrix composite material," *AIP Conference Proceedings*, vol. 2317, no. 1, article 020023, 2021.

[24] M. Rajesh and J. Pitchaimani, "Dynamic mechanical and free vibration behavior of natural fiber braided fabric composite: comparison with conventional and knitted fabric composites," *Polymer Composites*, vol. 39, no. 7, pp. 2479–2489, 2018.

[25] W. Lu, J. Fei, J. Yang et al., "A novel method to identify yak fiber in textile," *Textile Research Journal*, vol. 83, no. 8, pp. 773–779, 2013.

[26] F. J. Wortmann and G. Wortmann, "Quantitative fiber mixture analysis by scanning electron microscopy," *Textile Research Journal*, vol. 62, no. 7, pp. 423–431, 1992.

[27] N. Kumar, A. Singh, and R. Ranjan, "Fabrication and mechanical characterization of horse hair (HH) reinforced polypropylene (PP) composites," *Materials Today: Proceedings*, vol. 19, pp. 622–625, 2019.

[28] M. F. Ali, M. S. Hossain, S. Ahmed, and A. M. Sarwaruddin Chowdhury, "Fabrication and characterization of eco-friendly composite materials from natural animal fibers," *Heliyon*, vol. 7, no. 5, article e06954, 2021.

[29] V. Naik and M. Kumar, "A review on natural fiber composite material in automotive applications," *Engineered Science*, vol. 18, 2021.

[30] M. A. Azman, M. R. M. Asyraf, A. Khalina et al., "Natural fiber reinforced composite material for product design: a short review," *Polymers*, vol. 13, no. 12, p. 1917, 2021.

[31] R. Jagadeesan, I. Suyambulingam, D. Divakaran, and S. Siengchin, "Novel sesame oil cake biomass waste derived cellulose micro-fillers reinforced with basalt/banana fibre-based hybrid polymeric composite for lightweight applications," *Biomass Conversion and Biorefinery*, vol. 13, pp. 4443–4458, 2023.

[32] J. Rantheesh, S. Indran, S. Raja, and S. Siengchin, "Isolation and characterization of novel micro cellulose from *Azadirachta indica* A. *Juss* agro-industrial residual waste oil cake for futuristic applications," *Biomass Conversion and Biorefinery*, vol. 13, pp. 4393–4411, 2023.

[33] N. P. Sunesh, S. Indran, D. Divya, and S. Suchart, "Isolation and characterization of novel agrowaste-based cellulosic micro fillers from Borassus flabellifer flower for polymer composite reinforcement," *Polymer Composites*, vol. 43, no. 9, pp. 6476–6488, 2022.

[34] M. Ramesh, L. N. Rajeshkumar, N. Srinivasan, D. V. Kumar, and D. Balaji, "Influence of filler material on properties of fiber-reinforced polymer composites: a review," *E-Polymers*, vol. 22, no. 1, pp. 898–916, 2022.

[35] R. Vijay, A. Vinod, R. Kathiravan, S. Siengchin, and D. L. Singaravelu, "Evaluation of Azadirachta indica seed/spent Camellia sinensis bio-filler based jute fabrics–epoxy composites: experimental and numerical studies," *Journal of Industrial Textiles*, vol. 49, no. 9, pp. 1252–1277, 2020.

[36] P. Ravikumar, G. Rajeshkumar, P. Manimegalai, K. R. Sumesh, M. R. Sanjay, and S. Siengchin, "Delamination and surface roughness analysis of jute/polyester composites using response surface methodology: consequence of sodium bicarbonate treatment," *Journal of Industrial Textiles*, vol. 51, 1_suppl, pp. 360S–377S, 2022.

[37] S. Nagaraja, P. Bindiganavile Anand, R. N. Mahadeva Naik, and S. Gunashekaran, "Effect of aging on the biopolymer composites: mechanisms, modes and characterization," *Polymer Composites*, vol. 43, no. 7, pp. 4115–4125, 2022.

[38] K. R. Sumesh, V. Kavimani, G. Rajeshkumar, S. Indran, and G. Saikrishnan, "Effect of banana, pineapple and coir fly ash filled with hybrid fiber epoxy based composites for mechanical and morphological study," *Journal of Material Cycles and Waste Management*, vol. 23, no. 4, pp. 1277–1288, 2021.

[39] K. R. Sumesh and K. Kanthavel, "Synergy of fiber content, Al_2O_3 nanopowder, NaOH treatment and compression pressure on free vibration and damping behavior of natural hybrid-based epoxy composites," *Polymer Bulletin*, vol. 77, no. 3, pp. 1581–1604, 2020.

[40] K. R. Sumesh, G. Saikrishnan, P. Pandiyan et al., "The influence of different parameters in tribological characteristics of pineapple/sisal/TiO_2 filler incorporation," *Journal of Industrial Textiles*, vol. 51, 5_suppl, pp. 8626S–8644S, 2022.

[41] S. Keerthiveettil Ramakrishnan, K. Vijayananth, G. Pudhupalayam Muthukutti, P. Spatenka, A. Arivendan, and S. P. Ganesan, "The effect of various composite and operating parameters in wear properties of epoxy-based natural fiber composites," *Journal of Material Cycles and Waste Management*, vol. 24, no. 2, pp. 667–679, 2022.

[42] W. Baig and M. Mushtaq, "Experimental investigation of mechanical properties on tamarind shell-reinforced epoxy composite laminates," *Materials Today: Proceedings*, vol. 45, pp. 257–263, 2021.

[43] S. Naik, B. Halemani, and G. U. Raju, "Investigation of the mechanical properties of tamarind seed particles reinforced epoxy composites," *AIP Conference Proceedings*, vol. 2057, article 020023, 2019.

[44] G. U. Raju and S. Kumarappa, "Experimental study on mechanical properties of groundnut shell particle-reinforced epoxy composites," *Journal of Reinforced Plastics and Composites*, vol. 30, no. 12, pp. 1029–1037, 2011.

[45] M. A. Usman, I. Momohjimoh, and A. S. Gimba, "Effect of groundnut shell powder on the mechanical properties of recycled polyethylene and its biodegradability," *Journal of Minerals and Materials Characterization and Engineering*, vol. 4, no. 3, pp. 228–240, 2016.

[46] S. N. Nadzri, M. T. Sultan, A. U. Shah et al., "A comprehensive review of coconut shell powder composites: preparation, processing, and characterization," *Journal of Thermoplastic Composite Materials*, vol. 35, no. 12, pp. 2641–2664, 2022.

[47] S. K. Saw, R. Purwar, S. Nandy, J. Ghose, and G. Sarkhel, "Fabrication, characterization, and evaluation of Luffa cylindrica fiber reinforced epoxy composites," *BioResources*, vol. 8, no. 4, pp. 4805–4826, 2013.

[48] S. Noone, K. Purushothaman, and R. Pradhan, "An investigation on Luffa cylindrica fiber reinforced epoxy composite," *Materials Today: Proceedings*, vol. 33, pp. 1026–1031, 2020.

[49] D. Sreeramulu and N. Ramesh, "Synthesis, characterization, and properties of epoxy filled Luffa cylindrica reinforced composites," *Materials Today: Proceedings*, vol. 5, no. 2, pp. 6518–6524, 2018.

[50] N. Premalatha, S. S. Saravanakumar, M. R. Sanjay, S. Siengchin, and A. Khan, "Structural and thermal properties of chemically modified *Luffa cylindrica* fibres," *Journal of Natural Fibres*, vol. 18, no. 7, pp. 1038–1044, 2021.

[51] B. Stalin, N. Nagaprasad, V. Vignesh et al., "Evaluation of mechanical, thermal and water absorption behaviors of

Polyalthia longifolia seed reinforced vinyl ester composites," *Carbohydrate Polymers*, vol. 248, article 116748, 2020.

[52] R. Potluri, K. J. Paul, and P. Prasanthi, "Mechanical properties characterization of okra fiber based green composites & hybrid laminates," *Materials Today: Proceedings*, vol. 4, no. 2, pp. 2893–2902, 2017.

[53] N. A. Abdullah and M. K. Ab Wahab, "The effect of modified jackfruit (Artocarpus heterophyllus Lam.) seed starch on the properties of poly lactic acid," *IOP Conference Series: Materials Science and Engineering*, vol. 957, no. 1, article 012017, 2020.

[54] M. N. A. Marzuki, I. S. M. A. Tawakkal, M. S. M. Basri et al., "The effect of jackfruit skin powder and fiber bleaching treatment in PLA composites with incorporation of thymol," *Polymers*, vol. 12, no. 11, p. 2622, 2020.

[55] V. Aigbodion and C. Atuanya, "Improving the properties of epoxy/melon shell bio-composites: effect weight percentage and form of melon shell particles," *Polymer Bulletin*, vol. 73, no. 12, pp. 3305–3317, 2016.

[56] P. R. Sekaran, S. G. Kumar, J. A. Singh, and J. Vairamuthu, "Experiment investigation and analysis of fish scale reinforced polymer composite materials," *Materials Today: Proceedings*, vol. 33, pp. 4542–4545, 2020.

[57] K. R. Babu, V. Jayakumar, G. Bharathiraja, and S. Madhu, "Experimental investigation of fish scale reinforced polymer composite," *Materials Today: Proceedings*, vol. 22, pp. 416–418, 2020.

[58] S. Abhishek, M. R. Sanjay, R. George, S. Siengchin, J. Parameswaranpillai, and C. I. Pruncu, "Development of new hybrid *Phoenix pusilla*/carbon/fish bone filler reinforced polymer composites," *Journal of the Chinese Advanced Materials Society*, vol. 6, no. 4, pp. 553–560, 2018.

[59] G. L. C. Coura, R. T. S. Freire, J. C. . Santos, L. Á. . Oliveira, F. Scarpa, and T. H. Panzera, "Tensile and flexural properties of epoxy laminates with natural papaya bast fibre cellular layers," *Composites Part C: Open Access*, vol. 2, article 100017, 2020.

[60] T. Srinivasan, S. Bharani Kumar, G. Suresh et al., "Experimental investigation and fabrication of palmyra palm natural fiber with tamarind seed powder reinforced composite," *IOP Conference Series: Materials Science and Engineering*, vol. 988, no. 1, article 012022, 2020.

[61] A. Felix Sahayaraj, M. Muthukrishnan, and M. Ramesh, "Influence of *Tamarindus indica* seed nano-powder on properties of *Luffa cylindrica* (L.) fruit waste fiber reinforced polymer composites," *Polymer Composites*, vol. 43, no. 9, pp. 6442–6452, 2022.

[62] O. V. Potadar and G. S. Kadam, "Preparation and testing of composites using waste groundnut shells and coir fibres," *Procedia Manufacturing*, vol. 20, pp. 91–96, 2018.

[63] G. K. Chowdari, D. K. Prasad, and S. B. Devireddy, "Physical and thermal behaviour of areca and coconut shell powder reinforced epoxy composites," *Materials Today: Proceedings*, vol. 26, pp. 1402–1405, 2020.

[64] T. M. Somashekhar, P. Naik, V. Nayak, and S. Rahul, "Study of mechanical properties of coconut shell powder and tamarind shell powder reinforced with epoxy composites," *IOP Conference Series: Materials Science and Engineering*, vol. 376, article 012105, 2018.

[65] N. Santhosh, B. A. Praveena, H. V. Srikanth et al., "Experimental investigations on static, dynamic, and morphological characteristics of bamboo fiber-reinforced polyester composites," vol. 2022, Article ID 1916877, pp. 1–11, 2022.

[66] B. A. Praveena, N. Santhosh, A. Buradi et al., "Experimental investigation on density and volume fraction of void, and mechanical characteristics of areca nut leaf sheath fiber-reinforced polymer composites," *International Journal of Polymer Science*, vol. 2022, Article ID 6445022, 13 pages, 2022.

[67] A. Felix Sahayaraj, M. Muthukrishnan, M. Ramesh, and L. Rajeshkumar, "Effect of hybridization on properties of tamarind (*Tamarindus indica L.*) seed nano-powder incorporated jute-hemp fibers reinforced epoxy composites," *Polymer Composites*, vol. 42, no. 12, pp. 6611–6620, 2021.

[68] I. Jenish, A. F. Sahayaraj, M. Appadurai, E. F. Irudaya Raj, and P. Suresh, "Sea sand abrasive wear of red mud micro particle reinforced *Cissus quadrangularis* stem fiber/epoxy composite," *Journal of Natural Fibres*, vol. 19, no. 16, pp. 13216–13231, 2022.

[69] P. Hariprasad, M. Kannan, C. Ramesh et al., "Mechanical and Morphological Studies of *Sansevieria trifasciata* Fiber- Reinforced Polyester Composites with the Addition of SiO_2 and B_4C," *Advances in Materials Science and Engineering*, vol. 2022, Article ID 1634670, 5 pages, 2022.

[70] R. Premkumar, K. Sathish Kumar, J. Maniraj et al., "Experimental studies on mechanical and thermal properties of polyester hybrid composites reinforced with Sansevieria trifasciata fibers," *Advances in Materials Science and Engineering*, vol. 2022, Article ID 8604234, 6 pages, 2022.

[71] R. Prem Kumar, M. Muthukrishnan, and A. Felix Sahayaraj, "Experimental investigation on jute/snake grass/kenaf fiber reinforced novel hybrid composites with Annona reticulata seed filler addition," *Materials Research Express*, vol. 9, no. 9, article 095304, 2022.

[72] M. Hemath, J. Tengsuthiwat, S. Mavinkere Rangappa et al., "Effect of TiC nanoparticles on accelerated weathering of coir fiber filler and basalt fabric reinforced bio/synthetic epoxy hybrid composites: physicomechanical and thermal characteristics," *Polymer Composites*, vol. 42, no. 9, pp. 4897–4910, 2021.

[73] P. Jagadeesh, M. Puttegowda, Y. G. Thyavihalli Girijappa, S. M. Rangappa, and S. Siengchin, "Effect of natural filler materials on fiber reinforced hybrid polymer composites: an overview," *Journal of Natural Fibres*, vol. 19, no. 11, pp. 4132–4147, 2022.

[74] G. Ravichandran, G. Rathnakar, and N. Santhosh, "Enhancement of mechanical properties of epoxy/halloysite nanotube (HNT) nanocomposites," *SN Applied Sciences*, vol. 1, no. 4, pp. 1–8, 2019.

[75] G. Ravichandran, G. Rathnakar, N. Santhosh, and R. Suresh, "A comparative study on the effect of HNT and nano-alumina particles on the mechanical properties of vacuum bag moulded glass-epoxy nanocomposites, mechanics of advanced," *Composite Structures*, vol. 8, pp. 119–131, 2021.

[76] G. Ravichandran, G. Rathnakar, N. Santhosh, and R. Thejaraju, "Effects of Heat Treatment Conditions on Microstructure and Mechanical Properties of halloysite nanotube (HNT) filled Epoxy nanocomposites," *International Journal of Engineering and Advanced Technology*, vol. 9, no. 1, pp. 3314–3321, 2020.

[77] G. Ravichandran, G. Rathnakar, and N. Santhosh, "Effect of heat treated HNT on physico-mechanical properties of epoxy nanocomposites," *Composites Communications*, vol. 13, no. 2, pp. 42–46, 2019.

[78] G. Ravichandran, G. Rathnakar, N. Santhosh, and R. Suresh, "Wear characterization of HNT filled glass-epoxy composites using Taguchi's design of experiments and study of wear morphology," *Composites Theory and Practice*, vol. 20, no. 2, pp. 85–91, 2020.

[79] B. A. Praveena, N. Santhosh, D. P. Archana et al., "Influence of nanoclay filler material on the tensile, flexural, impact, and morphological characteristics of jute/E-glass fiber-reinforced polyester-based hybrid composites: experimental, modeling, and optimization study," *Journal of Nanomaterials*, vol. 2022, Article ID 1653449, 17 pages, 2022.

[80] B. A. Praveena, B. Abdulrajak, N. Santhosh, V. K. Kedambadi, H. Jaibheem, and D. Huliya, "Study on characterization of mechanical, thermal properties, machinability and biodegerability of natural fiber reinforced polymer composites and its applications, recent developments and future potentials: a comprehensive review," *Material Today Proceedings*, vol. 52, Part 3, pp. 1255–1259, 2021.

[81] G. Anand, N. Santhosh, and S. Vishvanathperumal, "Introduction to aging in bio composites," in *Aging Effects on Natural Fiber-Reinforced Polymer Composites, Composites Science and Technology*, C. Muthukumar, S. Krishnasamy, S. M. K. Thiagamani, and S. Siengchin, Eds., pp. 1–16, Springer, Singapore, 2022.

Hindawi
Advances in Polymer Technology
Volume 2023, Article ID 8639185, 18 pages
https://doi.org/10.1155/2023/8639185

Review Article

Challenges and Opportunities in Additive Manufacturing Polymer Technology: A Review Based on Optimization Perspective

S. Raja and A. John Rajan

Department of Manufacturing Engineering, School of Mechanical Engineering (SMEC), Vellore Institute of Technology, Vellore, Tamil Nadu, India

Correspondence should be addressed to A. John Rajan; ajohnrajan@vit.ac.in

Received 11 November 2022; Revised 12 December 2022; Accepted 27 March 2023; Published 19 April 2023

Academic Editor: Indran Suyambulingam

In the emerging modern technology of additive manufacturing, the need for optimization can be found in literature in many places. Additive manufacturing (AM) is making an object layer by layer directly from digital data. Previous works of literature have classified additive manufacturing processes into seven types. However, there is a lack of comprehensive review describing the optimization challenges and opportunities in the material extrusion process (polymer technology) and also the need for FDM polymer materials application in impeller making. In this review paper, a specific optimization method called multicriteria decision-making (MCDM) from the mathematical programming technique used in additive manufacturing polymer technology (AMPT) is discussed. The other topics such as different types of optimization techniques, applications of different MCDM tools and their applications in different fields including AM, and the optimization challenges and opportunities in AMPT particularly impeller application are discussed.

1. Introduction

Additive manufacturing (AM) has been used everywhere in the manufacturing industry in recent decades [1]. AM has many advantages such as less waste during production, lower production cost, and direct production from design data. In this, material extrusion process polymer technology is attracting more attention due to many features such as raw material availability, low cost of raw material, and low cost of production machinery [2]. The polymer raw materials are used to produce end products for many applications like automobile, medical, and civil engineering. A lot of research is being done to improve this technology, and one of the most important is operational research [3]. Operation research is a subject from the scientific mathematical technique used to make decisions in difficult situations [4]. It is divided into three categories and can be seen in Figure 1. Vijay et al. used optimization approaches to investigate the thermal conditions of several polymer composites and then ranked the composites as a result [5]. Jothibasu et al. explored the different polymer composite mechanical properties using optimization techniques, and the result selected the best composite for making an L-framed flower stand application [6].

Using the MCDM optimization technique, Singaravelu et al. performed the research on various polymer composite brake frictions. Their findings showed that the boron graphite composition is the best among the various compositions [7]. The natural fibre polymer composite was investigated by Manoharan et al. using the Taguchi optimization approach, with the goal of identifying the ideal process parameter for natural fibre [8]. With the aid of the Taguchi optimization approach, Binoj et al. examined the areca fruit natural polymer composite fibre process parameter optimization and determined the ideal process parameter [9]. Mannan et al. did research on natural polymer composite for

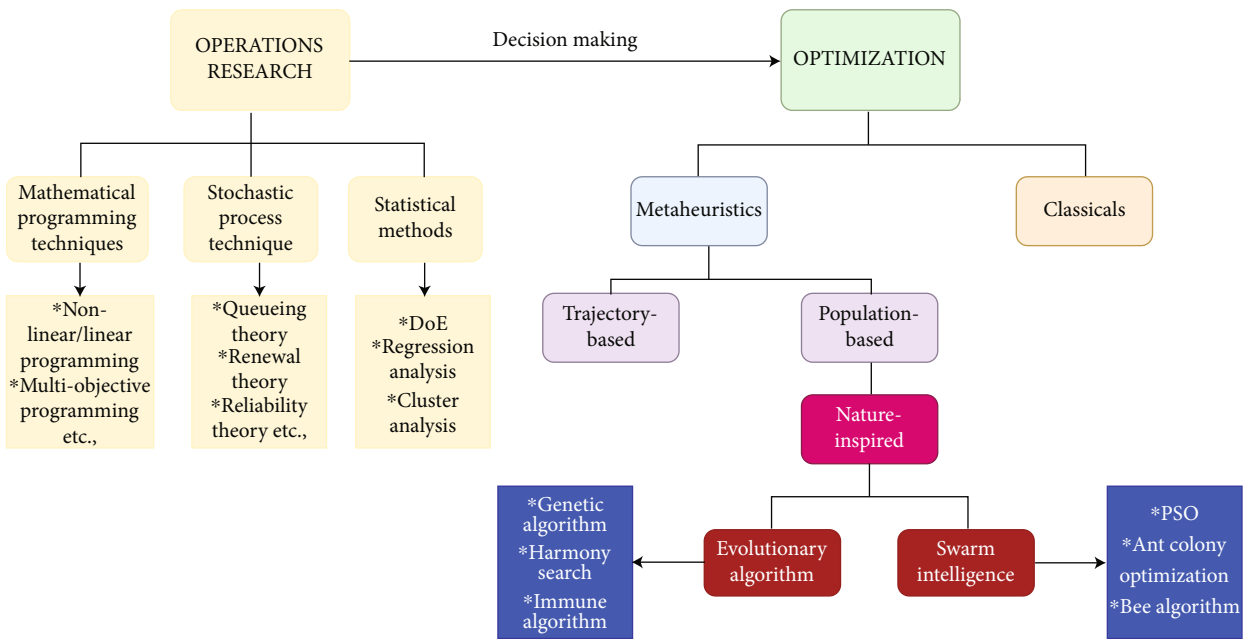

Figure 1: Classification of optimization techniques [13].

construction applications, and their findings produced a composition that was suitable for achieving a high level of mechanical strength [10, 11]. Natrayan et.al investigated the soybean oil-reinforced polymer composite shear strength with different compositions using an optimization method and their result ranked the high-strength composition [12]. Based on the literatures, optimization is the method of choosing the best and is a part of our daily life. There are several steps involved in optimization such as describing a system mathematically, finding the variables and conditions that are satisfying, describing the properties of the system, and finding the state of the system.

1.1. Optimization Techniques in Operation Research. De Leon-Aldaco et.al [13] reviewed the power converters' metaheuristic optimization methods and classified the operation research optimization techniques as follows.

1.1.1. Mathematical Programming Techniques. In this method, the decision maker's opinions are converted into numerical values and solved with a decision matrix, for example, MCDM (multicriteria decision-making) and linear and nonlinear programming.

1.1.2. Stochastic Process Techniques. This method application is known by previous researchers to give an approximate solution, for example, queuing theory and renewal theory.

1.1.3. Statistical Method. This method is used to evaluate the experimental results and select the appropriate one, for example, DOE and the Taguchi method.

From this, the application of MCDM methods in additive manufacturing' material extrusion process (polymer technology) has very less research only carried out. Therefore an extensive review of MCDM and also a few DOE methods are proposed to optimize problems in the additive manufacturing material extrusion process. In the first step, MCDM and DOE optimization methods, additive manufacturing, and, especially, the material extrusion process can be seen. Then, the optimization challenges and opportunities in additive manufacturing polymer technology are explained in detail. More specifically, the novelty of this research is focusing on optimization in additive manufacturing polymer technology in impeller applications. Finally, the summary and conclusion show how well the research purpose was accomplished.

1.2. MCDM (Multicriteria Decision-Making). MCDM is a method of selecting a suitable alternative from more than one alternative [14]. Previous researchers have applied this method to complex decision-making situations in many fields. The MCDM technique has been used in many names in previous literature such as multicriteria decision analysis (MCDA) [15], multiobjective decision analysis (MODA) [16], and multiattribute decision-making (MADM) [17]. Stojcic et al.'s [18] review explored how the MCDM method has been widely used in two ways, like qualitative and quantitative research, by previous literature. Figure 2 describes the hierarchy of the MCDM method and more details are given in Section 3. MCDM tools are AHP (analytical hierarchy process) [19], TOPSIS (technique for order of preference by similarity to ideal solution) [20], ANP (analytical network process) [21], BWM (best worst method) [22], FAHP (fuzzy analytical hierarchy process) [23], COPRAS (complex proportional assessment) [24], and PROMETHEE (preference ranking organization method for enrichment of evaluations) [25]. In this, a pairwise matrix is created based on the opinions of the decision maker, and it is converted into numerical values from 0 to 9 (based on the MCDM tool/technique) [26]. Then, the created pairwise matrix is evaluated by basic steps like criteria weight, consistency ratio, and random

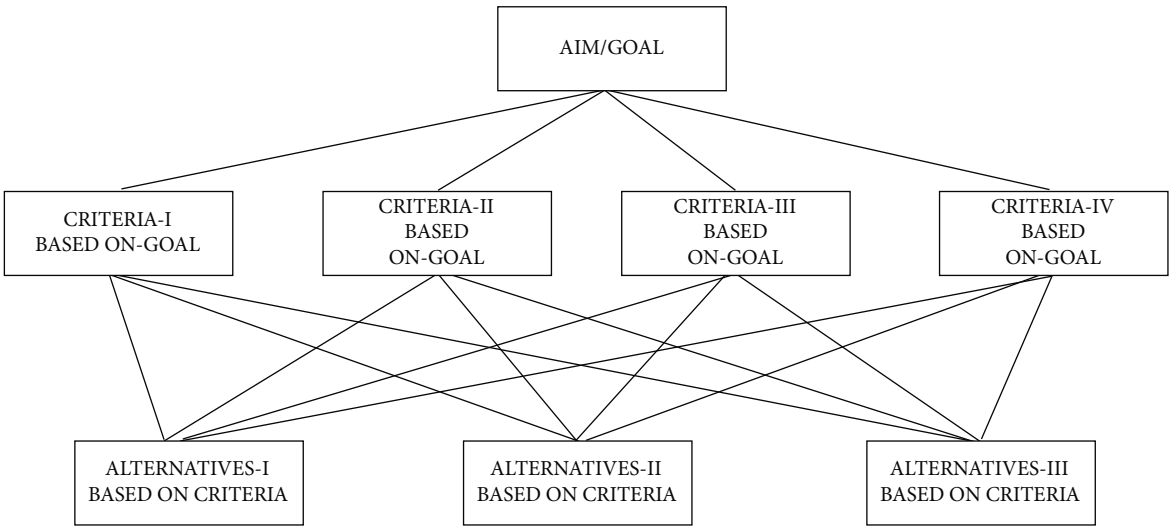

Figure 2: Hierarchy structure of multicriteria decision-making technique.

index [27]. Finally, the alternatives are ranked based on the decision matrix and priority values. On the basis of ranking, the necessary alternative is selected by the decision-maker.

1.3. DOE (Design of Experiment). The design of the experiment is considered as an optimization technique that helps to analyze the data by conducting an experiment easily through knowledge and techniques and to find its correlation [28]. DOE is a structured technique used to find the relationship between input and output variables [29]. Also, it is used to find which parameter most influenced the result. DOE is used in many fields like agriculture [30], engineering [31], and defense [32]. Three such DOE strategies have been used by previous researchers like examining multiple factors simultaneously [33] and examining multiple factors together [34], and one factor is examined at a time [35]. Anderson and McLean [36] have classified the DOE as the factorial design (finding main effects on prices), response surface design (finding the maximum and minimum response of various factors), mixture design (finding ideal proportion in mixture processes), and optimal design (used to find sufficient details).

Factorial design is divided into two categories such as full factorial design (experiment conducted for all factors and levels) and fractional factorial design (experiment conducted only for certain combination levels), and the Taguchi design is also a type of factorial design. It is also believed that sustainability can be achieved through the use of optimization techniques in many fields. Additive manufacturing is considered to be a growing field in the current manufacturing industry, and also, the optimization needs to find a lot of processes [37].

1.4. Additive Manufacturing. The contribution of additive manufacturing in the manufacturing sector has attracted a bit more attention in recent times as compared to conventional manufacturing [38]. The main reason for this is many advantages such as lightweight, low material wastage of material, low cost, less lead time, low emission, and facilities that can easily produce hard material [39]. As proof of this, the use of additive manufacturing in forming, castings, etc. industries has increased gradually [40]. It consists of seven methods as shown in Figure 3 with its modern technology and raw materials. Liquid polymer, discrete particle, molten material, and solid shield systems are several types of AM technology. In this binder jetting, 3D printing, ink jetting, S-print, and M-print technology are used in which metal polymer and ceramic raw materials are used. The vat photopolymerization process uses stereolithography and digital light processing technologies and uses photo polymer and ceramics raw materials. The sheet lamination method uses ultrasonic consolidation and laminated object manufacture technology and hybrid metallic ceramic raw material. The material extrusion process uses FDM technology and polymer raw material. Material jetting uses polyjet, ink jetting, thermojet technology, and wax raw material. The powder bed fusion process uses SLS, SLM, EBM, and DMLS technologies and raw materials like polymer, ceramic powders, metal powders, and ceramic. Finally, in direct energy deposition, technologies such as LP-DED, LW-DED, AW-DED, and EB-DED and metal, metal alloy, wire, powder, ceramic, and polymer raw materials are used. However, the material extrusion method only has the lowest technical cost and raw material costs. Although many researchers have conducted many researches on the material extrusion method, some research gaps can be seen in the optimization area. In particular, this review article describes current problems such as the selection of production machinery and supplier selection.

1.4.1. Material Extrusion Process (Polymer Technology). In the material extrusion process, the filament (polymers) is passed through a hot extruder to form a final product layer by layer according to the given (.STL) design [42]. Material extrusion is a method with very low-cost raw material and machine costs compared to all other AM processes. The lower cost of raw materials and machinery gets more

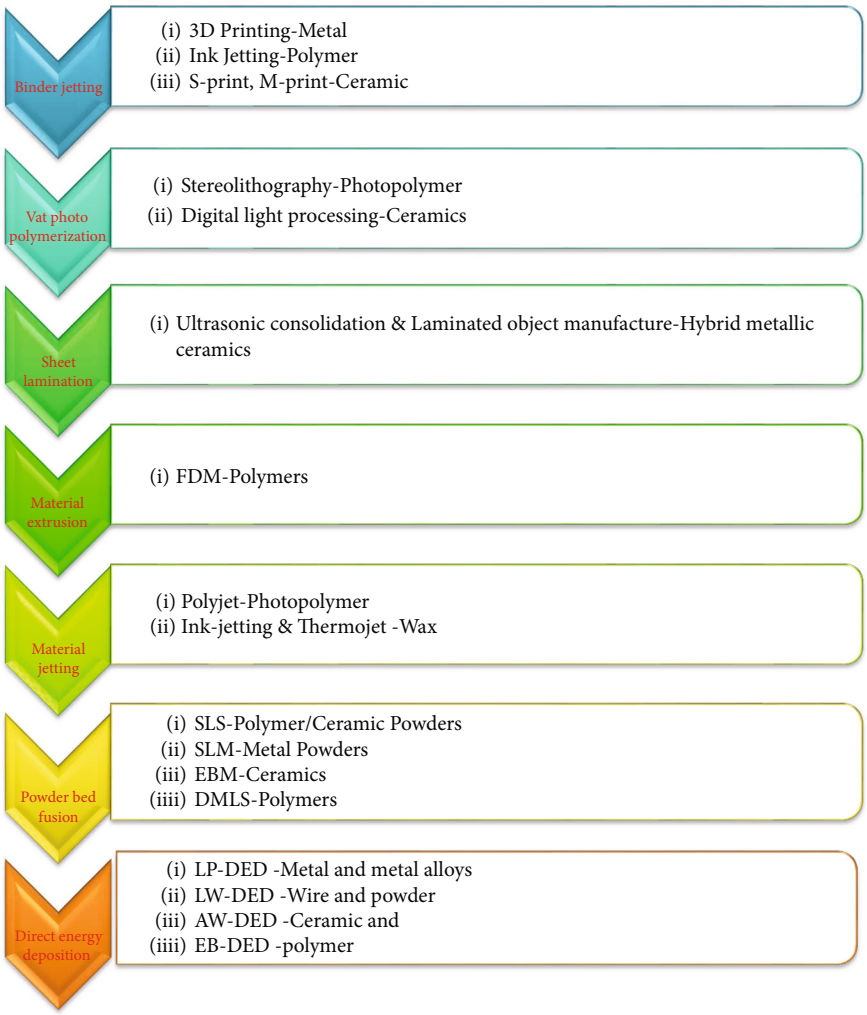

Figure 3: Different processes/technologies/materials in additive manufacturing [38–41].

attention in the market for increased producers and users of AM. Thermoplastic polymers like PLA (polylactic acid) and ABS (acrylonitrile butadiene styrene) are used as raw materials in the form of filament and the standard filament wire diameter used as 1.75 mm [43]. FDM machine and their important components such as filament spoof, filament, extruder, melting zones, molten filament, and object in the build platform are shown in Figure 4. Each polymer raw material has its unique properties, for example, PLA is a biodegradable material [44], and ABS is a toxic material [45]. So, it is used in many applications like medical [46], pipe making [47], and impeller making [48] based on the raw material properties. A previous literature review revealed that the FDM-fabricated impeller of the rotodynamic hydraulic pump performed similarly to the original impeller.

Filament spoof is the roll of polymer filament in the wire format, and it is connected with extruders. The extruders have heated with the melting zone when the wire filament passes through the melting zone.

Printing parameters play an important role in the material extrusion 3D printing process. One of the most important printing parameters is the infill pattern such as

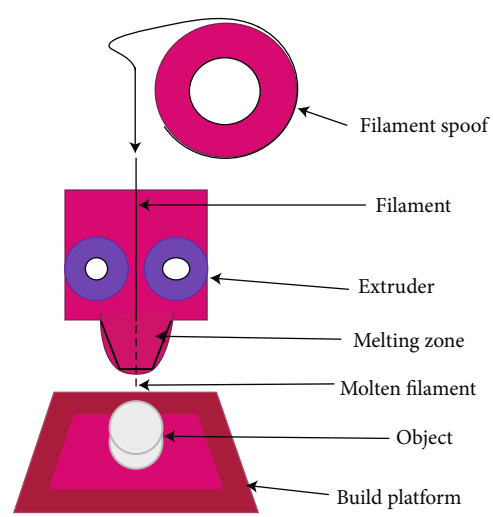

Figure 4: Material extrusion process (software: draw.io-online free software).

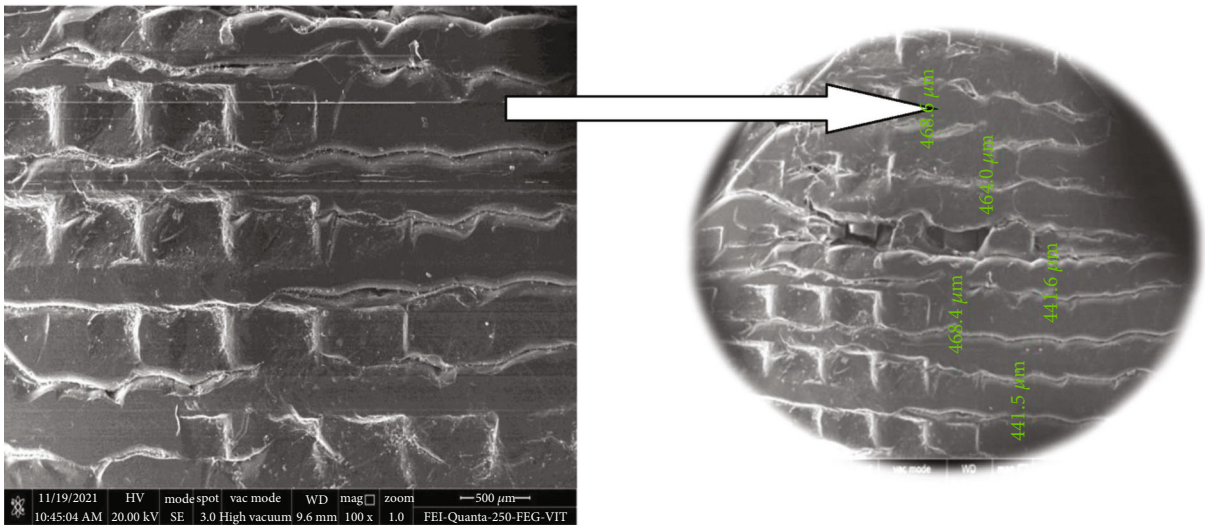

Hexagonal pattern and average 454.6 μm gap found

Figure 5: Hexagonal pattern morphology.

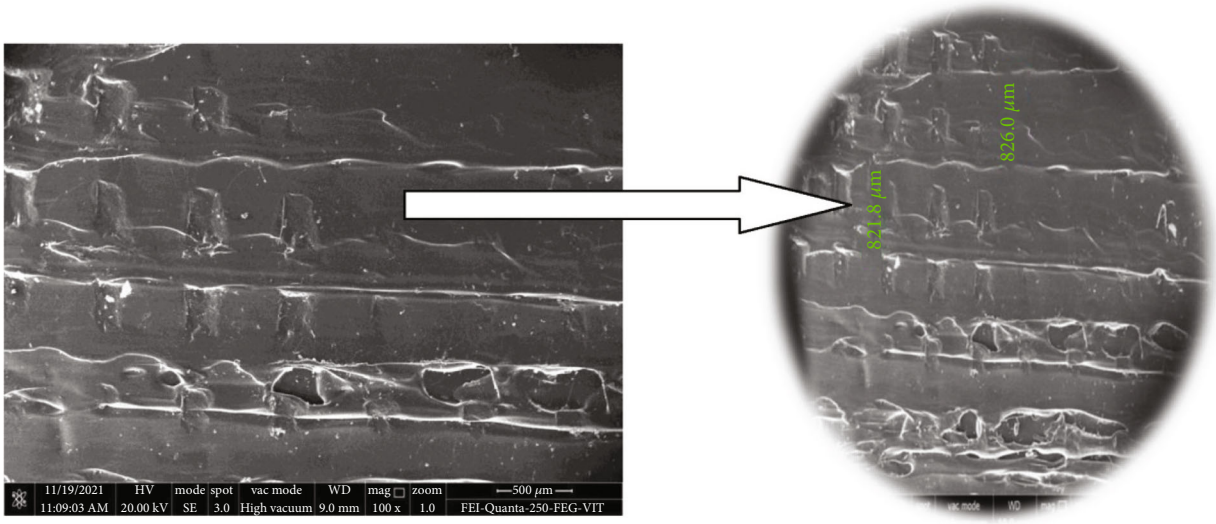

Line pattern and average 822.5 μm gap found

Figure 6: Line pattern morphology.

hexagonal, line, and triangle printing in which Figure 5 shows the microstructure of the hexagonal pattern. In this, the printing shape and distance of the hexagonal pattern and the average gap between the two layers are calculated as 454.6 μm.

Figure 6 illustrates the microstructure of the line pattern and the 822.5 μm average spacing for two adjacent lines.

Finally, Figure 7 describes the microstructure of the triangle pattern and the 612.7 μm average spacing between the two layers. These three remarkable patterns were produced by an FDM printer using PLA filament and described with the help of a FESEM image for this research. Based on this result, the hexagonal pattern is recommended for production in the material extrusion method because it is observed only for a low construction gap between two layers. Also, the solid infill pattern is having more conductivity after the spatter coating. Therefore, the microstructure of the solid infill pattern is unable to find with spatter coating. However, the remaining patterns can be selected according to the infill percentage, user's application, etc.

Figure 8 illustrates the entire additive manufacturing process and some important material extrusion raw materials and their applications.

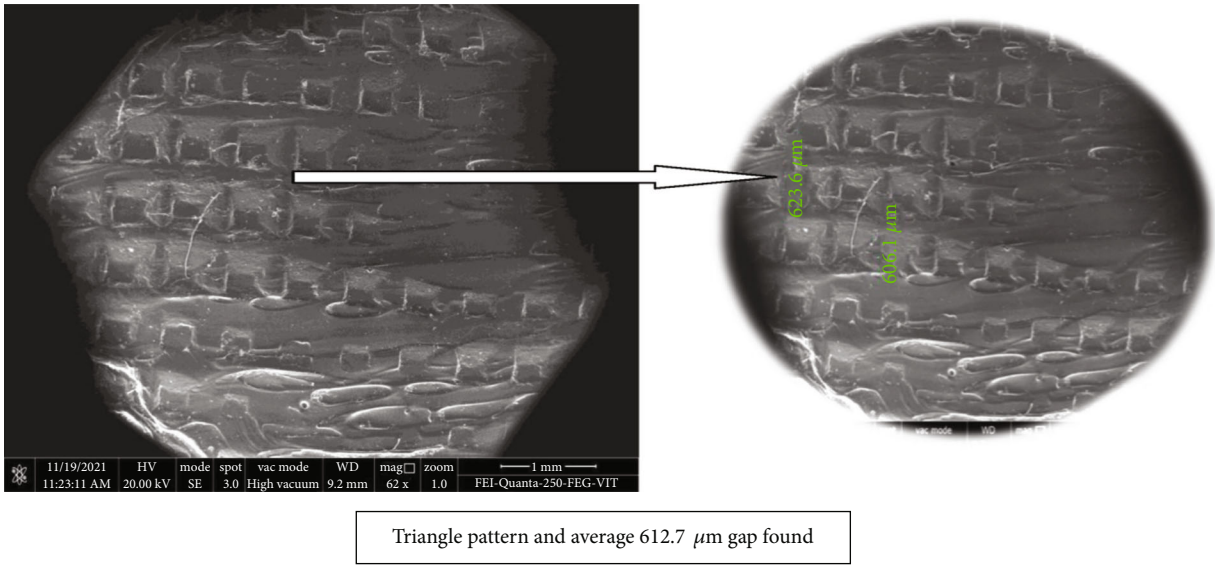

Triangle pattern and average 612.7 μm gap found

Figure 7: Triangle pattern morphology.

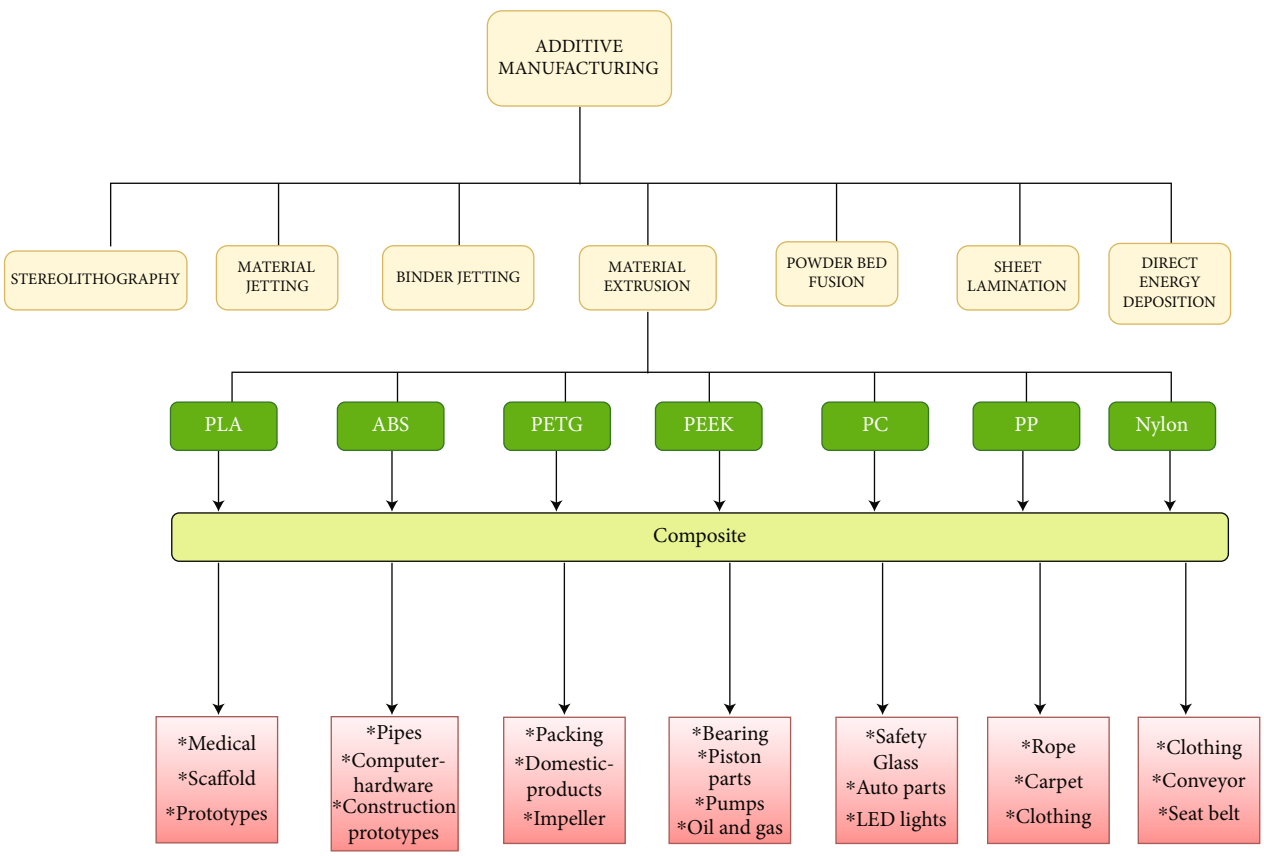

Figure 8: Additive manufacturing process and material extrusion's raw material with the application.

2. Optimization Challenges in Additive Manufacturing Polymer Technology

Optimization is the process of selecting the desired or suitable one from among several alternatives [49]. As illustrated in Figure 9, resource, weight, cost, and process are chosen for the optimization ways. The current optimization problem identified in the material extrusion process is as follows.

2.1. Machine Selection. The sales of similar FDM machines with slightly different features are increasing day by day in the market [10, 16, 50, 51]. Also, choosing the most suitable

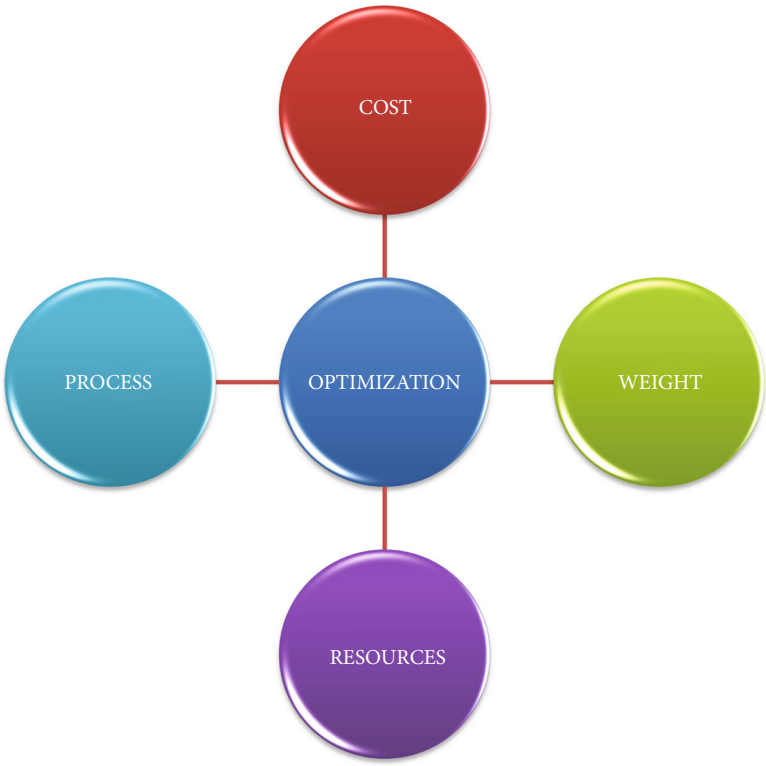

Figure 9: Different applications of optimization.

machine for the users from the various machines that have got the same sales rating on the online platforms is considered to be the current challenge so commercial companies can use optimization techniques to reduce investment and end product costs. Figure 10 described the optimization problems in the material extrusion process and proposed optimization tools.

2.2. Supplier Selection. FDM machine users suffer a lot because after purchasing a machine, services such as repair or replacement of parts are not available properly from suppliers. Therefore, it is considered very important for wholesalers to choose distributors [10, 17, 52, 53] who provide proper sales and service. Solving this using any suitable MCDM method would be a novelty.

2.3. Logistic Selections. 3D printing manufacturers are largely independent of production. So, logistics is a bit more expensive and takes delivery time [54–58]. Additive manufacturing can solve logistics problems when manufacturers combine production. Especially in India, known as small industries development corporations (SIDCO), governments adopt policies to consolidate clusters of similar industries. This makes logistics continuous and cost-effective. Therefore, integrating FDM commercial manufacturers is considered very important in choosing the right logistic partners.

2.4. Raw Material Selections. Large numbers of smaller molecules or repeating units, known as monomers, are joined together chemically to form polymers, which are referred to as macromolecules.

Within a single polymer molecule, the degree of order, the relative orientation, and the kind of monomer can all vary. The benefits of polymers, including their low price, flexibility of manufacture, water resistance, and suppleness, have led to their use such as industry. Depending on the manufacture, various types of polymers can be found as powders, granolas, filaments, and resins. Polymers called thermoplastic are used in the material extrusion. It is fusible when heated [59]. This review article describes the most important polymers and their properties and applications. It is a novelty to use MCDM methods to select the most suitable polymer for the user among polymers with similar uses. The various types of polymers and their applications are shown in Table 1.

2.4.1. PLA (Polylactic Acid). PLA is made from organic source sugarcane or corn starch. Its molecules are renewable so it can also be known as biodegradable material. It is often used to make medical, scaffolds, and prototypes as shown in Figure 8. Also, its melting point is calculated to be 195°C to 220°C. It is priced from INR 869 onwards in the Indian market. Moreover, PLA is not ideal for high-temperature applications. According to results from tests on creep behaviour, PLA's behaviour resembled that of a weakly cross-linked elastomer the most, which caused the creep curve to be held to a constant limit under light loads. Previous literature presented PLA as a material to consider when looking for long-term use based on their findings. Comparing this polymer to other polymers, its fair price, eco-friendly biocompatibility, and suitable physicomechanical characteristics have made it an excellent choice. [60–65].

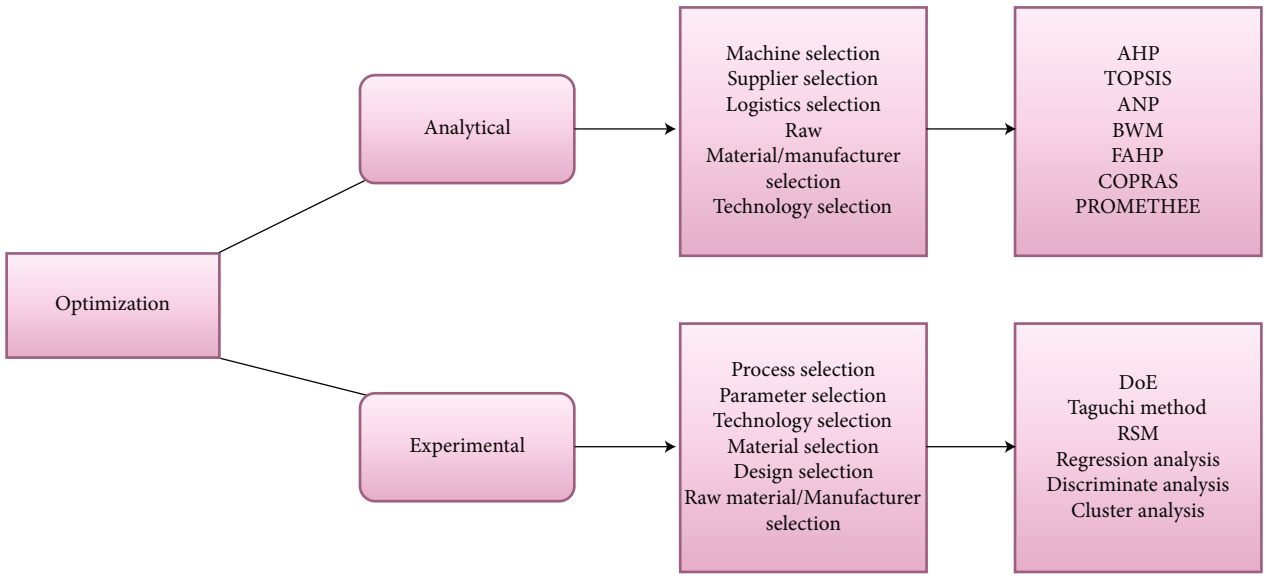

Figure 10: General optimization problems and methodology in the material extrusion process.

Table 1: Different types of polymers [84–87].

Type of polymer	Structure	Different polymer
High-performance polymers	Semicrystalline	Polyether ether ketone, liquid crystal polymer, polyphthalamide, polyphenylene sulfide, polycyclohexylenedimethylene terephthalate, and polyimide
	Amorphous	Polyethersulfone, polyethylenimine, and polyphenylsulfone
Engineering polymers	Semicrystalline	Polybutylene terephthalate, polyvinylidene difluoride, nylon, polyamide, and polyethylene terephthalate
	Amorphous	Poly(ADP-ribose), polycarbonate (PC), polysulfone, and modified polyphenylene oxide
General use polymers	Semicrystalline	Polylactic acid, polypropylene, and low-density polyethylene
	Amorphous	Polyethylene terephthalate glycol, acrylonitrile styrene acrylate, acrylonitrile butadiene styrene, poly(methyl methacrylate), polyvinyl chloride, high-impact polystyrene

2.4.2. ABS (Acrylonitrile Butadiene Styrene). ABS filament is styrene and acrylonitrile derived from polybutadiene. It is a toxic filament and is used for external use only and is also considered more suitable for higher temperature applications than PLA. As mentioned in Figure 8, computer hardware, prototypes, and pipe-making purpose ABS are used. The ABS melting point is calculated to be 210°C to 240°C. Previous research on ABS's mechanical characteristics in the manufacture of impeller pumps demonstrated that ABS can be thought of as a good choice for the manufacture of impellers [65–67].

2.4.3. PETG (Polyethylene Terephthalate Glycol). Chemical impact resistance hardness, ductility, and transparency are considered the main properties of PETG. As mentioned in Figure 5, it is used to make packing, domestic products, impellers, etc. PETG melting point is used between 220°C and 240°C. Previous research examined the use of PTEG impellers in pump-jet modules (PJM). A PTEG impeller exhibited the necessary characteristics while operating for this application, taking into account the 1200 rpm rotational speed that produced a thrust of 14 N. [68–71].

2.4.4. PEEK (Polyether Ether Ketone). PEEK is a colourless organic thermoplastic with excellent fire performance and excellent mechanical strength. As mentioned in Figure 8, PEEK is used for bearing, piston parts, pumps, oil, gas, etc. Moreover, its melting point is calculated at 230°C to 250°C. Extensive researches have focused on the use of PEEK impellers in centrifugal pumps for medical applications because of the enhanced strength and durability they provide [72–76].

2.4.5. PC (Polycarbonate). Bisphenol A is a toxic substance in polycarbonate, so it is used for external use only. However, PC has slightly higher strength and stiffness than other polymer filaments. As mentioned in Figure 8, it is used for safety glass production, auto parts, and led light production. PC melting point is used between 250°C and 285°C in the FDM printers [2, 77–80].

2.4.6. PP (Polypropylene). PP is lightweight, flexible, chemical resistant, and tough. Therefore, as mentioned in Figure 8, it is mostly used for rope, carpet, clothing, and packing, and its extruder melt temperature is calculated from 220°C to 250°C. Also, PP is slightly more flexible than PLA [81–83].

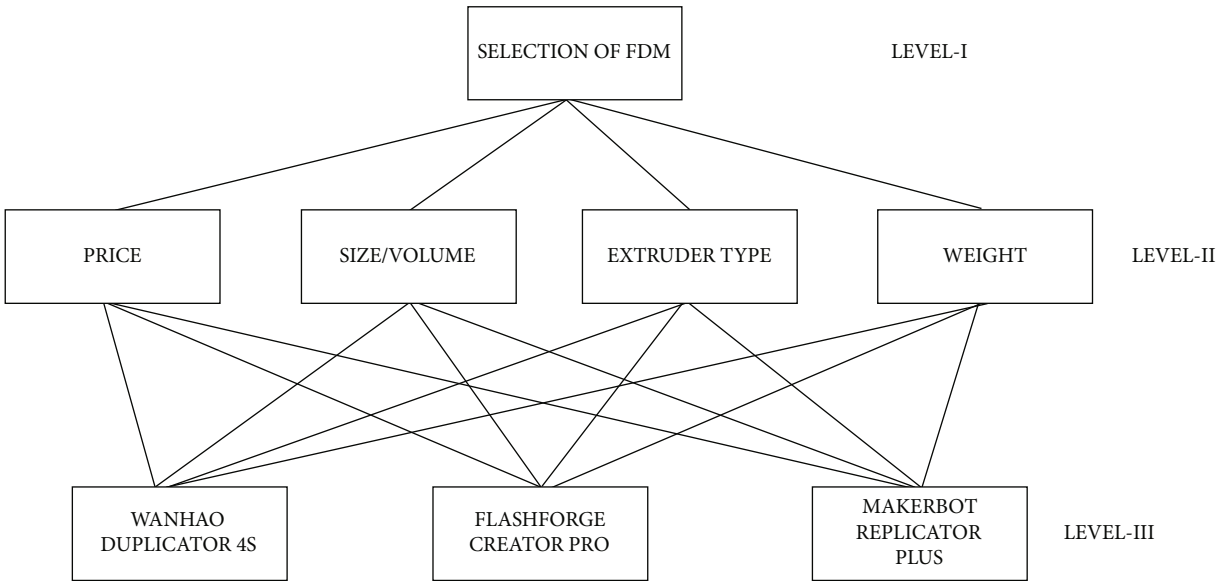

Figure 11: Hierarchy structure of machine selection problem [18].

2.4.7. Nylon. Nylon filament has high flexibility and high toughness. Its extruder melting point is calculated at 250°C, and also, nylon is used in clothing, seat belt, and conveyor applications as mentioned in Figure 8 [88–90].

In all polymer filament materials, composite filaments are available in the market with 90% parent polymer and 10% another polymer according to the application, for example, ABS+, ABS Premium, PLA Pro, PLA+, PLA carbon fibre, and PETG carbon fibre [91–94].

2.5. Raw Material Manufacturer Selection. The same polymer raw material or filaments are prepared by many manufacturers of different qualities in the Indian market. It is considered difficult to choose the best polymer raw material based on online ratings alone. Therefore, it is considered a novelty to investigate a polymer raw material using the optimization MCDM method based on the experimental result for different manufacturers same filament [95–97].

3. Opportunities of Optimization Techniques in AMPT

The purpose of this review article is how to solve all the optimization problems mentioned above using MCDM and the statistical method which is a common mathematical programming technique. Accordingly, Figure 2 illustrates the general hierarchy of the MCDM method, and the aim/goal means the problem to be solved. It is considered the first step in MCDM methods.

Then, the second step is to identify common criteria for alternatives depending on the objective. Finally, priority values are determined using any of the MCDM methods for the alternatives based on each criterion. Through this ranking, the alternative with the highest value is recommended to the decision-makers. This process is known as multicriteria decision-making [98–103].

For example, the hierarchy is illustrated in Figure 11, considering the machine selection problem. In which the selection of a suitable FDM machine is the aim/objective. The price of the machine, extruder type, build platform, safety guards, etc. is common criteria for alternatives. Finally, alternatives are FDM machines, namely, X (Wanhao Duplicator 4S), Y (Flashforge Creator Pro), and Z (MakerBot Replicator Plus). Moreover, if the MCDM tool called AHP is used to calculate the priority value for the alternatives, then the criteria weight, consistency ratio, random index, and pairwise matrix are found through the Saaty scale.

Then, it is confirmed whether the nature of the pairwise matrix is correct. Then, depending on each criterion, separate priority values are found through another pairwise matrix for alternatives with the help of the Saaty scale. Finally, by summing all the identified priority values, the final priority values are obtained for the alternatives. A high-value alternative is recommended to the decision maker.

Various important and significant MCDM methods and their uses in different fields can be seen in Table 2, and this method can also be done analytically (data collection—collect the opinions based on a numerical scale and solved). Therefore, in similar problem situations in the material extrusion process, the decision-maker can ease the use of the appropriate MCDM tool.

According to the statistical method, based on the experimental result, any optimization tool is applied, and a suitable solution is given to the end user. For example, taking the machine selection problem, innovative research can be carried out by producing a product on more than one machine and depending on the results, using an appropriate statistical tool. What is necessary to use the statistical tool in this is that the results obtained have distinct characteristics from each other. Statistical tools are used to make the decision-makers choose the appropriate option easily. It is worth noting that experimental optimization has been

Table 2: Different MCDM tools and their application.

Field	Purpose	Problem solved by previous literature	Applied MCDM	Reference
Transport and logistics	Selection	(i) Sustainable transport plan selection (ii) Transport infrastructure contractor selection (iii) Transport terminal location selection (iv) City logistics centre selection (v) Multimodal logistic selection	(i) WSM (ii) AHP and FAHP (iii) Fuzzy Delphi, fuzzy Delphi ANP, and fuzzy Delphi VIKOR (iv) Fuzzy MAGDM (v) DEMATEL-MAIRCA	[104–108]
	Evaluation	(i) Urban section roads evaluation (ii) Uncertain environment sustainable transport selection (iii) Logistics third-party evaluation	(i) AHP (ii) Fuzzy TOPSIS (iii) Fuzzy SWARA and fuzzy MOORA	[109–111]
	Others	(i) The sustainable urban transport project screening purpose (ii) The best-used component collection identification purpose	(i) AHP (ii) AHP-EW and MABAC	[112, 113]
Civil engineering and infrastructure	Selection	(i) Optimum solution selection for RC building and existing masonry construction (ii) Material selection projects (iii) Method selection for highway selection (iv) Location selection (v) Effective delivery system selection in power plants	(i) TOPSIS, ELECTRE, and VIKOR (ii) FEAHP (iii) ANP (iv) Rough BWM and rough WASPAS (v) SMART	[114–118]
	Evaluation	(i) Urban drainage plan evaluation (ii) Sewer pipe materials evaluation comparison and evaluation (iii) Green building construction evaluation	(i) Adaptive AHP, entropy, and TOPSIS (ii) AHP (iii) DEMATEL, ANP, and ZOGP	[119–121]
	Others	(i) Sewerage pipes sustainability analysis (ii) Worst passenger car parking indication	(i) AHP and MIVES (ii) SAW, TOPSIS, COPRAS, and AHP	[122, 123]
Energy	Selection	(i) Power generation selection (ii) Wind farm location selection (iii) PV project location selection	(i) LNN PW-CODAS (ii) Rough BWM and rough MAIRCA (iii) AHP	[124–126]
	Evaluation	(i) Wind farm sites evaluation (ii) Renewable energy source evaluation	(i) FAHP and fuzzy TOPSIS (ii) AHP and TOPSIS	[127, 128]
	Others	(i) Estimate thermal power plant quality	(i) ASPID	[129]
Supply chain Management	Selection	(i) Sustainable supplier selection (ii) Thermal power plant equipment supplier selection	(i) FPP and fuzzy TOPSIS (ii) Fuzzy entropy-TOPSIS	[130, 131]
	Evaluation	(i) Supplier performance evaluation (ii) Sustainable supplier selection evaluation	(i) Fuzzy Delphi, DEMATEL, and DEMATEL ANP-VIKOR (ii) AHP, VIKOR	[132, 133]
	Others	(i) Oil and gas industry sustainability classification	(i) ELECTRE TRI	[134]
Additive manufacturing	Selection	(i) Machine selection (3D printers) (ii) Technology selection (SLM, SLS, and FDM) (iii) Material selection (appropriate raw material from a similar property material)	(i) Analytical hierarchy process (AHP) (ii) Best worst method (BWM) (iii) Fuzzy technique for order of preference by similarity to ideal solution (TOPSIS)	[10, 16, 41, 135]

Table 2: Continued.

Field	Purpose	Problem solved by previous literature	Applied MCDM	Reference
	Evaluation	(i) Printing parameter optimization	(i) Fuzzy AHP-TOPSIS	[24, 25, 40]
	Others	(i) Comparison of different manufacturing processes	(i) AHP	[19]
Other engineering disciplines	Selection	(i) IC engine optimum biodiesel blend selection (ii) Agriculture product strategy selection (iii) Particulate matter sensor selection	(i) Fuzzy AHP-TOPSIS, fuzzy AHP-VIKOR, and fuzzy AHP-ELECTRE (ii) DEMATEL and MABAC (iii) DEMATEL and VIKOR	[136–138]
	Evaluation	(i) Evaluating the level of sustainability (ii) Site evaluations	(i) AHP (ii) WASPAS-SVNS	[139, 140]
	Others	(i) Sustainable environment design proposal	(i) ELECTRE III	[141]

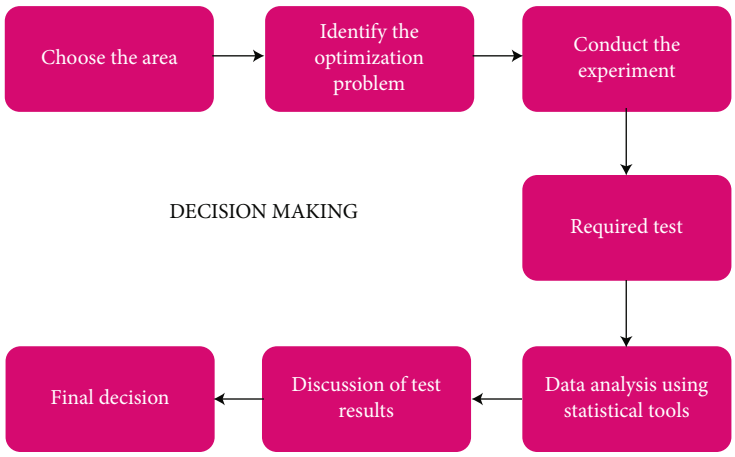

Figure 12: Steps of an experimental optimization tool.

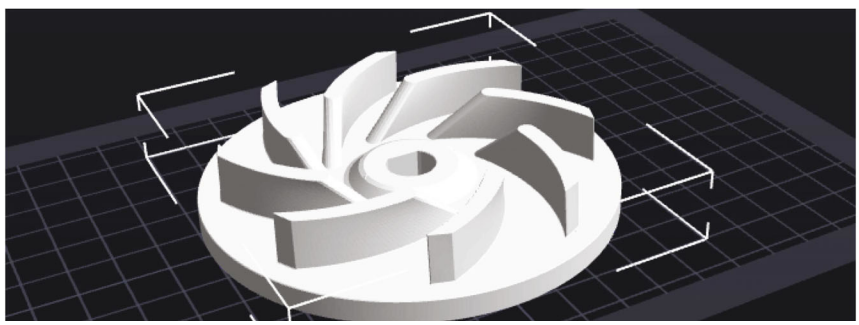

Figure 13: Polymer impeller CAD design into slicing softer image (online free software: Flashforge 5.0).

extensively explored by previous researchers [142–148]. Figure 12 explores the experimental optimization procedure.

4. Material Extrusion Polymers in Impeller Application

An impeller is considered the main part of turbomachinery. The work of the impeller is to convert the velocity of the working fluid into pressure due to the very fast rotation [149]. Impeller application also plays an important role in many fields, for example, pumps [150], medical [151], automobile [152], and aerospace [153]. In injection moulding and other traditional impeller production techniques, raw materials such as polymeric, metal glass, stainless steel, titanium, aluminium, and nickel alloy are frequently utilized. Metal impellers achieve only slightly lower efficiency due to their heavy weight. Efficiency can be increased when using thermoplastic polymer impellers with low weight and high strength. The main kinds of thermoplastics are amorphous and semicrystalline. Different thermoplastic polymer forms like powders, granules, and filaments. The benefits of this class of polymer include its capacity to be recycled, high ductility, and impact resistance when compared to thermosets. The modulus of the thermoplastic item is typically less than 5 GPa, though this might vary based on the object's chemical constitution and production process. At present, the AMPT method is used to produce the final product directly from the given design in less time and more accurately. Polymer impellers were first used in the heating ventilation and air conditioning (HVAC) and microorganic ranking cycle (mORC) and refrigeration systems. Polymers like PEEK, PLA, and ABS have been used for the first time for impeller application. The ABS impeller met the anticipated operating condition taking into consideration the working environment and safety factor (FoS), which is the ratio of elastic modulus to the maximum equivalent stress. One of the key benefits of employing this polymer was the ability to manufacture the impeller at a lower cost by using ABS, which enables the mass production of mORC. It is also noteworthy that only PEEK-GF30 [154] has been used in the composite rotary component. Impellers are manufactured using a minimal amount of polymers when using an additive manufacturing process.

PLA has been utilized in the manufacturing of impellers for pumps and marine applications. However, since PLA and ABS are both easily accessible, these two categories of thermoplastic have been investigated in various experiments as pump impellers. Pump and compressor applications for a variety of industries, including the automotive, aerospace, and medical sectors, place a high value on PEEK impellers. Pump and mORC applications have both utilized PETG impellers. For the production of pump blades, this polymer was chosen because of its excellent water resistance and biodegradability. Metals have been replaced by carbon fibre polymer-matrix composites, one of the most effective families of materials. These kinds of composites can be divided into categories based on the type of fibre condition, such as

short or continuous. Epoxy, which has been frequently utilized as a matrix for these composites, is a thermoset, and PPS, PEEK, PI, and PEI are thermoplastics. In the case of a microturbine generator, a PEEK carbon-reinforced impeller was suggested as a suitable material to replace an aluminium impeller. However, the time required to make an impeller using many polymers (directly or compositely blended like PLACF and PETG-CF) in the market, changing the printing parameters, making changes in the manufacturing geometry, etc. will be an optimization challenge and opportunity in AMPT for impeller application.

Figure 13 shows the flash forge software for slicing the impeller design. Choosing optimal process parameters using the MCDM method will be a novelty for future researchers because each polymer filament has different process parameters like different melting temperatures, printing speed, and infill.

5. Summary and Conclusions

In this review article, mathematical programming MCDM and statistical method optimization problems in additive manufacturing material extrusion are presented. In more than 147 AM material extrusion-related 3D printing selection, supplier selection, logistic selection, raw material selection, main properties of raw material (polymers), and raw material manufacturer selection, interesting new novel problems through this conclusion provide useful information to the researchers. This review article also describes the optimization challenges and opportunities in the use of polymers, especially in impeller applications. Although material extrusion polymers have many sectoral applications, only significant research has been done on impeller applications. Likewise, optimization challenges such as selecting the appropriate FDM and selecting the appropriate raw material have been highlighted. Moreover, the optimization opportunity is described with an example based on mathematical programming techniques and statistical techniques. Many fields like transport, logistics, energy, civil engineering, and other engineering disciplines have achieved sustainability by using optimization methods. It describes several applications of MCDMs so that future researchers can easily find the appropriate technique to suit their application. Finally, today's increasing use of optimization in all fields reflects its importance and nature of sustainable decision-making.

Data Availability

The data used to support the findings of this study are included in the article. Should further data or information be required, these are available from the corresponding author upon request.

Conflicts of Interest

There is no conflict of interest.

Acknowledgments

For their assistance in allowing us to conduct this research, we gratefully acknowledge and thank the Vellore Institute of Technology management. Additionally, we would like to extend our gratitude to the technician staff at the FESEM lab and the DIGI-MAN LAB in charge.

References

[1] B. Devarajan, R. Lakshmi Narasimhan, B. Venkateswaran, S. Mavinkere Rangappa, and S. Siengchin, "Additive manufacturing of jute fiber reinforced polymer composites: a concise review of material forms and methods," *Polymer Composites*, vol. 43, no. 10, pp. 6735–6748, 2022.

[2] B. O. Samuel, M. Sumaila, and B. Dan-Asabe, "Modeling and optimization of the manufacturing parameters of a hybrid fiber reinforced polymer composite PxGyEz," *The International Journal of Advanced Manufacturing Technology*, vol. 118, no. 5-6, pp. 1441–1452, 2022.

[3] M. Priyadharshini, D. Balaji, V. Bhuvaneswari, L. Rajeshkumar, M. R. Sanjay, and S. Siengchin, "Fiber reinforced composite Manufacturing with the aid of artificial intelligence–a state-of-the-art review," *Archives of Computational Methods in Engineering*, vol. 29, no. 7, pp. 5511–5524, 2022.

[4] D. Balaji, J. Ranga, V. Bhuvaneswari et al., "Additive manufacturing for aerospace from inception to certification," *Journal of Nanomaterials*, vol. 2022, Article ID 7226852, 18 pages, 2022.

[5] R. Vijay, D. L. Singaravelu, and R. Jayaganthan, "Development and characterization of stainless steel fiber-based copper-free brake liner formulation: a positive solution for steel fiber replacement," *Friction*, vol. 8, no. 2, pp. 396–420, 2020.

[6] S. Jothibasu, S. Mohanamurugan, R. Vijay, D. Lenin Singaravelu, A. Vinod, and M. R. Sanjay, "Investigation on the mechanical behavior of areca sheath fibers/jute fibers/glass fabrics reinforced hybrid composite for light weight applications," *Journal of Industrial Textiles*, vol. 49, no. 8, pp. 1036–1060, 2020.

[7] D. L. Singaravelu, R. Vijay, and P. Filip, "Influence of various cashew friction dusts on the fade and recovery characteristics of non-asbestos copper free brake friction composites," *Wear*, vol. 426-427, pp. 1129–1141, 2019.

[8] S. Manoharan, R. Vijay, D. L. Singaravelu, S. Krishnaraj, and B. Suresha, "Tribological characterization of recycled basalt-aramid fiber reinforced hybrid friction composites using grey-based Taguchi approach," *Materials Research Express*, vol. 6, no. 6, article 065301, 2019.

[9] J. S. Binoj, N. Manikandan, B. B. Mansingh et al., "Taguchi's optimization of areca fruit husk fiber mechanical properties for polymer composite applications," *Fibers and Polymers*, vol. 23, no. 11, pp. 3207–3213, 2022.

[10] K. T. Mannan, V. Sivaprakash, S. Raja, P. P. Patil, S. Kaliappan, and S. Socrates, "Effect of Roselle and biochar reinforced natural fiber composites for construction applications in cryogenic environment," *Materials Today: Proceedings*, vol. 69, pp. 1361–1368, 2022.

[11] K. T. Mannan, V. Sivaprakash, S. Raja, M. Kulandasamy, P. P. Patil, and S. Kaliappan, "Significance of Si_3N_4/Lime powder addition on the mechanical properties of natural calotropis

gigantea composites," *Materials Today: Proceedings*, vol. 69, pp. 1355–1360, 2022.

[12] L. Natrayan, S. Kaliappan, S. B. Sethupathy et al., "Investigation on interlaminar shear strength and moisture absorption properties of soybean oil reinforced with aluminium trihydrate-filled polyester-based nanocomposites," *Journal of Nanomaterials*, vol. 2022, Article ID 7588699, 8 pages, 2022.

[13] S. E. De Leon-Aldaco, H. Calleja, and J. Aguayo Alquicira, "Metaheuristic optimization methods applied to power converters: a review," *IEEE Transactions on Power Electronics*, vol. 30, no. 12, pp. 6791–6803, 2015.

[14] M. Sugavaneswaran, B. Prashanthi, and J. Rajan, "A multi-criteria decision making method for vapor smoothening fused deposition modelling part," *Rapid Prototyping Journal*, vol. 28, no. 2, pp. 236–252, 2022.

[15] Y. Zhijun, H. Wang, X. Wei, K. Yan, and C. Gao, "Multiobjective optimization method for polymer injection molding based on a genetic algorithm," *Advances in Polymer Technology*, vol. 2019, Article ID 9012085, 17 pages, 2019.

[16] Z. Shan, W. Wu, Y. Lei, and B. Zhao, "A new fuzzy rule based multi-objective optimization method for cross-scale injection molding of protein electrophoresis microfluidic chips," *Scientific Reports*, vol. 12, no. 1, article 13159, 2022.

[17] S. U. Sapkal and P. H. Warule, "Application of multi-attribute decision making methods for fused deposition modelling," in *Sustainability for 3D Printing. Springer Tracts in Additive Manufacturing*, K. Sandhu, S. Singh, C. Prakash, K. Subburaj, and S. Ramakrishna, Eds., pp. 55–75, Springer, Cham, Switzerland, 2022.

[18] M. Stojčić, E. K. Zavadskas, D. Pamučar, Ž. Stević, and A. Mardani, "Application of MCDM methods in sustainability engineering: a literature review 2008-2018," *Symmetry*, vol. 11, no. 3, p. 350, 2019.

[19] D. Schuhmann, M. Rupp, M. Merkel, and D. K. Harrison, "Additive vs. conventional manufacturing of metal components: selection of the manufacturing process using the AHP method," *Process*, vol. 10, no. 8, p. 1617, 2022.

[20] S. Raja and A. J. Rajan, "A decision-making model for selection of the suitable FDM machine using fuzzy TOPSIS," *Mathematical Problems in Engineering*, vol. 2022, Article ID 7653292, 15 pages, 2022.

[21] G. M. Magableh and M. Z. Mistarihi, "Applications of MCDM approach (ANP-TOPSIS) to evaluate supply chain solutions in the context of COVID-19," *Heliyon*, vol. 8, no. 3, article e09062, 2022.

[22] R. Agrawal, "Sustainable material selection for additive manufacturing technologies: a critical analysis of rank reversal approach," *Journal of Cleaner Production*, vol. 296, article 126500, 2021.

[23] T.-C. T. Chen and C.-W. Lin, "Assessing cloud manufacturing applications using an optimally rectified FAHP approach," *Complex & Intelligent Systems*, vol. 8, no. 6, pp. 5087–5099, 2022.

[24] A. Baroutaji, A. Arjunan, G. Singh, and J. Robinson, "Crushing and energy absorption properties of additively manufactured concave thin-walled tubes," *Results in Engineering*, vol. 14, article 100424, 2022.

[25] A. S. Bhaskar and A. Khan, "Comparative analysis of hybrid MCDM methods in material selection for dental applications," *Expert Systems with Applications*, vol. 209, article 118268, 2022.

[26] S. Raja, A. J. Rajan, V. P. Kumar et al., "Selection of additive manufacturing machine using analytical hierarchy process," vol. 2022, Article ID 1596590, pp. 1–20, 2022.

[27] R. Subramani, S. Kaliappan, P. V. Arul et al., "A recent trend on additive manufacturing sustainability with supply chain management concept, multicriteria decision making techniques," *Multicriteria Decision Making Techniques*, vol. 2022, article 9151839, pp. 1–12, 2022.

[28] V. Kumar, R. Singh, and I. Singh, "Online health monitoring of repaired non-structural cracks with innovative 3D printed strips in heritage buildings," *Materials Letters*, vol. 327, article 133033, 2022.

[29] M. Karthick, M. Meikandan, S. Kaliappan et al., "Experimental investigation on mechanical properties of glass fiber hybridized natural fiber reinforced penta-layered hybrid polymer composite," *International Journal of Chemical Engineering*, vol. 2022, Article ID 1864446, 9 pages, 2022.

[30] T. Jiang, Z. Guan, H. Li et al., "A feeding quantity monitoring system for a combine harvester: design and experiment," *Agriculture*, vol. 12, no. 2, p. 153, 2022.

[31] G. Velmurugan, V. S. Shankar, S. Kaliappan et al., "Effect of aluminium tetrahydrate nanofiller addition on the mechanical and thermal behaviour of luffa fibre-based polyester composites under cryogenic environment," *Journal of Nanomaterials*, vol. 2022, Article ID 5970534, 10 pages, 2022.

[32] P. Octorina, A. Böhm, D. Martin-Creuzburg, and D. Straile, "Morphological defences and defence–cost trade-offs in daphnia in response to two co-occurring invertebrate predators," *Freshwater Biology*, vol. 67, no. 5, pp. 883–892, 2022.

[33] K. C. Sekhar, R. Surakasi, P. Roy et al., "Mechanical Behavior of Aluminum and Graphene Nanopowder-Based Composites," *International Journal of Chemical Engineering*, vol. 2022, Article ID 2224482, 13 pages, 2022.

[34] R. Subramani, S. Kaliappan, S. Sekar et al., "Polymer filament process parameter optimization with mechanical test and morphology analysis," *Advances in Materials Science and Engineering*, vol. 2022, Article ID 8259804, 8 pages, 2022.

[35] S. Raja, A. P. Agrawal, P. P. Patil et al., "Optimization of 3D printing process parameters of Polylactic acid filament based on the mechanical test," *International Journal of Chemical Engineering*, vol. 2022, Article ID 5830869, 7 pages, 2022.

[36] V. L. Anderson and R. A. McLean, *Design of Experiments: A Realistic Approach*, CRC Press, 1st edition, 1974.

[37] L. Auffray, P. A. Gouge, and L. Hattali, "Design of experiment analysis on tensile properties of PLA samples produced by fused filament fabrication," *International Journal of Advanced Manufacturing Technology*, vol. 118, no. 11-12, pp. 4123–4137, 2022.

[38] V. Madhavadas, D. Srivastava, U. Chadha et al., "A review on metal additive manufacturing for intricately shaped aerospace components," *CIRP Journal of Manufacturing Science and Technology*, vol. 39, pp. 18–36, 2022.

[39] A. Garcia-Colomo, D. Wood, F. Martina, and S. W. Williams, "A comparison framework to support the selection of the best additive manufacturing process for specific aerospace applications," *International Journal of Rapid Manufacturing*, vol. 9, no. 2/3, pp. 194–211, 2020.

[40] S. M. S. Mukras, "Experimental-based optimization of injection molding process parameters for short product cycle time," *Advances in Polymer Technology*, vol. 2020, Article ID 1309209, 15 pages, 2020.

[41] S. M. Yusuf, S. Cutler, and N. Gao, "Review: the impact of metal additive manufacturing on the aerospace industry," *Metals*, vol. 9, no. 12, p. 1286, 2019.

[42] D. Popescu, A. Zapciu, C. Amza, F. Baciu, and R. Marinescu, "FDM process parameters influence over the mechanical properties of polymer specimens: a review," *Polymer Testing*, vol. 69, pp. 157–166, 2018.

[43] N. G. Olaiya, C. Maraveas, M. A. Salem et al., "Viscoelastic and properties of amphiphilic chitin in plasticised polylactic acid/starch biocomposite," *Polymers*, vol. 14, no. 11, p. 2268, 2022.

[44] G. Atakok, M. Kam, and H. B. Koc, "Tensile, three-point bending and impact strength of 3D printed parts using PLA and recycled PLA filaments: a statistical investigation," *Journal of Materials Research and Technology*, vol. 18, pp. 1542–1554, 2022.

[45] J. Zhang, D. Chen, and S. Chen, "A review of emission characteristics and control strategies for particles emitted from 3D fused deposition modeling (FDM) printing," *Building and Environment*, vol. 221, article 109348, 2022.

[46] A. Haryńska, J. Kucinska-Lipka, A. Sulowska, I. Gubanska, M. Kostrzewa, and H. Janik, "Medical-grade PCL based polyurethane system for FDM 3D printing-characterization and fabrication," *Materials*, vol. 12, no. 6, 2019.

[47] E. V. Chary and G. A. Kumar, "Overfcview of Manufacturing PMC's Using Traditional and 3D printing Technology (FDM)," *Metal Matrix Composites Journal, Taylor and Francis Publisher*, vol. 9, no. 1, pp. 6–10, 2022.

[48] N. Zirak, M. Shirinbayan, M. Deligant, and A. Tcharkhtchi, "Toward polymeric and polymer composites impeller fabrication," *Polymers*, vol. 14, no. 1, 2021.

[49] S. Raja, J. Logeshwaran, S. Venkatasubramanian et al., "OCHSA: Designing Energy-Efficient Lifetime-Aware Leisure Degree Adaptive Routing Protocol with Optimal Cluster Head Selection for 5G Communication Network Disaster Management," *Scientific Programming*, vol. 2022, Article ID 5424356, 11 pages, 2022.

[50] K. Ransikarbum and P. Khamhong, "Integrated fuzzy analytic hierarchy process and technique for order of preference by similarity to ideal solution for additive manufacturing printer selection," *Journal of Materials Engineering and Performance*, vol. 30, no. 9, pp. 6481–6492, 2021.

[51] M. Palanisamy, A. Pugalendhi, and R. Ranganathan, "Selection of suitable additive manufacturing machine and materials through best–worst method (BWM)," *International Journal of Advanced Manufacturing Technology*, vol. 107, no. 5-6, pp. 2345–2362, 2020.

[52] M. L. Tseng, T. D. Bui, M. K. Lim, M. Fujii, and U. Mishra, "Assessing data-driven sustainable supply chain management indicators for the textile industry under industrial disruption and ambidexterity," *International Journal of Production Economics*, vol. 245, article 108401, 2022.

[53] L. Peng, J. Lu, J. Luo, and Y. Wang, "A Combination of FDM, DEMATEL, and DANP for Disclosing the Interrelationship of Influencing Factors in Rural Homestay Business: Empirical Evidence from China," *Sustainability*, vol. 14, no. 16, article 10341, 2022.

[54] I. Valtonen, S. Rautio, and M. Salmi, "Capability development in hybrid organizations: enhancing military logistics with additive manufacturing," *Progress in Additive Manufacturing*, vol. 7, no. 5, pp. 1037–1052, 2022.

[55] S. Venkatasubramanian, S. Raja, V. Sumanth et al., "Fault diagnosis using data fusion with ensemble deep learning technique in IIoT," *Mathematical Problems in Engineering*, vol. 2022, Article ID 1682874, 8 pages, 2022.

[56] T. Santos, *A relação da logística reversa e manufatura aditiva com a sustentabilidade: revisão de literatura*, Engineering Archive, 2022.

[57] D. Version, *AMHUB-Additive Manufacturing Hubs for Radical Innovation in Digital Part Delivery Logistics Final Report*, VTT Technical Research Centre of Finland, 2022.

[58] B. Debnath, M. S. Shakur, F. Tanjum, M. A. Rahman, and Z. H. Adnan, "Impact of additive manufacturing on the supply chain of aerospace spare parts industry—a review," *Logistics*, vol. 6, no. 2, p. 28, 2022.

[59] A. Kumar, R. Agrawal, and V. Ashok, "Materials today: proceedings material selection for metal additive manufacturing process," *Materials Today: Proceedings*, vol. 66, pp. 1744–1749, 2022.

[60] R. A. D. N. V. Rajakaruna, B. Subeshan, and E. Asmatulu, "Fabrication of hydrophobic PLA filaments for additive manufacturing," *Journal of Materials Science*, vol. 57, no. 19, pp. 8987–9001, 2022.

[61] A. Rimkus, M. M. Farh, and V. Gribniak, "Continuously reinforced polymeric composite for additive manufacturing — development and efficiency analysis," *Polymers*, vol. 14, no. 17, p. 3471, 2022.

[62] J. Beniak, Ľ. Šooš, P. Križan, M. Matúš, and V. Ruprich, "Resistance and strength of conductive PLA processed by FDM additive manufacturing," *Polymers*, vol. 14, no. 4, p. 678, 2022.

[63] E. Brancewicz-Steinmetz and J. Sawicki, "Bonding and strengthening the PLA biopolymer in multi-material additive manufacturing," *Materials*, vol. 15, no. 16, p. 5563, 2022.

[64] J. Sasse, L. Pelzer, M. Schön, T. Ghaddar, and C. Hopmann, "Investigation of recycled and coextruded PLA filament for additive manufacturing," *Polymers*, vol. 14, no. 12, p. 2407, 2022.

[65] A. B. Stefaniak, L. N. Bowers, G. Cottrell et al., "Towards sustainable additive manufacturing: the need for awareness of particle and vapor releases during polymer recycling, making filament, and fused filament fabrication 3-D printing," *Resources, Conservation and Recycling*, vol. 176, 2023.

[66] Y. Hong, M. Mrinal, H. Si, V. Dung, X. Liu, and C. Luo, "In-situ observation of the extrusion processes of acrylonitrile butadiene styrene and polylactic acid for material extrusion additive manufacturing," *Additive Manufacturing*, vol. 49, article 102507, 2022.

[67] A. Goulas, J. R. Mcghee, T. Whittaker et al., "Synthesis and dielectric characterisation of a low loss $BaSrTiO_3$/ABS ceramic/polymer composite for fused filament fabrication additive manufacturing," vol. 55, Article ID 102844, 2022.

[68] R. Anandkumar and S. R. Babu, "FDM filaments with unique segmentation since evolution: a critical review," *Progress in Additive Manufacturing*, vol. 4, no. 2, pp. 185–193, 2019.

[69] K. Singh, C. Herrmann, P. Stief, J. Dantan, A. Etienne, and A. Siadat, "A Comparative Study on the Life Cycle Assessment of a 3D Printed Product with PLA, ABS & PETG Materials," *Procedia CIRP*, vol. 107, pp. 15–20, 2022.

[70] S. Rijckaert, L. Daelemans, L. Cardon, M. Boone, W. Van Paepegem, and K. De Clerck, "Continuous fiber-reinforced aramid/PETG 3D-printed composites with high fiber loading through fused filament fabrication," *Polymers*, vol. 14, no. 2, p. 298, 2022.

[71] M. A. Caminero and J. M. Chac, "Effects of carbon fibre reinforcement on the geometric properties of PETG-based filament using FFF additive manufacturing," *Composites Part B: Engineering*, vol. 235, 2022.

[72] H. Spece, P. M. Desantis, and S. M. Kurtz, "Development of an architecture-property model for triply periodic minimal surface structures and validation using material extrusion additive manufacturing with polyetheretherketone (PEEK)," *Journal of the Mechanical Behavior of Biomedical Materials*, vol. 133, article 105345, 2022.

[73] G. Ramesh, J. Logeshwaran, and K. Rajkumar, "The smart construction for image preprocessing of mobile robotic systems using neuro fuzzy logical system approach," *Neuro Quantology*, vol. 20, no. 10, pp. 6354–6367, 2022.

[74] W. Freudenberg, F. Wich, N. Langhof, and S. Schaff, "Additive manufacturing of carbon fiber reinforced ceramic matrix composites based on fused filament fabrication," *Journal of the European Ceramic Society*, vol. 42, no. 4, pp. 1822–1828, 2022.

[75] A. Diouf-lewis, R. D. Farahani, F. Iervolino et al., "Design and characterization of carbon fiber-reinforced PEEK/PEI blends for fused filament fabrication additive manufacturing," *Materials Today Communications*, vol. 31, article 103445, 2022.

[76] A. Lee, M. Wynn, L. Quigley, M. Salviato, and N. Zobeiry, "Effect of temperature history during additive manufacturing on crystalline morphology of PEEK," *Advances in Industrial and Manufacturing Engineering*, vol. 4, article 100085, 2022.

[77] M. Petousis, N. Vidakis, N. Mountakis et al., "Silicon carbide nanoparticles as a mechanical boosting agent in material extrusion 3D-printed polycarbonate," *Polymers*, vol. 14, no. 17, p. 3492, 2022.

[78] N. Vidakis, M. Petousis, S. Grammatikos, V. Papadakis, A. Korlos, and N. Mountakis, "High performance polycarbonate nanocomposites mechanically boosted with titanium carbide in material extrusion additive manufacturing," vol. 12, no. 7, p. 1068, 2022.

[79] S. J. Mohan, P. S. S. Devasahayam, I. Suyambulingam, and S. Siengchin, "Suitability characterization of novel cellulosic plant fiber from *Ficus benjamina* L. aerial root for a potential polymeric composite reinforcement," *Polymer Composites*, vol. 43, no. 12, pp. 9012–9026, 2022.

[80] A. Gupta, S. Hasanov, and I. Fidan, "Thermal characterization of short carbon fiber reinforced high temperature polymer material produced using the fused filament fabrication process," *Journal of Manufacturing Processes*, vol. 80, pp. 515–528, 2022.

[81] N. Vidakis, M. Petousis, E. Velidakis et al., "Fused filament fabrication 3D printed polypropylene/ alumina nanocomposites: effect of filler loading on the mechanical reinforcement," *Polymer Testing*, vol. 109, article 107545, 2022.

[82] D. Divya, I. Suyambulingam, M. R. Sanjay, and S. Siengchin, "Suitability examination of novel cellulosic plant fiber from *Furcraea selloa* K. *Koch* peduncle for a potential polymeric composite reinforcement," *Polymer Composites*, vol. 43, no. 7, pp. 4223–4243, 2022.

[83] A. N. Solodov, J. Shayimova, D. Balkaev et al., "High-throughput, low-cost and "green" production method for highly stable polypropylene/perovskite composites, applicable in 3D printing," *Additive Manufacturing*, vol. 59, article 103094, 2022.

[84] S. Ramasamy, A. Karuppuchamy, J. J. Jayaraj, I. Suyambulingam, S. Siengchin, and S. Fischer, "Comprehensive characterization of novel Robusta (AAA) banana bracts fibers reinforced polylactic acid based biocomposites for lightweight applications," *Polymer Composites*, vol. 43, no. 11, pp. 8569–8580, 2022.

[85] F. Jiang and D. Drummer, "Analysis of UV curing strategy on reaction heat control and part accuracy for additive manufacturing," *Polymers*, vol. 14, no. 4, p. 759, 2022.

[86] M. M. Zerankeshi, R. Bakhshi, and R. Alizadeh, "Polymer/metal composite 3D porous bone tissue engineering scaffolds fabricated by additive manufacturing techniques: a review," *Bioprinting*, vol. 25, article e00191, 2022.

[87] A. Pajonk, A. Prieto, U. Blum, and U. Knaack, "Multi-material additive manufacturing in architecture and construction: a review," *Journal of Building Engineering*, vol. 45, article 103603, 2022.

[88] V. Mishra, S. Negi, S. Kar, A. K. Sharma, Y. N. K. Rajbahadur, and A. Kumar, "Recent advances in fused deposition modeling based additive manufacturing of thermoplastic composite structures: a review," p. 089270572211028, 2022.

[89] R. Somasundaram, R. Rajamoni, I. Suyambulingam, D. Divakaran, S. Mavinkere Rangappa, and S. Siengchin, "Utilization of discarded Cymbopogon flexuosus root waste as a novel lignocellulosic fiber for lightweight polymer composite application," *Polymer Composites*, vol. 43, no. 5, pp. 2838–2853, 2022.

[90] L. Di and Y. Yang, "Towards closed-loop material flow in additive manufacturing: Recyclability analysis of thermoplastic waste," *Journal of Cleaner Production*, vol. 362, article 132427, 2022.

[91] M. Chandra, F. Shahab, K. E. K. Vimal, and S. Rajak, "Selection for additive manufacturing using hybrid MCDM technique considering sustainable concepts," *Rapid Prototyping Journal*, vol. 28, no. 7, pp. 1297–1311, 2022.

[92] Y. Abderrafai, M. Hadi, F. Sosa-rey et al., "Additive manufacturing of short carbon fiber-reinforced polyamide composites by fused filament fabrication: formulation, manufacturing and characterization," *Materials & Design*, vol. 214, article 110358, 2022.

[93] J. Logeshwaran, "AICSA - an artificial intelligence cyber security algorithm for cooperative P2P file sharing in social networks. ICTACT journal on data science and machine," *Learning*, vol. 3, no. 1, pp. 251–253, 2021.

[94] G. S. Sivagnanamani, S. R. Begum, R. Siva, and M. S. Kumar, "Experimental investigation on influence of waste egg Shell particles on polylactic acid matrix for additive manufacturing application," *Journal of Materials Engineering and Performance*, vol. 31, no. 5, pp. 3471–3480, 2022.

[95] H. Sonar, V. Khanzode, and M. Akarte, "Additive manufacturing enabled supply chain management: a review and research directions," *Vision*, vol. 26, no. 2, pp. 147–162, 2022.

[96] A. Mecheter, S. Pokharel, and F. Tarlochan, "Additive manufacturing technology for spare parts application: a systematic review on supply chain management," *Applied Sciences*, vol. 12, no. 9, p. 4160, 2022.

[97] M. K. Jha, S. Gupta, V. Chaudhary, and P. Gupta, "Material selection for biomedical application in additive manufacturing using TOPSIS approach," *Materials Today: Proceedings*, vol. 62, pp. 1452–1457, 2022.

[98] Ž. Stević, S. Miškić, D. Vojinović, E. Huskanović, M. Stanković, and D. Pamučar, "Development of a model for evaluating the efficiency of transport companies: PCA–DEA–MCDM model," *Axioms*, vol. 11, no. 3, p. 140, 2022.

[99] X. Wang, C. Zhang, J. Deng, C. Su, and Z. Gao, "Analysis of factors influencing miners' unsafe behaviors in intelligent mines using a novel hybrid MCDM model," *International Journal of Environmental Research and Public Health*, vol. 19, no. 12, p. 7368, 2022.

[100] A. I. Yoris-nobile, E. Lizasoain-arteaga, E. Blanco-fernandez, and S. Alonso-cañon, "Life cycle assessment (LCA) and multi-criteria decision-making (MCDM) analysis to determine the performance of 3D printed cement mortars and geopolymers," *Journal of Sustainable Cement-Based Materials*, vol. 11, pp. 1–18, 2022.

[101] J. Logeshwaran, M. J. Rex, T. Kiruthiga, and V. A. Rajan, "FPSMM: fuzzy probabilistic based semi morkov model among the sensor nodes for realtime applications," in *2017 International Conference on Intelligent Sustainable Systems (ICISS)*, pp. 442–446, Palladam, India, 2017.

[102] C. N. Wang, T. T. Dang, N. A. T. Nguyen, and J. W. Wang, "A combined data envelopment analysis (DEA) and Grey based multiple criteria decision making (G-MCDM) for solar PV power plants site selection: a case study in Vietnam," *Energy Reports*, vol. 8, pp. 1124–1142, 2022.

[103] Z. C. Wang, Y. Ran, Y. Chen, X. Yang, and G. Zhang, "Group risk assessment in failure mode and effects analysis using a hybrid probabilistic hesitant fuzzy linguistic MCDM method," *Expert Systems with Applications*, vol. 188, article 116013, 2022.

[104] M. R. Sanjay, S. Siengchin, J. Parameswaranpillai, M. Jawaid, C. I. Pruncu, and A. Khan, "A comprehensive review of techniques for natural fibers as reinforcement in composites: preparation, processing and characterization," *Carbohydrate Polymers*, vol. 207, pp. 108–121, 2019.

[105] S. Inti and V. Tandon, "Application of fuzzy preference-analytic hierarchy process logic in evaluating sustainability of transportation infrastructure requiring multicriteria decision making," *Journal of Infrastructure Systems*, vol. 23, no. 4, article 04017014, 2017.

[106] S. Zecevic, S. Tadic, and M. Krstic, "Intermodal transport terminal location selection using a novel hybrid MCDM model," *International Journal of Uncertainty, Fuzziness and Knowledge-Based Systems*, vol. 25, no. 6, pp. 853–876, 2017.

[107] J. Jasmine, N. Yuvaraj, and J. Logeshwaran, "DSQLR-A distributed scheduling and QoS localized routing scheme for wireless sensor network," *Recent Trends in Information Technology and Communication for Industry*, vol. 4, pp. 47–60, 2022.

[108] D. S. Pamucar, S. P. Tarle, and T. Parezanovic, "New hybrid multi-criteria decision-making DEMATEL-MAIRCA model: sustainable selection of a location for the development of multimodal logistics centre," *Economic Research-Ekonomska istraživanja*, vol. 31, no. 1, pp. 1641–1665, 2018.

[109] D. Baric, H. Pilko, and J. Strujic, "An analytic hierarchy process model to evaluate road section design," *Transport*, vol. 31, no. 3, pp. 312–321, 2016.

[110] A. Awasthi, S. S. Chauhan, and H. Omrani, "Application of fuzzy TOPSIS in evaluating sustainable transportation systems," *Expert Systems with Applications*, vol. 38, no. 10, pp. 12270–12280, 2011.

[111] R. K. Mavi, M. Goh, and N. Zarbakhshnia, "Sustainable third-party reverse logistic provider selection with fuzzy SWARA and fuzzy MOORA in plastic industry," *International Journal of Advanced Manufacturing Technology*, vol. 91, no. 5-8, pp. 2401–2418, 2017.

[112] S. Jones, M. Tefe, and S. Appiah-Opoku, "Proposed framework for sustainability screening of urban transport projects in developing countries: a case study of Accra, Ghana," *Transportation Research Part A: Policy and Practice*, vol. 49, pp. 21–34, 2013.

[113] H. Wang, Z. G. Jiang, H. Zhang, Y. Wang, Y. H. Yang, and Y. Li, "An integrated MCDM approach considering demands-matching for reverse logistics," *Journal of Cleaner Production*, vol. 208, pp. 199–210, 2019.

[114] A. Formisano and F. M. Mazzolani, "On the selection by MCDM methods of the optimal system for seismic retrofitting and vertical addition of existing buildings," *Computers and Structures*, vol. 159, pp. 1–13, 2015.

[115] P. O. Akadiri, P. O. Olomolaiye, and E. A. Chinyio, "Multi-criteria evaluation model for the selection of sustainable materials for building projects," *Automation in Construction*, vol. 30, pp. 113–125, 2013.

[116] J. Logeshwaran, "The topology configuration of protocol-based local networks in high speed communication networks," *Multidisciplinary Approach in Research*, vol. 15, pp. 78–83, 2022.

[117] Z. Stevic, D. Pamucar, M. Subotic, J. Antucheviciene, and E. K. Zavadskas, "The location selection for roundabout construction using rough BWM-rough WASPAS approach based on a new rough Hamy aggregator," *Sustainability*, vol. 10, no. 8, p. 2817, 2018.

[118] M. Marzouk and L. Elmesteckawi, "Analyzing procurement route selection for electric power plants projects using SMART," *Journal of Civil Engineering and Management*, vol. 21, no. 7, pp. 912–922, 2015.

[119] Y. T. Birgani and F. Yazdandoost, "An integrated framework to evaluate resilient-sustainable urban drainage management plans using a combined-adaptive MCDM technique," *Water Resources Management*, vol. 32, no. 8, pp. 2817–2835, 2018.

[120] S. Akhtar, B. Reza, K. Hewage, A. Shahriar, A. Zargar, and R. Sadiq, "Life cycle sustainability assessment (LCSA) for selection of sewer pipe materials," *Clean Technologies and Environmental Policy*, vol. 17, no. 4, pp. 973–992, 2015.

[121] W. H. Tsai, S. J. Lin, Y. F. Lee, Y. C. Chang, and J. L. Hsu, "Construction method selection for green building projects to improve environmental sustainability by using an MCDM approach," *Journal of Environmental Planning and Management*, vol. 56, no. 10, pp. 1487–1510, 2013.

[122] A. De la Fuente, O. Pons, A. Josa, and A. Aguado, "Multi-criteria decision making in the sustainability assessment of sewerage pipe systems," *Journal of Cleaner Production*, vol. 112, pp. 4762–4770, 2016.

[123] V. Palevicius, G. M. Paliulis, J. Venckauskaite, and B. Vengrys, "Evaluation of the requirement for passenger car parking spaces using multi-criteria methods," *Journal of Civil Engineering and Management*, vol. 19, no. 1, pp. 49–58, 2013.

[124] D. Pamucar, I. Badi, K. Sanja, and R. Obradovic, "A novel approach for the selection of power-generation technology using a linguistic neutrosophic CODAS method: a case study in Libya," *Energies*, vol. 11, no. 9, p. 2489, 2018.

[125] D. Pamucar, L. Gigovic, Z. Bajic, and M. Janosevic, "Location selection for wind farms using GIS multi-criteria hybrid model: an approach based on fuzzy and rough numbers," *Sustainability*, vol. 9, no. 8, p. 1315, 2017.

[126] H. Z. Al Garni and A. Awasthi, "Solar PV power plant site selection using a GIS-AHP based approach with application in Saudi Arabia," *Applied Energy*, vol. 206, pp. 1225–1240, 2017.

[127] J. M. Sanchez-Lozano, M. S. Garcia-Cascales, and M. T. Lamata, "GIS-based onshore wind farm site selection using fuzzy multi-criteria decision making methods. Evaluating the case of southeastern Spain," *Applied Energy*, vol. 171, pp. 86–102, 2016.

[128] Y. N. Wu, C. B. Xu, and T. Zhang, "Evaluation of renewable power sources using a fuzzy MCDM based on cumulative prospect theory: a case in China," *Energy*, vol. 147, pp. 1227–1239, 2018.

[129] P. Skobalj, M. Kijevcanin, N. Afgan, M. Jovanovic, V. Turanjanin, and B. Vucicevic, "Multi-criteria sustainability analysis of thermal power plant Kolubara-A unit 2," *Energy*, vol. 125, pp. 837–847, 2017.

[130] A. Fallahpour, E. U. Olugu, S. N. Musa, K. Y. Wong, and S. Noori, "A decision support model for sustainable supplier selection in sustainable supply chain management," *Computers and Industrial Engineering*, vol. 105, pp. 391–410, 2017.

[131] H. R. Zhao and S. Guo, "Selecting green supplier of thermal power equipment by using a hybrid MCDM method for sustainability," *Sustainability*, vol. 6, no. 1, pp. 217–235, 2014.

[132] J. Logeshwaran, N. Adhikari, S. S. Joshi, P. Saxena, and A. Sharma, "Deep DNA machine learning model to classify the tumor genome of patients with tumor sequencing," *International Journal of Health Sciences*, vol. 6, no. S5, pp. 9364–9375, 2022.

[133] S. Luthra, K. Govindan, D. Kannan, S. K. Mangla, and C. P. Garg, "An integrated framework for sustainable supplier selection and evaluation in supply chains," *Journal of Cleaner Production*, vol. 140, pp. 1686–1698, 2017.

[134] J. F. F. Barata, O. L. G. Quelhas, H. G. Costa, R. H. Gutierrez, V. D. Lameira, and M. J. Meirino, "Multi-criteria indicator for sustainability rating in suppliers of the oil and gas industries in Brazil," *Sustainability*, vol. 6, no. 3, pp. 1107–1128, 2014.

[135] N. Nag, M. Chandra, K. H. Kazmi, A. Shukla, and S. K. Sharma, "Selection of suitable powder bed fusion technique for medical applications using MCDM techniques," https://ssrn.com/abstract=4192942.

[136] C. M. Sivaraja and G. Sakthivel, "Compression ignition engine performance modelling using hybrid MCDM techniques for the selection of optimum fish oil biodiesel blend at different injection timings," *Energy*, vol. 139, pp. 118–141, 2017.

[137] A. Debnath, J. Roy, S. Kar, E. K. Zavadskas, and J. Antucheviciene, "A hybrid MCDM approach for strategic project portfolio selection of agro by-products," *Sustainability*, vol. 9, no. 8, p. 1302, 2017.

[138] C. Y. Huang, P. H. Chung, J. Z. Shyu et al., "Evaluation and selection of materials for particulate matter MEMS sensors by using hybrid MCDM methods," *Sustainability*, vol. 10, no. 10, p. 3451, 2018.

[139] H. Alwaer and D. J. Clements-Croome, "Key performance indicators (KPIs) and priority setting in using the multi- attribute approach for assessing sustainable intelligent buildings," *Building and Environment*, vol. 45, no. 4, pp. 799–807, 2010.

[140] E. K. Zavadskas, R. Bausys, and M. Lazauskas, "Sustainable assessment of alternative sites for the construction of a waste incineration plant by applying WASPAS method with single-valued neutrosophic set," *Sustainability*, vol. 7, no. 12, pp. 15923–15936, 2015.

[141] N. R. Khalili and S. Duecker, "Application of multi-criteria decision analysis in design of sustainable environmental management system framework," *Journal of Cleaner Production*, vol. 47, pp. 188–198, 2013.

[142] S. Mohammad, D. Tezerjani, M. S. Yazdi, and M. H. Hosseinzadeh, "The effect of 3D printing parameters on the shape memory properties of 4D printed polylactic acid circular disks: an experimental investigation and parameters optimization," *Materials Today Communications*, vol. 33, article 104262, 2022.

[143] J. C. Kurnia, L. A. F. Haryoko, I. Taufiqurrahman, L. Chen, L. Jiang, and A. P. Sasmito, "Optimization of an innovative hybrid thermal energy storage with phase change material (PCM) wall insulator utilizing Taguchi method," *Journal of Energy Storage*, vol. 49, article 104067, 2022.

[144] G. Yang, Y. Tao, P. Wang, X. Xu, and X. Zhu, "Optimizing 3D printing of chicken meat by response surface methodology and genetic algorithm: feasibility study of 3D printed chicken product," *LWT*, vol. 154, article 112693, 2022.

[145] R. Vijay, J. D. James Dhilip, S. Gowtham et al., "Characterization of natural cellulose fiber from the barks ofVachellia farnesiana," *Journal of Natural Fibers*, vol. 19, no. 4, pp. 1343–1352, 2022.

[146] B. Sampath, N. Naveenkumar, P. Sampathkumar, P. Silambarasan, A. Venkadesh, and M. Sakthivel, "Experimental comparative study of banana fiber composite with glass fiber composite material using Taguchi method," *Materials Today: Proceedings*, vol. 49, pp. 1475–1480, 2022.

[147] M. Sutharasan and J. Logeshwaran, "Design intelligence data gathering and incident response model for data security using honey pot system," *International Journal for Research & Development in Technology*, vol. 5, no. 5, pp. 310–314, 2016.

[148] M. Jayasudha, M. Elangovan, M. Mahdal, and J. Priyadarshini, "Accurate estimation of tensile strength of 3D printed parts using machine learning algorithms," *Processes*, vol. 10, no. 6, p. 1158, 2022.

[149] M. R. Sanjay, P. Madhu, M. Jawaid, P. Senthamaraikannan, S. Senthil, and S. Pradeep, "Characterization and properties of natural fiber polymer composites: a comprehensive review," *Journal of Cleaner Production*, vol. 172, pp. 566–581, 2018.

[150] M. Liu, L. Tan, and S. Cao, "Performance prediction and geometry optimization for application of pump as turbine: a review," *Frontiers in Energy Research*, vol. 9, pp. 1–16, 2022.

[151] M. Isametova, N. Dishovsky, P. Velev, and A. Duisengali, "Properties of glass-fiber reinforced polycarbonates for centrifugal pumps impellers," *Journal of Chemical Technology and Metallurgy*, vol. 57, no. 2, pp. 224–231, 2022.

[152] A. J. Humaidi, S. K. Kadhim, and A. S. Gataa, "Optimal adaptive magnetic suspension control of rotary impeller for artificial heart pump," *Cybernetics and Systems*, vol. 53, no. 1, pp. 141–167, 2022.

[153] X. Song, H. Y. Li, Y. Li, and X. Luo, "The development of a high-speed miniature pump with dynamic bearing," *Journal of Physics: Conference Series*, vol. 2217, no. 1, p. 012049, 2022.

[154] M. Isametova, R. Nussipali, D. Karaivanov, Z. Abilikhair, and A. Isametov, "Computational and experimental study of the composite material for the centrifugal pump impellers manufacturing," *Journal of Applied and Computational Mechanics*, vol. 8, no. 4, pp. 2383–4536, 2022.

Hindawi
Advances in Polymer Technology
Volume 2023, Article ID 6344193, 9 pages
https://doi.org/10.1155/2023/6344193

Research Article

A Decision-Making Carbon Reinforced Material Selection Model for Composite Polymers in Pipeline Applications

Mohammed Ahmed Mustafa,[1] S. Raja,[2] Layth Abdulrasool A. L. Asadi,[3] Nashrah Hani Jamadon,[4] N. Rajeswari,[5] and Avvaru Praveen Kumar[6]

[1]*University of Imam Jafar Al-Sadiq, College of Technology Department of Medical Laboratory Techniques, Iraq*
[2]*Managing Director, Research & Development, Mr. R Business Corporation, Karur, Tamil Nadu, India*
[3]*Department of Structures and Water Resources Engineering, Faculty of Engineering, University of Kufa, Najaf, Iraq*
[4]*Centre of Materials Engineering and Smart Manufacturing, Department of Mechanical and Manufacturing, Faculty of Engineering and Built Environment, The National University of Malaysia, Bangi, 43600 Selangor, Malaysia*
[5]*Department of Mechanical Engineering, Surya Engineering College, Erode, Tamil Nadu, India*
[6]*Department of Applied Chemistry, School of Applied Natural Science, Adama Science and Technology University, P O Box 1888, Adama, Ethiopia*

Correspondence should be addressed to S. Raja; engineerraja1995@gmail.com
and Avvaru Praveen Kumar; avvaru.praveen@astu.edu.et

Received 20 December 2022; Revised 1 February 2023; Accepted 22 March 2023; Published 11 April 2023

Academic Editor: Indran Suyambulingam

Pipes are manufactured primarily through the extrusion process. One of the material extrusion processes in recent digital manufacturing is additive manufacturing's fusion deposition modeling. Pipes are made from various materials such as metal and plastic/polymers, and the main challenge has been in selecting the pipe material for the customized application. For the creation of water-passing tubes, this research has chosen appropriate carbon-reinforced polymers that can be used with filament made of polyether ether ketone (PEEK) and polyethylene terephthalate glycol (PETG). For this goal, the analytical hierarchy process, also known as the AHP, is used to choose the best material based on factors such as cost, temperature resistance, printing speed, and mechanical properties of the material. The results revealed that PEEK-CF is a better material for the customized impeller application than PETG-CF. The PEEK-CF obtains the higher priority value of 0.6363, and the PETG-CF obtains 0.2791. This decision-making technique can be used to select other comparable customized applications.

1. Introduction

Researchers are still interested in carbon-fiber reinforced polymers (CFRPs), which are well-known for having high specific mechanical characteristics. However, due to the high degree of skill and substantial equipment expenditures needed, producing these composite materials is expensive. Cheaper manufacturing techniques are a crucial enabler technology for higher commercial acceptance of composites and quicker product development cycles since these decrease the growth of composite materials [1–3]. In recent decades, additive manufacturing methods have emerged, which use 3D printers to manufacture components layer by layer. Net-shaped parts can now be directly manufactured with more design freedom. The most common layer-by-layer technique is fused filament fabrication (FFF), also known as fused deposition modeling (FDM). Using this method, an object is constructed by depositing thermoplastic polymer material through a nozzle, a process also known as 3D printing. A relatively recent field of research [4–8] is the use of fiber-reinforced filament to produce composite parts using a completely automated method.

A hollow plastic cylinder or portion is known as a plastic pipe. It has a circular cross-section and is mostly used to

move fluids, such as liquids and gases, slurries, powders, and masses of tiny materials. Polyvinyl chloride (PVC), a combination of plastic and vinyl, is the most commonly used material for polymer pipes. There is also CPVC (chlorinated polyvinyl chloride) piping, PERT (polyethylene-raised temperature) piping, and other options available [9–12].

Previous researchers explored different polymers for water-passing pipes/tube-based various applications instead of metals.

Supian et al. [13] wrote a review on the polymer composite materials in the energy absorption tube application. Based on this review, authors revealed that polymer replaces the metal application. Zhao et al. [14] investigated the 1D polymer material for the pipeline application and revealed that aerogels replace the liquid solvents with air to replace the solid interlaminar.

An amorphous thermoplastic polymer called ABS has been used to fabricate the pumps, rotor blades for drones, and rotary parts for the microorganic Rankine cycle (mORC) [15]. A semicrystalline thermoplastic polymer called PLA is made from sustainable resources like sugarcane or maize starch. One or more of the characteristics of this polymer is that it is biodegradable and compassable. When compared to other polymers, this polymer has a reasonable price, environmentally favorable biocompatibility, and acceptable physicomechanical properties. Impellers for pumps, compressors, and maritime applications have been made using PLA [16].

In order to examine the mechanical impact behavior of short carbon fiber reinforced PEEK composites and unfilled PEEK, Garcia-Gonzalez et al. [17] looked into the energy absorbed. In transverse, longitudinal, and unfilled fiber PEEK conditions, the tensile elastic modulus was 12.6, 24, and 3.6 GPa, respectively.

According to Alam et al.'s [18] investigation of carbon-reinforced PEEK for biomedical structural applications, the material recovers a sizable portion of the mechanical losses in strength and modulus brought on by sulfonation, in one instance increasing superior than (nonsulfonated) printed PEEK in terms of yield and final strengths (graphene nanoplatelets reinforcement).

Siddikali et al. [19] investigated carbon-reinforced PETG for coating with an electroless metal layer application, and their findings show better mechanical properties. In a Pump-Jet Module application, the PETG impeller was studied by Odetti et al. [20]. Tests with a PETG impeller at 1200 rpm and 14 N of thrust revealed that it has the right characteristics for this application. A more advanced quasithermoplastic polymer is PEEK. This polymer exhibits exceptional thermal, mechanical, and chemical resistance qualities. Many academics are interested in the PEEK impeller found in centrifugal pumps because of its improved strength and dependability [21, 22]. Pumps have used PETG impellers. This polymer's good water resistance and biodegradability are reasons for using it in the manufacture of pump blades [23, 24]. The various types of polymers and applications are classified in Figure 1.

The manufacture of rotating components has been done using a variety of thermoplastic polymers, including ABS, PLA, polyethylene terephthalate glycol (PETG), PEEK, and polyphenylene sulfide (PPS) [26–29].

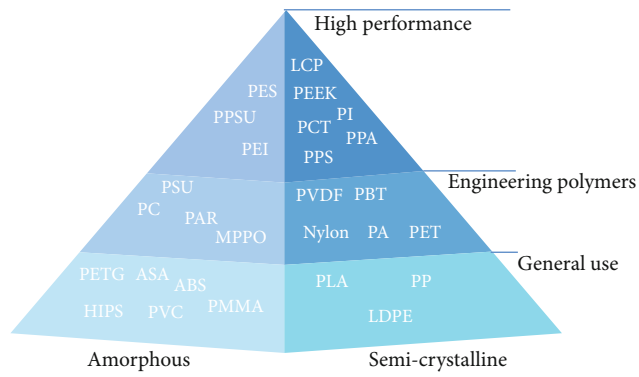

Figure 1: Various thermoplastic polymers and applications (open access article—Nader Zirak et al. [25]).

From this, previous literature has not done customized application material selection-based studies on carbon-reinforced polymer for water pipe making. Carbon-reinforced PEEK and PETG filaments are investigated in this study for use in the fabrication of customized water pipes. For obtaining this research objective, the detailed literature review has been carried out with MCDM methodology, particularly AHP procedures in the material selection problems as the first phase, and detailed materials and methods (how to apply) are discussed. The rest of the part elaborates on the result and discussion, and also, the conclusion shows research objective obtain or not.

2. Literature Review

2.1. Multicriteria Decision-Making. The act of choosing the best or appropriate option from a variety of options is known as decision-making. The primary goal of MCDM is to select the best alternative for a given situation including several criteria. The MCDM method makes use of criteria, options, and decision-makers' perspectives to determine the optimum course of action [30]. MCDM is a vital technique in operation research and can assist decision-makers when presented with a variety of options and requirements [31]. The MCDM contains a number of tools for making decisions, including AHP, FAHP, TOPSIS, and COPRAS, among others [32]. The FAHP, TOPSIS, and DEMATEL algorithms are frequently employed in the AM sector [33]. SCM [34], management science system engineering [35], sustainability [36], planning and product development assessment [37], and strategic management [38] all benefit from the application of MCDM. FTOPSIS and FMEA risk assessment have both been enhanced by MCDM [39].

2.2. Analytical Hierarchy Process (AHP). In this study, the AHP technique is covered first. The three primary techniques that make up the AHP approach's foundation are the hierarchy structure, priority examination, and consistency confirmation. This methodology was created to help with complex decision-making. The rational hierarchy is designed to enable a decision-maker or group of decision-

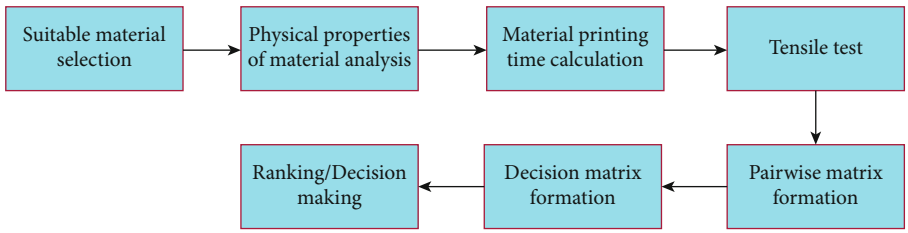

Figure 2: Research flow of the paper.

Table 1: Saaty scale of relative alternative, [4].

Saaty scale	
2, 4, 6, and 8	Intermittent values
1/3, 1/5, 1/7, 1/9	Inverted comparison values
1	Equal significance
3	Moderate significance
5	Strong significance
7	Extremely significance
9	Very extremely significance

makers to pairwise compare criteria and the related alternatives, resulting in global weight syncing, and then use the results to decide on alternative priority. Additionally, one of the main contributions of AHP and what sets it apart from other MCDA methodologies is that it permits the evaluation of judgement consistency [40].

The top level of the AHP hierarchy structure may be the aim or objective, with criteria and/or subcriteria appearing at the intermediate level. Then, the possibilities that correlate can be pursued at the most basic level. To create numerical weights, all pairwise comparison matrices will be collected, assessed, and then normalized. However, given the existence of uncertain situations in the decision-making process, this work suggests the integrative AHP and fuzzy logic (i.e., FAHP), which can be further researched [41].

3. Methodology

The research flow of the manuscript is shown in Figure 2. The research objective is to select a suitable carbon-reinforced material for pipe application. For this, the physical properties of material analysis such as price, mechanical property, printing time, and temperature withstand. Then, the third criteria of time have been calculated during the printing.

Then, the printed samples were involved in the tensile test, and based on all the criteria results, the pairwise matrix formed. In this paper's research, the AHP is used for finding suitable materials from the selected carbon-reinforced materials. The AHP processes have the Saaty scale as shown in Table 1. The Saaty scale is used to evaluate the criteria and alternatives. Figure 3 expresses the methodology of the manuscript. The objective of the research is the selection of suitable materials based on criteria such as price, temperature, printing time, and mechanical property.

4. Fabrication and Testing

4.1. Physical Properties of Material Analysis. The physical properties of PEEK and PETG are analyzed using criteria such as price and temperature. As a consequence, the cost and temperature of both materials are as follows.

PEEK is a liquid crystalline thermoplastic with high-temperature chemical and mechanical resistance properties. PEEK CF is one of the most advanced thermoplastics ever created. It is employed in some of the most demanding applications in industries such as automobiles, aerospace, defense, semiconductors, and oil and gas. PEEK is used by engineers in applications where failure is not an option. With tensile strengths between 90 and 100 MPa and a Young's modulus of 3.6 GPa, PEEK is both stiff and powerful. Polyether ether ketone is also referred to as PEEK. It is a colorless organic thermoplastic polymer that produces some of the best results of any thermoplastic on the market. It belongs to the polyether ether ketone (PEEK) family of compounds. PEEK filament has a variety of distinct properties. PETG filament is a quasi-industrial strength material with excellent UV and impact resistance and a slightly softer surface. It is simple to postprocess to achieve the desired surface finish [42–45].

Their main distinctions are their properties, applications, and material costs. PETG is more durable and stronger than PLA. PLA, on the other hand, is commonly used as an FDM/FFF filament due to its superior melt and cooling properties. However, comparable materials, PETG and PEEK, have superior materials compared to PLA. PETG is more expensive than PLA in terms of cost. PETG CF is a material designed for users that need to create structural elements that are subjected to significant mechanical pressures. As a result, many disciplines of engineering, including medicine, utilize this material to create prototypes and final items.

PETG is mainly remembered for its strength and durability, and the plastic is resistant to high temperatures, UV rays, water, chemical solvents, and other environmental factors. All of this makes PETG an excellent filament material choice for printing parts that will be exposed to harsh environments or will be subjected to a high level of physical stress [46–49].

The price of PETG carbon fiber filament starts onwards (Indian rupee) INR.1150 and PEEK carbon fiber filament price INR 4800 onwards, as shown in Figure 4. PETG has a significant melting point of 210°C and a fairly low temperature for glass transition of about 85°C. This means that, while the printing process necessitates hotter temperatures,

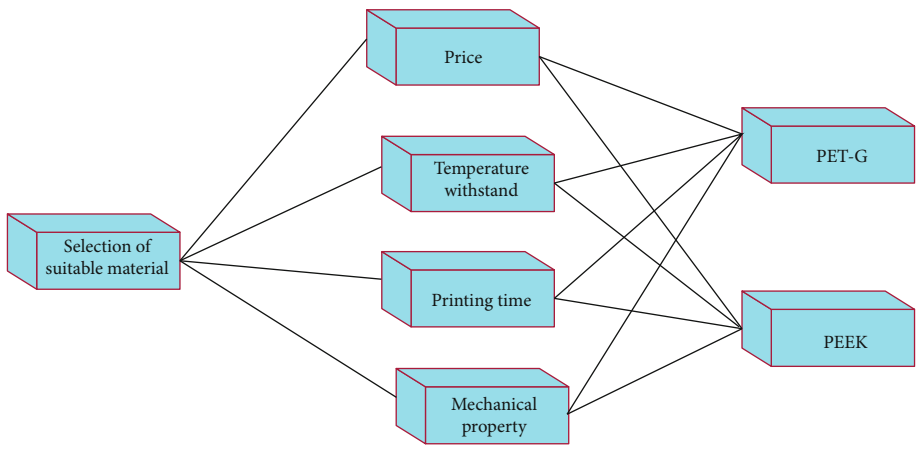

Figure 3: Methodology.

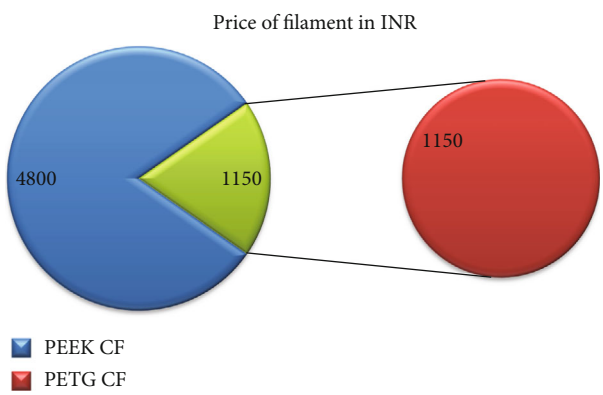

Figure 4: Comparison of the price of filaments.

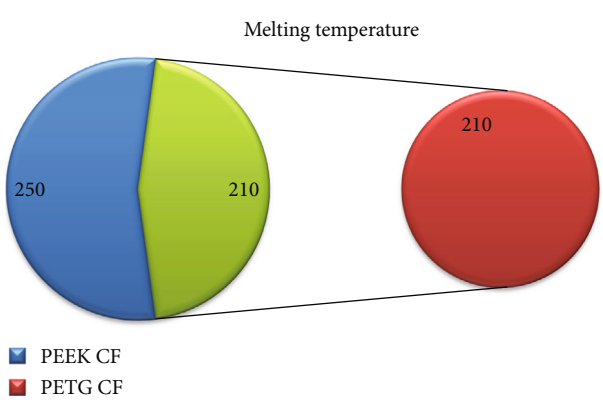

Figure 5: Comparison of the melting temperature of filaments.

PETG components are not well-known for their thermal properties. PEEK has a roughly 143°C (289°F) transition temperature and a roughly 250°C (662°F) melting temperature, and the comparison between the two selected polymers is shown in Figure 5 [44, 50, 51].

4.2. Printing the Samples. FDM has risen in popularity among additive manufacturing techniques because of its accessibility and material adaptability. This technique has been used over the years to generate a variety of materials

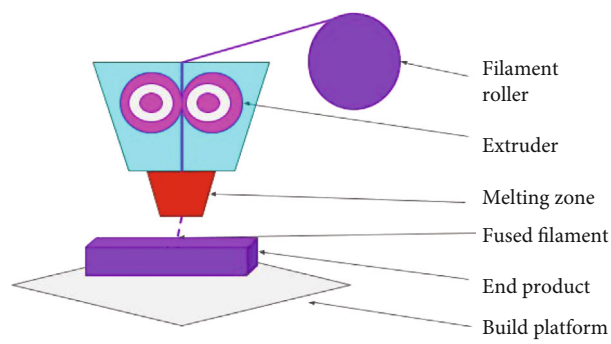

Figure 6: FDM components.

Table 2: Time recorded for printing ASTM D638 samples.

PETG-CF	Time taken in "min"	PEEK-CF	Time taken in "min"
Sample 1	9	Sample 1	15
Sample 2	10	Sample 2	15
Sample 3	9	Sample 3	16
Total	28	Total	46
Average	9.33	Average	15.33

for application in the aerospace [52], medical [53], and automotive industries, including plastics, powder, ceramics, and composites [54]. This procedure involves layering a partially built object with semisolid filament material that has been extruded through a heated nozzle. The process uses a build platform, print bed, liquefier head, and build material spool, as shown in Figure 6. The geometry development program is used to create the STL (standard triangular language) file format for the manufactured part model. It is then entered into the software and split into thin, two-dimensional layers.

This two-dimensional contour information is used to produce the tool path motion. The movement of the liquefier head is controlled by a 3-axis mechanism. It moves in the X-Y plane in accordance with the tool path of the

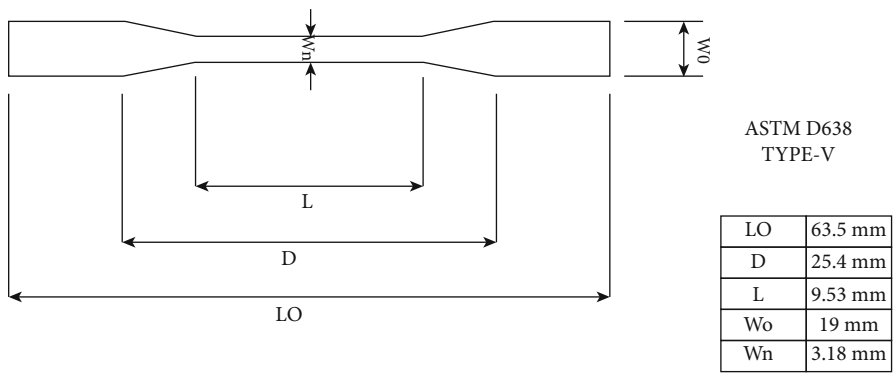

Figure 7: Geometrical standard of ASTM D638 type V [45].

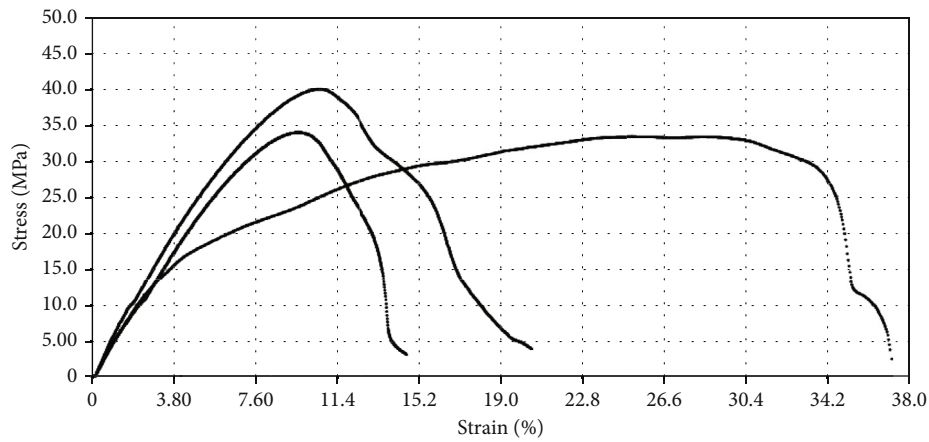

Figure 8: Stress and strain diagram for PEEK-CF.

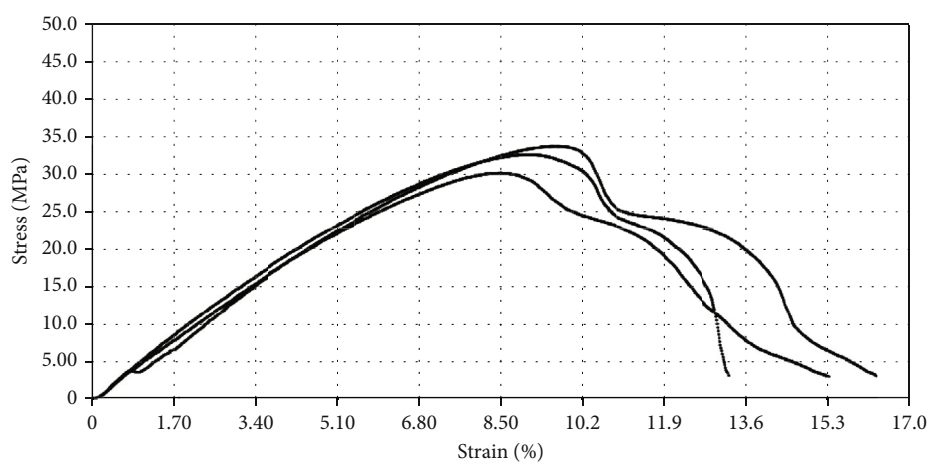

Figure 9: Stress and strain diagram for PETG-CF.

Table 3: Tensile test results for carbon-reinforced PETG AND PEEK.

PETG-CF	UTS in "MPa"	PEEK-CF	UTS in "MPa"
Sample 1	39.9	Sample 1	79.8
Sample 2	33.9	Sample 2	81.2
Sample 3	33.3	Sample 3	84.5
Total	107.1	Total	245.5
Average	35.7	Average	81.83

software and deposits the first layer while doing so. The recently added layer and the recently deposited layer are joined. Until the entire section is finished, the material will be deposited in successive layers.

After completion, the structure can be manually or chemically removed from the print platform by destroying the support structure [25, 55–57]. Fused deposition modeling (FDM) or material extrusion additive manufacturing are other names for this process that are permissible in

Table 4: Pairwise matrixes for analyzing criteria.

Based on aim	Price	Printing time	Temperature withstand	Mechanical property
Price	1	3	4	6
Printing time	1/3	1	1/2	3
Temperature withstand	1/4	2	1	3
Mechanical property	1/6	1/3	1/3	1

Table 5: Decision matrix with criteria.

Criteria weight	0.56 Priority-1	0.18 Priority-2	0.24 Priority-3	0.07028 Priority-4
PEEK-CF	0.613	0.667	0.643	0.641
PETG-CF	0.095	0.107	0.072	0.136

Table 6: Final decision matrix.

	Total rows	Priority value	Rank
PEEK-CF	0.337 + 0.112 + 0.143 + 0.0452	0.6363	I
PETG-CF	0.165 + 0.032 + 0.063 + 0.0158	0.2791	II

ASTM F42 (additive manufacturing technologies) (AM). The FDM components and operation are shown in Figure 1.

4.3. Printing Time Calculation. Based on the printing time, carbon-reinforced PETG had 15 minutes, and PEEK took 19 minutes. Table 2 expresses the time recorded for printing the tensile samples.

Each tensile sample of PETG carbon fiber takes a minimum of 9 minutes and a maximum of 10 min for printing the ASTM D638. Similarly, the PEEK carbon fiber samples take a minimum of 15 minutes and a maximum of 16 minutes. The average time of PETG carbon fiber is better than that of PEEK carbon fiber.

4.4. Tensile Test. The tensile test has been prepared from 3 out of 6 samples for PETG-CF and the rest of 3 out of 6 samples for PEEK-CF. The polymer tensile specimen standard ASTMD638 type V has been used for the experiment, and its geometrical size is shown in Figure 7.

The stress-strain curves of carbon-reinforced PEEK polymer are depicted in Figure 8, and PETG polymer is depicted in Figure 9.

Table 3 expresses the ultimate tensile strength values of carbon-reinforced PETG and PEEK. From the result, the PEEK carbon-reinforced polymer has a much superior tensile mechanical property.

Based on the tensile strength, the carbon-reinforced PETG has 35.7 MPa, and PEEK has 81.83 MPa. The tensile test was carried out by Instron machine, and the maximum load of 10000 N is applied to the specimen at the strain rate of 1 mm/min.

5. Result and Discussion

According to time, PETG-CF takes 9.33 minutes, and PEEK-CF takes 15.33 minutes. PETGCF compare to PEEK-CF takes less time. Based on tensile test results, PETG-CF has less strength compared to PEEK-CF. The other parameter comparison is discussed in detail in section 4.0. The pairwise matrix shown below has been created based on the discussion of the criteria and the Saaty scale. The pairwise matrixes formed in the first row indicated that price is considered equally important for both alternatives. Then, column 3 compares the price versus printing time; it takes 3 which means moderate importance. Column 4, in the first row, compares the price versus temperature withstands of material; it takes 4 which means intermediate of moderate and strong importance. Finally, column 5 compares the price versus mechanical property; it takes 6 which means intermediate between strong and very strong importance. Table 4 shows the pairwise matrix for the selected criteria.

Consistency index,

$$\text{C.I} = \frac{\lambda\max - n}{n - 1.} \tag{1}$$

where: $\lambda\max$ = (Sum of ratio of weight sum value and criteria weight)/(number of criteria) and n is the number of criteria.

Based on the consistency ratio verification,

$$\text{C.R} = 0.05 < 0.10 \tag{2}$$

As a result, the criteria are acceptable, and the consistency ratio is reasonable. If the consistency is less than one, it means that the created pairwise matrix is acceptable.

Table 5 shows the four criteria with priority values to form the decision matrix. Table 6 expresses that the PEEK-CF has been the most suitable material for the pipe-making customized application. The PEEK-CF material has the highest priority value of 0.6363, and the PETG-CF materials have the lowest priority value of 0.2791.

6. Conclusion

The purpose of this research is to select suitable materials from two different carbon-reinforced materials for manufacturing customized pipes. For this, a technique called AHP has been used in the mathematical programming technique of multicriteria decision-making. In this, both materials are evaluated based on the common criteria of time, temperature resistance, printing time, and tensile strength which are mechanical properties. In terms of price, PETG carbon fiber is slightly less when compared to PEEK-CF. And in terms of temperature, PEEK-CF is considered superior to PETG carbon fiber. Then, in terms of time, it is found

that PETG carbon fiber can produce products in slightly less time when compared to PEEK-CF. Finally, PEEK carbon fiber is known to be stronger than PETG carbon fiber in terms of mechanical properties. Based on these four criteria, the pairwise matrix is generated with the help of Saaty scale. And through it, the consistency index is found, and the criteria are evaluated. Accordingly, this research indicates that PEEK carbon fiber is more suitable for pipe application than PETG carbon fiber. This research will be useful for future researchers to choose customized materials and equipment problems.

Data Availability

The article contains all the data required to back up the investigation's conclusions. The author in question can provide more details upon request if necessary.

Conflicts of Interest

The authors declare that they have no conflict of interest.

References

[1] R. Guo, C. Li, Y. Niu, and G. Xian, "The fatigue performances of carbon fiber reinforced polymer composites - a review," *Journal of Materials Research and Technology*, vol. 21, pp. 4773–4789, 2022.

[2] J. N. Hani, M. A. Ahmad, H. N. M. Fuad, and S. Adzila, "Mechanical properties of injection-molded poly-lactic acid (PLA) reinforced with magnesium hydroxide for biomedical application," in *Advances in Material Science and Engineering*, Lecture Notes in Mechanical Engineering, S. S. Emamian, M. Awang, J. A. Razak, and P. J. Masset, Eds., pp. 363–370, Springer, Singapore, 2023.

[3] X. Liu, E. Zhang, J. Liu et al., "Self-healing, reprocessable, degradable, thermadapt shape memory multifunctional polymers based on dynamic imine bonds and their application in nondestructively recyclable carbon fiber composites," *Chemical Engineering Journal*, vol. 454, article 139992, 2023.

[4] S. Raja, A. J. Rajan, V. P. Kumar et al., "Selection of additive manufacturing machine using analytical hierarchy process," *Scientific Programming*, vol. 2022, Article ID 1596590, 20 pages, 2022.

[5] K. I. Ismail, T. C. Yap, and R. Ahmed, "3D-printed fiber-reinforced polymer composites by fused deposition modelling (FDM): fiber length and fiber implementation techniques," *Polymers*, vol. 14, no. 21, p. 4659, 2022.

[6] M. Karthick, M. Meikandan, S. Kaliappan et al., "Experimental investigation on mechanical properties of glass fiber hybridized natural fiber reinforced penta-layered hybrid polymer composite," *International Journal of Chemical Engineering*, vol. 2022, Article ID 1864446, 9 pages, 2022.

[7] N. R. Madhu, H. Erfani, S. Jadoun, M. Amir, Y. Thiagarajan, and N. P. S. Chauhan, "Fused deposition modelling approach using 3D printing and recycled industrial materials for a sustainable environment: a review," *The International Journal of Advanced Manufacturing Technology*, vol. 122, no. 5-6, pp. 2125–2138, 2022.

[8] S. Raja, A. P. Agrawal, P. P. Patil et al., "Optimization of 3D printing process parameters of polylactic acid filament based on the mechanical test," *International Journal of Chemical Engineering*, vol. 2022, Article ID 5830869, 2022.

[9] J. C. Montes, D. Cadoux, J. Creus, S. Touzain, E. Gaudichet-Maurin, and O. Correc, "Ageing of polyethylene at raised temperature in contact with chlorinated sanitary hot water. Part I–Chemical aspects," *Polymer Degradation and Stability*, vol. 97, no. 2, pp. 149–157, 2012.

[10] N. B. Samarth and P. A. Mahanwar, "Degradation of polymer & elastomer exposed to chlorinated water—a review," *Open Journal of Organic Polymer Materials*, vol. 11, no. 1, pp. 1–50, 2021.

[11] S. Ravichandran, R. Duraiswamy, and F. S. Arockiasamy, "Tool and formability multi-response optimization for ultimate strength and ductility of AA8011 during axial compression," *Advances in Mechanical Engineering*, vol. 14, no. 10, 2022.

[12] S. Kumar, "Recent developments of biobased plasticizers and their effect on mechanical and thermal properties of poly (vinyl chloride): a review," *Industrial & Engineering Chemistry Research*, vol. 58, no. 27, pp. 11659–11672, 2019.

[13] A. B. M. Supian, S. M. Sapuan, M. Y. M. Zuhri, E. S. Zainudin, and H. H. Ya, "Hybrid reinforced thermoset polymer composite in energy absorption tube application: a review," *Defence Technology*, vol. 14, no. 4, pp. 291–305, 2018.

[14] G. Zhao, L. Shi, G. Yang, X. Zhuang, and B. Cheng, "3D fibrous aerogels from 1D polymer nanofibers for energy and environmental applications," *Journal of Materials Chemistry A*, vol. 11, no. 2, pp. 512–547, 2023.

[15] I. Hernandez-Carrillo, C. J. Wood, and H. Liu, "Advanced materials for the impeller in an ORC radial microturbine," *Energy Procedia*, vol. 129, pp. 1047–1054, 2017.

[16] N. Zirak, M. Shirinbayan, S. Farzaneh, and A. Tcharkhtchi, "Effect of Molecular Weight on Crystallization Behavior of Poly Lactic Acid (PLA) under Isotherm and Non-Isotherm Conditions," *Polymers for Advanced Technologies*, vol. 33, no. 4, pp. 1307–1316, 2022.

[17] D. Garcia-Gonzalez, M. Rodriguez-Millan, A. Rusinek, and A. Arias, "Investigation of mechanical impact behavior of short carbon-fiber-reinforced PEEK composites," *Composite Structures*, vol. 133, pp. 1116–1126, 2015.

[18] F. Alam, K. M. Varadarajan, J. H. Koo, B. L. Wardle, and S. Kumar, "Additively manufactured polyetheretherketone (PEEK) with carbon nanostructure reinforcement for biomedical structural applications," *Advanced Engineering Materials*, vol. 22, no. 10, article 2000483, 2020.

[19] P. Siddikali and P. R. Sreekanth, "Performance evaluation of CNT reinforcement on electroless plating on solid free-form-fabricated PETG specimens for prosthetic limb application," *Polymers*, vol. 14, no. 16, p. 3366, 2022.

[20] A. Odetti, M. Altosole, G. Bruzzone, M. Caccia, and M. Viviani, "Design and construction of a modular pump-jet thruster for autonomous surface vehicle operations in extremely shallow water," *Journal of Marine Science and Engineering*, vol. 7, no. 7, p. 222, 2019.

[21] G. Velmurugan, V. S. Shankar, S. Kaliappan et al., "Effect of aluminium tetrahydrate nanofiller addition on the mechanical and thermal behaviour of luffa fibre-based polyester composites under cryogenic environment," *Journal of Nanomaterials*, vol. 2022, Article ID 5970534, 10 pages, 2022.

[22] K. Pedersen, A. F. Bengtsson, J. S. Edlund, and L. C. Eriksson, "Sulphate-controlled diversity of subterranean microbial

communities over depth in deep groundwater with opposing gradients of sulphate and methane," *Geomicrobiology Journal*, vol. 31, no. 7, pp. 617–631, 2014.

[23] K. C. Sekhar, R. Surakasi, P. Roy et al., "Mechanical behavior of aluminum and graphene nanopowder-based composites," *International Journal of Chemical Engineering*, vol. 2022, Article ID 2224482, 13 pages, 2022.

[24] D. Garcia-Gonzalez, A. Rusinek, T. Jankowiak, and A. Arias, "Mechanical impact behavior of polyether-ether-ketone (PEEK)," *Composite Structures*, vol. 124, pp. 88–99, 2015.

[25] H. Ramazani and A. Kami, "Metal FDM, a new extrusion-based additive manufacturing technology for manufacturing of metallic parts: a review," *Progress in Additive Manufacturing*, vol. 7, no. 4, pp. 609–626, 2022.

[26] A. Machalski, J. Skrzypacz, P. Szulc, and D. Błoński, "Experimental and numerical research on influence of winglets arrangement on vortex pump performance," *Journal of Physics Conference Series*, vol. 1741, no. 1, article 012019, 2021.

[27] N. G. Olaiya, C. Maraveas, M. A. Salem et al., "Viscoelastic and properties of amphiphilic chitin in plasticised polylactic acid/starch biocomposite," *Polymers*, vol. 14, no. 11, p. 2268, 2022.

[28] Z. Yu, M. Lei, Y. Ou, and G. Yang, "Toughening of polyethylene terephthalate/amorphous copolyester blends with a maleated thermoplastic elastomer," *Journal of Applied Polymer Science*, vol. 89, no. 3, pp. 797–805, 2003.

[29] A. Kumar, B. Sah, A. R. Singh et al., "A review of multi criteria decision making (MCDM) towards sustainable renewable energy development," *Renewable and Sustainable Energy Reviews*, vol. 69, pp. 596–609, 2017.

[30] F. E. Boran, S. Genç, M. Kurt, and D. Akay, "A multi-criteria intuitionistic fuzzy group decision making for supplier selection with TOPSIS method," *Expert Systems with Applications*, vol. 36, no. 8, pp. 11363–11368, 2009.

[31] S. Raja and A. J. Rajan, "A decision-making model for selection of the suitable FDM machine using fuzzy TOPSIS," *Mathematical Problems in Engineering*, vol. 2022, Article ID 7653292, 15 pages, 2022.

[32] M. Zoghi, G. Rostami, A. Khoshand, and F. Motalleb, "Material selection in design for deconstruction using Kano model, fuzzy-AHP and TOPSIS methodology," *Waste Management & Research*, vol. 40, no. 4, pp. 410–419, 2022.

[33] R. Subramani, S. Kaliappan, P. V. Arul et al., "A recent trend on additive manufacturing sustainability with supply chain management concept, multicriteria decision making techniques," *Multicriteria Decision Making Techniques*, vol. 2022, article 9151839, 12 pages, 2022.

[34] K. T. Mannan, V. Sivaprakash, S. Raja, P. P. Patil, S. Kaliappan, and S. Socrates, "Materials Today : Proceedings Effect of Roselle and Biochar Reinforced Natural Fiber Composites for Construction Applications in Cryogenic Environment," *Materials Today: Proceedings*, vol. 69, pp. 1361–1368, 2022.

[35] S. Raja, J. Logeshwaran, S. Venkatasubramanian et al., "OCHSA : designing energy-efficient lifetime-aware leisure degree adaptive routing protocol with optimal cluster head selection for 5G communication network disaster management," *Scientific Programming*, vol. 2022, Article ID 5424356, 2022.

[36] K. T. Mannan, V. Sivaprakash, S. Raja, M. Kulandasamy, P. P. Patil, and S. Kaliappan, "Materials today : proceedings significance of Si 3 N 4/lime powder addition on the mechanical properties of natural calotropis gigantea composites," *Materials Today: Proceedings*, vol. 69, pp. 1355–1360, 2022.

[37] Z. J. Wang, "A note on "a group decision making model based on a generalized ordered weighted geometric average operator with interval preference matrices"," *Fuzzy Sets and Systems*, vol. 341, pp. 145–153, 2018.

[38] J. E. Leal, "AHP-express: A simplified version of the analytical hierarchy process method," *Methods X*, vol. 7, article 100748, 2020.

[39] A. F. Firdaus, S. Madelan, and A. B. Saluy, "Supplier/partnership selection system analysis based on analytic hierarchy method process in oil and gas drilling project (case study: PT KMI)," *International Journal of Innovative Science and Research Technology*, vol. 6, no. 3, pp. 403–411, 2021.

[40] P. Ferretti, G. M. Santi, C. Leon-Cardenas, E. Fusari, M. Cristofori, and A. Liverani, "Production readiness assessment of low cost, multi-material, polymeric 3D printed moulds," *Heliyon*, vol. 8, no. 10, article e11136, 2022.

[41] L. Musa, N. K. Kumar, S. Z. Abd Rahim et al., "A review on the potential of polylactic acid based thermoplastic elastomer as filament material for fused deposition modelling," *Journal of Materials Research and Technology*, vol. 20, pp. 2841–2858, 2022.

[42] L. Natrayan, S. Kaliappan, S. B. Sethupathy et al., "Investigation on interlaminar shear strength and moisture absorption properties of soybean oil reinforced with aluminium trihydrate-filled polyester-based nanocomposites," *Journal of Nanomaterials*, vol. 2022, Article ID 7588699, 8 pages, 2022.

[43] R. C. Ogle, J. Lee, and U. K. Vaidya, "Improved specimen design for interlayer adhesion parameter optimization of material extrusion," 2022, Available at SSRN 4239104.

[44] N. H. Jamadon, A. W. Tan, F. Z. Yusof, T. Ariga, Y. Miyashita, and M. Hamdi, "Utilization of a porous cu interlayer for the enhancement of Pb-free Sn-3.0ag-0.5Cu solder joint," *Metals*, vol. 6, no. 9, p. 220, 2016.

[45] R. Subramani, S. Kaliappan, S. Sekar et al., "Polymer filament process parameter optimization with mechanical test and morphology analysis," *Advances in Materials Science and Engineering*, vol. 2022, Article ID 8259804, 8 pages, 2022.

[46] A. Basir, A. B. Sulong, N. H. Jamadon, N. Muhamad, and U. B. Emeka, "Process parameters used in macro/micro powder injection molding: an overview," *Metals and Materials International*, vol. 27, no. 7, pp. 2023–2045, 2021.

[47] F. Harden, R. Kral, B. Schädel, R. Adelung, and O. Jacobs, "Precise non-assembly mechanisms by multi-material fused layer modeling and subsequent heat treatment," 2022, Available at SSRN 4245482.

[48] M. R. Mazlan, N. H. Jamadon, A. Rajabi et al., "Necking mechanism under various sintering process parameters – a review," *Journal of Materials Research and Technology*, vol. 23, pp. 2189–2201, 2023.

[49] S. Venkatasubramanian, S. Raja, V. Sumanth et al., "Fault diagnosis using data fusion with ensemble deep learning technique in IIoT," *Mathematical Problems in Engineering*, vol. 2022, Article ID 1682874, 8 pages, 2022.

[50] J. Kechagias, D. Chaidas, N. Vidakis, K. Salonitis, and N. M. Vaxevanidis, "A multi-parametric process evaluation of the mechanical response of PLA in FFF 3D printing," *Materials and Manufacturing Processes*, pp. 1–13, 2022.

[51] J. Zhang, D. R. Chen, and S. C. Chen, "A review of emission characteristics and control strategies for particles emitted from

3D fused deposition modeling (FDM) printing," *Building and Environment*, vol. 221, p. 109348, 2022.

[52] L. Sandanamsamy, W. S. W. Harun, I. Ishak et al., "A comprehensive review on fused deposition modelling of polylactic acid," *Progress in Additive Manufacturing*, vol. 7, no. 5, pp. 1–25, 2022.

[53] R. Patel, C. Desai, S. Kushwah, and M. H. Mangrola, "A Review Article on FDM Process Parameters in 3D Printing for Composite Materials," *Materials Today: Proceedings*, vol. 60, pp. 2162–2166, 2022.

[54] A. Wazeer, A. Das, A. Sinha, K. Inaba, S. Ziyi, and A. Karmakar, "Additive manufacturing in biomedical field: a critical review on fabrication method, materials used, applications, challenges, and future prospects," *Progress in Additive Manufacturing*, vol. 7, pp. 1–33, 2022.

[55] P. A. Hatwalne and S. B. Thakare, "Evaluating torsional properties of FDM components for various Layer Heights," in *Recent Advances in Manufacturing Processes and Systems*, pp. 437–443, Springer, Singapore, 2022.

[56] E. Manzo, N. Downey, P. Cheetham, and S. Pamidi, "Fabrication and characterization of additively manufactured electrical insulation system components using SLA and FDM printers," in *2022 IEEE Electrical Insulation Conference (EIC)*, pp. 69–72, Knoxville, TN, USA, 2022.

[57] N. Zirak, M. Shirinbayan, M. Deligant, and A. Tcharkhtchi, "Toward polymeric and polymer composites impeller fabrication," *Polymers*, vol. 14, no. 1, p. 97, 2022.